WASHINGTON UNIVERSITY
THE HENRY EDWIN SEVER GRADUATE SCHOOL
DEPARTMENT OF CIVIL ENGINEERING

CONTROL STRATEGIES FOR 3D SMART BASE ISOLATION SYSTEMS USING MODAL AND NODAL APPROACHES

by
Yumei Wang
Prepared under the direction of Professor Shirley J. Dyke

A dissertation presented to the Henry Edwin Sever Graduate School of
Washington University in partial fulfillment of the
requirements of the degree of
DOCTOR OF SCIENCE

May 2006
Saint Louis, Missouri

WASHINGTON UNIVERSITY
THE HENRY EDWIN SEVER GRADUATE SCHOOL
DEPARTMENT OF CIVIL ENGINEERING

ABSTRACT

CONTROL STRATEGIES FOR 3D SMART BASE ISOLATION SYSTEMS USING MODAL AND NODAL APPROACHES

by

Yumei Wang

ADVISOR: Professor Shirley J. Dyke

May 2006
Saint Louis, Missouri

Application of control technologies to structures is expected to be able to enhance a structure's performance in response to natural hazards. Specifically, smart base isolation systems, which consist of a passive isolator at the base with controllable semiactive devices, attract much attention for efficacy and economical reasons. This study focuses on the development of control design strategies using physical knowledge of the system dynamics that had not been investigated systematically and applied for civil structures previously. Structural characteristics that are helpful to disclose structural properties yet are often ignored by civil engineers are integrated with these control techniques in both nodal and modal coordinates to construct indices for the determination of the control actions to take full advantage of their capabilities. A 3D base isolated building is employed for the demonstration and validation of these strategies. MR dampers are used as the smart control devices. Effective design for this complex system requires the use of control device and sensor placement techniques and optimal control weighting selection, which is achieved through the application of the structural physical properties. A correlation technique is proposed and is first applied for the placement problem to minimize redundancies. Controller order reduction is also examined for more implementable controllers, where both open-loop and closed-loop balancing are taken into account. Responses of this system to seven specified earthquakes demonstrate that the proposed strategies are effective for the control of the base isolation system. The modal approach is advocated because it has explicit physical interpretation and is more straightforward for the design engineer.

copyright by
Yumei Wang
2006

CONTENTS

List of Figures vi

List of Tables ix

Acknowledgements x

Chapter 1

Introduction 1

1.1 Literature Review 3
1.1.1 Semiactive Control Devices 3
1.1.2 Control Design and Implementation 7
1.1.3 Smart Base Isolation 13
1.2 Objectives of This Research 14
1.3 Organization of This Dissertation 16

Chapter 2

Modal Approach for Structural Dynamics and Control 18

2.1 Modal Structural Models 19
2.1.1 Signal Flow Diagrams of Nodal Form and Modal Form 19
2.1.2 Transformation Between Modal Forms 24
2.2 Controllability and Observability 29
2.2.1 Definitions 29
2.2.2 Properties in Modal Coordinates 32
2.3 Grammian Ellipsoids and Balanced Model Reduction 34
2.4 Illustrative Example 40
2.5 Summary 47

Chapter 3

The Isolation System of the Benchmark Building 48

3.1 Description of the Smart Base Isolation Benchmark Problem 48
3.2 Optimal Linear Isolation System 57

3.2.1 Isolation System for a One-Dimensional Model 58
3.2.2 Isolation System for the 3D Building 61
3.3 Summary 63

Chapter 4

Actuator and Sensor Placement Using Modal Approach 64

4.1 Effects of the Cross Couplings on Norms in the Feedback Loop 65
4.2 Placement Indices..... 69
4.3 Placement Strategy..... 72
4.4 Control Device and Sensor Placement for the Benchmark Problem..... 74
4.5 Summary 83

Chapter 5

LQG Control in Nodal Coordinates 84

5.1 Linear Quadratic (LQ) Control 85
5.1.1 Linear Quadratic Regulator (LQR) 85
5.1.2 Kalman Filter and Noise-Shaping Filter 87
5.1.3 Selection of the Weighting Matrices..... 94
5.2 Control of the Benchmark Building Subjected to Earthquakes..... 97
5.2.1 Modeling and Control of MR Dampers 97
5.2.2 Weighting Determination 104
5.2.3 Earthquake Simulation Results 108
5.3 Pole Assignment and Order Reduction in Nodal Coordinates 115
5.4 Summary 118

Chapter 6

LQG Control and Order Reduction Using the Modal Approach 119

6.1 LQG Balancing and Order Reduction 120
6.1.1 LQG Control in Modal Coordinates 120
6.1.2 LQG-Balanced and Approximately LQG-Balanced Controllers..... 124
6.1.3 Reduction Index and Reduction Strategy 127
6.1.4 Spillover in Modal Control..... 130
6.2 Application to the Benchmark Building..... 131
6.2.1 LQG-Balanced Controller for the Benchmark Building 131
6.2.2 Earthquake Simulations..... 139
6.2.3 Control Performances for Different Weightings 146
6.3 Sources of Error 154
6.4 Summary 154

Chapter 7

Conclusions and Recommendations.....155

Appendix A Structural Parameters of the Benchmark Building 159

Appendix B Properties of Modal Low-Authority LQG Controllers.....162

References 164

Vita 176

LIST OF FIGURES

Chapter 1

Figure 1-1 (a) Force-Displacement Curve of Piezoelectric Friction Damper (b) Acceleration at the Second Floor of a Three-Story Building 4
Figure 1-2 Schematic of the VAD-Damper System 5
Figure 1-3 (a) Photograph of the 20-Ton MR Damper (b) Force-Displacement Loops of the MR Damper 6

Chapter 2

Figure 2-1 Signal Flow Diagram of a System in Nodal Form 20
Figure 2-2 Signal Flow Diagram of a System in Jordan Diagram for Distinct Roots..... 23
Figure 2-3 Signal Flow Diagram of Modal Form 1 25
Figure 2-4 Signal Flow Diagram of Modal Form 3 for a Pair of Complex Mode..... 26
Figure 2-5 Signal Flow Diagram of Modal Form 2 for a Pair of Complex Mode..... 27
Figure 2-6 Controllability Ellipsoids..... 36
Figure 2-7 Unbalanced System Ellipsoids 37
Figure 2-8 Six-Story Building Model 40
Figure 2-9 Poles of the Full-Order and Nodal Reduced-Order Models..... 44
Figure 2-10 Poles of the Full-Order and Modal Reduced-Order Models 46

Chapter 3

Figure 3-1 Plan View of the Fundamental Level and the Nominal Bearing Locations .. 49
Figure 3-2 Elevation View of the Asymmetric Base Isolated Benchmark Building..... 50
Figure 3-3 Maximum RMS of Base-Drift – Acceleration Curves of the 1D System..... 59
Figure 3-4 Maximum RMS Responses of the Actively Controlled System..... 60
Figure 3-5 Maximum RMS of Base-Drift – Acceleration Curves of the 2D System..... 61
Figure 3-6 10% Damped Response Spectra of the Design Earthquakes 62

Chapter 4

Figure 4-1 General Diagram of a Feedback Control System 66
Figure 4-2 Diagram of a Constant-Gain Feedback Control System 67
Figure 4-3 Control Device Placement Indices vs. Control Device Locations 76
Figure 4-4 Schematic of Control Device Installation 78
Figure 4-5 Plan View of the Base Level and the Control Device Locations 79
Figure 4-6 Sensor Placement Indices vs. Floors 80
Figure 4-7 Sensor Corner Placement Indices for Floor 3 81

Figure 4-8 Sensor Locations 82
Figure 4-9 Responses at Corner 1 in the x-Direction with Full- and Reduced-Sensors .. 83

Chapter 5

Figure 5-1 Frequency Content of Design Earthquakes and the Kanai-Tajimi Filter 91
Figure 5-2 Flow Chart of the Nominal Controller Design Using the Nodal Approach .. 93
Figure 5-3 Weighting Observability Grammians for Cases AA and AID 95
Figure 5-4 Weighting Observability Grammians for Cases BDAA and BDBA 96
Figure 5-5 Weighting Observability Grammians for Cases BDBATA and BD5ATA ... 97
Figure 5-6 (a)Schematic of an MR Damper (b)Bouc-Wen Model of the MR Damper .. 98
Figure 5-7 Force-Time Response of the MR Damper to 20sin(πt) 100
Figure 5-8 Force-Displacement Loop of the MR Damper to 20sin(πt) 101
Figure 5-9 Force-Velocity Loop of the MR Damper to 20sin(πt) 101
Figure 5-10 Graphical Representation for Selecting Command Signal 103
Figure 5-11 Simulink Block Diagram for Simulations 104
Figure 5-12 q-Maps of Base Drift Responses 107
Figure 5-13 q-Maps of Acceleration Responses 107
Figure 5-14 Maximum Responses to the Design Earthquakes (Nodal) 109
Figure 5-15 Performance Indices of the Passive-on System 111
Figure 5-16 Performance Indices of the Semiactive System (Nodal) 111
Figure 5-17 Base Drift Responses at Corner 1 to the Newhall Earthquake (Nodal) 112
Figure 5-18 Acceleration Responses at Roof Corner 1 to the Newhall Earthquake (Nodal) 112
Figure 5-19 Response Profiles to the Newhall Earthquakes (Nodal) 113
Figure 5-20 Effective Bearing Forces and Control Forces (Nodal) 114
Figure 5-21 Desired and Actual Control Forces in MR Damper at Bearing 3 in the Newhall Earthquake (Nodal) 115
Figure 5-22 Poles of the Open-Loop and the Closed-Loop Plants (Nodal) 116
Figure 5-23 Poles of the Open-Loop Plant and the Closed-Loop Controller (Nodal) 117
Figure 5-24 Zoom-In of the Poles of the Open-Loop Plant and the Closed-Loop Controller 117

Chapter 6

Figure 6-1 Coefficient β_c vs. Weight q or Hankel Singular Value γ^2 122
Figure 6-2 Hankel Singular Values from SVD of Balanced Nodal Model and from Approximation of Balanced and Unbalanced Modal Model 131
Figure 6-3 Block Diagram of Control Using the Modal Approach 132
Figure 6-4 Test of Low-Authority Property 134
Figure 6-5 Poles of the Open-Loop and the Closed-Loop Plants (Modal, 1) 135
Figure 6-6 Poles of the Open-Loop Plant and the Closed-Loop Controller (Modal, 1) 136
Figure 6-7 MIMO Bode Magnitude Plots of Base Drifts to MR Damper at Bearing 3 of the Open- and Closed-Loop Systems (Modal, 1) 137

Figure 6-8 MIMO Bode Magnitude Plots of Roof Corner Accelerations to MR Damper at Bearing 3 of the Open- and Closed-Loop Systems (Modal, 1) 138
Figure 6-9 LQG Characteristic Values and Order Reduction Indices (Modal, 1) 138
Figure 6-10 Response Profiles with Full-Sensor, Full-Order Controller to the Newhall Earthquake (Modal, 1) 140
Figure 6-11 Response Profiles with Reduced-Sensor, Full-Order Controller to the Newhall Earthquake (Modal, 1) 141
Figure 6-12 Response Profiles with Reduced-Sensor, 12-Mode Controller to the Newhall Earthquake (Modal, 1) 142
Figure 6-13 Base Drift Responses at Corner 1 to the Newhall Earthquake (Modal, 1) .. 143
Figure 6-14 Acceleration Responses at Roof Corner 1 to the Newhall Earthquake (Modal, 1) 143
Figure 6-15 Effective Bearing Forces and Control Forces (Modal, 1) 144
Figure 6-16 Maximum Responses to the Design Earthquakes (Modal, 1) 145
Figure 6-17 Performance Indices of the Semiactive System (Modal, 1) 145
Figure 6-18 Poles of the Open-Loop Plant and the Closed-Loop Controller (Modal, 2) 147
Figure 6-19 LQG Characteristic Values and Order Reduction Indices (Modal, 2) 148
Figure 6-20 Step Responses of the Closed-Loop Plant and the Full-Order LQG Controller (Modal, 2) 149
Figure 6-21 Effective Bearing Forces and Control Forces (Modal, 2) 149
Figure 6-22 Poles of the Open-Loop and the Closed-Loop Plants (Modal, 2) 150
Figure 6-23 MIMO Bode Magnitude Plots of Base-Drifts to MR Dampers at Bearing 3 of the Open- and Closed-Loop Systems (Modal, 2) 151
Figure 6-24 Response Profiles with Reduced-Sensor, 18-Mode Controller to the Newhall Earthquake (Modal, 2) 152
Figure 6-25 Base Drift Responses at Corner 1 to the Newhall Earthquake (Modal, 2) .. 152
Figure 6-26 Step Responses of the Closed-Loop Plant and the Full-Order LQG Controller (Modal, 2) 153

LIST OF TABLES

Chapter 2

Table 2-1 Structural Model Parameter (Kelly et al., 1987) 41
Table 2-2 Eigenvalues and Dominant Eigenvectors of the Controllability and Observability Grammians 42

Chapter 3

Table 3-1 Floor Masses of the Benchmark Building 51
Table 3-2 First Nine Natural Periods of the Superstructure 51
Table 3-3 Performance Indices (Normalized) to be used in This Study 52
Table 3-4 Parameters of the 1D Base Isolated Benchmark Building 58

Chapter 4

Table 4-1 Membership Index of the Control Device Locations 77
Table 4-2 Correlation Membership of the Control Device Locations 78

Chapter 5

Table 5-1 Weighting Matrix Alternatives 94
Table 5-2 Performance Indices 110

ACKNOWLEDGMENTS

In the first instance, I would like to thank my advisor, Dr. Shirley J. Dyke. Her continuous support and guidance helped me in all the time of this research. She provided all the convenience in facilitating this work and proofread all the revisions as well.

I also want to thank Prof. Bergman and Prof. Sridharan, who read my draft very closely, corrected grammar and symbol errors, and proposed valuable advice for improvement. I am also obliged to Prof. Kenneth L. Jerina, who allowed me to sit in his class of aircraft simulation and control, where I learned advanced control techniques that are helpful to this research.

This work was supported in part by the Mid-America Earthquake Center through NSF grant EEC-9701785. This dissertation would not be possible without their support.

Dr. Xiuxia Du supplied me lot of materials and information on structural control. Her friendship and help was a great backup to me.

Last, my thankfulness would forward to my family and my other friends. Thanks for their continuous love and understanding. I couldn't have made it through this long process without them.

Yumei Wang

Washington University in St. Louis
May 2006

Chapter 1

Introduction

The primary focus of most model building codes is to ensure life safety for the design level ground shaking. The design of the seismic load resisting system is based on a pseudo seismic load using a reduction factor "R". The same reduction factor applies to the entire building. Continued operation of a facility and reduction of economic losses associated with earthquake damage to the facility are secondary considerations. Economic losses sustained in previous earthquakes have highlighted the need for a design methodology that allows people to choose a desired level of seismic performance for buildings and nonstructural components when they are subjected to a specified level of ground motion. Performance based seismic design is such methodology that allows the building owner, architect, and engineer to work together to determine the appropriate levels of ground motion and performance objectives in order to meet the owner's expectations. It delineates at least two levels performance to which structures can be designed including: (1) to prevent injury to the occupants and damage to the contents; and (2) to protect the integrity and function of the structure (Meirovitch and Stemple, 1997).

Promising new systems have been developed which can be incorporated into structures to provide enhanced behavior for improved service and safety. These systems are known as control systems. By integrating real-time, mechanical force-generation devices within the structure, the structural system can respond intelligently to the specific excitation, and thus can achieve the desired performance in the most efficient way. One particular application of structural control systems, smart base isolation systems, is the subject of this dissertation. The following paragraphs will provide some background for control systems in general with a focus on their application to base isolated structures.

Because of their simplicity, passive control strategies are relatively well understood and widely accepted by the engineering community. Passive systems rely on energy supplemental devices such as dampers, isolators, and absorbers to respond to the motion of

the structure to dissipate vibrational energy. Among passive control systems, base isolation systems are the most widely accepted, and they have been applied to many structures and types of equipment (Kelly et al., 1985; Tsai et al., 1989; Manolis et al., 1990; Naeim and Kelly, 1999; Nagarajaiah et al., 2000). However, passive approaches can only adapt to structural and loading changes in a narrow band and often need additional measures to help to overcome their inherent weaknesses.

To date, extensive research has been conducted in the area of active structural control. Active control systems operate by using external energy supplied by the actuators to impart forces on the structure. The control action is determined by the measurement of structural responses. These systems have been installed in over twenty commercial buildings and more than ten bridges (Ni et al., 2002a,b). Active control applications in civil engineering structures were initially proposed and applied for seismic protection or seismic performance improvement in conventional (fixed base) structures (Kelly et al., 1987). However, some potential users of this technology are concerned with the stability, cost effectiveness, reliability, power requirements, etc. of active control. Cost considerations call for hybrid control, a blend of passive and active control. Under certain stringent design specifications when passive isolation can not ensure the desired performance, the introduction of active control systems along with passive isolation techniques constitutes a viable alternative (Inaudi et al., 1993a). The hybrid use of active schemes for base-isolated structures has been considered for many years (Fujita et al., 1988; Inaudi et al., 1990; Talbot et al., 1990; Kobori et al., 1991). There are still some questions about power requirements and cost-effectiveness.

Semiactive control systems offer an appealing alternative to both active and hybrid control. Semiactive devices have the ability to dynamically vary their properties, indicating they will be effective for a wide variety of disturbances. Additionally, they typically have low power requirements, eliminating the need for a large external power source. Moreover, they are inherently stable because they do not have the ability to input energy into the structural system. Both experimental and analytical studies have demonstrated that the performance of semiactive devices is superior to that of comparable passive systems. In

some cases, these devices also outperform comparable active systems (Dyke, 1996, Jansen and Dyke, 2000, Yoshida, 2003).

Several algorithms and semiactive devices have been developed to be implemented in civil engineering structures. For near-term acceptance and implementation of this technology, we still require a greater understanding of the issues associated with the modeling and simulation of these devices and how to implement them in structures to best exploit their unique capabilities (Dyke et al., 2005). In this literature review, some of the recent accomplishments made by researchers in the US in the area of structural control using semiactive devices (specifically, MR dampers) will be summarized first. The second portion will turn toward some important control design issues (device placement and model reduction, etc.) and implementations of semiactive devices. The third portion of the literature review summarizes the recent work of smart base isolation problems using semiactive devices.

1.1 Literature Review

1.1.1 Semiactive Control Devices

Semiactive devices are essentially passive devices that can be controlled. The promise of semiactive control has lead to research resulting in significant advances in semiactive devices. This section will summarize some of the recent research in the varied implementations of semiactive control systems for civil engineering structures.

As an appealing alternative to their passive counterpart, semiactive tuned mass dampers (STMD) have gained recent recognition. STMD can be based on variable stiffness devices, controllable tuned sloshing dampers, and controllable tuned liquid column dampers. For instance, the design of next generation of liquid dampers has been studied at the NatHaz Modeling Laboratory at the University of Notre Dame (Yalla et al., 2000, 2003). Nagarajaiah and Nadathur (2005) have also developed a novel STMD, with variable stiffness that has the advantage of continuously retuning its natural frequency in real time thus making it robust to changes in building stiffness and damping. This is based on a

semiactive continuously and independently variable stiffness (SAIVS) device that can vary the stiffness continuously and smoothly (Nagarajaiah et al., 1998).

He et al. (2003) have also proposed a continuously sliding semiactive friction controller which dissipates vibratory energy using surface frictional forces. Piezoelectric actuators have recently been integrated into a friction device to make the device semiactive in responding to structural responses (Chen and Chen, 2004b). A prototype damper was designed, characterized as shown in Figure 1-1(a), and successfully implemented on a ¼-scale three-story building (Chen and Chen, 2004a) for effective reduction of the building response as illustrated in Figure 1-1(b).

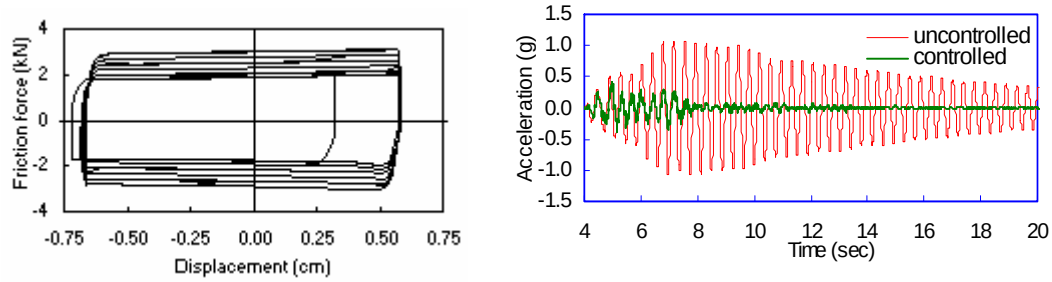

(a) (b)

Figure 1-1 (a) Force-Displacement Curve of Piezoelectric Friction Damper
(b) Acceleration at the Second Floor of a Three-Story Building

Another new semiactive damping system is comprised of a novel variable amplification device (VAD) connected in series with a supplemental damper. When installed on a structure, the VAD is connected between a damping element and the structural frame (Figure 1-2). It consists of a series of gears mounted on parallel shafts. The amplification factors of the device are given by the ratio of the radii of any two gears in a pair. Therefore, changing the gear pair changes its amplification state. When the amplification state is selected via a semiactive control algorithm, forces may be delivered to the structure at various levels as required throughout the duration of a dynamic event. In this way, the VAD-damper system behaves like a semiactive control system even when a passive damper is used (Walsh 2005).

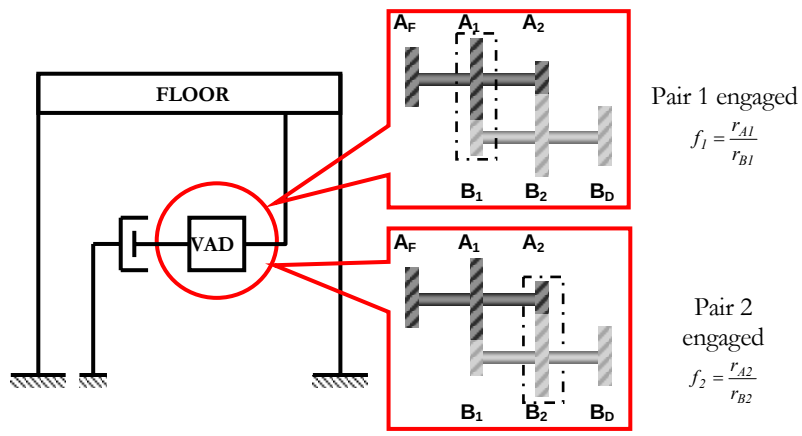

Figure 1-2 Schematic of the VAD-Damper System

Much of the research in semiactive control has made use of control devices with variable mechanical parameters. However, it is also possible for energy to be dissipated electrically, using electric machines to facilitate electromechanical energy conversion, and then using controllable circuitry to regulate dissipation. Such electromechanical systems of devices are referred to as regenerative force actuation (RFA) networks. Unlike ordinary semiactive systems, RFA systems have the capability to store and reuse energy, as well as transmit energy from one device to another in actuation networks. Currently, RFA networks are being implemented in scale-model structural control experiments at Caltech (Scruggs and Iwan, 2004, 2005).

Shape memory alloy (SMA) materials are capable of repeatedly absorbing large amounts of energy under a combination of loading and thermal cycles without exhibiting permanent deformation. This prominent property of SMA materials has made them a promising candidate for use in the design of alternative structural damping devices, which have attracted a great attention from civil engineering communities, especially for hazard mitigation applications. Recently, a SMA wire (SMAW) damper with tunable hysteretic behavior has been developed by Zhang and Zhu (2005) and the results of a numerical simulation study which involves a 3-story steel frame building used for the ASCE control benchmark study has demonstrated the effectiveness of the SMAW damper in controlling seismic responses of building structures.

Recently at the University of Nevada, Reno, researchers have designed, constructed and tested, a new modular, large-scale, magnetorheological fluid (MRF) by-pass damper for seismic mitigation applications (Wang et al., 2004; Gordaninejad et al., 2004a,b). The modular feature of the new MRF valve provides flexibility of adding as much force as needed to the damper with minimal modification to an existing passive damper.

Magnetorheological (MR) dampers that use MR fluids to create controllable characteristics have recently become popular new semiactive control devices because they have the ability to generate large forces, offer high reliability, demand small power requirements, and respond in milliseconds. A phenomenological model for an MR damper was developed by Spencer et al. (1997) based on the Bouc-Wen hysteresis model (Wen 1976) and then used to demonstrate the capabilities of MR dampers (Dyke et al. 1996a, b). Several other modeling techniques have been applied to small (1.5 kN) MR dampers (see, for example, Gavin et al. 2001; Chang and Roschke 1999; Wereley et al. 1999; Zhang and Roschke 1998; Xu et al. 2003). Models for larger scale (200 kN) devices were later developed and validated experimentally by Yang (2001) and Yang et al. (2002a, b) based on the Bouc-Wen model. MR devices of this size are now commercially available for implementation in civil engineering structures (Figure 1-3). MR devices built by Lord Corporation have also been applied recently to the National Museum of Emerging Science and Innovation in Tokyo, Japan, and to control cable vibration using constant command voltages (passive mode) in the Dongting Lake Bridge in China (Ko et al., 2002).

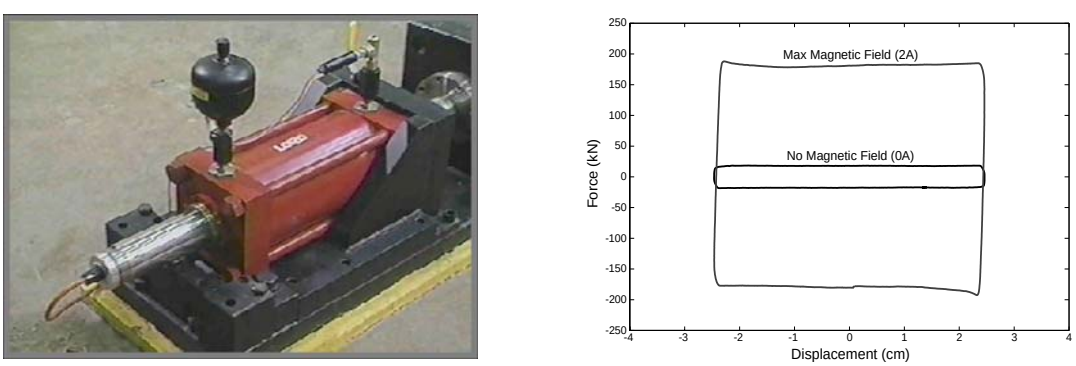

(a) (b)

Figure 1-3 (a) Photograph of the 20-Ton MR Damper

(b) Force-Displacement Loop of the MR Damper

1.1.2 Control Design and Implementation

The capabilities of a structural control system depend on a great deal more than device selection. The nonlinear nature of the control devices and the strong potential for nonlinear behavior in the structure itself under severe dynamic loads increase the challenge to the designers. Placement schemes must be employed to appropriately place the devices within the structure, and modern optimal control design for MIMO systems needs a reasonable order controller. This section focuses on current research in each of these topics.

The nonlinear nature of semiactive devices and the broad range of nonlinearities exhibited by the various devices in this class pose a challenge to the control system designer. Some control algorithms have been developed for the various devices. Several of the most recent algorithms will be described in the following paragraphs.

A supervisory fuzzy logic controller (SVFLC) has been developed by Symans and Reigles (2004) to optimize semiactive controllers for base isolation systems. The basic concept is to develop a supervisory controller to determine the more appropriate one of the two separate lower-level controllers. Numerical studies of the SVFLC were performed using the first generation of base isolation benchmark problems with controllable fluid viscous dampers used as control devices within the isolation system. The results from the numerical simulations are promising and experimental validation tests are planned for the near future. A performance evaluation study of various semiactive control strategies was recently completed (Reigles and Symans, 2005a, b). Results demonstrate that semiactive control can provide improved performance compared with passive control in many cases.

Wilson and Abdullah (2005b) also developed a fuzzy controller to regulate the damping properties of MR dampers and to reduce floor displacements and accelerations in a SDOF seismically excited structure. In this study, two additional tuning strategies were employed (Wilson et al. 2005a), leading to the development of a gain-scheduled fuzzy controller and a self-tuning fuzzy controller. This mechanism involves the introduction of a fuzzy reasoning system to select appropriate parameters at each time step. Comparison with results obtained with the fuzzy controller with constant value (Wilson et al., 2005b) showed that tuning of these parameters can improve the controller's performance. Numerical simulations showed that the fuzzy controller successfully reduced maximum and root-

mean-square (RMS) responses of the structure under four different earthquake loads. Furthermore, this controller was found to outperform the control algorithm presented in Liu et al. (2001).

Another strategy for application to active and semiactive control of structures excited by winds and earthquakes is the model predictive control (MPC) (Mei et al. 2001, 2002). MPC is employed to develop real-time, feed-forward and feedback control. The MPC scheme is based on the system response of an explicit prediction model to obtain the control action by minimizing an objective function. Optimization objectives include minimization of the difference between the predicted and reference response and minimization of the control effort subjected to constraints. The effectiveness of the control schemes is validated through small scale experiments on a shaking table. The design and development of the MPC scheme has been effectively implemented in structural control applications at the NatHaz Modeling Laboratory.

Research has also been conducted at Caltech in the area of reliability-based structural control design. Recent investigations have concentrated on the derivation of active control laws which explicitly minimize the probability of structural failure. Here, "failure" is defined as the first-passage of the system trajectory across a generalized set of hyperplanes in the system response space. Versions of the approach have been developed for the case with no structural model uncertainty, as well as for the case with uncertain model parameters with probabilistically-distributed values. This concept is applied to an ASCE benchmark problem concerning an active base isolation system (Scruggs et al., 2005). Currently, the concept of reliability-based control design is being extended to nonlinear actuation systems, such as semiactive and regenerative systems.

Since the design requirements for civil engineering structures are multi-objective, Yang et al. (2004a) developed a multi-objective control strategy using linear matrix inequality (LMI) approaches and applied them to various structural control benchmark problems. Yang et al. (2002) also proposed an optimal design approach for passive energy dissipation devices (PEDD). Based on active control theories, various active control theories have been used advantageously to design PEDDs in terms of optimal location and capacity. The 76-story, wind-excited benchmark concrete office tower (Yang et al., 2004

a,b) proposed for Melbourne, Australia was designed to test these control algorithms and for the convenience of comparison.

Controllable fluid dampers (including MR and ER devices) exhibit physical properties similar to a simple dashpot element: they dissipate energy from the system to which they are attached. Decentralized (McClamroch and Gavin, 1995) and neural network (Zhang and Roschke, 1998) based controllers have been employed in numerical studies with controllable fluid devices. However, the most successful strategy to date for control of systems using controllable fluid devices is the clipped optimal algorithm developed by Dyke, et al. (1996a,b). In this case a controller is designed based on linear control strategies as if the control device were active. However, a decision block and measured force feedback are integrated to appropriately adjust the control command to accommodate the device's dissipative characteristics and the nonlinearities in the device behavior. This strategy has been used widely by other researchers (Yi et al., 1998; Jansen and Dyke, 2000; Yi et al., 2001). The efficacy has been demonstrated for various investigations, such as multiple device application (Jansen, et al, 1999).

For the semiactive control approaches mentioned previously, dissipativity of the selected linear control theory is the leading factor that affects the performance of the smart damper. Johnson et al. (2002a,b, 2004) introduced two new dissipativity indices to quantify the dissipativity of a linear control algorithm. Also, using convex multi-objective optimization methods in linear matrix inequality (LMI) framework, a well-known control strategy, linear quadratic regulator (LQR) is redefined in a form that is suitable to be modified by one of the dissipativity constraints introduced. Therefore, this new representation of LQR allows one to design the controller, possibly with better dissipativity characteristics.

Irregular structures are appealing for aesthetic reasons and often necessary for some facilities, but this is a source of damage in many such structures during earthquakes. If a structure has an asymmetric distribution of mass or stiffness, torsional motions may be coupled with lateral responses and result in amplification and stress concentration. Yoshida and Dyke (2005) have conducted research to utilize smart devices to control the responses of structures that are plan and vertically irregular. Experimental validation was first

conducted on a two-story, four-DOF structure in the laboratory. The experimental results demonstrate that the performance of the semiactive controller using MR dampers is significantly better than passive control system where constant voltages are applied to the MR dampers (Dyke et al., 1997; Yoshida, 2003). Numerical studies on full-scale structures were also performed to demonstrate the effectiveness of smart devices for this application (Yoshida et al., 2003; Yoshida et al., 2005).

Other control algorithms include a continuously sliding semiactive friction controller (He et al., 2003), and bridge connections between adjacent civil structures with the control forces developed based on Fixed Point Theory (Richardson et al., 2003). The effectiveness of the algorithms in decreasing the structural vibration has been verified on selected structures.

It is obvious that the number and location of sensors and actuators have greater influence upon the closed-loop performance than any specific control law itself because the issue directly links to the structural performance and the control effort. This issue is especially important for 3D, multi-story buildings with lateral-torsional behavior, because not only does the vertical distribution across the building height but also the horizontal distribution at floor levels are essential for structural performance. These problems become more critical when the number of control devices and sensors increases and the mode shapes becomes more complicated.

Researchers have studied the problem of optimal placement using different methodologies. Geromel (1989) presented a procedure of convex analysis and global optimization for actuator location using LMI. Oliveira and Geromel (2000) proposed a linear output feedback controller design with joint selection of sensor and actuator.

The technique mostly mentioned and cited in the literature is the genetic algorithm (GA). Using GA, the placement of collocated sensors / control devices is coded into a genetic string known as a chromosome. Subsets of the chromosomes, known as genes, contribute in different ways to the chromosome's 'fitness'. The aim of the GA is to produce chromosomes with increasing fitness. It does so by generating successive chromosome populations using features of the fittest chromosomes from previous populations. The final population of chromosomes contains information about the best controller locations.

Abdullah (2001) proposed a genetic algorithm (GA) with a gradient-based optimization technique to simultaneously place control devices and determine the optimal gains for each controller. The proposed method is compared with a previous study using sequential placement (Abdullah, 1999). Tan et al (2005c) further extended the concepts to propose an integrated H_2/LQG design and placement approach using GA. The advantage of this approach lies in its flexibility and practicality for design. Design objectives, disturbance characteristics, actuator dynamics, and control resources (limitations) can all be integrated into the placement/design procedure. Each control design is evaluated by calculating its performance index, and the strings which yield the best fitness are kept.

The development of optimal methods of designing controllers with order constraints is an interesting topic. High order controllers are sometimes difficult to implement due to hardware and software limitations. A wide variety of techniques exist for generating reduced-order controllers. The classical control ideas allow the design of non-optimal, low-order controllers. Reduced-order approximation of SISO controllers can be accomplished by removing poles and zeros. This technique can be extended to MIMO systems, but is presented primarily to increase intuitive understanding of controller approximation.

The computation of the H_∞-norm is of particular importance in the validation of reduced-order models. In the literature various iterative methods for the calculation of this norm have been proposed. The problem is usually considered by using linear matrix inequalities (LMI), where the main focus is on solving a non-convex optimization problem (Gahinet et al., 1994; Iwasaki et al., 1995). Watanabe et al. (2002) proposed and studied the structure of algorithms for deriving the H_∞ reduced controllers for both continuous and discrete time systems. The reduction in order is related to unstable transmission zeros of the subsystem from disturbance inputs to measurement outputs. In the case where the subsystem has no infinite zeros, the resulting order of the H_∞ controller is lower than that of the existing reduced-order H_∞ controller designs which are based on reduced-order observer design. Furthermore, the mechanism of the controller order reduction is analyzed on the basis of the two Riccati equations approach.

A method for reduced-order controller approximation based on balanced realizations can be directly applied to MIMO controllers. Balanced reduction relies on the internal

balancing of the controllability and observability grammians to eliminate weakly observable and controllable modes (Moore, 1981). Fortuna et al. (1993a) presented some results relative to the parameterization of SISO discrete-time models in open-loop balanced form. Given the singular values, the results allow discrete-time, open-loop balanced systems to be obtained. The problem of the closed-loop balancing of discrete-time systems was addressed later (Fortuna et al., 1993b). In this work a new nonlinear matrix equation of the cross-Riccati type is introduced. The equation allows the right balancing of discrete-time MIMO systems, avoiding the solution of the two traditional Riccati equations for the Kalman filter and the LQ regulator. Some characteristic properties of the cross-Riccati equation are also proven and a method is suggested to obtain approximations of discrete-time models, by using the equation introduced, which appears suitable for the approximation of LQG compensators.

The reduction of the order of an LQG controller is considered by Nunnari et al. (1994). The proposed approach takes advantage of the formulation of the stability of the closed-loop system as a structured perturbation problem of a linear state space system.

A system can be expressed in either a nodal or a modal representation. Structural analysis and testing usually gives preference to the modal representation, due to its compactness, simplicity, and explicit physical interpretation. Also, many useful structural characteristics are properly exposed only in modal coordinates (Gawronski, 1998). The modal control method allows one to unveil structural characteristics and gives insights into the control laws. Also, it makes it easier to design control laws. To date, numerous procedures and algorithms concerning modal control or pole assignment have been proposed in literature (Yang, 1982; Lu, 2001; Lu and Chung, 2001). The modal approach is more pertinent and useful in many engineering applications, such as actuator and sensor placement, model reduction, pole assignment, etc. It usually has more explicit physical interpretation as well. However, one must be careful to properly consider the effects of modeling errors at high frequencies, often called “spillover”, when using modal control. This phnomenon can severely degrade the system performance and even generate instabilities in the controlled system when an active controller is used (Mark, 1978; Cho et al., 2005). Some methods of mitigating the spillover effect for semiactive systems were

discussed by Bhatia (2001) and Whalen et al. (2002). Additionally, Dyke (1996a) discussed a technique to avoid exerting significant control effort at the higher frequencies based on the examination of the loop gain transfer function (see also, Dyke et al., 1996d; Dyke et al., 1996e).

1.1.3 Smart Base Isolation

Because semiactively controlled base isolation systems combine the best features of passive and active control, they appear to have significant potential to advance the acceptance of structural control as a viable means for dynamic hazard mitigation (Park et al., 2003). Makris (1997) showed that the use of friction-type forces (rigid-plastic behavior) such as those provided by electrorheological (ER) dampers could reduce displacements while keeping accelerations at low levels for both near-field and far-field earthquakes. Another particular promising class of semiactive control devices for smart base isolation systems is found in magnetorheological (MR) dampers. These devices offer mechanical simplicity, low operating power requirements, environmental robustness, and demonstrated potential for developing forces sufficient for full scale applications.

A number of numerical and experimental studies have shown that smart base isolation using MR dampers could achieve notable decreases in base drifts over comparable passive systems with no accompanying increase in base shears or in accelerations. In the United States, these applications on buildings can be found in Barbat et al. (1995), Ramallo et al. (2002), Ahmadi et al. (2005), and Ribakov et al. (2002); on bridges, there are Agrawal et al. (2003), He et al. (2005), Tan and Agrawal (2005a,b), and Sahasrabudehe et al.(2005). Research on semiactive control of base isolations systems has also been considered extensively in Japan (Midorikawa et al., 2004) and China (Xia et al., 2005).

To progress toward the goal of multi-level performance based design for varying load conditions, analytical and design techniques, evaluation procedures, and suitable test cases are needed to demonstrate and examine the reliability in a consistent manner. Thus, the ASCE Committee on Structural Control has recently developed a base isolated benchmark problem. The objective of this benchmark study is to provide a systematic and standardized means by which competing control strategies, including devices, algorithms, sensors, etc.,

can be evaluated in terms of their ability to achieve specific performance objectives. The benchmark model is an eight story base isolated building with lateral-torsional behavior. The framework of this benchmark study has been provided, from problem definition to sample control system design. The first paper defines the benchmark problem (Narasimhan et al., 2004), the second paper includes sample controllers for linear and friction isolation (Nagarajaiah and Narasimhan, 2005), and the third paper provides a sample controller for the bilinear isolation (Erkus et al. 2004). These studies are intended to serve as a guide to the participants to investigate systematically the performance of smart base isolation systems.

1.2 Objectives of this Research

The purpose of this research is to examine the behavior and design of a smart base isolation system and to bring together effective control and placement methods to synthesize controllers that can take advantage of the unique characteristics of this problem. Effective control techniques that use physical knowledge of the system, specifically the special modal characteristics of a structure, for the design of the control law are sought. These approaches are expected to be more acceptable to current practicing civil engineers, while facilitating specific design objectives. Optimization of the control device and sensor locations is also important in the design of a cost-effective system (i.e. maximum control effect using minimal effort and fewer devices) for this class of system.

Because smart base isolation systems are considered to be economical and effective for earthquake protection, a controllable base isolation system is considered here to demonstrate and assess the placement techniques and control design strategies proposed herein. Naturally, the base isolation benchmark problem is adopted because the mathematical model has been well established and is interesting to the research community. This benchmark problem is complex and challenging due to the coupled 3D motions and the clear benefits and tradeoffs in the performance of the system. It consists of an eight-story, three dimensional, base isolated, bi-directionally excited building, and the building is both planar and vertically irregular. In addition to control algorithms and devices, 3D

dynamics, lateral-torsional behavior and effective device placement are factors that must be considered to achieve effective performance. MR dampers are the semiactive device used throughout this dissertation.

The reminder of this section will introduce the strategies employed herein in the synthesis of an approach to controlling civil engineering structures: modal structural dynamics, control concepts and methods (such as system norms, grammians), device placement, and controller order reduction.

The modal method can facilitate effective control design. Modal control is especially desirable in the vibration control of civil engineering structures, which are usually large in size and involve hundreds or even thousands of degrees of freedom. Their response is usually dominated by a few modes. Therefore, the responses of the structures can be effectively suppressed by merely controlling a few modes of the system. Modal representation can be approximately balanced (open-loop and closed-loop) using appropriate scale factors. These concepts are employed herein.

Though GA techniques can find good results in device placement, these techniques do not necessarily yield the optimal solution (Silva and Lopes Jr., 2002). This approach can also be time-consuming because computation of the objective function to find the best control design already involves the controller design. Thus, for each candidate location, the controller must be synthesized and its performance must be evaluated. However, it is well known that the degree of controllability and observability of a linear system is conveniently captured by the singular values of the grammians. These singular values have a wide range of applications. This study will integrate controllability-observability based measures, system Hankel singular norms, into the problem of control design for determination of effective device and sensor placement. The adoption of this approach eliminates the need to evaluate the performance of the candidate location for placement, and it is applicable to the case where performance / measurement and sensors / control devices are not collocated.

Among many candidate control algorithms, LQG control is adopted in this study because of its many advantages, effectiveness, and successful previous application in civil engineering problems (Dyke, 1996a, Dyke et al., 1996b,c). There have been many investigations into the analysis and design of LQG controllers. Good insight into the variety

of approaches can be obtained from Kwakernaak and Silvan (1972), Maciejowski (1989), and Furuta et al. (1988). Controller order reduction in this study is achieved through the so called LQG-balanced model, where the solutions of the two Ricatti equations of LQG algorithm are equal and diagonal. These solutions are important factors to determine the mode / state importance.

The synthesis of physical behavior with control design concepts gives new insights into the potential of the control laws. This study will examine the performance of smart base isolation systems with various controllers for seven specified earthquakes using the proposed approaches. The performance of the system is assessed using certain common evaluation criteria. Comparisons are made between the nodal and modal approaches. The resulting properties of these concepts and information disclosed by the modal approach will be demonstrated through simulations.

1.3 Organization of This Dissertation

This dissertation is organized as follows:

Chapter 1 reviews the background of this study and the related work done by previous researchers.

Chapter 2 presents a number of concepts essential in structural control and to this study in particular. First, various structural modal representations are introduced with the illustrations of signal flow diagrams. Then, the important concepts such as controllability and observability, grammians, Hankel singular norms, etc. are introduced in both algebraic and geometric ways. Their closed-form approximations are summarized herein. The connection between balanced model and modal coordinates is given. A simple example demonstrates the computations of some of these measures.

Chapter 3 describes the structural model to be used for illustration of the techniques synthesized in this study: the base isolation benchmark building. The construction of the three-dimension mathematical model and design unknowns, constraints and performance criteria are provided in detail. Also, the optimal passive systems are identified for both the 1D system and 3D cases.

Chapter 4 proposes a method for control device and sensor placement. The placement indices adopted are based on Hankel singular values which reflect a system's controllability and observability properties despite similarity transformations. Placement indices for each mode and location are arranged in matrices, and location indices are normalized considering the importance of all control devices / sensors to a single mode. A membership index is introduced to reject highly correlated locations.

Chapter 5 reviews the LQG control law in the nodal coordinates, as well as the phenomenological modeling and clipped-optimal control of MR dampers. The LQG weighting matrix is determined using the controllability / observability properties and the closed-loop stability requirements. Optimal weighting values are determined by numerical simulations resulting in weighting trade-off plots referred to herein as q-maps. Finally, the responses are provided for the controlled benchmark structure when subjected to the earthquakes.

Chapter 6 introduces the modal LQG approach, the LQG-balanced model reduction and their closed-form approximations. The close relationships between the weightings and the pole locations are demonstrated in examples, and performance with different weightings is given. It turns out that the application of the modal approach is very straightforward in use, and very effective in suppressing earthquake responses.

Chapter 2

Modal Approach for Structural Dynamics and Control

The synthesis of feedback control systems and the analysis of their response characteristics are often considerably simplified when the plant and control matrices in the matrix state equation have particular forms. Because equations of motion of a system are usually obtained from Newton's 2nd law with structural conditions as the independent variables, state equations are thus conveniently expressed using displacement and velocity dependent at structural locations. The use of these as state variables is also referred to as using nodal coordinates. As state variables are not unique; the nodal system can be converted to other forms by a means of linear similarity transformation. State variables that are commonly used in control system design are defined through modal displacements and their derivatives. Systems with such state variables are said to use modal coordinates.

Modal state variables are not unique either. Modal state variables can be phase variables, or any linear combinations of them. Particularly, the transformation can be selected such that the state matrix $\mathbf{A}$ is rewritten in diagonal or block diagonal forms. There are many advantages of having a diagonal $\mathbf{A}$ matrix. For example, in this form $e^{\mathbf{A}t}$ is also diagonal and is easily obtained; the equations are uncoupled, and so on. The advantages become more prominent for multi-input-multi-output (MIMO) systems.

To provide background needed to understand the remaining chapters of this dissertation, this chapter introduces several forms of modal representations, their application in the study of controllability/observability and model reduction, and structural properties that can be exposed when systems are expressed in modal coordinates. Finally, an example is presented to illustrate the computations relevant to the study of controllability and observability of base isolation systems using a modal approach.

2.1 Modal Structural Models

2.1.1 Signal Flow Diagrams of Nodal Form and Modal Form

A general linear, constant coefficient differential equation takes the form

$$y^{(n)} + a_{n-1}y^{(n-1)} + a_{n-2}y^{(n-2)} + \cdots + a_1\dot{y} + a_0 y = u \tag{2-1}$$

where the superscript in parentheses denotes the order of differentiation with respect to time higher than 2, y represents the output, and u represents the input. Selecting state variables as phase variables defined by

$$\begin{aligned} x_1 &= y \\ x_2 &= \dot{x}_1 = \dot{y} \\ x_3 &= \dot{x}_2 = \ddot{y} \\ &\vdots \\ x_n &= \dot{x}_{n-1} = y^{(n-1)} \end{aligned} \tag{2-2}$$

it follows that

$$\dot{x}_n + a_{n-1}x_n + a_{n-2}x_{n-1} + \cdots + a_1 x_2 + a_0 x_1 = u\ . \tag{2-3}$$

Defining a state vector as $\mathbf{x} = \begin{bmatrix} x_1 & x_2 & \cdots & x_n \end{bmatrix}^T$, the resulting state equations using phase variables is

$$\dot{\mathbf{x}} = \begin{bmatrix} 0 & 1 & & & & \\ & 0 & 1 & & \mathbf{0} & \\ & & & \ddots & & \\ & \mathbf{0} & & \ddots & & \\ & & & & 0 & 1 \\ -a_0 & -a_1 & -a_2 & \cdots & -a_{n-2} & -a_{n-1} \end{bmatrix}\mathbf{x} + \begin{bmatrix} 0 \\ 0 \\ \vdots \\ \vdots \\ 0 \\ 1 \end{bmatrix}\mathbf{u}\ . \tag{2-4}$$

In equation (2-4), the state matrix (the coefficient matrix of the state vector) has values of 1 in the super-diagonal and the negative of the coefficients of the original differential equation in the *n*th row. This is referred to as the companion matrix form (Barnett, 1975).

Equations of motion of structures are second order differential equations. Consider a MDOF system without external disturbances that is expressed in the nodal state-space form of

$$\dot{\mathbf{x}} = \mathbf{A}\mathbf{x} + \mathbf{B}\mathbf{u} \tag{2-5a}$$

$$\mathbf{y} = \mathbf{C}_{\mathbf{y}}\mathbf{x} + \mathbf{D}_{\mathbf{y}}\mathbf{u} \tag{2-5b}$$

where $\mathbf{x} = [\mathbf{y}_s \quad \dot{\mathbf{y}}_s]^T$ is the state vector, $\mathbf{y}_s$ is the vector of structural displacement, $\mathbf{u}$ is the vector of control inputs. The state matrix $\mathbf{A}$ is in the well-known block companion form of

$$\mathbf{A} = \begin{bmatrix} \mathbf{0} & \mathbf{I} \\ \mathbf{M}^{-1}\mathbf{K} & \mathbf{M}^{-1}\mathbf{C} \end{bmatrix} \tag{2-6}$$

where $\mathbf{M}$, $\mathbf{C}$, and $\mathbf{K}$ are the mass, damping and stiffness of the structure, respectively.

A signal flow diagram of the nodal equation (2-5) is shown in Figure 2-1, where the Laplace transformation of variables is represented by capital letters, and the initial conditions of the state variables for Laplace transform are assumed to be zero.

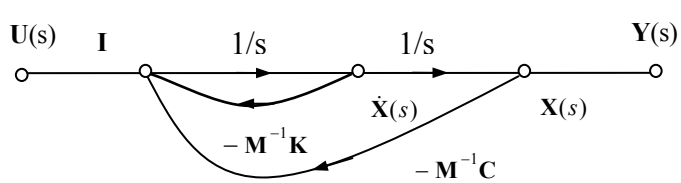

Figure 2-1 Signal Flow Diagram of a System in Nodal Form

In nodal form all equations are coupled, so the equations must be expressed using vector phase variables. Figure 2-1 shows both the multifold signal flow paths and the states. This form of representation generally is not conveniently physically controlled.

As state variables are not unique, the equations can be expressed in other forms through a similarity transformation, as mentioned previously. Let $\mathbf{T}$ be the transformation matrix transforming the state vector $\mathbf{x}$ to a new state vector $\bar{\mathbf{x}}$, that is, $\mathbf{x} = \mathbf{T}\bar{\mathbf{x}}$. Substituting $\mathbf{x} = \mathbf{T}\bar{\mathbf{x}}$ into the state equation (2-5) produces

$$\mathbf{T}\dot{\bar{\mathbf{x}}} = \mathbf{A}\mathbf{T}\bar{\mathbf{x}} + \mathbf{B}\mathbf{u}\,. \tag{2-7}$$

Thus

$$\dot{\bar{\mathbf{x}}} = \mathbf{T}^{-1}\mathbf{A}\mathbf{T}\bar{\mathbf{x}} + \mathbf{T}^{-1}\mathbf{B}\mathbf{u} \tag{2-8}$$

and the corresponding output equation is

$$\mathbf{y} = \mathbf{C}_{\mathrm{y}}\mathbf{T}\bar{\mathbf{x}} + \mathbf{D}_{\mathrm{y}}\mathbf{u}\,. \tag{2-9}$$

It is clear that the eigenvalues are invariant for this type of linear transformation. When $\mathbf{T}^{-1}\mathbf{A}\mathbf{T}$ is diagonal (or block diagonal), the system equations are written as

$$\dot{\bar{\mathbf{x}}} = \mathbf{A}_m\bar{\mathbf{x}} + \mathbf{B}_m\mathbf{u} \tag{2-10a}$$

$$\mathbf{y} = \mathbf{C}_m\bar{\mathbf{x}} + \mathbf{D}_m\mathbf{u} \tag{2-10b}$$

where $\mathbf{A}_m$, $\mathbf{B}_m$, $\mathbf{C}_m$ and $\mathbf{D}_m$ are modal state matrices, and

$$\mathbf{A}_m = \mathbf{\Lambda} = \mathbf{T}^{-1}\mathbf{A}\mathbf{T}\,,\quad \mathbf{B}_m = \mathbf{T}^{-1}\mathbf{B}\,,\quad \mathbf{C}_m = \mathbf{C}_{\mathrm{y}}\mathbf{T}\,,\quad \mathbf{D}_m = \mathbf{D}_{\mathrm{y}}\,. \tag{2-11}$$

The system has the state-space representation denoted by the triple $(\mathbf{A}_m, \mathbf{B}_m, \mathbf{C}_m)$ (matrix $\mathbf{D}$ is invariant in linear similarity transformation) and is independently obtained from equation (2-10) and (2-11) such that

$$\mathbf{y} = \sum_{i=1}^{n} \mathbf{y}_i \tag{2-12}$$

where $i = 1, 2, \ldots, n$ is the ith mode.

Suppose the eigenvalues λ_i are distinct. If the diagonal elements are eigenvalues, i.e.,

$$\mathbf{T}^{-1}\mathbf{A}\mathbf{T} = \mathbf{A}_m = \begin{bmatrix} \lambda_1 & & & \mathbf{0} \\ & \lambda_2 & & \\ & & \ddots & \\ \mathbf{0} & & & \lambda_n \end{bmatrix} \tag{2-13}$$

then the transformation matrix $\mathbf{T}$ for it is called the modal matrix. The corresponding state variables are called canonical variables. When $\mathbf{T}^{-1}\mathbf{A}\mathbf{T}$ is not in this form, $\mathbf{T}$ is just called the transformation matrix. If the state matrix $\mathbf{A}$ has distinct eigenvalues, the modal matrix is easily obtained by

$$\mathbf{T} = \begin{bmatrix} 1 & 1 & \cdots & 1 \\ \lambda_1 & \lambda_2 & \cdots & \lambda_n \\ \lambda_1^2 & \lambda_2^2 & \cdots & \lambda_2^2 \\ \cdots & \cdots & \cdots & \cdots \\ \lambda_1^{n-1} & \lambda_2^{n-1} & \cdots & \lambda_n^{n-1} \end{bmatrix} \tag{2-14}$$

and this is referred to as the Vandermond matrix (Barnett, 1975).

There are several other methods to obtain the modal matrix $\mathbf{T}$. When $\mathbf{T}$ is selected so that $\mathbf{B}_m = \mathbf{T}^{-1}\mathbf{B}$ contains only unit elements, equation (2-10) takes the form

$$\dot{\bar{\mathbf{x}}} = \mathbf{A}_m \bar{\mathbf{x}} + \mathbf{b}_m \mathbf{u} \tag{2-15}$$

where $\mathbf{b}_m = \begin{bmatrix} 1 & \cdots & 1 \end{bmatrix}^T$. In the case of equation (2-15), if $\mathbf{D}_m = \mathbf{0}$, the signal flow graph of equation (2-15) is shown in Figure 2-2, where $Y_{m,i}(s)$ represents the Laplace transform of

the contribution of the *i*th mode to the output, and $C_{m,i}$ represents the output gain of the *i*th mode (the coefficient of the *i*th partial fraction of the transfer function). C_n is the feed-forward path gain, which appears only when the denominator and numerator of the transfer function are of the same order.

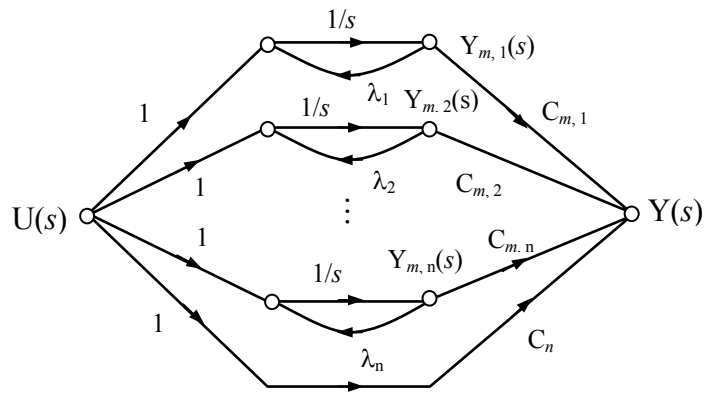

Figure 2-2 Signal Flow Diagram of a System in Jordan Form for Distinct Roots

Figure 2-2 and equation (2-15) correspond to the Jordan form of the system. Due to decoupled modes, the signals flow in parallel branches. Each branch only involves scalar values and can be represented by a first-order differential equation and transfer function of the form (D'Azzo and Houpis, 1988)

$$\dot{y}_{m,i} - \lambda_i y_{m,i} = u\,, \quad G_i(s) = \frac{Y_{m,i}(s)}{U(s)} = \frac{C_{m,i}}{s - \lambda_i} \tag{2-16}$$

where $G_i(s)$ denotes the transfer function matrix.

An advantage to using parallel form is that, when the state matrix is diagonal, the diagonal elements provide information regarding the structural modes, i.e., the eigenvalues or frequencies. Parallel forms are easier to employ for examining control action. The state variables for a diagonal state matrix are canonical variables or their combinations (modal

coordinates). Manipulation of these equations is referred to as the modal approach in contrast to the manipulation using nodal coordinates (equation (2-5) and Figure (2-1)).

2.1.2 Transformation between Modal Forms

In the previous section, a general modal form was introduced in which the diagonal entries are the system eigenvalues. However, there are other means to decouple the equations. This section introduces other forms for modal representations and the transformations between them.

When decoupling a set of differential equations, it is most common to use modal decomposition to differential equations instead of using state equations. It results in a set of n independent equations for each modal displacement q as in

$$\ddot{q}_i + 2\zeta_i \omega_i \dot{q}_i + \omega_i^2 q_i = b_i u \tag{2-17}$$

where ζ_i is the *i*th modal damping ratio, and ω_i the *i*th natural frequency.

Assuming the system is underdamped, the eigenvalues are $\lambda_{1,2} = -\zeta_i \omega_i \pm j\omega_{d,i}$, where $\omega_{d,i} = \omega_i \sqrt{1-\zeta_i^2}$. Introducing the state vector $\bar{\mathbf{x}}_i = \begin{bmatrix} q_i & \dot{q}_i \end{bmatrix}^T$ for the *i*th equation, the state matrices corresponding to the equation governing the *i*th mode are

$$\mathbf{A}_{m,i} = \begin{bmatrix} 0 & 1 \\ -\omega_i^2 & -2\zeta_i \omega_i \end{bmatrix}, \quad \mathbf{B}_{m,i} = \begin{bmatrix} 0 \\ b_i \end{bmatrix}. \tag{2-18}$$

This form is denoted modal form 1 herein. $\mathbf{A}_{m,i}$ is in companion form. The signal flow diagram for this form of the equation is shown in Figure 2-3.

The entire system is decoupled for this expression, i.e., $\mathbf{A}_m$ is diagonal with each of the diagonal terms as $\mathbf{A}_{m,i}$. So the signal flow diagram is still shown in parallel. But each equation in modal form 1 is expressed using phase variables, so the signal flow for each branch is still multifold. This form is still not conveniently physically controlled.

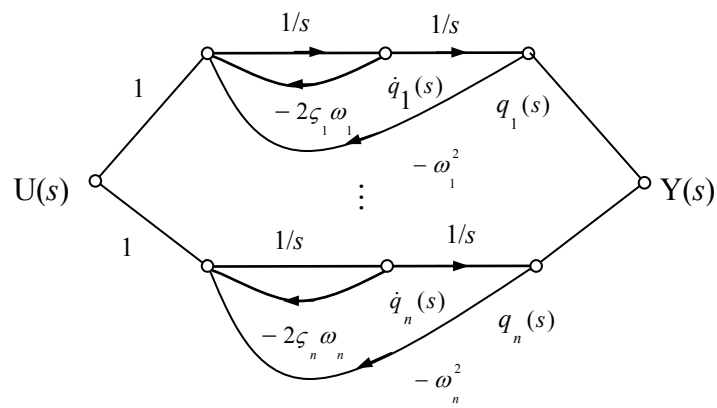

Figure 2-3 Signal Flow Diagram of Modal Form 1

Now transform the individual equation from the companion form (modal form 1) to diagonal form, with the complex-conjugate eigenvalues on the diagonal as

$$\dot{\overline{\mathbf{x}}} = \begin{bmatrix} -\zeta_i\omega_i + j\omega_{d,i} & 0 \\ 0 & -\zeta_i\omega_i - j\omega_{d,i} \end{bmatrix}\overline{\mathbf{x}} + \frac{b_i}{2j\omega_{d,i}}\begin{bmatrix} 1 \\ -1 \end{bmatrix}\mathbf{u}. \tag{2-19}$$

In this study, this form of $\mathbf{A}_m$ is referred to as modal form 3. To transform modal form 1 to modal form 3, we use the transformation $\mathbf{x}_i = \mathbf{T}_{13,i}\overline{\mathbf{x}}_i$, where $\mathbf{T}_{13,i}$ is the Vandermonde matrix

$$\mathbf{T}_{13,i} = \begin{bmatrix} 1 & 1 \\ -\zeta_i\omega_i + j\omega_{d,i} & -\zeta_i\omega_i - j\omega_{d,i} \end{bmatrix}. \tag{2-20}$$

The simulation diagram for one mode (equation (2-19)) is like Figure 2-2 but with complex-valued parameters, which is shown in Figure 2-4.

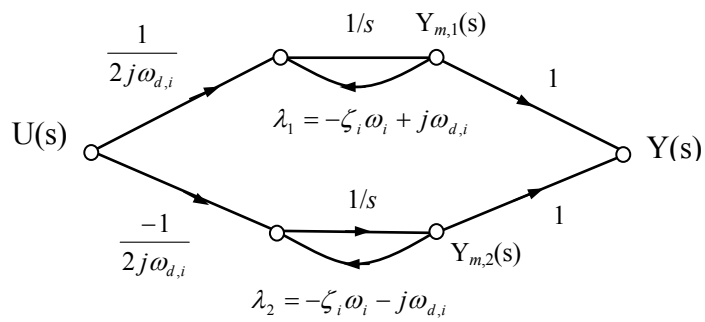

Figure 2-4 Signal Flow Diagram of Modal Form 3 for a Pair of Complex Mode

The complex quantities increase the difficulty when obtaining mathematical solutions. Thus, it is desirable to perform another transformation in order to obtain representation which contains only real quantities. It is necessary to apply an additional transformation so that modal form 3 (equation (2-19)) changes into modal form 2, i.e.,

$$\dot{\bar{\mathbf{x}}} = \begin{bmatrix} -\zeta_i\omega_i & \omega_i \\ -\omega_i & -\zeta_i\omega_i \end{bmatrix}\bar{\mathbf{x}} + \frac{1}{\omega_{d,i}}\begin{bmatrix} 0 \\ 1 \end{bmatrix}\mathbf{u} \ . \tag{2-21}$$

The transformation matrix needed is

$$\mathbf{T}_{32,i} = \frac{1}{2}\begin{bmatrix} 1 & -j \\ 1 & j \end{bmatrix}. \tag{2-22}$$

With this modification the two vibration modes produced by the two sets of the complex eigenvalues are decoupled. Note that the column vectors contained in $\mathbf{T}_{32}$ are for the conjugate eigenvalues $-\zeta_1\omega_1 \pm j\omega_{d,1}$ and $-\zeta_2\omega_2 \pm j\omega_{d,2}$ and are also conjugates. The simulation diagram for modal form 2 is shown in Figure 2-5.

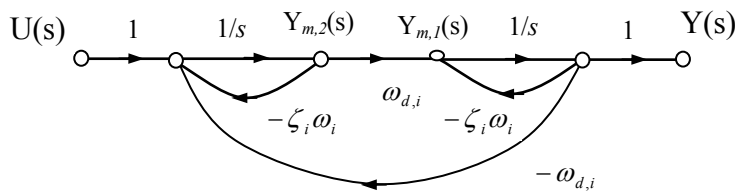

Figure 2-5 Signal Flow Diagram of Modal Form 2 for a Pair of Complex Mode

Note that only real quantities appear. Also, the two modes have not been isolated. This result is an advantage for complex-conjugate roots (D'Azzo and Houpis, 1988).

Assuming small damping values, i.e., $\omega_i \cong \omega_{d,i}$, the transformation matrix from modal form 2 to modal form 1 is

$$\mathbf{T}_{21,i} = \begin{bmatrix} 1 & 0 \\ -\varsigma_i \omega_i & \omega_i \end{bmatrix}. \tag{2-23}$$

Other modal forms are not introduced herein because they are not relevant to the study. In this study, form 1 is used throughout chapters 3 and 5, while chapters 4 and 6 primarily consider form 2. Each modal form can be transferred to any others using approximate transformation matrices.

Note that for MDOF systems, modal form 3 is obtained from the decoupled differential equations. The entire state matrix is block diagonal, and the state vector is given by $\begin{bmatrix} q_1 & \dot{q}_1 & q_2 & \dot{q}_2 & \cdots & \cdots & q_n & \dot{q}_n \end{bmatrix}^T$. If the state matrix is obtained from the matrix of decoupled equations, or transformed from nodal state matrices, the state vector would be $\begin{bmatrix} q_1 & q_2 & \cdots & q_n & \dot{q}_1 & \dot{q}_2 & \cdots & \dot{q}_n \end{bmatrix}^T$. To rearrange the states into the former modal form, a transformation matrix needs to be applied. This matrix is (Gawronski, 1998)

$$\mathbf{T}_{q1} = \begin{bmatrix} \mathbf{0} & \mathbf{e}_1 \\ \mathbf{e}_1 & \mathbf{0} \\ \mathbf{0} & \mathbf{e}_2 \\ \mathbf{e}_2 & \mathbf{0} \\ \vdots & \vdots \\ \mathbf{0} & \mathbf{e}_n \\ \mathbf{e}_n & \mathbf{0} \end{bmatrix} \tag{2-24}$$

where $\mathbf{e}_i$ is an n-element row vector with all elements equal to zero except the ith which is equal to one. Then with $\bar{\mathbf{x}} = \begin{bmatrix} \bar{\mathbf{x}}_1 & \bar{\mathbf{x}}_2 & \cdots & \bar{\mathbf{x}}_n \end{bmatrix}^T$, the modal state-space representation has a triple $(\mathbf{A}_m, \mathbf{B}_m, \mathbf{C}_m)$ characterized by the block diagonal matrix $\mathbf{A}_m$, and the related input and output matrices

$$\mathbf{A}_m = diag(\mathbf{A}_{m,i}),\ \mathbf{B}_m = \begin{bmatrix} \mathbf{B}_{m,1} \\ \vdots \\ \mathbf{B}_{m,n} \end{bmatrix},\ \mathbf{C}_m = \begin{bmatrix} \mathbf{C}_{m,1} & \cdots & \mathbf{C}_{m,n} \end{bmatrix} \tag{2-25}$$

where $\mathbf{A}_{m,i}$, $\mathbf{B}_{m,i}$, and $\mathbf{C}_{m,i}$ are 2×2, 2×s, and r×2 blocks, respectively. The three modal forms introduced before are summarized here

$$\text{form 1 } \mathbf{A}_{mi} = \begin{bmatrix} 0 & 1 \\ -\omega_i^2 & -2\zeta_i\omega_i \end{bmatrix} \text{ for state } i \ \mathbf{x}_i = \begin{Bmatrix} q_i \\ \dot{q}_i \end{Bmatrix} \tag{2-26a}$$

$$\text{form 2 } \mathbf{A}_{mi} = \begin{bmatrix} -\zeta_i\omega_i & \omega_i \\ -\omega_i & -\zeta_i\omega_i \end{bmatrix} \text{ for state } i \ \mathbf{x}_i = \begin{Bmatrix} q_i \\ \dot{q}_{oi} \end{Bmatrix} \tag{2-26b}$$

$$\text{form 3 } \mathbf{A}_{mi} = \begin{bmatrix} -\zeta_i\omega_i + j\omega_{d,i} & 0 \\ 0 & -\zeta_i\omega_i - j\omega_{d,i} \end{bmatrix} \text{ for state } i \ \mathbf{x}_i = \begin{Bmatrix} q_i - jq_{oi} \\ q_i + jq_{oi} \end{Bmatrix} \tag{2-26c}$$

where $q_{oi} \cong \zeta_i q_i + \dot{q}_i/\omega_i$ (for small damping) and $\mathbf{x} = \begin{bmatrix} \mathbf{x}_1 & \cdots & \mathbf{x}_n \end{bmatrix}^T$.

2.2 Controllability and Observability

2.2.1 Definitions

Controllability and observability are structural properties of a dynamic system that carry useful information for structural testing and control, yet are often overlooked by structural engineers. A structure is controllable if the installed actuators together have the capability to excite all its structural modes. It is observable if the installed sensors have the ability to measure the motions of all its structural modes. In other words, controllability and observability indicate how well the states can be "reached" by inputs and how well the states can be "recovered" from outputs, respectively. For state feedback control, controllability ensures the assignability of the eigenvalues of the closed-loop state matrix (Dullerud and Paganini, 2000). Uncontrollable eigenvalues cannot be modified by adding control no matter which gain is used for feedback. Steady-state optimal control is possible if either the plant is stable, or the plant is both controllable and observable (Burl, 1999).

Controllability, as a coupling between the inputs and the states, involves the system matrix $\mathbf{A}$ and the input matrix $\mathbf{B}$. Observability, as a coupling between the states and outputs, involves the system matrix $\mathbf{A}$ and the output matrix $\mathbf{C}_{\mathrm{y}}$. Generally, two criteria are used to determine the system's controllability and observability properties. The first criterion is related to the rank of the controllability or observability matrices. An LTI system with s inputs is completely controllable (*c.c.*) if and only if the $n \times sn$ matrix

$$\mathbf{Q}_c = \begin{bmatrix} \mathbf{B} & \mathbf{AB} & \mathbf{A}^2\mathbf{B} & \cdots & \mathbf{A}^{n-1}\mathbf{B} \end{bmatrix} \tag{2-27}$$

has rank n. An LTI system with r outputs is completely observable (*c.o.*) if and only if the $rn \times n$ matrix

$$\mathbf{Q}_o = \begin{bmatrix} \mathbf{C}_{\mathrm{y}} \\ \mathbf{C}_{\mathrm{y}}\mathbf{A} \\ \mathbf{C}_{\mathrm{y}}\mathbf{A}^2 \\ \vdots \\ \mathbf{C}_{\mathrm{y}}\mathbf{A}^{n-1} \end{bmatrix} \tag{2-28}$$

has rank n. For SISO systems, if either $\mathbf{Q}_c$ or $\mathbf{Q}_o$ does not have full rank (singular), an appropriate linear transformation can be used to transform the system into a staircase structure where the controllable (observable) and uncontrollable (unobservable) states are separated. Eliminating all uncontrollable and unobservable states, the resulting representation contains only controllable or observable states. The representation is referred to as a minimal realization.

The above criterion, although simple, has two serious drawbacks. First, the answer to the controllability and observability question is either yes or no. If the system is not *c.c.*, it would be misleading to call it "uncontrollable", since the implication of the definition is that for a non- *c.c.* system there are only certain states which cannot be reached by any choice of control (Barnett, 1975). Moreover, $\mathbf{Q}_c$ and $\mathbf{Q}_o$ can typically be considered full-rank given a sufficiently low tolerance, but some states might be too weakly represented to be practically controlled or observed. Second, these criteria are useful only for a system of small dimensions. Assume, for example, that the system is of dimension n = 100. In order to answer the controllability and observability question one has to find powers of $\mathbf{A}$ up to 99 and $\mathbf{A}^{99}$ for a 100×100 matrix is a task that easily results in numerical overflow.

The alternative approach is to use grammians to determine the system properties. Grammians express the controllability and observability properties qualitatively, and avoid numerical difficulties. The controllability and observability grammians are defined as

$$\mathbf{W}_c = \int_0^\infty e^{-\mathbf{A}t}\mathbf{B}\mathbf{B}^T e^{-\mathbf{A}^T t}dt, \qquad \mathbf{W}_o = \int_0^\infty e^{-\mathbf{A}^T t}\mathbf{C}_\mathbf{y}^T\mathbf{C}_\mathbf{y} e^{-\mathbf{A}t}dt \tag{2-29}$$

Alternatively, the grammians can be determined from the following Lyapunov equations

$$\mathbf{A}\mathbf{W}_c + \mathbf{W}_c\mathbf{A}^T + \mathbf{B}\mathbf{B}^T = \mathbf{0} \quad \text{and} \quad \mathbf{A}^T\mathbf{W}_o + \mathbf{W}_o\mathbf{A} + \mathbf{C}_\mathbf{y}^T\mathbf{C}_\mathbf{y} = \mathbf{0} \tag{2-30}$$

For stable $\mathbf{A}$, the grammians $\mathbf{W}_c$ and $\mathbf{W}_o$ are positive definite. Equations (2-30) show that the controllability grammian is the stable covariance of the states if the input to the system

$(\mathbf{A},\mathbf{B})$ is a white Gaussian noise (Franklin et. al., 2002). Similarly, the observability grammian is the stable covariance of the states if the input to the system $(\mathbf{A}^T,\mathbf{C}_\mathbf{y}^T)$ is a white Gaussian noise (Franklin et. al., 2002). This is one physical interpretation of the grammians.

Grammians do vary with coordinate systems. But the eigenvalues of the product of the grammians are invariant under linear transformations. These invariants are called Hankel singular values of the system, denoted by γ_i, i.e.,

$$\gamma_i = \sqrt{\lambda_i(\mathbf{W}_c\mathbf{W}_o)} \tag{2-31}$$

where $\lambda(.)$ denotes the eigenvalue. These values reflect the combined controllability and observability of individual states of the balanced model. If a given γ_i is small compared to the others, the corresponding state has the interpretation of being weakly controllable and observable.

System norms serve as measures of a system "size". In this capacity, they are used in model reduction and in actuator/sensor placement strategies. Three system norms, H_2, H_∞, and Hankel, are introduced below.

Let $\mathbf{G}(\omega) = \mathbf{C}_m(j\omega\mathbf{I} - \mathbf{A}_m)^{-1}\mathbf{B}_m$ be the transfer function of the structure. The H_2 norm is defined as

$$\|\mathbf{G}\|_2 = \sqrt{\frac{1}{2\pi}\int_{-\infty}^{\infty} tr(\mathbf{G}^*(\omega)\mathbf{G}(\omega))d\omega} \tag{2-32}$$

where * denotes complex conjugate. A convenient way to determine the numerical value of the H_2 norm is to use (Gawronski, 1998)

$$\|\mathbf{G}\|_2 = \sqrt{tr(\mathbf{C}_\mathbf{y}\mathbf{C}_\mathbf{y}^T\mathbf{W}_c)} \text{ or } \|\mathbf{G}\|_2 = \sqrt{tr(\mathbf{B}^T\mathbf{B}\mathbf{W}_o)}\,. \tag{2-33}$$

The H_∞ norm is defined as

$$\|\mathbf{G}\|_\infty = \max_\omega(\sigma_{\max}(\mathbf{G}(\omega))) \tag{2-34}$$

where $\sigma_{\max}(\mathbf{G}(\omega))$ is the largest singular value of $\mathbf{G}(\omega)$. The H_∞ norm is the peak of the transfer function magnitude for SISO (single-input-single-output) systems.

The Hankel norm is a measure of the effect of the past input on the future output, or the amount of energy stored in and subsequently retrieved from the system (Boyd and Barratt, 1991). It is given by

$$\|G\|_h = \left(\lambda_{\max}\left(\mathbf{W}_o\mathbf{W}_c\right)\right)^{1/2}. \tag{2-35}$$

Equation (2-35) shows that the Hankel norm is the largest Hankel singular value, i.e., $\|G\|_h = \gamma_{\max}$.

2.2.2 Properties in Modal Coordinates

The modal state-space representation has specific controllability and observability properties, and its grammians are of a specific form. These forms and properties hold for flexible structures (Here, flexible structures refer to linear systems that have finite dimensions, non-clustered and small real-part poles.) with small dampings ($\zeta_i << 1$, i = 1, 2, …, n.). For proofs, refer to Gawronski (1998).

1. In modal coordinates, the controllability and observability grammians are diagonally dominant, i.e.,

$$\mathbf{W}_c \cong diag(w_{c,i}\mathbf{I}_2),\ \ w_{ci} > 0, \qquad i = 1, \ldots, n \tag{2-36a}$$

$$\mathbf{W}_o \cong diag(w_{o,i}\mathbf{I}_2),\ \ w_{ci} > 0, \qquad i = 1, \ldots, n \tag{2-36b}$$

where $w_{c,i}$ and $w_{o,i}$ are the modal controllability and observability coefficients. The approximate Hankel singular values are obtained as a geometric mean of the modal controllability and observability $\gamma_i = \sqrt{w_{c,i} w_{o,i}}$. Because grammians are solutions to Lyapunov equations (equation 2-30), this property means that under a white noise, the modes are almost independent.

2. In modal coordinates, the dominant diagonal entries can be obtained by approximation with a closed-form formula, as in

$$w_{c,i} = \frac{\left\|\mathbf{B}_{m,i}\right\|_2^2}{4\zeta_i \omega_i}, \quad w_{c,o} = \frac{\left\|\mathbf{C}_{m,i}\right\|_2^2}{4\zeta_i \omega_i}, \quad \gamma_i = \frac{\left\|\mathbf{B}_{m,i}\right\|_2 \left\|\mathbf{C}_{m,i}\right\|_2}{4\zeta_i \omega_i} \tag{2-37}$$

where the $\|.\|_2$ denotes the 2-norm.

Note that, for application to the determination of modal norms, the modal equivalent output matrix $\mathbf{C}_m$ is defined as $C_{m,i} = C_{mq,i} / \omega_i + C_{m\dot{q},i}$ for the output equation $\mathbf{y} = \mathbf{C}_{mq}\mathbf{q} + \mathbf{C}_{m\dot{q}}\dot{\mathbf{q}}$.

This property is very appealing because, on the one hand, the computation of grammians is greatly simplified without the involvement of $\mathbf{A}_m$. On the other hand, these equations show that the controllability grammian of the *i*th mode is proportional to the square of the *i*th modal input gain. Similarly, the observability grammian of the *i*th mode is proportional to the square of the *i*th modal output gain. They are both inversely proportional to the *i*th modal damping and frequency. The Hankel singular value is the geometric mean of the two. Input gains are dependent on actuator location and output gains on selected sensor location. This property is useful for the future study of actuator and sensor placement.

3. Consider the *i*th mode in state-space form $(\mathbf{A}_{m,i}, \mathbf{B}_{m,i}, \mathbf{C}_{m,i})$, or the second-order form $(\omega_i, \zeta_i, b_i, c_i)$, and let $\mathbf{G}(\omega) = \mathbf{C}_m (j\omega\mathbf{I} - \mathbf{A}_m)^{-1} \mathbf{B}_m$ be the transfer function of the

structure. Then the H_2 norm, H_∞ norm, and the Hankel norm H_h have the following expressions and relationships:

$$\|G_i\|_2 \cong \frac{\|\mathbf{B}_{m,i}\|_2 \|\mathbf{C}_{m,i}\|_2}{2\sqrt{\zeta_i \omega_i}}, \quad \|G_i\|_\infty \cong \frac{\|\mathbf{B}_{m,i}\|_2 \|\mathbf{C}_{m,i}\|_2}{2\zeta_i \omega_i}, \quad \|G_i\|_h \cong \frac{\|\mathbf{B}_{m,i}\|_2 \|\mathbf{C}_{m,i}\|_2}{4\zeta_i \omega_i} \tag{2-38}$$

$$\|G_i\|_\infty \cong 2\|G_i\|_h \cong \sqrt{\zeta_i \omega_i}\,\|G_i\|_2 \tag{2-39}$$

$$\|G\|_2 \cong \sqrt{\sum_{i=1}^{n} \|G_i\|_2^2}\ . \tag{2-40}$$

These equations indicate the superposition property of modal transfer functions, and thus, of the norms. They also show that the Hankel norm is about half of the peak value of the transfer function.

2.3 Grammian Ellipsoids and Balanced Model Reduction

Given a system, it is often necessary to reduce the order of a state-space realization, while keeping the system input-output properties approximately the same. A reduced-order model is obtained by truncating the states. It is reasonable to assume that the states that are only weakly coupled to both the input and the output can be deleted from the model without greatly impacting the input-output behavior of the system. However, deleting the weakly coupled states is not straightforward. As the modal state matrix can be partitioned into separate modes, model reduction can be achieved through modal truncation with explicit knowledge of which modes and states are retained. For example, using modal forms, the system representation can be partitioned as

$$\begin{Bmatrix} \dot{\hat{\mathbf{x}}}_r \\ \dot{\hat{\mathbf{x}}}_t \end{Bmatrix} = \begin{bmatrix} \mathbf{A}_r & \mathbf{0} \\ \mathbf{0} & \mathbf{A}_t \end{bmatrix} \begin{Bmatrix} \hat{\mathbf{x}}_r \\ \hat{\mathbf{x}}_t \end{Bmatrix} + \begin{bmatrix} \mathbf{B}_r \\ \mathbf{B}_t \end{bmatrix} \mathbf{u} + \begin{bmatrix} \mathbf{E}_r \\ \mathbf{E}_t \end{bmatrix} \mathbf{w} \tag{2-41}$$

$$\mathbf{y} = \begin{bmatrix} \mathbf{C}_{\mathbf{y},r} & \mathbf{C}_{\mathbf{y},t} \end{bmatrix} \begin{Bmatrix} \mathbf{x}_r \\ \mathbf{x}_t \end{Bmatrix} \tag{2-42}$$

where the subscript *r* denotes "retained" while the subscript *t* denotes "truncated".

States may be strongly coupled to the input, but only weakly coupled to the output, or vice versa. This phenomenon can be described geometrically. Consider the system given by equations (2-5a, b), with the conditions $\mathbf{x}(-\infty) = 0$ and $\mathbf{x}(0) = \mathbf{x}_0$. The solution of this equation is $\mathbf{C}_\mathbf{y} e^{-\mathbf{A}\tau}\mathbf{x}_0$. One can define the controllability and observability operators $\boldsymbol{\psi}_c$ and $\boldsymbol{\psi}_o$ that define the maps of $\mathbf{u}(t) \to \mathbf{x}_0$ and $\mathbf{x}_0 \to \mathbf{y}(t)$ as

$$\boldsymbol{\psi}_c : \mathbf{u} \to \int_{-\infty}^{0} e^{-\mathbf{A}\tau}\mathbf{B}\mathbf{u}(\tau)d\tau \quad \text{or} \quad \boldsymbol{\psi}_c\mathbf{u} = \mathbf{x}_0, \ \ t \le 0 \tag{2-43}$$

$$\boldsymbol{\psi}_o : \mathbf{x}_0 \to \mathbf{C}_\mathbf{y} e^{-\mathbf{A}\tau}\mathbf{x}_0 \quad \text{or} \quad \boldsymbol{\psi}_o\mathbf{x}_0 = \mathbf{y}, \ \ t \ge 0 \tag{2-44}$$

From equation (2-35), the Hankel norm is the largest eigenvalue of the Hankel operator $\boldsymbol{\Gamma}_h = \boldsymbol{\psi}_o\boldsymbol{\psi}_c$. The controllability and observability operators relate to the grammians as (Dullerud and Paganini, 2000)

$$\mathbf{W}_c = \boldsymbol{\psi}_c\boldsymbol{\psi}_c^T = \int_0^\infty e^{-\mathbf{A}t}\mathbf{B}\mathbf{B}^T e^{-\mathbf{A}^T t}dt, \ \text{ and } \mathbf{W}_o = \boldsymbol{\psi}_o^T\boldsymbol{\psi}_o = \int_0^\infty e^{-\mathbf{A}^T t}\mathbf{C}_\mathbf{y}^T\mathbf{C}_\mathbf{y} e^{-\mathbf{A}t}dt. \tag{2-45}$$

It can be seen that $\mathbf{u}_{opt} = \boldsymbol{\psi}_c^T\mathbf{W}_c^{-1}\mathbf{x}_0$ is a solution to $\boldsymbol{\psi}_c\mathbf{u} = \mathbf{x}_0$. Also, for a general $\mathbf{u}$ in this set, $\|\mathbf{u}\| \ge \|\mathbf{u}_{opt}\|$ (Dullerud and Paganini, 2000), i.e., if we want to reach a state $\mathbf{x}_0$, then $\mathbf{u}_{opt} = \boldsymbol{\psi}_c^T\mathbf{W}_c^{-1}\mathbf{x}_0$ is the most economical input in terms of energy. This input energy is given by

$$\|\mathbf{u}_{opt}\|^2 = \left\langle \boldsymbol{\psi}_c^T\mathbf{W}_c^{-1}\mathbf{x}_0, \boldsymbol{\psi}_c^T\mathbf{W}_c^{-1}\mathbf{x}_0 \right\rangle = \mathbf{x}_0^T\mathbf{W}_c^{-1}\mathbf{x}_0 \tag{2-46}$$

where $\langle . \rangle$ denotes the inner product.

To consider a geometric interpretation of the controllability grammian, the question is, what are the final states $\mathbf{x}_0 = \boldsymbol{\psi}_c\mathbf{u}$ that can result from an input $\mathbf{u}$ of unit norm? The

answer is that all the states reachable with $\|\mathbf{u}\| \le 1$ are given by $\mathbf{W}_c^{1/2}\mathbf{x}_c$, where $\|\mathbf{x}_c\| \le 1$, if the pair $(\mathbf{A}, \mathbf{B})$ is controllable. This outcome can be proven from two perspectives: On the one hand, examine the vector $\mathbf{x}_c = \mathbf{W}_c^{1/2}\boldsymbol{\psi}_c\mathbf{u}$ with $\|\mathbf{u}\| \le 1$. It has the norm

$$\|\mathbf{x}_c\|^2 = \left\langle \mathbf{W}_c^{1/2}\boldsymbol{\psi}_c\mathbf{u}, \mathbf{W}_c^{1/2}\boldsymbol{\psi}_c\mathbf{u} \right\rangle = \left\langle \mathbf{u}, \boldsymbol{\psi}_c^T\mathbf{W}_c^{-1}\boldsymbol{\psi}_c\mathbf{u} \right\rangle \le \|\mathbf{u}\|^2 \le 1. \tag{2-47}$$

On the other hand, choose the input of minimum norm that gives $\boldsymbol{\psi}_c\mathbf{u} = \mathbf{W}_c^{1/2}\mathbf{x}_c$, it yields

$$\|\mathbf{u}_{opt}\|^2 = (\mathbf{W}_c^{1/2}\mathbf{x}_c)^T\mathbf{W}_c^{-1}(\mathbf{W}_c^{1/2}\mathbf{x}_c) = \|\mathbf{x}_c\|^2 \le 1. \tag{2-48}$$

This means that $\mathbf{x}_c$ has unit length. Notice that the norm squared of any such states is $\mathbf{x}_c^T\mathbf{W}_c\mathbf{x}_c$. Such reachable states also contain directional information. Define the set

$$E_c = \left\{ \mathbf{W}_c^{1/2}\mathbf{x}_c : \|\mathbf{x}_c\| = 1 \right\} \tag{2-49}$$

which is a collection of all such states, where $\mathbf{x}_c$ is in the *n*-dimensional vector space. Because $\mathbf{W}_c$ is positive semi-definite, this set represents an ellipsoid, and is depicted two dimensionally in Figure 2-6. This shape is named as the controllability ellipsoid. It tells us the reachable state norms associated with a particular direction in state space. The length of the principle axes (maximum eigenvalue) represents the strongest controllability, and the corresponding eigenvector represents the direction with the "strongest" controllability.

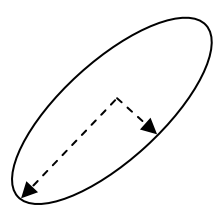

Figure 2-6 Controllability Ellipsoid

For observability, let us examine the energy associated with the output $\mathbf{y} = \boldsymbol{\psi}_o \mathbf{x}_0$ starting from an initial condition $\mathbf{x}_0$. It is given by

$$\|\mathbf{y}\|^2 = \langle \boldsymbol{\psi}_o \mathbf{x}_0, \boldsymbol{\psi}_o \mathbf{x}_0 \rangle = \langle \mathbf{x}_0, \boldsymbol{\psi}_o^T \boldsymbol{\psi}_o \mathbf{x}_0 \rangle = \langle \mathbf{x}_0, \mathbf{W}_o \mathbf{x}_0 \rangle = \mathbf{x}_o^T \mathbf{W}_o \mathbf{x}_0 . \tag{2-50}$$

If only the states $|\mathbf{x}_o| = 1$ are considered, then clearly some states will yield higher output norms than others. Therefore, the observability grammian measures "how observable" a given initial condition is. This idea can be described geometrically considering the vectors $\mathbf{W}_o^{1/2} \mathbf{x}_o$ with $|\mathbf{x}_o| = 1$. Similar to the controllability ellipsoid, define the set

$$E_o = \left\{ \mathbf{W}_o^{1/2} \mathbf{x}_0 : \|\mathbf{x}_0\| = 1 \right\} \tag{2-51}$$

These vectors depict the observability ellipsoid, where $\mathbf{x}_0$ is in the *n*-dimensional vector space. It tells us the output norm associated with a particular direction in state space. The eigenvalues represent the length in the principal axes, and eigenvectors represent the direction of the principal axes.

From above discussions, we can conclude that the states corresponding to small eigenvalues of the grammians are not very controllable or observable. However, the weak observable states might be very controllable because the controllability and observability ellipsoids might be aligned orthogonally, as shown in Figure 2-7 (Dullerud and Paganini, 2000).

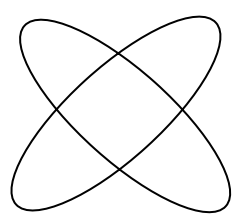

Figure 2-7 Unbalanced System Ellipsoids

Therefore, model reduction is usually performed in a balanced state-space representation. The idea of "balancing" the state-space representation of a system can be credited to Moore (1981). In a balanced state-space representation, the individual states have the same degree of controllability and observability, i.e., they are equally strongly coupled to both the input and the output, and thus states can be deleted when this coupling is weak.

A Moore-balanced model has exactly aligned ellipsoids such that the most controllable states are also the most observable states. It can be obtained by changing the base to the state space of the system. Let $\mathbf{T}$ be the transformation matrix of the original state such that $\mathbf{x} = \mathbf{T}\overline{\mathbf{x}}$; the controllability and observability grammians associated with this new realization are

$$\widetilde{\mathbf{W}}_c = \mathbf{T}\mathbf{W}_c\mathbf{T}^T, \quad \widetilde{\mathbf{W}}_o = (\mathbf{T}^T)^{-1}\mathbf{W}_o\mathbf{T}^{-1}. \tag{2-52}$$

Through singular value decomposition techniques (see, for instance, Burl 1999), a $\mathbf{T} = \mathbf{T}_b$ can be found such that

$$\widetilde{\mathbf{W}}_c = \widetilde{\mathbf{W}}_o = \mathbf{\Gamma}, \text{ and } \mathbf{\Gamma} = diag(\gamma_1, \cdots, \gamma_n) \tag{2-53}$$

where $\gamma_i > 0$ is the ith Hankel singular value of the system. The resulting system representation with equal and diagonal grammians is called open-loop-balanced realization, or Moore-balanced representation. Balanced realizations are widely used for model-order-reduction, because the states corresponding to small diagonal grammians (or Hankel singular values) are weakly controllable and observable and thus can be truncated, while the most important input-output characteristics of the original system can be retained. This model-reduction method is referred to as balanced truncation.

The balanced realization is not strictly unique, but the subspace of the state space associated with each singular value is invariant for all balanced realizations. Multiple balanced realizations can only be obtained by sign changes in the state basis, and by rotations of the bases for subspaces associated with repeated singular values. Therefore, the

reduced order controller generated by truncating the states of a balance realization associated with a given set of singular values is unique (Burl, 1999).

As the grammians are diagonally dominant, the transformation matrix from the modal to the balanced coordinates must be diagonally dominant itself. The system matrix in the balanced coordinates is therefore diagonally dominant. Actually, the matrix $\mathbf{A}_m$ in modal form 2 can be a balanced state matrix, as the fourth property states (Gawronski, 1998):

4. In a balanced representation the system matrix $\mathbf{A}_{mb}$ is block diagonally dominant with 2×2 blocks on the diagonal, and $\mathbf{B}_{mb}$, $\mathbf{C}_{mb}$ are divided into $2\times s$ and $r\times 2$ blocks as

$$\mathbf{A}_{mb} = diag(\mathbf{A}_{mb,i}), \text{ where } \mathbf{A}_{mbi} = \mathbf{A}_{mi} = \begin{bmatrix} -\zeta_i\omega_i & \omega_i \\ -\omega_i & -\zeta_i\omega_i \end{bmatrix}. \tag{2-54}$$

$\mathbf{B}_{mb}$ and $\mathbf{C}_{mb}$ can be obtained using the same transformation matrix.

The question that arises here is, can the modal representation be almost-balanced in the sense that its grammians are almost equal and diagonally dominant, i.e., $\mathbf{\Gamma} \cong \mathbf{W}_c \cong \mathbf{W}_o$, by a simple manipulation? The answer is yes. An almost-balanced model can be obtained by scaling matrix $\mathbf{B}_m$ and $\mathbf{C}_m$ only, leaving $\mathbf{A}_m$ unchanged, as stated in the fifth property:

5. By scaling the modal representation $(\mathbf{A}_m, \mathbf{B}_m, \mathbf{C}_m)$, one obtains an almost balanced representation $(\mathbf{A}_{ab}, \mathbf{B}_{ab}, \mathbf{C}_{ab})$, such that its grammians are almost equal and diagonally dominant as in

$$\mathbf{x}_{ab} = \mathbf{T}_{ab}\bar{\mathbf{x}}, \text{ and } \mathbf{A}_{ab} = \mathbf{A}_m,\ \mathbf{B}_{ab} = \mathbf{T}_{ab}^{-1}\mathbf{B}_m, \mathbf{C}_{ab} = \mathbf{C}_m\mathbf{T}_{ab}. \tag{2-55}$$

Here the transformation matrix $\mathbf{T}_{ab}$ is a diagonal matrix

$$\mathbf{T}_{ab} = diag(\mathbf{T}_{ab,i}),\ \ \mathbf{T}_{ab,i} = r_i \mathbf{I}_2, \text{ and } r_i = \left(\frac{w_{c,i}}{w_{o,i}}\right)^{1/4} = \sqrt{\frac{\|\mathbf{B}_{m,i}\|_2}{\|\mathbf{C}_{m,i}\|_2}}\ . \tag{2-56}$$

The advantage of the modal approach is apparent. The almost-balanced representation can be obtained using a closed-form equation, and thus tedious computation is avoided. Moreover, the diagonal form 2 matrix $\mathbf{A}_m$ remains unchanged, which provides more convenience and insight for researchers to examine the structural properties.

The computations utilizing the above definitions and properties are illustrated in the example below.

2.4 Illustrative Example

An example of a five-story building model given by Kelly et al. (1987) and used for the study of smart isolation by Ramallo et al (2002), is adopted here to illustrate the controllability/observability properties and model reduction techniques using modal form 2. Control devices are installed at the base level. The structural parameters of the five-DOF fixed-base structure and base and bearings are given in Table 2-1 and shown in Figure 2-8.

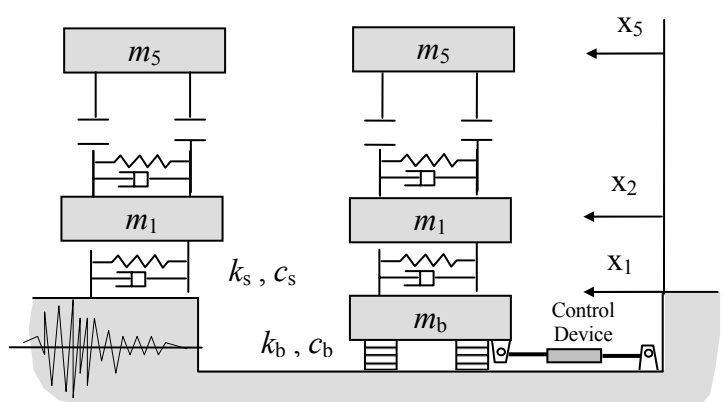

Figure 2-8 Six-Story Building Model

Table 2-1 Structural Model Parameter (Kelly et al., 1987)

Floor masses(kg)	Stiffness coefficient(kN/m)	Damping coefficient(kN.s/m)	Natural frequencies(Hz)	Natural periods(sec)
$m_b = 6800$	$k_b = 232$	$c_b = 3.74$	0.3978	2.5138
$m_1 = 5897$	$k_1 = 33732$	$c_1 = 67$	5.4647	0.1830
$m_2 = 5897$	$k_2 = 29093$	$c_2 = 58$	10.2932	0.0972
$m_3 = 5897$	$k_3 = 28621$	$c_3 = 57$	14.7186	0.0679
$m_4 = 5897$	$k_4 = 24954$	$c_4 = 50$	18.3980	0.0544
$m_5 = 5897$	$k_5 = 19059$	$c_5 = 38$	21.3127	0.0469

k_b and c_b are so chosen such that the isolation mode period is 2.5 sec and the isolation mode damping ratio is 2%. To examine the observability properties, the displacements with respect to the ground and the absolute accelerations of all floors are selected as outputs.

The rank of a matrix can be readily computed using the Matlab routine *rank.m*. For this example, the dimensions of $\mathbf{Q}_c$ and $\mathbf{Q}_o$ are 12 by 12, while their ranks are 6 and 10 respectively using the default tolerance. However, further computations show that the ranks are actually full when smaller, more appropriate tolerances are selected. So the system is completely controllable (c.c.) and completely observable (c.o.), but there are weakly controllable and observable states that could not be detected with larger tolerances. The information is all that $\mathbf{Q}_c$ and $\mathbf{Q}_o$ can provide.

Unlike the $\mathbf{Q}_c$ and $\mathbf{Q}_o$ matrices, grammians carry more qualitative information. Table 2-2 gives the eigenvalues of the grammians and the eigenvectors corresponding to the first two dominant eigenvalues. It shows that there are five dominant states for both controllability and observability. However, the principal directions of the dominant states for the two grammians are not aligned. Apparently, model reduction cannot be performed on this unbalanced model.

For the nodal representation, the balanced realization can be computed manually using equation (2-53), where the transformation matrix $\mathbf{T}_b$ is obtained using the singular value decomposition technique. Here Matlab routine *balreal.m* is used to perform the calculations required. Hankel singular values are provided by *balreal.m* as well. So, the equal values of the grammians for the balanced realization can be obtained. The transformation matrix

$\mathbf{T}_b =$

$$\begin{bmatrix}
0.0071 & 0.0011 & 0.0006 & 0.0002 & -0.0002 & -0.0004 & 0.0006 & 0.0006 & 0.0006 & 0.0006 & 0.0006 & 0.0006 \\
0.0046 & -0.0016 & -0.0022 & -0.0027 & -0.0031 & -0.0034 & 0.0006 & 0.0005 & 0.0005 & 0.0005 & 0.0005 & 0.0005 \\
0.1208 & 0.0374 & 0.0024 & -0.0288 & -0.0554 & -0.0736 & 0.0026 & 0.0019 & 0.0008 & -0.0005 & -0.0019 & -0.0030 \\
-0.0511 & -0.0856 & -0.0463 & 0.0068 & 0.0636 & 0.1101 & 0.0027 & 0.0015 & 0.0004 & -0.0007 & -0.0016 & -0.0022 \\
-0.3393 & 0.1827 & 0.1977 & 0.0692 & -0.0392 & -0.0732 & -0.0035 & -0.0001 & 0.0037 & 0.0039 & 0.0004 & -0.0044 \\
-0.0909 & -0.2244 & 0.2056 & 0.3207 & 0.0775 & -0.2899 & 0.0041 & -0.0018 & -0.0026 & -0.0005 & 0.0008 & 0.0001 \\
-0.4182 & 0.5262 & -0.1386 & -0.0122 & 0.2404 & -0.1991 & -0.0035 & 0.0061 & 0.0021 & -0.0049 & -0.0034 & 0.0037 \\
0.3757 & -0.2988 & -0.5010 & 0.3449 & 0.3823 & -0.3019 & -0.0039 & 0.0040 & -0.0019 & 0.0010 & 0.0044 & -0.0036 \\
0.2229 & -0.1257 & -0.1179 & -0.5071 & 0.9907 & -0.4620 & 0.0028 & -0.0088 & 0.0073 & 0.0004 & -0.0020 & 0.0003 \\
0.5979 & -1.1902 & 0.5805 & 0.3069 & -0.3847 & 0.0906 & -0.0032 & 0.0003 & 0.0036 & 0.0051 & -0.0106 & 0.0047 \\
0.1517 & -0.9818 & 2.2386 & -2.4256 & 1.3506 & -0.3338 & -0.0025 & 0.0063 & -0.0034 & -0.0045 & 0.0066 & -0.0025 \\
-0.5277 & 1.2478 & -0.9714 & -0.0557 & 0.5519 & -0.2455 & 0.0012 & 0.0055 & -0.0187 & 0.0201 & -0.0104 & 0.0023
\end{bmatrix}$$

The resulting diagonal entries of the controllability and observability grammians are thus ($\times 10^{-3}$): 0.8756 0.8418, 0.5996 0.5584, 0.3030 0.2729, 0.1760 0.1581, 0.0827 0.0756, 0.0252 0.0236. These grammians show that there are states that are weakly controllable and observable, and only a few states can be strongly affected by the control action.

Table 2-2 Eigenvalues and Dominant Eigenvectors of the Controllability and Observability Grammians

Controllability			Observability		
Eigenvalues (10^{-7})	Eigenvector 1 (10^{-8})	Eigenvector 2 (10^{-8})	Eigenvalues (10^{6})	Eigenvector 1 (10^{3})	Eigenvector 2 (10^{3})
0.0000	0.0000	0.0001	0.0000	-0.0091	-0.0138
0.0000	0.0001	0.0001	0.0002	0.0046	-0.0453
0.0000	0.0001	0.0001	0.0002	-0.0236	0.0541
0.0000	0.0001	0.0001	0.0002	0.0106	-2.0254
0.0000	0.0001	0.0000	0.0002	-1.5470	3.6980
0.0001	0.0000	-0.0001	0.0002	1.5647	-1.6673
0.0004	0.3379	0.3467	0.0003	-0.0348	-0.0358
0.0012	0.3459	0.3547	0.2794	-0.0309	-0.0319
0.0031	0.3610	0.3699	1.0384	-0.0323	-0.0336
0.0140	0.3827	0.3899	2.1424	-0.0348	-0.0418
0.0362 (2)	0.4133	0.4075	3.3499 (2)	-0.0432	0.2167
0.2265 (1)	0.4467	0.4133	4.5026 (1)	0.2061	-0.0432

If six states are retained and the other six truncated, the balanced truncation model is

$\mathbf{A}_b =$

$$\begin{array}{c} \\ x_1 \\ x_2 \\ x_3 \\ x_4 \\ x_5 \\ x_6 \end{array} \begin{array}{c} \begin{array}{cccccc} x_1 & x_2 & x_3 & x_4 & x_5 & x_6 \end{array} \\ \begin{bmatrix} -0.0506 & 2.501 & 0.4136 & 0.5377 & -0.1546 & 0.2435 \\ -2.505 & -0.0519 & 0.4138 & 0.659 & -0.1242 & 0.3008 \\ -0.6925 & -0.7175 & -1.209 & 34.51 & -1.012 & 2.782 \\ -0.7644 & -0.8726 & -34.63 & -1.378 & -1.505 & 3.874 \\ 0.5037 & 0.5098 & 3.172 & 3.76 & -2.895 & -68.72 \\ -0.6916 & -0.7336 & -4.905 & -5.918 & 69.81 & -6.013 \end{bmatrix} \end{array}$$

$\mathbf{B}_b =$

$$\begin{array}{c} \\ x_1 \\ x_2 \\ x_3 \\ x_4 \\ x_5 \\ x_6 \end{array} \begin{array}{c} \mathrm{u}_1 \\ \begin{bmatrix} 0.00941 \\ 0.00935 \\ 0.03808 \\ 0.03922 \\ -0.04189 \\ 0.05729 \end{bmatrix} \end{array}$$

$\mathbf{C}_b$ matrix is 12×6 and $\mathbf{D}_b$ matrix is 12×1. They are given by

$\mathbf{C}_b =$

$$\begin{array}{c} \\ y_1 \\ y_2 \\ y_3 \\ y_4 \\ y_5 \\ y_6 \\ y_7 \\ y_8 \\ y_9 \\ y_{10} \\ y_{11} \\ y_{12} \end{array} \begin{array}{c} \begin{array}{cccccc} x_1 & x_2 & x_3 & x_4 & x_5 & x6 \end{array} \\ \begin{bmatrix} 0.0005726 & -0.0006004 & 1.995\text{e-}005 & -1.602\text{e-}005 & -5.766\text{e-}006 & -5.556\text{e-}006 \\ 0.0005757 & -0.0006039 & 1.542\text{e-}005 & -1.275\text{e-}005 & -4.291\text{e-}007 & -5.007\text{e-}008 \\ 0.0005783 & -0.0006073 & 7.677\text{e-}006 & -5.494\text{e-}006 & 2.992\text{e-}006 & 6.979\text{e-}006 \\ 0.0005803 & -0.00061 & -3.664\text{e-}007 & 4.022\text{e-}006 & 2.16\text{e-}006 & 8.283\text{e-}006 \\ 0.0005817 & -0.0006121 & -7.822\text{e-}006 & 1.446\text{e-}005 & -1.533\text{e-}007 & 1.951\text{e-}006 \\ 0.0005827 & -0.0006134 & -1.336\text{e-}005 & 2.306\text{e-}005 & -1.366\text{e-}006 & -8.388\text{e-}006 \\ -0.005012 & 0.00223 & -0.02424 & 0.01473 & 0.0287 & 0.02244 \\ -0.004298 & 0.003034 & -0.014 & 0.01604 & -0.01084 & 0.006249 \\ -0.003563 & 0.00385 & -0.001455 & 0.01047 & -0.02456 & -0.02512 \\ -0.003236 & 0.004228 & 0.007951 & -0.001165 & -0.01071 & -0.03196 \\ -0.003152 & 0.004352 & 0.01486 & -0.01525 & 0.004909 & -0.00725 \\ -0.003138 & 0.004396 & 0.0195 & -0.02685 & 0.008501 & 0.03216 \end{bmatrix} \end{array}$$

$\mathbf{D}_b =$

$$\begin{array}{c} \\ y_1 \\ y_2 \\ y_3 \\ y_4 \\ y_5 \\ y_6 \\ y_7 \\ y_8 \\ y_9 \\ y_{10} \\ y_{11} \\ y_{12} \end{array} \begin{array}{c} u_1 \\ \begin{bmatrix} 3.805\text{e-}009 \\ -3.579\text{e-}009 \\ -2.231\text{e-}009 \\ 3.186\text{e-}011 \\ 8.458\text{e-}010 \\ 6.745\text{e-}010 \\ 0.0001083 \\ 5.402\text{e-}005 \\ 3.794\text{e-}006 \\ -1.084\text{e-}005 \\ -5.44\text{e-}006 \\ 3.047\text{e-}006 \end{bmatrix} \end{array}$$

The natural frequencies and periods of the reduced model can be obtained from the eigenvalues of the matrix $\mathbf{A}_b$. They are 0.3978 Hz (2.5137 sec), 5.4740 Hz (0.1827 sec), 11.1145 Hz (0.0900 sec), which are the first three modes corresponding to the original

isolation system: 0.3978 Hz (2.5137 sec), 5.4647 Hz (0.1830 sec), 10.2932 Hz (0.0972 sec). Notice that the 2nd and the 3rd modes deviate some from the original model. This can be clearly seen from the open-loop poles of the building and the reduced model (Figure 2-9), where the green dots represent the poles of full-order model and red ones the poles of the reduce-order model.

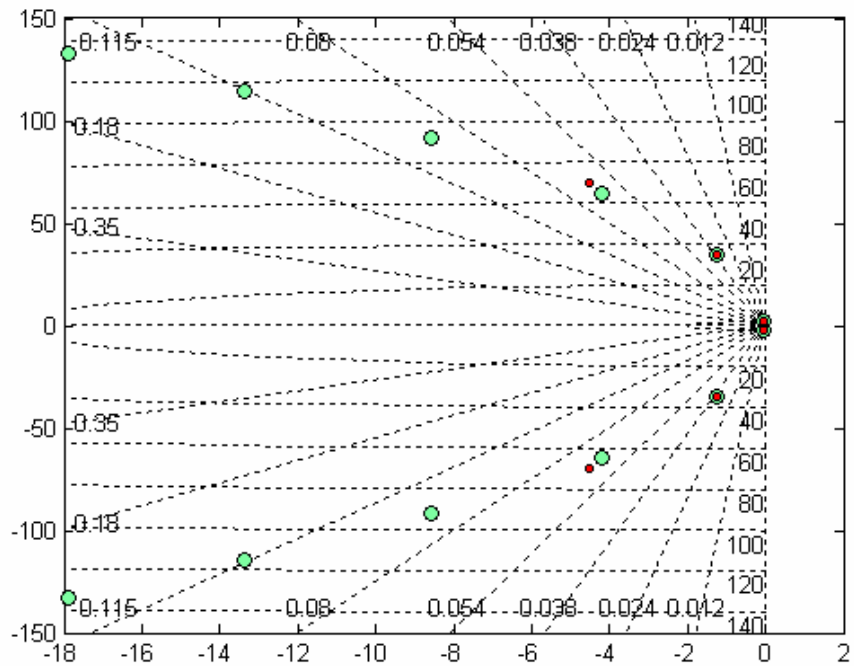

Figure 2-9 Poles of the Full-Order and Nodal Reduced-Order Models

Using the modal representation, the above process can be simplified. The controllability grammians computed in closed-form approximation (equations (2-36) and (2-37)) are ($\times 10^{-11}$): 2628.3 140.27 30.806 10.383 5.0889 2.1031 and the observability grammians are: 28.045 236.66 247.74 249.91 250.14 250.75.

Consequently, the Hankel singular values are ($\times 10^{-3}$): 0.8585 0.5762 0.2763 0.1611 0.1128 0.0726. These approximate values are very close to the accurate values from the balanced model computation. So model truncation using the approximate method is not expected to cause significant errors for this system.

Using modal form 2, the state-space matrix,

$\mathbf{A}_m =$

$$\left[\begin{array}{cccccc|cccccc}
-0.0492 & 2.499 & 0 & 0 & 0 & 0 & 0 & 0 & 0 & 0 & 0 & 0 \\
-2.499 & -0.0492 & 0 & 0 & 0 & 0 & 0 & 0 & 0 & 0 & 0 & 0 \\
0 & 0 & -1.244 & 34.313 & 0 & 0 & 0 & 0 & 0 & 0 & 0 & 0 \\
0 & 0 & -34.313 & -1.244 & 0 & 0 & 0 & 0 & 0 & 0 & 0 & 0 \\
0 & 0 & 0 & 0 & -4.220 & 64.536 & 0 & 0 & 0 & 0 & 0 & 0 \\
0 & 0 & 0 & 0 & -64.536 & -4.220 & 0 & 0 & 0 & 0 & 0 & 0 \\
\hline
0 & 0 & 0 & 0 & 0 & 0 & -8.554 & 92.083 & 0 & 0 & 0 & 0 \\
0 & 0 & 0 & 0 & 0 & 0 & -92.083 & -8.554 & 0 & 0 & 0 & 0 \\
0 & 0 & 0 & 0 & 0 & 0 & 0 & 0 & -13.355 & 114.82 & 0 & 0 \\
0 & 0 & 0 & 0 & 0 & 0 & 0 & 0 & -114.82 & -13.355 & 0 & 0 \\
0 & 0 & 0 & 0 & 0 & 0 & 0 & 0 & 0 & 0 & -17.877 & 132.71 \\
0 & 0 & 0 & 0 & 0 & 0 & 0 & 0 & 0 & 0 & -132.71 & -17.88
\end{array}\right]$$

$\mathbf{A}_m$ is block-diagonal and is arranged by the frequencies in ascending order. However, the model represented by the triple $(\mathbf{A}_m, \mathbf{B}_m, \mathbf{C}_m)$ is not balanced. To obtain an almost-balanced model, only matrices $\mathbf{B}_m$ and $\mathbf{C}_m$ need to be scaled using the easily formed matrix $\mathbf{T}_{ab}$, while matrix remains $\mathbf{A}_m$ unchanged. The transformation matrix $\mathbf{T}_{ab}$ is

$\mathbf{T}_{ab} =$

$$\left[\begin{array}{cc}
0.0055 & 0 \\ 0 & 0.0055
\end{array}\right.$$
$$\begin{array}{cc}
0.0016 & 0 \\ 0 & 0.0016
\end{array}$$
$$\begin{array}{cc}
0.0011 & 0 \\ 0 & 0.0011
\end{array}$$
$$\begin{array}{cc}
0.0008 & 0 \\ 0 & 0.0008
\end{array}$$
$$\begin{array}{cc}
0.0007 & 0 \\ 0 & 0.0007
\end{array}$$
$$\left.\begin{array}{cc}
0.0005 & 0 \\ 0 & 0.0005
\end{array}\right]$$

If we want to retain, say, the first three modes, it is necessary to eliminate the last six columns of $\mathbf{A}_m$ and $\mathbf{C}_{ab}$, and the last six rows and $\mathbf{A}_m$ and $\mathbf{B}_{ab}$. The reduced model with the almost-balanced truncation will retain the modes exactly from the original system, as shown in Figure 2-10. It shows that the reduced-order model retains exactly the modes desired.

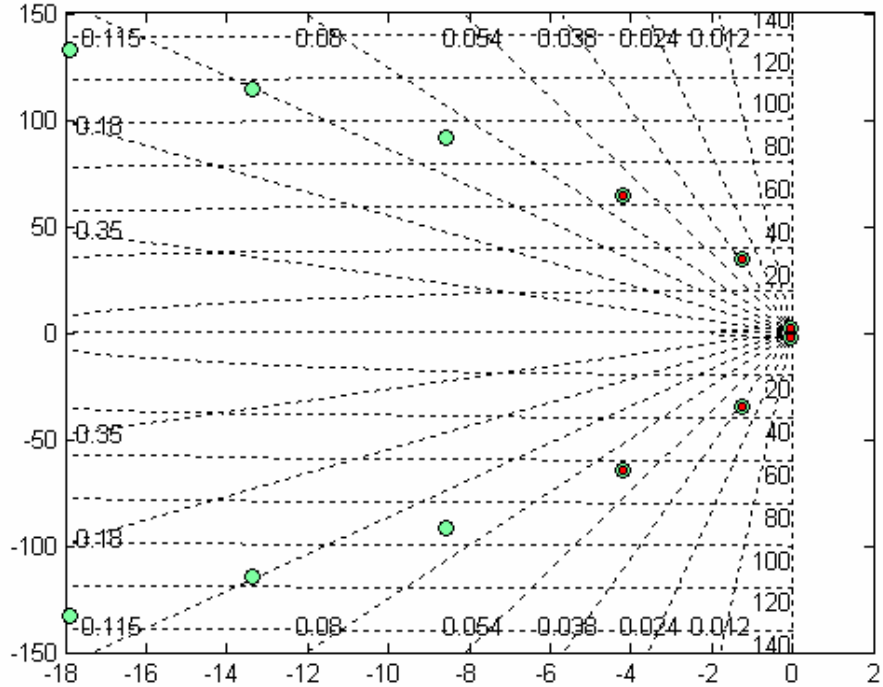

Figure 2-10 Poles of the Full-Order and Modal Reduced-Order Models

The grammians and singular values in this example show that, for a base isolation system with the control force applied at the base mass, the lower frequency modes are strongly controllable and observable, whereas the higher frequency modes are weakly controllable and observable. This conclusion coincides with engineering practice, i.e., for a base isolated building, it is easier to control the translational motion than to control the inter-story drifts if the force is applied at the base mass.

It is of interest to examine how the controllability and observability properties change with the degree of isolation. More simulations show that highly isolated buildings (with smaller k_b values) have stronger controllability and observability in the lower modes (especially the isolation mode), but their higher modes are less controllable and observable. Increasing the k_b value has the reverse effect. However, if k_b is too large, neither lower modes nor higher modes are controllable. These results are understandable. For a base isolated building, the isolation mode dominates its dynamic behavior, so control devices are more efficient in controlling the base drift and sensors are more efficient in detecting

the dominant responses instead of secondary responses of higher modes. As the bearing stiffness k_b grows larger, the structural system becomes more rigid, higher modes participate more and so their response becomes more detectable. However, if the structure is as rigid as a fixed-base structure, the control devices and sensors at the base would not have any significant effects on the building.

Accelerometers are more practical for civil engineering structures. Note that the observability grammian does not depend on the feed-through term $\mathbf{D}_{\mathbf{y}}$, which is introduced by the absolute accelerations as measured responses. The output for the accelerometers is in the form $\mathbf{y} = \mathbf{C}_{\mathbf{y}}\mathbf{x} + \mathbf{D}_{\mathbf{y}}\mathbf{u}$, and the transfer function is $\mathbf{G}(\omega) = \mathbf{C}_m(j\omega\mathbf{I} - \mathbf{A}_m)^{-1}\mathbf{B}_m + \mathbf{D}_m$ instead of $\mathbf{G}(\omega) = \mathbf{C}_m(j\omega\mathbf{I} - \mathbf{A}_m)^{-1}\mathbf{B}_m$. As is shown in the equations (2-38), (2-39) and (2-40), the norms of the modes equipped with accelerometers should be re-scaled if accelerometer dynamics is crucial to the study.

2.5 Summary

This chapter introduces the background knowledge of this study, modal structural models and the concepts of the controllability and observability. The advantages of using modal models for control application are extensively stated. An important base to perform model reduction, the open-loop balancing technique is explained in depth using the geometric description of controllability and observability ellipsoids. The computations regarding the controllability and observability are illustrated using a six-story base isolated building model, and the controllability and observability properties for general base isolation systems are discussed.

Chapter 3

The Isolation System of the Benchmark Building

3.1 Description of the Smart Base Isolation Benchmark Problem

The application of active schemes to base isolation systems are considered to be an effective way to enhance their performance. However, the relative merits of these schemes have not been investigated systematically on a benchmark problem. Due to the effectiveness of the fixed base building benchmark effort (Spencer et al., 1998a, b; Ohtori et al., 2004), the ASCE Committee on Structural Control voted to develop a new smart base isolation benchmark problem for use by the international research community to evaluate their competing control strategies, including the control devices, algorithms, and sensors, etc. As is introduced in the Introduction, the framework of this benchmark study has been provided, from problem definition (Narasimhan et al. 2004) to sample control system design (Nagarajaiah et al., 2005; Erkus et al., 2004). These sample designs are not competitive but are intended to serve as a guide to the participants.

Based on the input from the ASCE Committee on Structural Control, Narasimhan and Nagarajaiah (2002, 2004) have developed a 3D model of the entire system. The benchmark model is an eight story base isolated building with lateral-torsional behavior. It is similar to existing buildings in Los Angeles, California. This building is 270.4 ft (81.9 m) by 178 ft (53.9 m) in plan and 116 ft (35.1 m) in elevation. The floor plan is L-shaped and has setbacks above the fifth floor. Metal decking and a grid of steel beams support all concrete floor slabs. The superstructure is supported on a reinforced concrete base slab, which is integrated with the underneath concrete beams and drop panels at the bottom of the columns. The isolators are connected between these drop panels and footings. The developed 3D model has the capability to model three different commonly used base isolation systems: linear elastomeric systems with low damping or supplementary damping, friction systems, and bilinear or nonlinear-elastomeric systems. Any combination of these

can be considered as well. The nominal isolation system consists of 61 friction pendulum bearings and 31 linear elastomeric bearings. The sample controller positions and the nominal isolation system are shown in Figure 3-1. Participants may replace the nominal bearings with other types of bearings, develop their own device models, and place their devices at their desired locations.

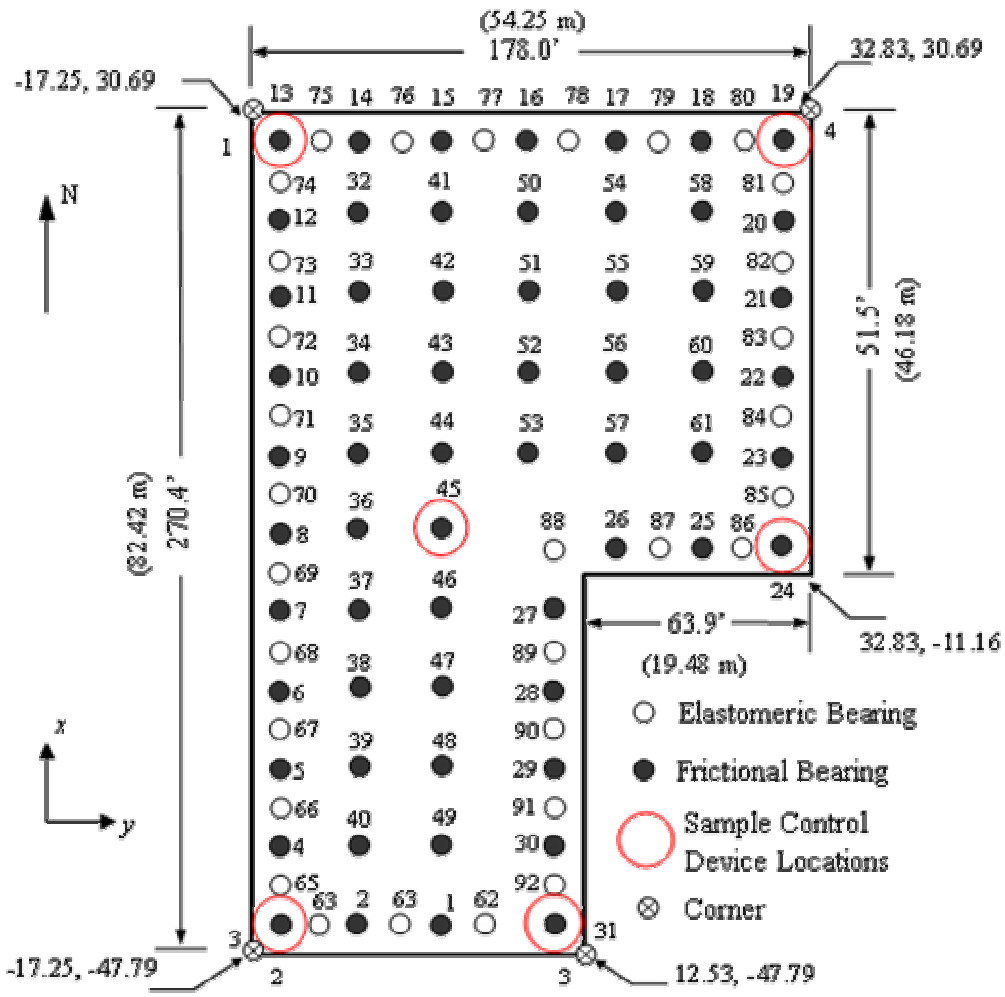

Figure 3-1 Plan View of the Fundamental Level and the Nominal Bearing Locations

Figure 3-2 shows the elevation view of the asymmetric model subjected to bidirectional ground excitations and the coordinate system that determines the relative location of the center of the masses and stiffnesses.

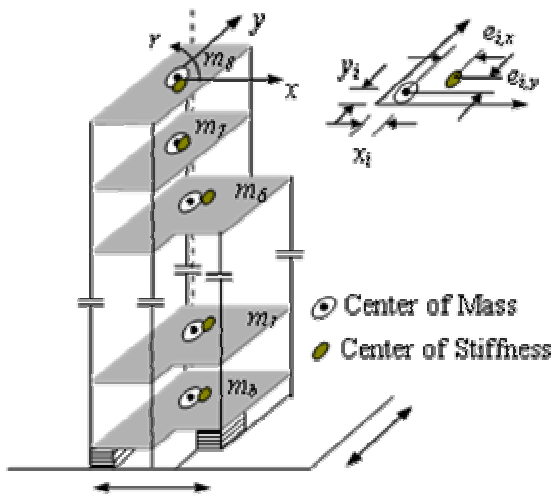

Figure 3-2 Elevation View of the Asymmetric Base Isolated Benchmark Building

When subjected to earthquake excitations, multistory buildings with eccentric centers of mass and resistance respond with coupled lateral-torsional motion to earthquake ground motion, even when the motion is uniform over the base and contains no rotational components (Chopra, 1977). Although coupled lateral-torsional response is reduced in base isolated structures compared to conventional designs (Skinner et al., 1993), it cannot be overlooked in practical design due to the fact that torsional response can cause excessive displacements at the corner bearings and lead to instabilities in the bearings. Analysis of such buildings requires torsional degrees of freedom in addition to translational degrees of freedom. The floors and the base of the building are assumed to be infinitely rigid in plane. Hence, a 3D building with 3 degrees of freedom (DOFs) per floor at the center of mass is assumed to adequately represent the elastic superstructure. The combined model of the superstructure (24 DOFs) and isolation system (3 DOFs) consists of 27 DOFs.

Base isolation buildings are designed such that the superstructure remains elastic. The localized nonlinearities at the isolation level allow the superstructure to be modeled by a condensed linear elastic system. The elastic superstructure is not assumed to be a shear building but a fully three dimensional building, so in modeling the superstructure, it is the eigenvalues and eigenvectors for the fixed base condition instead of the stiffness matrix that are provided. The equations of motion are developed in such a way that the fixed-base properties are used for modeling the linear superstructure. Damping ratios are assumed to be 5% in all fixed-base modes. The masses of the floors are shown in Table 3-1 and the computed natural periods for the first nine fixed modes are shown in Table 3-2. Other parameters of the building that are to be used in this study are shown in Appendix A.

Table 3-1 Floor Masses of the Benchmark Building

Floor	base	1	2	3	4	5	6	7	8
Mass (kN-s^2/m)	3565.73	2051	2051	2051	2051	2051	2057	2247	2580

Table 3-2 First Nine Natural Periods of the Superstructure

	N-S(x-direction)			E-W (y-direction)			Torsion (r-direction)		
Mode	1	2	3	1	2	3	1	2	3
Period (sec)	0.78	0.27	0.15	0.89	0.28	0.15	0.66	0.21	0.12

In this benchmark study, no control devices are allowed to be installed within the superstructure. Control devices may only be installed at the base level. Each isolation bearing and control device is modeled explicitly using the specified model, and the forces in the bearings and the devices are transformed to the center of the mass of the base using the rigid base slab assumption.

The benchmark problem also proposed seven earthquakes to be used to evaluate the performance of the candidate controllers designed by the participants. These earthquakes are the Newhall, Sylmar, El Centro, Rinaldi, Kobe, Ji-ji, and Erzincan, all containing fault-normal (FN) and fault-parallel (FP) components.

A set of evaluation criteria that is particularly relevant for base isolated structures have been developed to compare various control strategies. The definitions of six of the

performance indices that will be used in this study are shown in Table 3-3, where ^ denotes the uncontrolled (passively isolated) system. RMS denotes "root mean square".

Table 3-3 Performance Indices (Normalized) to be Used in This Study

Peak Base Drift	$J_3(q) = \dfrac{\max_{t,i}\lVert d_i(t,q)\rVert}{\max_{t,i}\lVert \hat{d}_i(t,q)\rVert}$	RMS Base Drift	$J_7(q) = \dfrac{\max_{i}\lVert \sigma_d(t,q)\rVert}{\max_{i}\lVert \sigma_{\hat{d}}(t,q)\rVert}$
Peak Floor Acceleration	$J_4(q) = \dfrac{\max_{t,f}\lVert d_f(t,q)\rVert}{\max_{t,f}\lVert \hat{d}_f(t,q)\rVert}$	RMS Floor Accelerations	$J_{11}(q) = \dfrac{\max_{f}\lVert \sigma_{d_f}(t,q)\rVert}{\max_{f}\lVert \sigma_{\hat{d}_f}(t,q)\rVert}$
Peak Inter-Story Drift	$J_5(q) = \dfrac{\max_{t,f}\lVert a_f(t,q)\rVert}{\max_{t,f}\lVert \hat{a}_f(t,q)\rVert}$	RMS Inter-Story Drift	$J_8(q) = \dfrac{\max_{f}\lVert \sigma_a(t,q)\rVert}{\max_{f}\lVert \sigma_{\hat{a}}(t,q)\rVert}$

For more details refer to Narasimhan et al. (2004) and the problem definition provided on the website: http://www.usc.edu/dept/civil_eng/johnsone/baseisobench/ .

This chapter focuses on the selection of the linear elastomeric bearings only, which are placed at all 92 locations. The 3D dynamics for asymmetrical buildings has been studied extensively by (Narasimhan et al., 1991). In light of the 3D dynamics proposed by that study, and taking into account of the assumptions made above, the equations of motion of the superstructure and base are expressed in the form (Narasimhan et al., 2004)

$$\begin{cases} \mathbf{M}\ddot{\mathbf{Z}}_s + \mathbf{C}\dot{\mathbf{Z}}_s + \mathbf{K}\mathbf{Z}_s = -\mathbf{M}\boldsymbol{\Gamma}(\ddot{\mathbf{X}}_g + \ddot{\mathbf{Y}}_b) \\ \mathbf{M}_b\ddot{\mathbf{Y}}_b + \mathbf{C}_b\dot{\mathbf{Y}}_b + \mathbf{K}_b\mathbf{Y}_b + \mathbf{f}_c = -\mathbf{M}_b\boldsymbol{\Gamma}\ddot{\mathbf{X}}_g - \boldsymbol{\Gamma}^T\mathbf{M}[\ddot{\mathbf{Z}}_s + \boldsymbol{\Gamma}(\ddot{\mathbf{X}}_g + \ddot{\mathbf{Y}}_b)] \end{cases} \tag{3-1}$$

where $\mathbf{M}$, $\mathbf{C}$, and $\mathbf{K}$ are the mass, damping and stiffness of the superstructure, respectively. The subscript b denotes the base and c denotes the controller. $\mathbf{M}_b$, $\mathbf{C}_b$, and $\mathbf{K}_b$ are the mass, damping and stiffness of the base, respectively. $\mathbf{f}_c$ is the vector of the control force. $\ddot{\mathbf{X}}_g$ represents the ground acceleration vector, $\mathbf{Z}_s$ is the displacement of the superstructure with respect to the base, $\mathbf{Y}_b$ is the displacement with respect the ground, and $\mathbf{X}$ is the absolute displacement. The coordinates have the relationship

$$\mathbf{X}_s = \mathbf{Z}_s + \mathbf{\Gamma}(\mathbf{X}_g + \mathbf{Y}_b) = \mathbf{Z}_s + \mathbf{\Gamma}\mathbf{Y}_b + \mathbf{\Gamma}\mathbf{X}_g \tag{3-2}$$

where $\mathbf{\Gamma} = \begin{bmatrix}\mathbf{\Gamma}_8 & \mathbf{\Gamma}_7 & \cdots & \mathbf{\Gamma}_1\end{bmatrix}^T$ is the influence coefficient matrix of the disturbance, i. e., resulting displacements and rotations at the center of mass of each floor due to a unit displacement and rotation of the center of mass of the base. In this case the entry of *i*th floor in $\mathbf{\Gamma}$ is

$$\mathbf{\Gamma}_i = \begin{bmatrix} 1 & 0 & -y_i \\ 0 & 1 & x_i \\ 0 & 0 & 1 \end{bmatrix} \tag{3-3}$$

that is, unlike the symmetric case, $\mathbf{\Gamma}_i \neq \mathbf{I}_{3\times3}$, where x_i and y_i are the offsets of the center of the mass of the *i*th floor in the *x*- and *y*-directions with respect to the base, respectively. The mass matrices $\mathbf{M}$ and $\mathbf{M}_b$ are diagonal. The damping and stiffness matrices of the substructure are given by

$$\mathbf{C}_b = \mathbf{\Gamma}_b \mathbf{C}^{is} \mathbf{\Gamma}_b^T, \quad \mathbf{K}_b = \mathbf{\Gamma}_b \mathbf{K}^{is} \mathbf{\Gamma}_b^T \tag{3-4}$$

$$\mathbf{C}^{is} = \begin{bmatrix} \mathbf{C}_1^{is} & & \\ & \ddots & \\ & & \mathbf{C}_{nb}^{is} \end{bmatrix}, \quad \mathbf{K}^{is} = \begin{bmatrix} \mathbf{K}_1^{is} & & \\ & \ddots & \\ & & \mathbf{K}_{nb}^{is} \end{bmatrix} \tag{3-5}$$

where $\mathbf{C}_i^{is}$ and $\mathbf{K}_i^{is}$ are the 3×3 damping and stiffness matrices of the *i*th bearing, and nb is the total number of the bearings. The bearings have only axial force components. Therefore the third column and row of each $\mathbf{C}_i^{is}$ and $\mathbf{K}_i^{is}$ is zero. $\mathbf{\Gamma}_b$ is a matrix related to the location of the bearings, as in

$$\mathbf{\Gamma}_b = \begin{bmatrix}\mathbf{r}_1^{is} & \cdots & \mathbf{r}_{nb}^{is}\end{bmatrix} \tag{3-6}$$

and

$$\mathbf{r}_i^{is} = \begin{bmatrix} 1 & 0 & 0 \\ 0 & 1 & 0 \\ -y_i^{is} & x_i^{is} & 1 \end{bmatrix} \tag{3-7}$$

where (x_i^{is}, y_i^{is}) is the coordinate of the *i*th bearing.

Let $\mathbf{\Phi}$ be the mass-normalized eigenvector matrix of the superstructure, i.e., $\mathbf{Z_s} = \mathbf{\Phi\eta}$. Then equations of the superstructure can be written in modal form as

$$\ddot{\boldsymbol{\eta}} + \widetilde{\mathbf{C}}\dot{\boldsymbol{\eta}} + \widetilde{\mathbf{K}}\boldsymbol{\eta} = -\mathbf{\Phi}^T\mathbf{M}\mathbf{\Gamma}(\ddot{\mathbf{X}}_\mathbf{g} + \ddot{\mathbf{Y}}_b) \tag{3-8}$$

where $\boldsymbol{\eta}$ is the vector of modal coordinates of the superstructure with respect to the base, and $\widetilde{\mathbf{C}}$ and $\widetilde{\mathbf{K}}$ are normalized damping and stiffness of the superstructure, respectively.

Equations (3-1) have a similar form to equations characterizing structures with multiple support excitations. Both cases have the effects of asymmetry. For the analysis of such problems, the equations should include the degrees of freedom at supports in the states (Chopra, 1999). Rewriting equation (3-1) in modal coordinate form (Erkus et al., 2004), it follows that

$$\overline{\mathbf{M}}\begin{Bmatrix} \ddot{\boldsymbol{\eta}} \\ \ddot{\mathbf{Y}}_b \end{Bmatrix} + \overline{\mathbf{C}}\begin{Bmatrix} \dot{\boldsymbol{\eta}} \\ \dot{\mathbf{Y}}_b \end{Bmatrix} + \overline{\mathbf{K}}\begin{Bmatrix} \boldsymbol{\eta} \\ \mathbf{Y}_b \end{Bmatrix} = \mathbf{S}_1\mathbf{f}_c - \mathbf{S}_2\mathbf{\Gamma}_3\ddot{\mathbf{X}}_g \tag{3-9}$$

where

$$\overline{\mathbf{M}} = \begin{bmatrix} \mathbf{I} & \mathbf{\Phi}^T\mathbf{M}^T\mathbf{\Gamma} \\ \mathbf{\Gamma}^T\mathbf{M}\mathbf{\Phi} & \mathbf{\Gamma}^T\mathbf{M}\mathbf{\Gamma} + \mathbf{M}_b \end{bmatrix} \quad \overline{\mathbf{C}} = \begin{bmatrix} \widetilde{\mathbf{C}} & \mathbf{0} \\ \mathbf{0} & \mathbf{C}_b \end{bmatrix} \quad \overline{\mathbf{K}} = \begin{bmatrix} \widetilde{\mathbf{K}} & \mathbf{0} \\ \mathbf{0} & \mathbf{K}_b \end{bmatrix} \tag{3-10}$$

$$\mathbf{\Gamma}_3 = \begin{bmatrix} 1 & 0 \\ 0 & 1 \\ 0 & 0 \end{bmatrix}, \quad \mathbf{S}_1 = \begin{bmatrix} \mathbf{0}_{24x24} \\ \mathbf{I}_{3x3} \end{bmatrix}, \quad \mathbf{S}_2 = \begin{bmatrix} \mathbf{\Phi}\mathbf{M}\mathbf{\Gamma} \\ \mathbf{\Gamma}^T\mathbf{M}\mathbf{\Gamma} + \mathbf{M}_b \end{bmatrix}. \tag{3-11}$$

Let $\mathbf{q} = \begin{Bmatrix} \boldsymbol{\eta}^T & \mathbf{Y}_b^T & \dot{\boldsymbol{\eta}}^T & \dot{\mathbf{Y}}_b^T \end{Bmatrix}^T$ be the state vector; the equation can be written in state space form as

$$\dot{\mathbf{q}}(t) = \mathbf{A}\mathbf{q}(t) + \mathbf{B}\mathbf{u}(t) + \mathbf{E}\ddot{\mathbf{X}}_g(t) \tag{3-12}$$

where

$$\mathbf{A} = \begin{bmatrix} \mathbf{0} & \mathbf{I} \\ -\overline{\mathbf{M}}^{-1}\overline{\mathbf{K}} & -\overline{\mathbf{M}}^{-1}\overline{\mathbf{C}} \end{bmatrix}, \quad \mathbf{B} = \begin{bmatrix} \mathbf{0} \\ \overline{\mathbf{M}}^{-1}\mathbf{S}_1\boldsymbol{\Gamma}_c \end{bmatrix}, \quad \mathbf{E} = \begin{bmatrix} \mathbf{0} \\ \overline{\mathbf{M}}^{-1}\mathbf{S}_2 \end{bmatrix}, \quad \mathbf{u} = \begin{bmatrix} \mathbf{0} \\ \mathbf{f_c} \end{bmatrix} \tag{3-13}$$

and $\boldsymbol{\Gamma}_c$ is a matrix related to the location of the controller, as in

$$\boldsymbol{\Gamma}_c = \begin{bmatrix} \mathbf{r}_1^{cl} & \cdots & \mathbf{r}_{nc}^{cl} \end{bmatrix} \tag{3-14}$$

and

$$\mathbf{r}_i^{cl} = \begin{cases} \begin{bmatrix} 1 & 0 & -y_i^{cl} \end{bmatrix}^T \\ \begin{bmatrix} 0 & 1 & x_i^{cl} \end{bmatrix}^T \end{cases} \tag{3-15}$$

where (x_i^{cl}, y_i^{cl}) are the coordinates of the *i*th control device, and nc is the total number of control devices.

The measurement output and regulated output equations take the forms

$$\mathbf{y} = \mathbf{C}_y\mathbf{q} + \mathbf{D}_y\mathbf{u} + \mathbf{E}_y\ddot{\mathbf{x}}_\mathbf{g} + \mathbf{v} \tag{3-16}$$

$$\mathbf{z} = \mathbf{C}_z\mathbf{q} + \mathbf{D}_z\mathbf{u} + \mathbf{E}_z\ddot{\mathbf{x}}_\mathbf{g} \tag{3-17}$$

where $\mathbf{v}$ is the vector of measurement noise. Here, the measured output vector $\mathbf{y}$ includes the accelerations of the floors of the structure and any additional measurements used for feedback in the control system. The regulated output vector $\mathbf{z}$ may consist of any linear

combination of the states of the system and components of the control input vector $\mathbf{u}$, depending on the control objectives.

The outputs (i.e., measurements) in this study are all corner outputs. Consider the outputs as corner inter-story drifts and absolute floor accelerations. The output vector is in the form of

$$\mathbf{z} = \begin{bmatrix} d\mathbf{X}_b & d\mathbf{X}_1 & \cdots & d\mathbf{X}_8 & \ddot{\mathbf{X}}_b & \ddot{\mathbf{X}}_1 & \cdots & \ddot{\mathbf{X}}_8 \end{bmatrix}^T \tag{3-18}$$

where $d\mathbf{X}_i = \begin{bmatrix} d\mathbf{X}_i^1 & \cdots & d\mathbf{X}_i^{ncr} \end{bmatrix}^T$ and $d\mathbf{X}_i^j = \begin{bmatrix} d\mathbf{X}_{i,x}^j & d\mathbf{X}_{i,y}^j \end{bmatrix}^T$, and similarly for accelerations. The state-space equation matrices for this set of outputs are given by

$$\mathbf{C}_\mathbf{z} = \begin{bmatrix} \mathbf{T}_3\mathbf{T}_2\mathbf{T}_1 & \mathbf{0} \\ -\mathbf{T}_4\mathbf{T}_1\mathbf{M}^{-1}\mathbf{K} & -\mathbf{T}_4\mathbf{T}_1\mathbf{M}^{-1}\mathbf{C} \end{bmatrix} \tag{3-19a}$$

$$\mathbf{D}_\mathbf{z} = \begin{bmatrix} \mathbf{0} \\ \mathbf{T}_4\mathbf{T}_1\mathbf{M}^{-1}\mathbf{S}_1\mathbf{\Gamma}_c \end{bmatrix}, \quad \mathbf{E}_\mathbf{z} = \begin{bmatrix} \mathbf{0} \\ \mathbf{T}_4\mathbf{T}_1\mathbf{M}^{-1}\mathbf{S}_2 + \mathbf{\Gamma}_4 \end{bmatrix} \tag{3-19b}$$

where

$$\mathbf{T}_1 = \begin{bmatrix} \mathbf{0} & \mathbf{I} \\ \mathbf{\Gamma}_5\mathbf{\Phi} & \mathbf{\Gamma}_1 \end{bmatrix}, \quad \mathbf{T}_2 = \begin{bmatrix} \mathbf{I}_{3\times3} & & & & \\ -\mathbf{I}_{3\times3} & \mathbf{I}_{3\times3} & & & \\ & -\mathbf{I}_{3\times3} & \mathbf{I}_{3\times3} & & \\ & & \ddots & \ddots & \\ & & & -\mathbf{I}_{3\times3} & \mathbf{I}_{3\times3} \end{bmatrix}_{27\times27} \tag{3-20a}$$

$$\mathbf{T}_3 = \begin{bmatrix} \mathbf{P}_b & & & \\ & \mathbf{P}_1 & & \\ & & \ddots & \\ & & & \mathbf{P}_8 \end{bmatrix}, \quad \mathbf{T}_4 = \begin{bmatrix} \mathbf{\Gamma}_3^T & & \\ & \ddots & \\ & & \mathbf{\Gamma}_3^T \end{bmatrix}_{18\times27}, \quad \mathbf{\Gamma}_5 = \begin{bmatrix} & & \mathbf{I}_{3\times3} \\ & \iddots & \\ \mathbf{I}_{3\times3} & & \end{bmatrix}_{24\times24} \tag{3-20b}$$

$$\mathbf{P}_i = \begin{bmatrix} \mathbf{P}_i^1 \\ \vdots \\ \mathbf{P}_i^{ncr} \end{bmatrix}, \quad \mathbf{P}_i^j = \begin{bmatrix} 1 & 0 & -Y_i^j \\ 0 & 1 & X_i^j \end{bmatrix}, \quad \mathbf{\Gamma}_4 = \begin{bmatrix} \mathbf{I}_{2\times2} \\ \vdots \\ \mathbf{I}_{2\times2} \end{bmatrix}_{18\times2}. \tag{3-20c}$$

Here, (X_i^j, Y_i^j) are the coordinates of the *j*th corner of the *i*th floor in the *x*- and *y*-directions, respectively, and ncr is the number of the corners. It is also assumed that the number of the corners for all floors is the same and is equal to ncr. If they were not equal, the equations would be modified accordingly.

3.2 Optimal Linear Isolation System

A base isolation system has the effect of producing low acceleration levels and small relative motions under strong ground motions at the cost of large absolute deformations at the isolation level. In an isolation system, the bearing stiffness k_b defines how "soft" the isolation system may be designed and how effectively it controls the floor accelerations. The introduction of damping (c_b or ξ_b) in the isolation mode increases the energy dissipation capacity and reduces the deformation demand in low-frequency ground motions. However, isolator energy dissipation has adverse effects on floor accelerations (Inaudi et al., 1993b). The purpose of isolation system design is to find a trade-off between the base deformation and the floor accelerations for various k_b and c_b. Studies show that such a point does exist. Given the characteristics of the primary structure, there is an optimal value of damping for minimizing the acceleration response. This fact puts boundaries on the dynamic performance achievable by passive isolation (Inaudi et al, 1993b). Based on this fact, the "optimal" passive system is defined as the system which produces minimal floor acceleration responses while rendering acceptable deformation in the isolation system.

Before studying the complex three-dimensional benchmark building, its equivalent one-dimensional counterpart is investigated first in the following section.

3.2.1 Isolation System for a One-Dimensional Model

The structural parameters in the *y*-direction (E-W) are shown in Table 3-4. The first three calculated natural frequencies are 1.42 Hz, 3.68 Hz, 5.92 Hz. The corresponding natural periods are 0.70 sec, 0.27 sec, and 0.17 sec. The damping ratios are assumed to be

5% in all modes. The weight of the base plate is 3565.73 kN-s^2/m. All bearings are assumed to be linear. The total stiffness and damping ratio of the bearings are to be designed.

Table 3-4 Parameters of the 1D Base Isolated Benchmark Building

Story	8	7	6	5	4	3	2	1
Weight (kN)	10435	13949	14935	19803	20081	20136	21994	25253
Total stiffness	24902	24558	26190	27904	37249	36929	41564	46216

The optimal bearing parameters are to be determined for a white-noise excitation in this section. Inaudi and Kelly (1992) have indicated that the optimum damping values for minimizing peak acceleration response are approximately equal to those that minimize the mean-square acceleration response with only minor variation. The stable RMS responses to white noise can be obtained from a Lyapunov equation (Soong et al., 1996) and the solution can be obtained using the Matlab routine *lyap2.m* within the control toolbox. The optimal pair of (k_b, c_b) is selected from a series of curves of the maximum RMS accelerations versus the maximum RMS base displacement relative to the ground (referred to as base drift) for various k_b and c_b.

Figure 3-3 shows the curves of maximum RMS acceleration (top floor) versus the RMS base drift of the one-dimensional model with varying bearing parameters to white noise with magnitude of $S_0 = \pi$. Each curve represents the RMS response with same stiffness but different damping values. The values in this figure are not important because they change proportionally with S_0 for the linear system. It can be seen that larger k_b curves are always located at higher positions where accelerations are larger. However, for each k_b there is an optimal damping ratio at which floor acceleration reaches its minimum. These curves are obtained for a white noise. Ground accelerations in reality are band-limited, typically having dominant periods within 0.1~1 sec, with maximum severity often in the range of 0.2~0.6 sec (Skinner et al., 1993). However, Inaudi et al. (1993b) showed that the optimal damping parameter is not sensitive to the frequency content of the excitation, where the white-noise was filtered by Kanai-Tajimi filters.

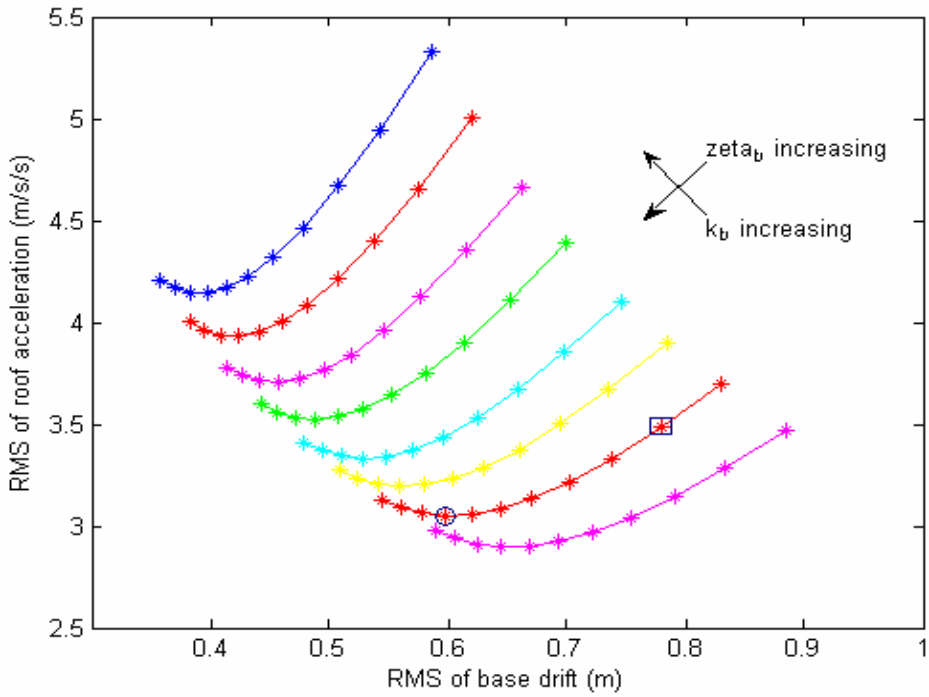

Figure 3-3 Maximum RMS of Base Drift -Acceleration Curves of the 1D System

For base isolation systems, k_b is usually determined such that the fundamental period of the isolated structure is beyond the frequency range of most earthquakes (0.1 ~1 sec). The sample designs provided in the benchmark papers (Narasimhan et al., 2004; Erkus et al., 2004) designed the structure with the fundamental period of 3.0 sec, corresponding to $k_b = 80{,}000$ kN/m in this model, and a damping ratio of 6% at the base level. This point is marked by a square in Figure 3-3. However, the optimum damping ratio for this k_b is 15%, as marked by the circle.

To examine if active control can further improve the performance of the selected optimal passive system, an LQG controller is applied to the optimal passive system. Equal weighting is put on each of the floor accelerations, while weighting on the base drift is 85 times of the weightings on accelerations. The performance of three systems is shown in Figure 3-4, including the passive system used in the benchmark paper (square), the optimal passive system determined from Figure 3-3 for the same k_b (circle), and the system with an active controller applied on this optimal passive system with various weightings

(crosses). The various crosses shown each represent different weightings (0 ~ 8×10^8), and consequently, different control forces.

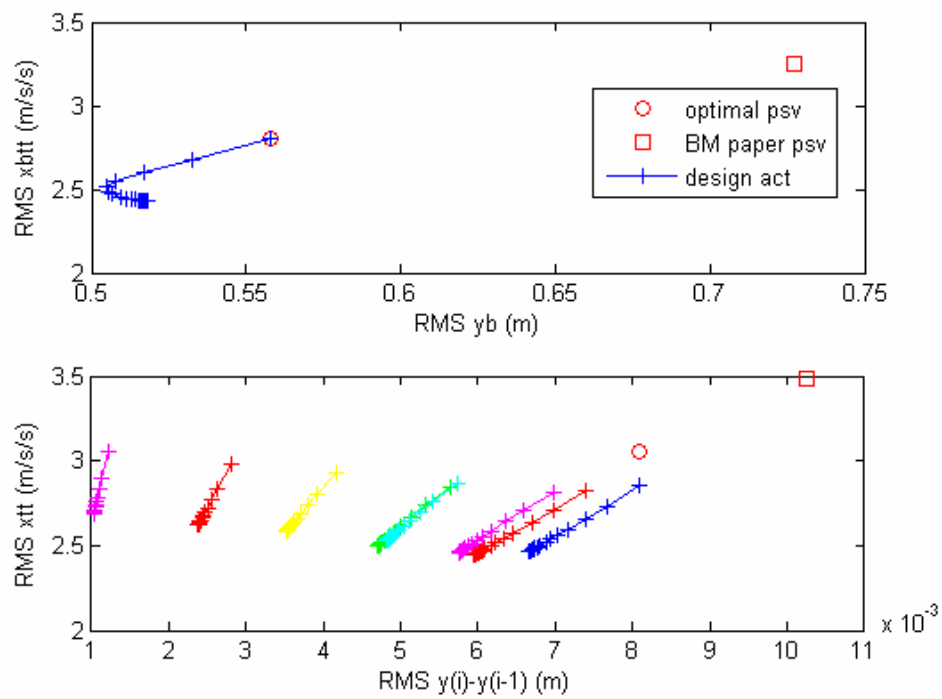

Figure 3-4 Maximum RMS Responses of the Actively Controlled System

The upper plot shows the RMS base acceleration versus RMS base drift. The lower plot shows the RMS accelerations (floors 2 to 8) versus RMS inter-story drifts. The blue curve represents the second floor, red the third floor, and so on. Apparently, the circle is lower, left to the square in both plots, indicating that all responses (the base drift, base and roof acceleration, and inter-story drift) of the optimal passive system are smaller than the responses using the (k_b, c_b) pair proposed in the sample design (Nagarajaiah and Narasimhan, 2005). Starting from a weighting of zero, the controlled system further improves the optimal passive system. However, performance is not improved in proportion to the weights. For a certain weight (the apex of the parabola), the base drift reaches the minimum while accelerations and inter-story drifts are low. This weight is the design weight for the active control system.

3.2.2 Isolation System for the 3D Building

Similar to the 1D case, the maximum RMS accelerations versus maximum RMS base drifts of the 3D building to two-directional white noise disturbances ($S_0 = \pi$) are computed and plotted in Figure 3-5. A curve represents a constant k_b bearing system. Arrows show the direction of increasing k_b or c_b.

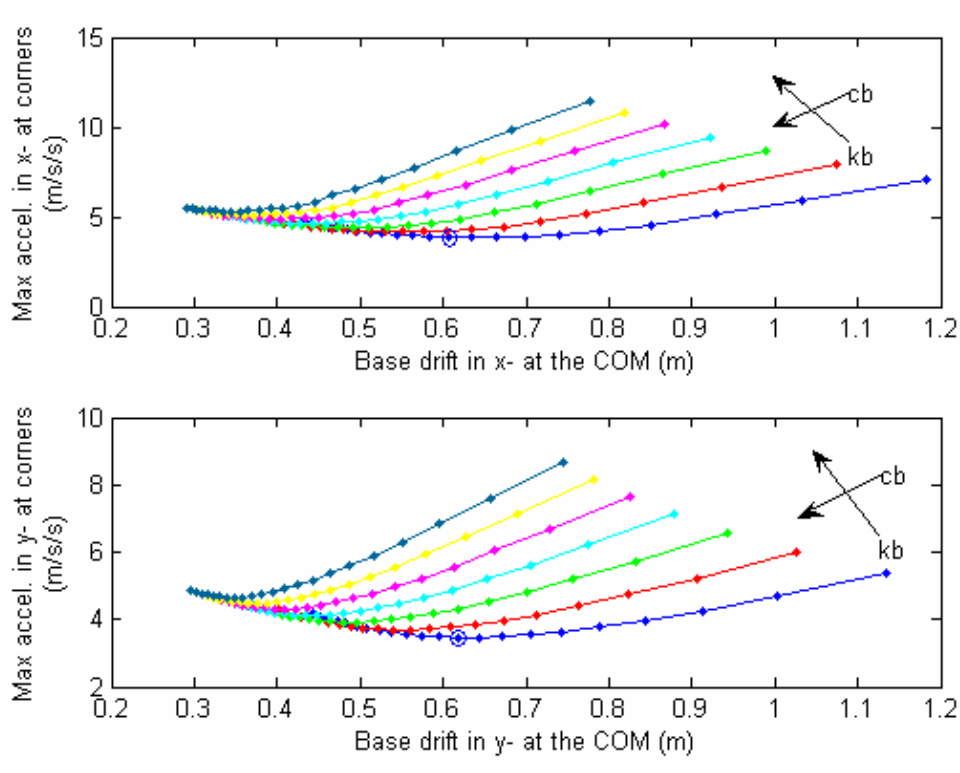

Figure 3-5 Maximum RMS of the Base Drift - Acceleration Curves of the 3D system

Similarly, optimal damping coefficients c_b exist for each k_b. The determination of k_b relies on the earthquake statistical properties, because seismic design is up to the excitation the structure will experience. As seven design earthquakes have been provided for this benchmark problem, their response spectra are computed and plotted. Figure 3-6 shows the $\xi = 10\%$ damped response spectra.

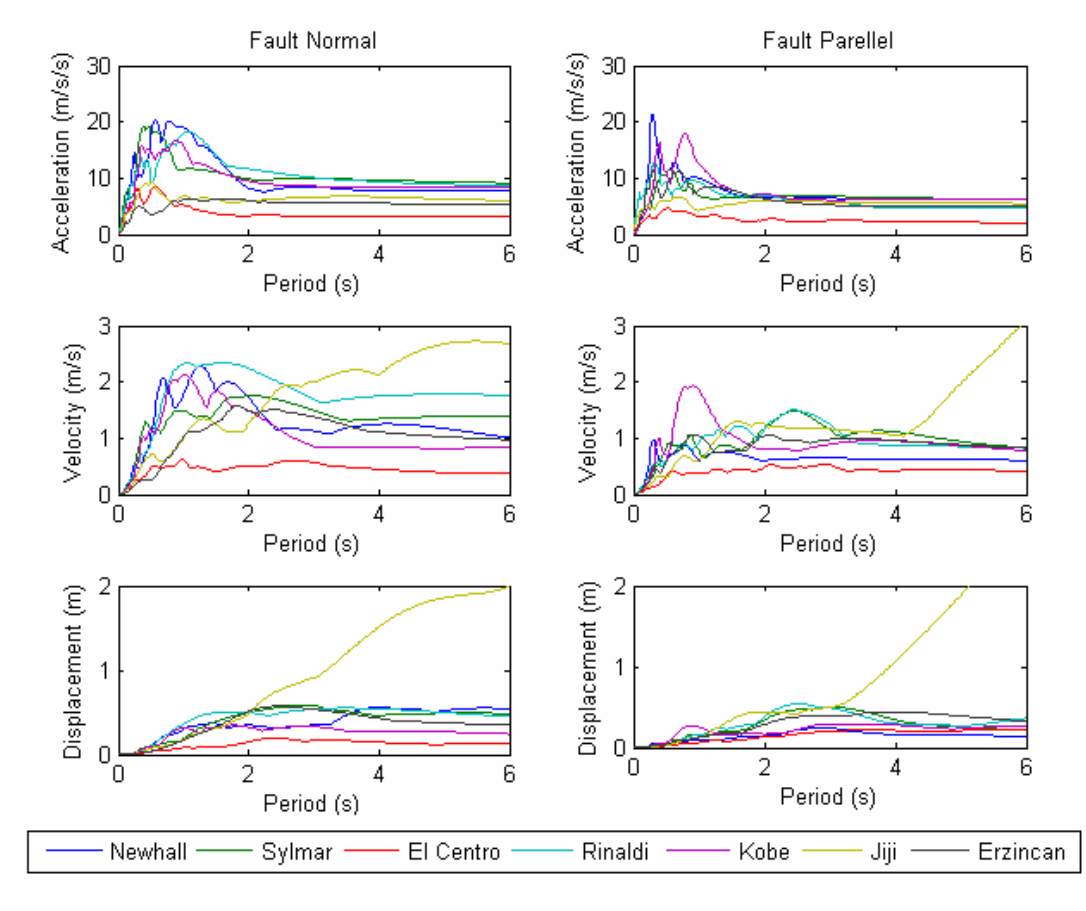

Figure 3-6 10% Damped Response Spectra of the Design Earthquakes

The dominant periods of these earthquakes are from about 1 sec to nearly 2 sec. The Ji-Ji earthquake is exceptionally extreme. Figure 3-6 shows that SDOF systems that have natural periods longer than 2 sec could shift their dynamics out of the high acceleration response region.

Most isolation periods of base-isolated buildings are between 2 and 3 sec, though some stiff isolation systems results in isolation as low as 0.6 sec (Makris, 1997). Although highly isolated structures (smaller k_b or longer period) are preferable for decreasing accelerations, the base deformations are usually so large that they lead to bearing damage. More control effort is required to decrease the deformation. For the eight-story building, fundamental periods of 2.28 sec (*x*-), 2.18 sec (*y*-), and 1.86 sec (*r*-), corresponding to $k_b = 2119$ kN/m (the blue line) in Figure 3-5, is an appropriate design choice. At this period, the $\xi = 10\%$

SDOF system will experience 15-55 cm base displacement, and specifically, 35 cm for the Newhall earthquake. With smart control force applied, the displacements are hopefully limited to 45 cm for most damaging near-field earthquakes. In Figure 3-5, the optimal damping for the $k_b = 2119$ kN/m curve should be the tenth point from right (circled in Figure 3-5), corresponding to a damping coefficient of $c_b = 241.44$ kN.sec/m and damping ratios of $\xi_1 = 14.7\%$ (*x*-direction), $\xi_2 = 14.9\%$ sec (*y*-direction), and $\xi_3 = 17.9\%$ (*r*-direction). It is appropriate for a traditional passive isolation design for near-source protection. The damping ratios are less than 20%, so it is reasonable if additional damping from an MR damper is to be applied on this passive optimal system.

Large bearing dampings also increase the modal damping ratios of the first flexible modes to $\xi_4 = 12.7\%$ (*x*-direction), $\xi_5 = 12.0\%$ sec (*y*-direction), and $\xi_6 = 13.2\%$ (*r*-direction) from 5%, respectively. Damping ratios of other modes do not change significantly. It is important to keep this fact in mind because the approximate methods to be used later have relatively larger errors to highly damped modes.

3.3 Summary

This chapter introduces the smart base isolation benchmark problem, its equations of motion, state and output equations, evaluation criteria and other constraints to be considered. Further, the optimal passive base isolation system is also defined and a method to design the optimal passive system is proposed. The design procedures are illustrated for the one-dimensional system and then applied to the three-dimensional system.

Chapter 4

Actuator and Sensor Placement Using Modal Approach

A large number of techniques for the optimal placement of sensors and actuators in a vibration control system have been developed in recent years. Many of these methods are based on the concepts of controllability and observability. Controllability and observability properties can be shaped by changing the configuration of the actuators and sensors. This is an optimization problem that is closely related to achieving high performance with minimal cost. For example, a system in which actuators and sensors are placed at or near the nodes of vibration modes may require an exceptionally large control force, or even may be uncontrollable. This approach is facilitated by the establishment of explicit relationships between controllability and observability and vibration modes (Longman et al, 1982; Moore, 1981; Hamdan and Nayfeh, 1989, etc), among which Hamdan and Nayfeh's measures are particularly attractive. They introduced a generalized angle between the two vector spaces on which controllability and observability are based: the left eigenvectors and the column vectors of input influence matrix, and the right eigenvectors and the column vectors of output measurement matrix. Choi et al (2000) further improved the method by extending the results to be used with a balanced coordinate system, and introducing the magnitude of the measures, the norms of eigenvectors, when used in that coordinate system. A balanced coordinate system is desirable because it ensures that the system is equally controllable and observable.

This study will use another controllability-observability based approach proposed by Panossian et al. (1998) in a practical application and described in detail by Gawronski (1998). This approach involves the computation of the system norms of each device location for selected modes, and then grades them according to their participation in the system norm. It agrees with the control objective of the LQR algorithm to be used in this study, whose cost function is actually a 2-norm, and it is relatively simple compared with

other algorithms. Silva and Lopes (2004) adopted the H_∞ norm of this approach in their study in the second phase, actuator and sensor location selection, of their smart structure design.

The method proposed in this chapter uses the Hankel singular norm instead of the H_∞ and H_2 norms. The Hankel norm is advantageous because it reflects both controllability and observability, and is invariant under linear similarity transformations. The placement indices proposed by Gawronski (1998) took into consideration the closed-loop effects when the actuators are not placed at the disturbance locations and sensors are not at the performance evaluation locations in index normalization. To make the approach more applicable to civil engineering problems, this study considers only the case when the actuators are collocated with disturbances and sensors collocated with performances. This assumption simplifies the normalization procedure, but still could reflect some closed-loop effects, as discussed in section 4.1, though it might decrease the accuracy. The simplified methodology is applied to the smart control device and sensor placement in the base isolation benchmark problem in the last section of this chapter.

4.1 Effects of the Cross Couplings on Norms in the Feedback Loop

A structure's inputs are composed of both disturbance and control inputs, and plant outputs include regulated outputs and measurements. In engineering practice, control devices and sensors are placed at available locations, not necessarily collocated with the disturbance and outputs used for performance evaluations. It is shown that the cross couplings between the inputs and outputs all impact on the structural norms due to the feedback loop (Gawronski, 1998), so it is necessary to examine these effects for placement rules based on properties of the structural norms.

First, define a general model of a feedback control system that explicitly includes the desired inputs and outputs. The block diagram of a general feedback control system is shown Figure 4-1.

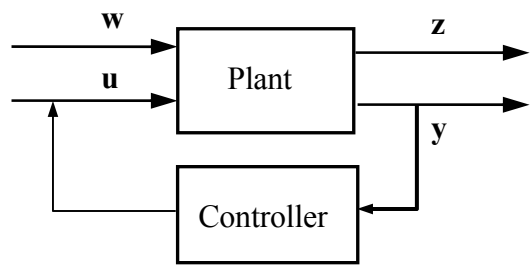

Figure 4-1 General Diagram of a Feedback Control System

$\mathbf{w}$ is the general disturbance. The control input $\mathbf{u}$ to the plant is generated by the controller. The output consists of the regulated output $\mathbf{z}$ and the measurement output $\mathbf{y}$. The feedback loop is closed between the measurement output and controller (actuator). In general, the measurement output is distinct from the regulated output, though they may be identical in some applications. The state model of the plant for the closed-loop system in Figure 4-1 is

$$\dot{\mathbf{x}}(t) = \mathbf{A}\mathbf{x}(t) + \begin{bmatrix}\mathbf{B} & \mathbf{E}\end{bmatrix}\begin{bmatrix}\mathbf{u}(t)\\ \mathbf{w}(t)\end{bmatrix} \tag{4-1}$$

$$\begin{bmatrix}\mathbf{z}(t)\\ \mathbf{y}(t)\end{bmatrix} = \begin{bmatrix}\mathbf{C}_\mathbf{z}\\ \mathbf{C}_\mathbf{y}\end{bmatrix}\mathbf{x}(t) + \begin{bmatrix}\mathbf{D}_\mathbf{z} & \mathbf{E}_\mathbf{z}\\ \mathbf{D}_\mathbf{y} & \mathbf{E}_\mathbf{y}\end{bmatrix}\begin{bmatrix}\mathbf{u}(t)\\ \mathbf{w}(t)\end{bmatrix} \tag{4-2}$$

Let $\mathbf{G}_{\mathbf{wz}}$ be the transfer function matrix from $\mathbf{w}$ to $\mathbf{z}$, $\mathbf{G}_{\mathbf{wy}}$ be the transfer function matrix from $\mathbf{w}$ to $\mathbf{y}$, $\mathbf{G}_{\mathbf{uz}}$ be the transfer function matrix from $\mathbf{u}$ to $\mathbf{z}$, and $\mathbf{G}_{\mathbf{uy}}$ be transfer function matrix from $\mathbf{u}$ to $\mathbf{y}$. These open-loop transfer functions are expressed by

$$\begin{aligned}
\mathbf{G}_{\mathbf{uz}}(s) &= \mathbf{C}_\mathbf{z}(s\mathbf{I}-\mathbf{A})^{-1}\mathbf{B} + \mathbf{D}_\mathbf{z}\\
\mathbf{G}_{\mathbf{uy}}(s) &= \mathbf{C}_\mathbf{y}(s\mathbf{I}-\mathbf{A})^{-1}\mathbf{B} + \mathbf{D}_\mathbf{y}\\
\mathbf{G}_{\mathbf{wz}}(s) &= \mathbf{C}_\mathbf{z}(s\mathbf{I}-\mathbf{A})^{-1}\mathbf{E}_\mathbf{z} + \mathbf{E}_\mathbf{z}\\
\mathbf{G}_{\mathbf{wy}}(s) &= \mathbf{C}_\mathbf{y}(s\mathbf{I}-\mathbf{A})^{-1}\mathbf{E}_\mathbf{y} + \mathbf{E}_\mathbf{y}
\end{aligned} . \tag{4-3}$$

Denote the Laplace transforms of the vectors $\mathbf{y}$, $\mathbf{z}$, $\mathbf{u}$, and $\mathbf{w}$ with capital letters. The transfer function of the plant is then

$$\begin{bmatrix} \mathbf{Z} \\ \mathbf{Y} \end{bmatrix} = \mathbf{G}(s)\begin{bmatrix} \mathbf{U} \\ \mathbf{W} \end{bmatrix} = \begin{bmatrix} \mathbf{G}_{\mathbf{uz}} & \mathbf{G}_{\mathbf{wz}} \\ \mathbf{G}_{\mathbf{uy}} & \mathbf{G}_{\mathbf{wy}} \end{bmatrix}\begin{bmatrix} \mathbf{U} \\ \mathbf{W} \end{bmatrix} = \begin{bmatrix} \mathbf{G}_{\mathbf{uz}}\mathbf{U} + \mathbf{G}_{\mathbf{wz}}\mathbf{W} \\ \mathbf{G}_{\mathbf{uy}}\mathbf{U} + \mathbf{G}_{\mathbf{wy}}\mathbf{W} \end{bmatrix}. \tag{4-4}$$

The transfer function of the controller is

$$\mathbf{U} = \begin{bmatrix} \mathbf{G}_{\mathbf{cr}} & \mathbf{G}_{\mathbf{cy}} \end{bmatrix}\begin{bmatrix} \mathbf{R} \\ \mathbf{Y} \end{bmatrix} = \mathbf{G}_{\mathbf{cr}}\mathbf{R} + \mathbf{G}_{\mathbf{cy}}\mathbf{Y}\ . \tag{4-5}$$

Substituting $\mathbf{Y}$ from the second equation of (4-4) into equation (4-5) yields

$$\mathbf{U} = (\mathbf{I} - \mathbf{G}_{\mathbf{cy}}\mathbf{G}_{\mathbf{uy}})^{-1}\mathbf{G}_{\mathbf{cy}}\mathbf{G}_{\mathbf{wy}}\mathbf{W}\ . \tag{4-6}$$

Substituting equation (4-6) into the first equation of (4-4) yields the closed-loop transfer function from $\mathbf{w}$ to $\mathbf{z}$ of the feedback control system

$$\mathbf{Z} = (\mathbf{G}_{\mathbf{uz}}(\mathbf{I} - \mathbf{G}_{\mathbf{cy}}\mathbf{G}_{\mathbf{uy}})^{-1}\mathbf{G}_{\mathbf{cy}}\mathbf{G}_{\mathbf{wy}} + \mathbf{G}_{\mathbf{wz}})\mathbf{W}\ . \tag{4-7}$$

If $\mathbf{G}_{\mathbf{cy}} = \mathbf{K}(s)$, the transfer function diagram representing Figure 4-1 is shown in Figure 4-2.

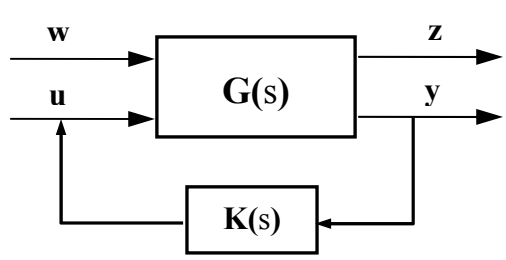

Figure 4-2 Diagram of a Constant-Gain Feedback Control System

The closed-loop transfer function from $\mathbf{w}$ to $\mathbf{z}$ then becomes

$$\mathbf{G}_{\mathbf{wz-cl}} = \mathbf{G}_{\mathbf{uz}}(\mathbf{I} - \mathbf{G}_{\mathbf{cy}}\mathbf{G}_{\mathbf{uy}})^{-1}\mathbf{K}\mathbf{G}_{\mathbf{wy}} + \mathbf{G}_{\mathbf{wz}} . \tag{4-8}$$

Equation (4-8) shows that the controller impacts the closed-loop performance not only through the action from $\mathbf{u}$ to $\mathbf{y}$, but also through the cross-actions from $\mathbf{u}$ to $\mathbf{z}$ and $\mathbf{w}$ to $\mathbf{y}$. If the transfer function matrices $\mathbf{G}_{wy}$ or $\mathbf{G}_{\mathbf{uz}}$ were zero, the controller could not reach the responses $\mathbf{z}$. Therefore, for non-collocated systems, the actuator and sensor connectivity $\mathbf{G}_{\mathbf{uy}}$ is not the only factor that determines the closed-loop performance. This makes the placement problem complicated because the above effort would be in vain if $\mathbf{G}_{\mathbf{wy}}$ or $\mathbf{G}_{\mathbf{uz}}$ decreases while the importance of locations (placement indices) is determined by large $\mathbf{G}_{\mathbf{uy}}$.

Fortunately, this is not the case. Denote subscript *i* for the *i*th mode, the following multiplicative property of modal norms holds (Gawronski, 1998)

$$\left\|\mathbf{G}_{\mathbf{wz},i}\right\|\left\|\mathbf{G}_{\mathbf{uy},i}\right\| \cong \left\|\mathbf{G}_{\mathbf{wy},i}\right\|\left\|\mathbf{G}_{\mathbf{uz},i}\right\| \tag{4-9}$$

where $\|.\|$ denotes either H_2, H_∞, or Hankel norms, and subscript *i* denotes the *i*th mode.

This property can be shown directly using the approximate relationship between the transfer function and the norms (equations (2-38) and (2-39)). This property indicates that for each mode the product of norms of the performance loop (from disturbance to response) and the control loop (from actuators to sensor response) is approximately equal to the product of the norms of the cross-couplings between the disturbance and sensors, and between the actuators and performance. It also indicates that improvement in $\mathbf{G}_{\mathbf{uy}}$ automatically leads to improvement in $\mathbf{G}_{\mathbf{wy}}$ and $\mathbf{G}_{\mathbf{uz}}$. Thus, the actuator and sensor location problems can be performed by manipulating $\mathbf{G}_{\mathbf{uy}}$ alone. This conclusion is important for the placement problem. It means the placement strategy proposed in sections 4.2 and 4.3 will be applicable for non-collocated systems.

4.2 Placement Indices

To define the controllability-observability based actuator and sensor location model, consider the system defined by equations (2-5a, b). Information about the location and size of the actuator is contained in the control input influence matrix $\mathbf{B}$. Information about the sensor location is contained in the matrix $\mathbf{C}$. Because there is no explicit disturbance in equations (2-5a, b), the placement strategy here only considers the case that actuators are collocated with the disturbance, and sensors are collocated with the performance outputs.

Note that, for the purpose of describing the methodology, the term "actuator" will be used for generality, although the focus of this thesis is on smart control devices which are not technically actuators. Also sensors mainly refer to accelerometers in this study.

For this benchmark problem, control devices are required to be placed at base level and, conveniently, at bearing locations. So there are 92 candidate locations for control devices. Accelerometers may be placed at the four corners (Figure 3-1) of each floor including the base. Each corner has one accelerometer in the *x*- and one in the *y*-direction, giving eight available accelerometer locations for each floor. Note that three sensors would be enough for each floor to capture the responses because each floor has three DOFs. Thus, the problem of placement is to determine a reasonable subset of locations for control devices that offer high controllability of the desired modes, and a reasonable subset of sensors that offer high observability in detection of the desired modes.

It is known that controllability and observability for linear systems are conveniently captured by the singular values of the grammians or Hankel singular values. Hankel singular values do not vary with coordinate transformations. An almost-balanced realization can be obtained without changing the $\mathbf{A}$ matrix. A logical conclusion to draw is that Hankel norms are appropriate measures for placement.

Consider a model of a structure in modal state-space representation $(\mathbf{A}_m, \mathbf{B}_m, \mathbf{C}_m)$. The Hankel norm of the *i*th mode is given by

$$\|G_i\|_h = \gamma_i \cong \frac{\|\mathbf{B}_{mi}\|_2 \|\mathbf{C}_{mi}\|_2}{4\xi_i \omega_i}. \tag{4-10}$$

Quantitatively, the Hankel norm is approximately one-half of the H_∞ norm, that is, about half of the resonant peak of transfer function (equation (2-39)).

The question arises as to how the Hankel norm of a structure with a single control device or sensor relates to the Hankel norm with a set of *s* actuators or *r* sensors. It turns out that, for each mode, the Hankel norm with a set of actuators or sensors is the *rms* sum of the Hankel norm with each single actuator or sensor from this set, i.e.,

$$\gamma_i = \sqrt{\sum_{j=1}^{s} \gamma_{ij}^2} \text{ or } \gamma_i = \sqrt{\sum_{k=1}^{r} \gamma_{ik}^2} . \tag{4-11}$$

Finally, the Hankel norm of the system is the largest norm of its mode, i.e.,

$$\|G\|_h \cong \max_i \|G_i\|_h = \gamma_{\max} = 0.5\|G\|_\infty . \tag{4-12}$$

where $\gamma_{\max}$ is the largest Hankel singular value of the system. Equations (4-10), (4-11) and (4-12) provide a means to normalize the indices using Hankel norms so that the indices are between 0 and 1.

For actuator placement, the index σ_{ij} that evaluates the *j*th actuator at the *i*th mode in terms of Hankel norm is defined with respect to all modes and control devices as

$$\sigma_{ij} = \frac{\|G_{ij}\|_h}{\|G\|_h} . \tag{4-13}$$

Similarly, in the sensor placement, the placement index that evaluates the *k*th sensor at the *i*th mode is defined as

$$\sigma_{ik} = \frac{\|G_{ik}\|_h}{\|G\|_h} . \tag{4-14}$$

It is convenient to arrange the placement indices in the placement index matrix. The resulting actuator placement index matrix is

$$\begin{array}{cc} \begin{bmatrix} \sigma_{11} & \sigma_{21} & \cdots & \sigma_{i1} & \cdots & \sigma_{n1} \\ \sigma_{21} & \sigma_{22} & \cdots & \sigma_{i2} & \cdots & \sigma_{n2} \\ \cdots & \cdots & \cdots & \cdots & \cdots & \cdots \\ \sigma_{1j} & \sigma_{2j} & \cdots & \sigma_{ij} & \cdots & \sigma_{nj} \\ \cdots & \cdots & \cdots & \cdots & \cdots & \cdots \\ \sigma_{1s} & \sigma_{2s} & \cdots & \sigma_{is} & \cdots & \sigma_{ns} \end{bmatrix} & \begin{array}{l} \\ \\ \\ \Leftarrow j\text{th actuator} \\ \\ \\ \end{array} \\ \Uparrow & \\ i\text{th mode} & \end{array} \tag{4-15}$$

The sensor placement index matrix is

$$\begin{array}{cc} \begin{bmatrix} \sigma_{11} & \sigma_{21} & \cdots & \sigma_{i1} & \cdots & \sigma_{n1} \\ \sigma_{21} & \sigma_{22} & \cdots & \sigma_{i2} & \cdots & \sigma_{n2} \\ \cdots & \cdots & \cdots & \cdots & \cdots & \cdots \\ \sigma_{1k} & \sigma_{2k} & \cdots & \sigma_{ik} & \cdots & \sigma_{nk} \\ \cdots & \cdots & \cdots & \cdots & \cdots & \cdots \\ \sigma_{1s} & \sigma_{2s} & \cdots & \sigma_{is} & \cdots & \sigma_{ns} \end{bmatrix} & \begin{array}{l} \\ \\ \\ \Leftarrow k\text{th sensor} \\ \\ \\ \end{array} \\ \Uparrow & \\ i\text{th mode} & \end{array} \tag{4-16}$$

The placement index can be studied from two points of views. First, one may examine the importance of a single actuator/sensor over all modes

$$\text{Actuator index vector (column): } \sigma_A = \begin{bmatrix} \sigma_{A1} & \sigma_{A2} & \cdots & \sigma_{As} \end{bmatrix}^T \tag{4-17}$$

$$\text{Sensor index vector (column): } \sigma_S = \begin{bmatrix} \sigma_{S1} & \sigma_{S2} & \cdots & \sigma_{Sr} \end{bmatrix}^T \tag{4-18}$$

where the kth entry is the placement index of the kth control device/sensor. In the case of the Hankel norm,

$$\sigma_{Ak} = \max_i(\sigma_{ik}) \,,\; \sigma_{Sk} = \max_i(\sigma_{ik}) \,. \tag{4-19}$$

This method focuses on the overall importance of an actuator or sensor regardless of its importance to a specified mode, so it could possibly result in large indices from the higher modes. It does not agree with the design goal for base isolation systems where the first several modes dominate, so it is not adopted in this study.

One may examine the importance of all control devices/sensors to a single mode using

$$\text{Actuator index vector (row): } \sigma_{Am} = \begin{bmatrix} \sigma_{Am1} & \sigma_{Am2} & \cdots & \sigma_{Amn} \end{bmatrix} \tag{4-20}$$

$$\text{Sensor index vector (row): } \sigma_{Sm} = \begin{bmatrix} \sigma_{Sm1} & \sigma_{Sm2} & \cdots & \sigma_{Smn} \end{bmatrix} \tag{4-21}$$

where

$$\sigma_{Ami} = \sqrt{\sum_j^s \sigma_{ij}^2} \,, \qquad \sigma_{Smi} = \sqrt{\sum_k^r \sigma_{ik}^2} \,. \tag{4-22}$$

Herein this second approach is adopted to determine the index vector for every available device location. The placement index characterizes the contribution of each device to each mode, so it serves as a placement solution. Locations with small indices for lower modes would be removed.

4.3 Placement Strategy

When one considers the placement of a very large number of candidate actuators and sensors, the maximum placement indices alone may not be a sufficient criterion (Gawronski, 1998). Suppose that a specific location gives a high performance index. Inevitably, locations close to it will have a high performance index as well. But the

locations in the neighborhood are not necessarily the best choice because the performance gains achieved using devices at these locations can also be achieved by appropriate gain adjustments (Gawronski, 1998). The best strategy is to find locations that cannot be compensated for by gain adjustment. Naturally, correlation coefficients are used to remove highly correlated locations. Below is a description of the approach recommended by Gawronski (1998).

Define a vector of the squares of the *i*th Hankel modal norms,

$$g_i = \begin{bmatrix} \|G_{i1}\|_h^2 \\ \|G_{i2}\|_h^2 \\ \vdots \\ \|G_{in}\|_h^2 \end{bmatrix} \tag{4-23}$$

where $\|G_{ik}\|_h$ is the Hankel norm of the *k*th mode at the *i*th control device or sensor. The correlation coefficient ρ_{ik} is defined as

$$\rho_{ik} = \frac{g_i^T g_k}{\|g_i\|_2 \|g_k\|_2}, \quad i = 1, \cdots, r, \quad k = i+1, \cdots, r. \tag{4-24}$$

Given a small positive number ε, say $\varepsilon = 0.001$, denote the membership index $I(k)$, $k = 1, \cdots, r$, where r is the number of sensors (control devices). This index is determined as

$$I(k) = \begin{cases} 0 & \rho_{ik} > 1-\varepsilon \quad and \quad \sigma_k < \sigma_i \quad for \quad k > i \\ 1, & elsewhere \end{cases}. \tag{4-25}$$

If $I(k) = 1$, then the *k*th sensor (actuator) is accepted. If $I(k) = 0$, the *k*th sensor (actuator) is rejected. In the case of $I(k) = 0$, the two locations *i* and *k* are either highly correlated $(\rho_{ik} > 1-\varepsilon)$, or the *i*th location has a higher performance σ_i.

Based on the above analysis the placement strategy is established. For this 3D base isolation benchmark problem, sensor placement is more flexible, so actuator locations are decided first. The placement procedure is described as follows:

- Place the control devices in order at the 92 bearing locations, one in the *x*-direction and one in the *y*-direction. Assume each admissible sensor location has two sensors, one in the *x*- and one in the *y*-direction, so that the $\mathbf{C}_m$ matrix is fixed. For each location, compute the modal $\mathbf{B}_m$ matrix and then the Hankel placement indices for all modes, until the 92×27 (total 27 modes) placement index matrix is formed.
- Roughly choose 20~25 locations with the largest placement indices in the lower modes.
- Check the correlation coefficients for the selected locations. Reject actuators with $I(k) = 0$. The resulting values (say, 10) are the final locations. If the number is less then 10, add more locations in step 2; if the number is more than 10, decrease ε so that rejection condition is stricter.
- Fix the $\mathbf{B}_m$ matrix for the resulting set of actuator locations. Compute the floor sensor placement indices, assuming sensors are put at all four corners on this floor while none are on other floors to determine $\mathbf{C}_m$ matrix. Repeat for each floor until the 9×27 placement index matrix is formed.
- Reject insignificant floors that have very low sensor placement indices.
- For the remaining floors, compute the corner placement indices one by one. Retain the non-correlated corners.

All control device and sensor locations are thus determined following the above procedure.

4.4 Control Device and Sensor Placement for the Benchmark Problem

The 3D dynamics of the benchmark problem have been introduced in Chapter 3. The parameters of the superstructure are known. The optimal isolation parameters, bearing stiffness and damping coefficient of the linear elastomeric bearings, have been determined

in Chapter 3. They are: $k_b = 2119.4$ kN/m, $c_b = 241.44$ kN-s/m. Matrices $\mathbf{B}_m$ and $\mathbf{C}_m$ in the computation of Hankel norms and placement indices are dependent upon the device locations.

Control device (MR damper) locations are to be determined first. Assume accelerometers are placed at all available locations (named as full sensor placement here). Consider control devices placed at bearing location #1, one in the *x*-direction and one in the *y*-direction. Follow the placement procedures summarized in section 4.3. Use equations (4-10), (4-13) and (4-14) to compute placement indices of all modes. Repeat this process for all other 91 bearing locations. The resulting control device placement index matrix has a dimension of 92×27. Figure 4-3 shows the indices of first 18 modes (first 6 modes in each of the *x*-, *y*- and *r*-directions, versus bearing locations.

As shown in Figure 4-3, locations with large placement indices almost coincide for all modes, though they may vary in the *x*-, *y*- and *r*-directions. Comparing Figure 4-3 and Figure 3-1, it is found that these locations are on the outer base corners and the south edge (see Appendix A for corner numbers). Particularly, locations near corner 2 (bearing 19) and 4 (bearing 80) and the south edge influence the *r*-direction modes most. They are the farthest points away from the center of mass. Locations that influence the *x*-direction modes (blue) are along or near the south edge (bearing 1-3, 31, 60-65, 90, etc.). These locations are near the *x*-axis across the center of the mass. It is not apparent what locations influence the low *y*-direction modes most in Figure 4-3. One reason for this is that control devices are placed in the *x*- and *y*-directions at the same time when computing the placement indices. Because the structure is irregular, the *x*- device would also impact on the *y*- mode, and vice versa. The structure is more eccentric in the *x*-direction than in the *y*-direction, so the result of interaction is that the *y*-direction indices are less significant relative to the *x*-direction indices for this strategy. If the *y*-direction indices were examined with the control devices placed in the *y*-direction only, things may be different. Anyway, for the results shown in Figure 4-3, it is preferable to include points near the *y*-axis across the center of mass and the other corner (corner 1), though they do not show high indices for this placement strategy. Taking into account all possible high correlations, primary

selection also includes some inner locations and the inner corner. These location numbers are (22 in total):

1, 2, 3, 12, 13, 19, 30, 31, 40, 43, 49, 62, 63, 64, 73, 74, 75, 80, 81, 87, 91, 92

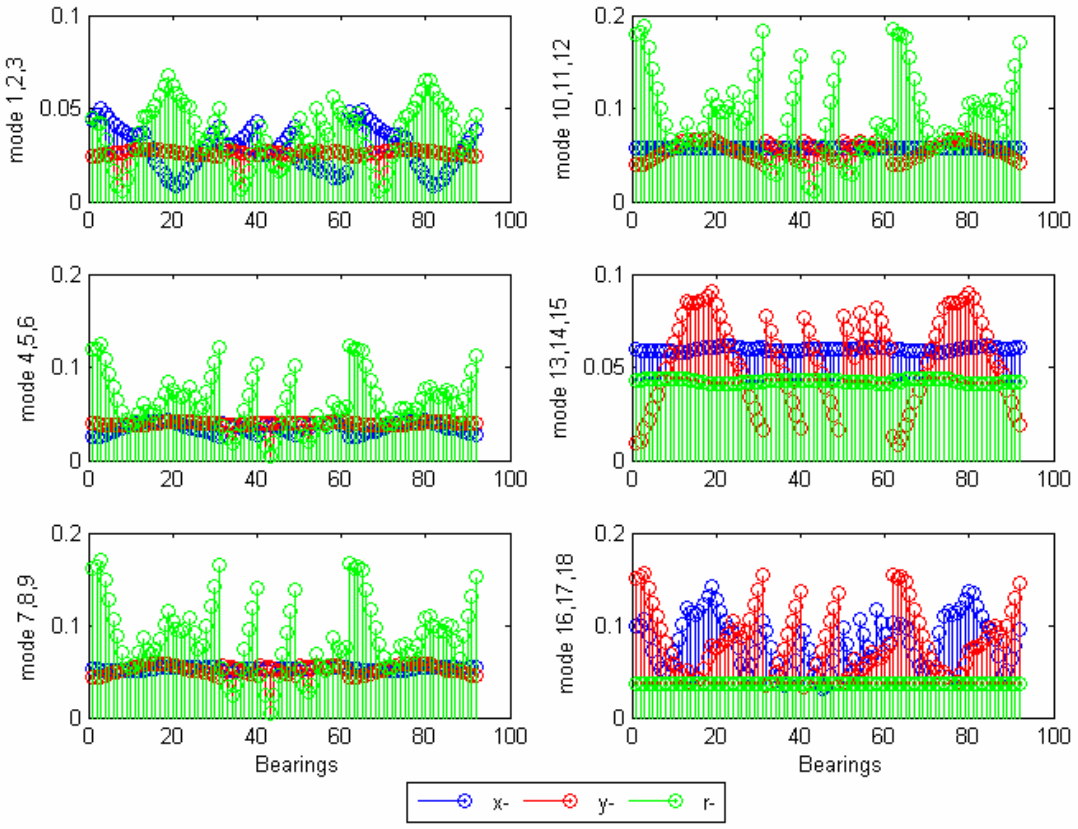

Figure 4-3 Control Device Placement Indices vs. Control Device Locations

The benchmark constraints require that the control force not exceed the bearing force, and it is desirable not to exceed 10% of the total weight of the structural system for practicality. The total weight of the building is 2.031×10^5 kN. Simulations show that the maximum bearing forces for the passive isolation case are 33%, 18%, and 21% of the total weight in the *x*-, *y*-, and *r*-directions, respectively. As the MR dampers to be used in this study have capacity of 1000 kN, the total number of MR dampers should not exceed 40. So in this study, it was decided to use 40 MR dampers.

With the 22 primary selections, the next step is to reject the highly correlated locations. For this problem, the small number $\varepsilon = 0.001$; that is, locations i and k are regarded as highly correlated if $r_{ik} > 0.999$. Table 4-1 provides the membership indices (those with $I(k) = 0$ are to be rejected).

Table 4-1 Membership Index of the Control Device Locations

location	1	2	3	12	13	19	30	31	40	43	49	62	63	64	73	74	75	80	81	87	91	92
1	0	1	1	1	1	1	1	1	1	1	1	1	1	1	1	1	1	1	1	1	1	0
2		0	1	1	1	1	1	1	1	1	1	1	0	0	1	1	1	1	1	1	1	0
3			0	1	1	1	1	0	1	1	1	0	0	0	1	1	1	1	1	1	1	1
12				0	1	1	1	1	1	1	1	1	1	1	1	1	1	1	1	1	1	1
13					0	1	1	1	1	1	1	1	1	1	1	1	1	1	1	1	1	1
19						0	1	1	1	1	1	1	1	1	1	1	1	0	0	1	1	1
30							0	1	0	1	0	1	1	1	1	1	1	1	1	1	0	1
31								0	1	1	1	1	0	0	1	1	1	1	1	1	1	0
40									0	1	0	1	1	1	1	1	1	1	1	1	0	1
43										0	1	1	1	1	1	1	1	1	1	1	1	1
49											0	1	1	1	1	1	1	1	1	1	0	1
62												0	0	0	1	1	1	1	1	1	1	0
63													0	1	1	1	1	1	1	1	1	0
64														0	1	1	1	1	1	1	1	0
73															0	1	1	1	1	1	1	1
74																0	1	1	1	1	1	1
75																	0	1	1	1	1	1
80																		0	0	1	1	1
81																			0	1	1	1
87																				0	1	1
91																					0	1
92																						0

Based on Table 4-1, the original locations (1st column) and highly correlated locations (2nd column, $I(k) = 0$) are shown in Table 4-2. Location numbers that do not show up in this table, such as 12, 13, 72, 73, 74, have $I(k) = 1$ and thus are accepted.

Table 4-2 Correlation Membership of Control Device Locations

Original location	Membership Locations
1	92
2	92
3	31, 62, 63, 64
19	80, 81
30	40, 49
31	63, 64
40	49

Eliminating the highly correlated locations leaves 12 remaining locations. Considering planar distribution, 10 locations are finally selected. They are:

3, 13, 19, 30, 31, 43, 65, 74, 81, 87.

Placing two MR dampers in the *x*-direction and two in the *y*-direction at each location, the total number of control devices (MR dampers) is 40. The schematic of the control device installation is shown in Figure 4-4 and the planar placement on the base level is shown in Figure 4-5.

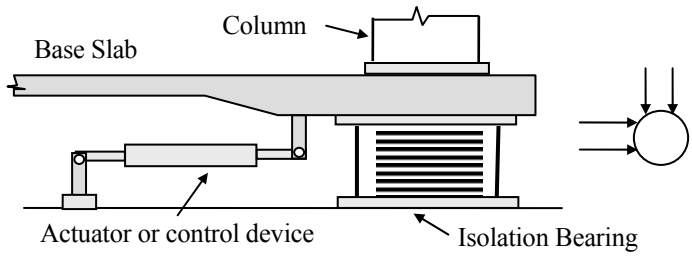

Figure 4-4 Schematic of Control Device Installation

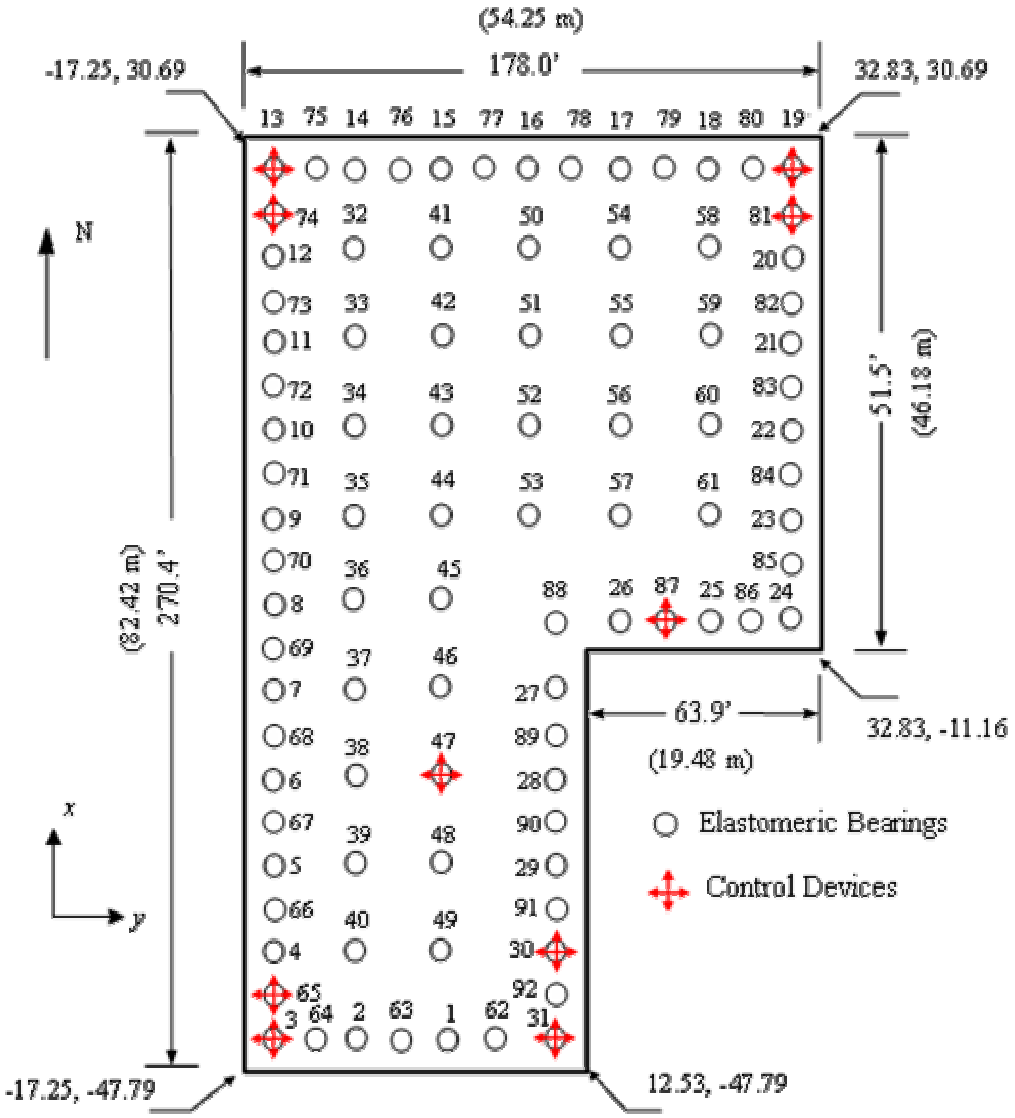

Figure 4-5 Plan View of the Base Level and the Control Device Locations

Full sensor placement was assumed in the determination of the control device locations. Now that the control device locations have been determined, the next step is to examine the sensor (accelerometer) floor placement indices according to step 4 in placement procedures. Figure 4-6 shows the first 18 mode indices versus floor numbers. Floor 0 represents the base.

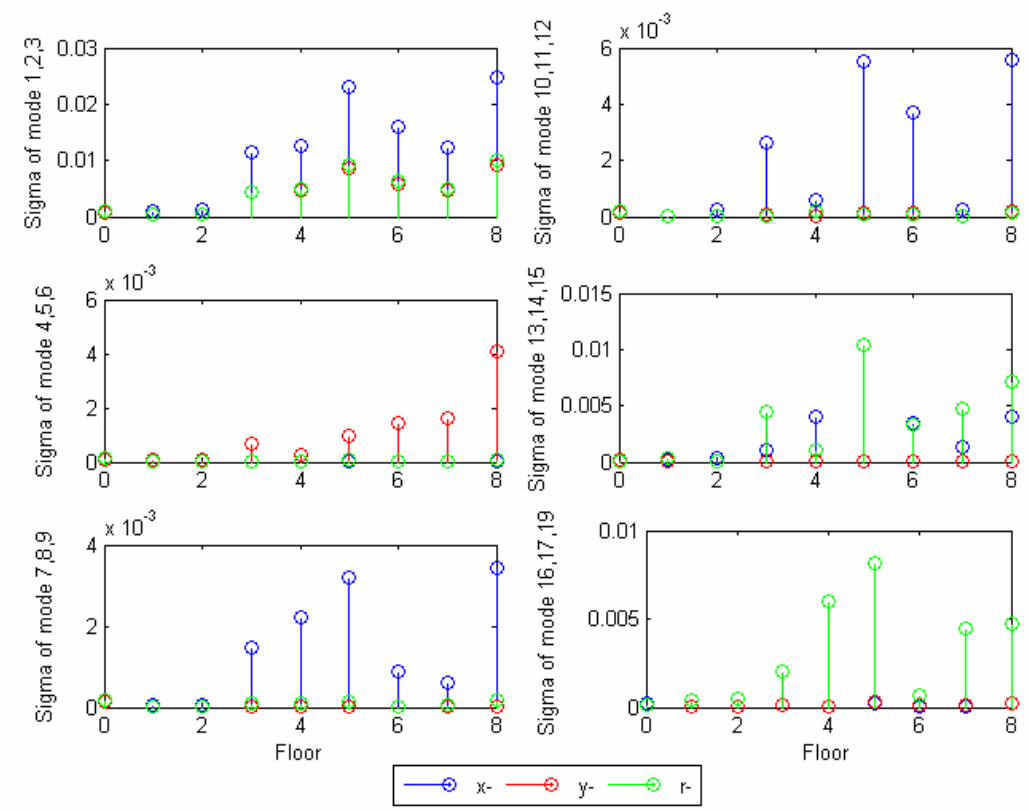

Figure 4-6 Sensor Placement Indices vs. Floors

It is clear that floors 1 and 2 and the base always have small indices for modes 1-19. This result indicates that sensors placed on the two floors do not correspond to high observability, and thus are not very important in detecting response signals. So accelerometers will be placed on floors 3 to 8.

There are four corners, and thus eight available locations for accelerometers for each floor, some of which are redundant. Three accelerometers per floor (24 total accelerometers) would provide a measure of all motions of that particular floor. So the following step is to compute the corner indices of floors 3 to 8. Place two accelerometers (one in the *x*-direction and one in the *y*-direction) at each corner of floor 3 and compute the indices and then repeat this procedure for the remaining floors (4~8).

Figure 4-7 shows the sensor corner indices of floor 3. Corner 4 (pink) has a different index than corners 1, 2, and 3, which are identical. For floors 4~8, computation shows that the indices corresponding to the four corners are exactly equal to each other. For computing

convenience, accelerometers are placed at corners 2 and 4 from floor 3 through 8 in this benchmark problem because the two corners are farthest from the center of the mass and thus the responses are large. In addition, displacement sensors are placed at corners 2 and 4 at the isolation level to measure the bearing deformations. They are necessary for the determination of the control force. This completes the sensor placement. Note that the number of accelerometers might be further reduced if the indices were computed with accelerometers placed at single directions, because currently there are four accelerometers at each floor.

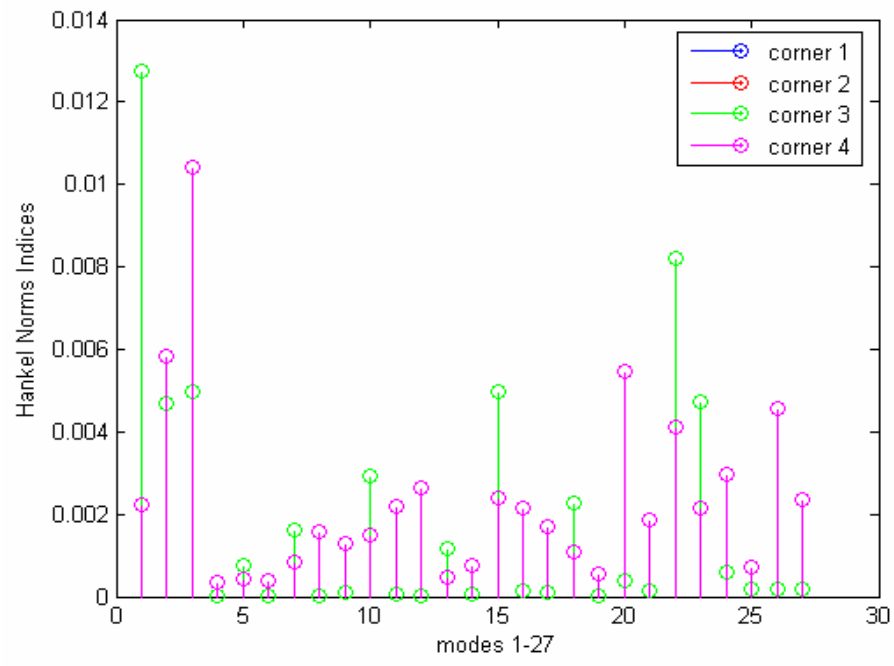

Figure 4-7 Sensor Corner Placement Indices for Floor 3

Figure 4-8 shows the locations of the accelerometers (red) and displacement sensors (yellow). No sensors are installed on floors 1 and 2.

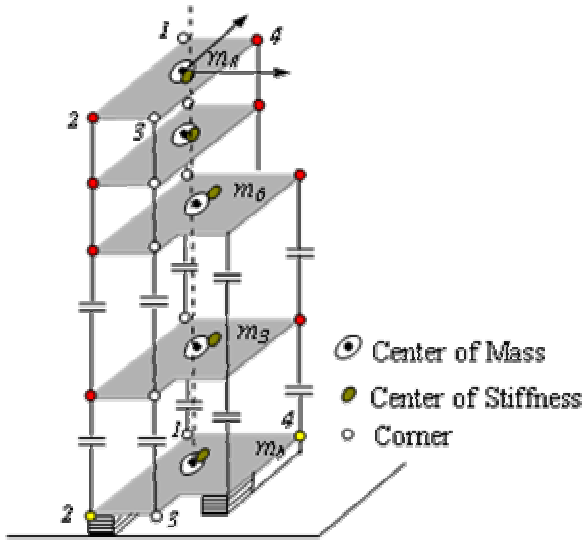

Figure 4-8 Sensor Locations

To evaluate the performance with the reduced set of sensors, comparisons are performed for responses of the isolated benchmark building subjected to the Newhall earthquake. The control algorithm is chosen as LQG, and MR dampers are adopted as the control devices to examine the performance of these systems. Weights are placed on the corner base drifts, corner base accelerations, and corner top floor accelerations ($q_{drift} = 4.642 \times 10^8$, $q_{accelration} = 1.145 \times 10^9$, $\mathbf{R} = \mathbf{I}_{20\times20}$, $\mathbf{S}_{\ddot{x}_g \ddot{x}_g} = 25\mathbf{I}_2$, and $S_{v_i v_i} = \mathbf{I}_{ns\times20}$, where *ns* is the number of sensors). Noise in the sensors is simulated by adding a band-limited white noise to each signal that is scaled to have an RMS of approximately 3% of the corresponding maximum RMS responses of the passive system. The approach to control design will be described in detail in Chapters 5 and 6. Time history responses of the base drift, inter-story drift between the fifth and sixth floors, and roof accelerations at corner 1 in the *x*-direction for full sensor placement and reduced sensor placement are shown in Figure 4-9. It can be seen that the response values are very close and differences in the resulting performance of the two systems are not significant.

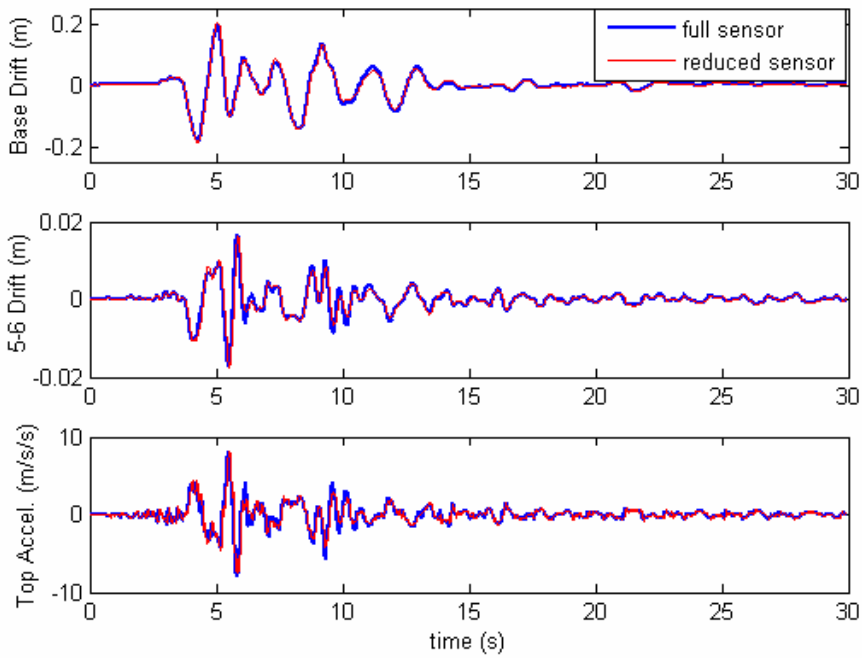

Figure 4-9 Responses at Corner 1 in the *x*-Direction with Full- and Reduced-Sensors

4.5 Summary

A controllability/observability-based approach has been proposed to effectively place control devices and sensors. The placement indices are based on Hankel singular values, which are invariant for both unbalanced and balanced systems. Validation of the technique for control devices (MR dampers) not collocated with disturbances, and for sensors not collocated with performance, is mathematically demonstrated. Correlations between locations are examined to avoid duplication of control effort, and locations with high indices and high correlations are rejected. The efficacy of the reduced set of sensors is confirmed by earthquake responses.

Chapter 5

LQG Control in Nodal Coordinates

A variety of control algorithms have been developed for civil engineering applications, each of which has its proponents. This study focuses the on linear quadratic regulator (LQR), a modern optimal control technique that uses quadratic cost functions with solutions based on a common variational approach. The methodology yields matrix equations for the control gains that can be solved using readily available tools (Matlab, 2005). It provides the designers with great insight into the design and the flexibility to perform trade-offs among various performance objectives. This chapter first reviews LQR, and then states how LQG techniques overcome the limitations of LQR through the use of the separation principle and Kalman filter. Also, this chapter considers an important issue regarding the procedures for the design of LQG controllers: the selection of the responses to be weighted. Simply weighting many responses does not necessarily help to close all loops and result in larger gains for the desired modes. The principles and techniques for selecting the weighting matrix are applied to the base isolation benchmark problem, followed by the introduction of the modeling and control of the control device to be used of this study, MR dampers. Optimal weighting values for the semiactively controlled system are determined by the test and error method in the nodal coordinate system. Responses of the benchmark building subjected to the design earthquakes with the selected weightings are presented. The limitation and inconvenience of the nodal approach in closed-loop pole assignment and controller order reduction are discussed at the end of this chapter.

5.1 Linear Quadratic (LQ) Control

5.1.1 Linear Quadratic Regulator (LQR)

The governing equation for a general feedback control system in state space form is given in (4-1) and (4-2). Rewriting (4-1) and (4-2) with sensor noise included in measurement yields

$$\dot{\mathbf{x}} = \mathbf{A}\mathbf{x} + \mathbf{B}\mathbf{u} + \mathbf{E}\mathbf{w} \tag{5-1}$$

$$\mathbf{y} = \mathbf{C}_y\mathbf{x} + \mathbf{D}_y\mathbf{u} + \mathbf{E}_y\mathbf{w} + \mathbf{v} \tag{5-2}$$

$$\mathbf{z} = \mathbf{C}_z\mathbf{x} + \mathbf{D}_z\mathbf{u} + \mathbf{E}_z\mathbf{w} \tag{5-3}$$

The objective of a regulator is to drive any initial condition errors to zeros, thus guaranteeing stability. This objective is achieved by selecting the control input $\mathbf{u}(t)$ to minimize a quadratic performance criterion or cost function. The problem is referred as the least-squares (optimal) control problem. The cost function often takes a form that minimizes the norm, covariance, or other inner-product space. An appropriate form for this study is

$$J = \lim_{\tau\to\infty}\frac{1}{\tau}E\left[\int_0^{\tau}\left\{(\mathbf{C_z}\mathbf{x} + \mathbf{D_z}\mathbf{u})^T\mathbf{Q}(\mathbf{C_z}\mathbf{x} + \mathbf{D_z}\mathbf{u}) + \mathbf{u}^T\mathbf{R}\mathbf{u}\right\}dt\right]. \tag{5-4}$$

where $E[.]$ represents expectation, $\mathbf{u}$ is the vector of command forces, $\mathbf{R}$ is a positive definite input weighting matrix, and $\mathbf{Q}$ is a positive semi-definite state weighting matrix. The relative magnitude of $\mathbf{Q}$ and $\mathbf{R}$ may be selected to trade off requirements on the magnitude of the performance against requirements on the magnitude of the input. For example, a larger $\mathbf{R}$ penalizes the control more, and a larger $\mathbf{Q}$ makes $\mathbf{z}$ approach zero more quickly with time.

In LQR control, the task is to find an optimal feedback gain $\mathbf{K}$ to achieve the control objectives. State variables are typically used for feedback, i.e., $\mathbf{y} = \mathbf{x}$, yielding the control law

$$\mathbf{u} = -\mathbf{K}\mathbf{x}. \tag{5-5}$$

For more general output feedback, the solution for $\mathbf{K}$ involves three coupled nonlinear matrix equations, whereas for full-state feedback, the solution reduces to the Riccati equation. Moreover, full-state feedback has powerful stability properties that are not guaranteed for other types of output feedback (Stevens and Lewis, 2003).

The solution to the LQ regulator with state feedback is well developed. The optimal gain matrix is given by

$$\mathbf{K} = \widetilde{\mathbf{R}}^{-1}(\widetilde{\mathbf{N}}^T + \mathbf{B}^T\mathbf{S}_c) \tag{5-6}$$

where $\mathbf{S}_c$ is the solution of the controller algebraic Riccati equation (CARE) given by

$$\mathbf{0} = \mathbf{S}_c\widetilde{\mathbf{A}} + \widetilde{\mathbf{A}}^T\mathbf{S}_c - \mathbf{S}_c\mathbf{B}\widetilde{\mathbf{R}}^{-1}\mathbf{B}^T\mathbf{S}_c + \widetilde{\mathbf{Q}} \tag{5-7}$$

where

$$\widetilde{\mathbf{Q}} = \mathbf{C}_\mathbf{z}^T\mathbf{Q}\mathbf{C}_\mathbf{z} - \widetilde{\mathbf{N}}\widetilde{\mathbf{R}}^{-1}\widetilde{\mathbf{N}}^T \tag{5-8a}$$

$$\widetilde{\mathbf{A}} = \mathbf{A} - \mathbf{B}^T\widetilde{\mathbf{R}}^{-1}\widetilde{\mathbf{N}} \tag{5-8b}$$

$$\widetilde{\mathbf{N}} = \mathbf{C}_\mathbf{z}^T\mathbf{Q}\mathbf{D}_\mathbf{z} \tag{5-8c}$$

$$\widetilde{\mathbf{R}} = \mathbf{R} + \mathbf{D}_\mathbf{z}^T\mathbf{Q}\mathbf{D}_\mathbf{z}. \tag{5-8d}$$

Calculations to determine $\mathbf{K}$ can be done using Matlab routine *lqry.m* in the control toolbox. Note that if $\mathbf{D}_\mathbf{z} = \mathbf{0}$, the procedures would be greatly simplified without losing generality.

Note that the above control law results in

$$\dot{\mathbf{x}} = (\mathbf{A} - \mathbf{BK})\mathbf{x} + \mathbf{Ew}\,. \tag{5-9}$$

We see that the values of the closed-loop poles depend on the control gain $\mathbf{K}$. The optimal control gain should stabilize the closed-loop $(\mathbf{A} - \mathbf{BK})$. We say $(\mathbf{A}, \mathbf{B})$ is stabilizable if such a feedback gain exists. For a stabilizable system, closed-loop poles may be arbitrarily assigned. For the LQ regulator with full-state feedback, the closed-loop stability is guaranteed if the matrix pair $(\sqrt{\mathbf{C}_\mathbf{z}^T\mathbf{C}_\mathbf{z}}, \mathbf{A})$ in the open-loop is detectable (Steven and Lewis, 2003). Other output feedback amounts to partial feedback, so it is clear that closed-loop stability cannot be expected. This is an advantage of using full-state LQ control. The detectability condition basically means that $\sqrt{\mathbf{C}_\mathbf{z}^T\mathbf{C}_\mathbf{z}}$ should be chosen so that all unstable states are weighted in the cost function, so that the open-loop unstable states will be forced to zero through the action of the control. From the numerical point of view, if $(\sqrt{\mathbf{C}_\mathbf{z}^T\mathbf{C}_\mathbf{z}}, \mathbf{A})$ is observable, a positive definite solution $\mathbf{S}_c$ results; otherwise, $\mathbf{S}_c$ may be singular. Because $\mathbf{S}_c$ helps determine $\mathbf{K}$, it is found that if $\mathbf{S}_c$ is singular, it may result in some zero-gain elements in $\mathbf{K}$. That is, if $(\sqrt{\mathbf{C}_\mathbf{z}^T\mathbf{C}_\mathbf{z}}, \mathbf{A})$ is not observable, the LQ algorithm can refuse to close some of the feedback loops (Stevens and Lewis, 2003).

5.1.2 Kalman Filter and Noise-Shaping Filter

Though LQR with full state feedback has some advantages and robust characteristics, all the states are not available for measurement in most real world problems. The observer design technique enables one to estimate the full state given only partial information in the measured output if the measured outputs capture enough information about the dynamics of the system. The combination of the state estimates $\hat{\mathbf{x}}$ and the state feedback gain $\mathbf{K}$ is then a dynamic regulator similar to the static regulator. It yields a control force of

$$\mathbf{u} = -\mathbf{K}\hat{\mathbf{x}}\,. \tag{5-10}$$

Equation (5-10) is well-known as the separation principle, which states that the feedback gain and observer may be designed separately and then concatenated (Stevens and Lewis, 2003). The separation principle also makes it possible to reduce the order of the controllers.

The state estimator is a dynamical system. For systems without disturbance and noise measurement, the state estimator is described by

$$\dot{\hat{\mathbf{x}}} = \mathbf{A}\hat{\mathbf{x}} + \mathbf{B}\mathbf{u} + \mathbf{L}(\mathbf{y} - \hat{\mathbf{y}}) = (\mathbf{A} - \mathbf{L}\mathbf{C}_{\mathrm{y}})\hat{\mathbf{x}} + (\mathbf{B} - \mathbf{L}\mathbf{D}_{\mathrm{y}})\mathbf{u} + \mathbf{L}\mathbf{y} \tag{5-11}$$

That is, the observer consists of two parts: a model of the system, and an error-correcting portion that involves the output error multiplied by the observer gain $\mathbf{L}$. Observers of this type are called output-injection observers.

To demonstrate that equation (5-11) is indeed an observer, define the estimation error as $\tilde{\mathbf{x}} = \mathbf{x} - \hat{\mathbf{x}}$. It is seen that the estimation error has dynamics given by

$$\dot{\tilde{\mathbf{x}}} = (\mathbf{A} - \mathbf{L}\mathbf{C}_{\mathrm{y}})\tilde{\mathbf{x}} \tag{5-12}$$

It is important for the estimation error to vanish with time for any initial estimate, ensuring that $\hat{\mathbf{x}}(t)$ will approach $\mathbf{x}(t)$. This will occur if $(\mathbf{A} - \mathbf{L}\mathbf{C}_{\mathrm{y}})$ is asymptotically stable, so the observer design problem is to select $\mathbf{L}$ to stabilize $(\mathbf{A} - \mathbf{L}\mathbf{C}_{\mathrm{y}})$. It is well known that the poles of $(\mathbf{A} - \mathbf{L}\mathbf{C}_{\mathrm{y}})$ may be arbitrarily assigned if and only if $(\mathbf{C}_{\mathrm{y}}, \mathbf{A})$ is observable. Also note that equation (5-12) is very similar to equation (5-9), and

$$(\mathbf{A} - \mathbf{L}\mathbf{C}_{\mathrm{y}})^T = \mathbf{A}^T - \mathbf{C}_{\mathrm{y}}^T\mathbf{L}^T \tag{5-13}$$

$(\mathbf{A}^T - \mathbf{C}_{\mathrm{y}}^T\mathbf{L}^T)$ is similar to $(\mathbf{A} - \mathbf{B}\mathbf{K})$. This outcome is called duality, i.e., state feedback and output injections are duals. The duality indicates that the same theory for selecting the state-feedback gain $\mathbf{K}$ may be used to select the observer gain $\mathbf{L}$, i.e., $\mathbf{Q}$ and $\mathbf{R}$ may be taken as design parameters for output-injection observers without noises (Stevens and

Lewis, 2003). It enables us to design an observer by replacing $\mathbf{A}$, $\mathbf{B}$ and $\mathbf{K}$ with $\mathbf{A}^T$, $\mathbf{C}_\mathbf{y}^T$ and $\mathbf{L}^T$ in equation (5-7), respectively.

However, in reality, modeling inaccuracies, disturbances, and noises are present in the system and in the measurements. The observer gain could not be solved using the duality property for this situation. A Kalman filter is an observer that is used for applications that require the reconstruction of the state from a stochastically disturbed (e.g., seismically excited) system and noisy measurements based on probability theory. The process disturbance $\mathbf{w}(t)$ and measurement noise $\mathbf{v}(t)$ are unknown, but it is reasonable to assume them to be zero-mean Gaussian white noise processes and orthogonal to each other, i.e.,

$$\mathrm{E}\{\mathbf{w}\mathbf{w}^T\} = \mathbf{H}\delta(\tau), \quad \mathrm{E}\{\mathbf{v}\mathbf{v}^T\} = \mathbf{P}\delta(\tau), \quad \mathrm{E}\{\mathbf{w}\mathbf{v}^T\} = \mathbf{0} \tag{5-14a}$$

$$\mathbf{w}(t) \sim (\mathbf{0}, \mathbf{H}), \quad \mathbf{v}(t) = (\mathbf{0}, \mathbf{P}) \tag{5-14b}$$

where $\mathbf{H}$ and $\mathbf{P}$ are positive semi-definite covariance matrices.

The assumption that $\mathbf{w}(t)$ and $\mathbf{v}(t)$ are white noise processes may in some applications be too simplistic to facilitate good performance in the controller. For instance, wind-gust noise and near-field earthquakes consist mainly of low-frequency components. To inform the controller about the frequency content of the perturbation (ground motion for this study), suppose $\mathbf{w}(t)$ is not white. We can determine a filter system description

$$\dot{\mathbf{x}}_\mathbf{w} = \mathbf{A}_\mathbf{w}\mathbf{x}_\mathbf{w} + \mathbf{B}_\mathbf{w}\mathbf{n} \tag{5-15a}$$

$$\mathbf{w} = \mathbf{C}_\mathbf{w}\mathbf{x}_\mathbf{w} \tag{5-15b}$$

which has a white noise input $\mathbf{n}(t)$ and output $\mathbf{w}(t)$. Equations (5-15a, b) are called a noise-shaping filter. Its dynamics may be combined with the plant (equation (5-1) and (5-3)) to obtain the augmented dynamics

$$\begin{bmatrix} \dot{\mathbf{x}} \\ \dot{\mathbf{x}}_\mathbf{w} \end{bmatrix} = \begin{bmatrix} \mathbf{A} & \mathbf{E}\mathbf{C}_\mathbf{w} \\ \mathbf{0} & \mathbf{A}_\mathbf{w} \end{bmatrix} \begin{bmatrix} \mathbf{x} \\ \mathbf{x}_\mathbf{w} \end{bmatrix} + \begin{bmatrix} \mathbf{B} \\ \mathbf{0} \end{bmatrix}\mathbf{u} + \begin{bmatrix} \mathbf{0} \\ \mathbf{B}_\mathbf{w} \end{bmatrix}\mathbf{n} = \mathbf{A}_a\mathbf{x}_a + \mathbf{B}_a\mathbf{u} + \mathbf{E}_a\mathbf{n} \tag{5-16}$$

$$\mathbf{y} = \begin{bmatrix}\mathbf{C}_{\mathbf{y}} & \mathbf{E}_{\mathbf{y}}\mathbf{C}_{\mathbf{w}}\end{bmatrix}\begin{bmatrix}\mathbf{x} \\ \mathbf{x}_{\mathbf{w}}\end{bmatrix} + \begin{bmatrix}\mathbf{D}_{\mathbf{y}} \\ \mathbf{0}\end{bmatrix}\mathbf{u} = \mathbf{C}_{\mathbf{y}a}\mathbf{x}_a + \mathbf{D}_{\mathbf{y}a}\mathbf{u} \tag{5-17}$$

where the subscript a denotes the augmented system. This augmented system does have a white process noise $\mathbf{n}(t)$. A similar procedure is applied if $\mathbf{v}(t)$ is non-white.

In this study, a Kanai-Tajimi shaping filter that is widely applied in civil engineering is adopted. The Kanai-Tajimi shaping filter takes the form

$$G_{nw}(s) = \frac{2\varsigma_g \omega_g s + \omega_g^2}{s^2 + 2\varsigma_g \omega_g s + \omega_g^2} \tag{5-18}$$

where, $\omega_g = 1.5$ rad/s, and $\varsigma_g = 0.2$.

Note that the benchmark building is subjected to bi-directional excitations, so the perturbation (ground motion) is modeled as process

$$\mathbf{W}(s) = \begin{bmatrix} G_{ns}(s) & 0 \\ 0 & G_{ew}(s) \end{bmatrix}\mathbf{n}(s) \tag{5-19}$$

The state-space matrices $\mathbf{A}_{\mathbf{w}}$, $\mathbf{B}_{\mathbf{w}}$, and $\mathbf{C}_{\mathbf{w}}$ for the filter are obtained from the transfer function (5-19).

The magnitude of the shaping filter as a function of frequency, as well as the frequency content (power spectral density) of the seven historical design earthquakes, is plotted in Figure 5-1.

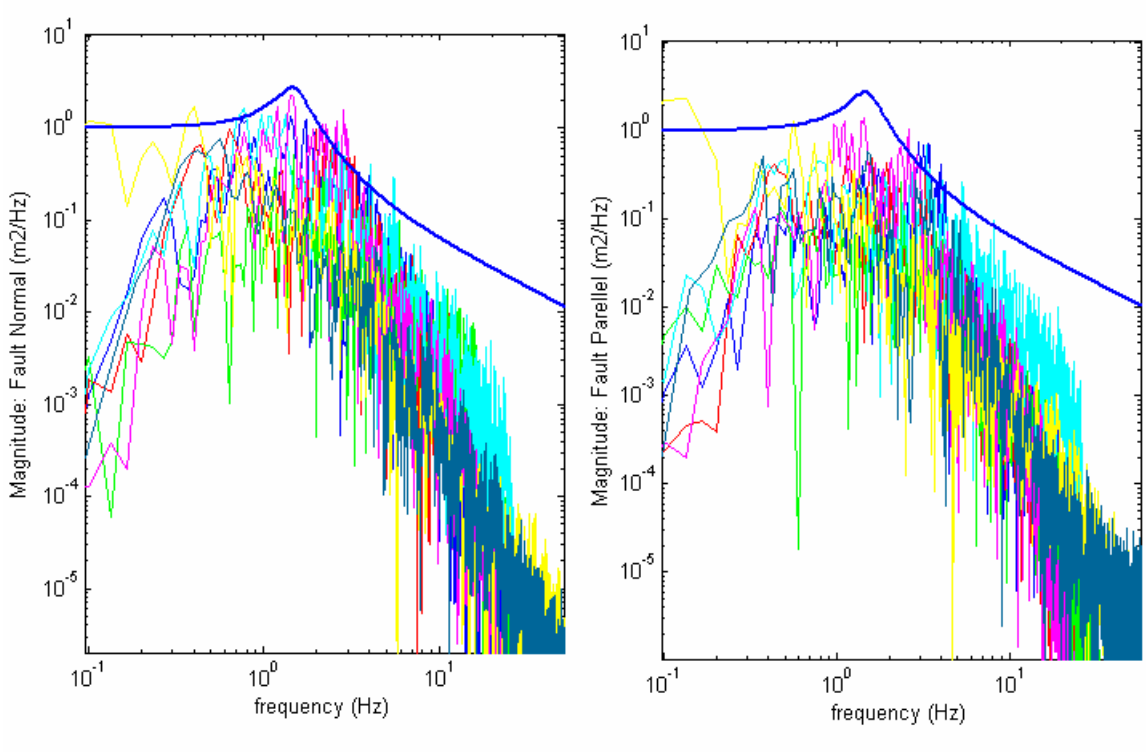

Figure 5-1 Frequency Content of Design Earthquakes and the Kanai-Tajimi Filter

With the augmented model, the observer gain matrix is given by

$$\mathbf{L} = \mathbf{S}_e \mathbf{C}_{ya}^T \mathbf{P}^{-1} \tag{5-20}$$

where $\mathbf{S}_e$ is the solution of the filter algebraic Riccati equation (FARE) given by

$$\mathbf{0} = \mathbf{S}_e \mathbf{A}_a + \mathbf{A}_a^T \mathbf{S}_e - \mathbf{S}_e \mathbf{C}_{ya}^T \mathbf{P}^{-1} \mathbf{C}_{ya} \mathbf{S}_e + \mathbf{E}_a \mathbf{H} \mathbf{E}_a^T . \tag{5-21}$$

Calculations to determine $\mathbf{L}$ are done using the Matlab routine *lqew.m* within the control toolbox. For design purposes, $\mathbf{H} = 25\mathbf{I}_2$ and $\mathbf{P} = \mathbf{I}$ are used in LQG controller design in this chapter, where $\mathbf{I}$ represents the identity matrix.

If the feedback gain matrix $\mathbf{K}$ is selected using the LQR Riccati equation (5-6) and (5-7), and estimator gain matrix $\mathbf{L}$ is selected using the Kalman filter Riccati equation (5-20)

and (5-21), this procedure is called the LQG (Linear system, Quadratic cost, Gaussian noise) design.

Now an output-projection observer for the stochastic system (5-16) and (5-17) is in the form

$$\dot{\hat{\mathbf{x}}} = \mathbf{A}_a\hat{\mathbf{x}} + \mathbf{B}_a\mathbf{u} + \mathbf{L}(\mathbf{y} - \hat{\mathbf{y}}) = (\mathbf{A}_a - \mathbf{L}\mathbf{C}_{\mathbf{y}a})\hat{\mathbf{x}} + (\mathbf{B}_a - \mathbf{L}\mathbf{D}_{\mathbf{y}a})\mathbf{u} + \mathbf{L}\mathbf{y}\,. \qquad (5\text{-}22)$$

For the estimation error $\tilde{\mathbf{x}} = \mathbf{x} - \hat{\mathbf{x}}$, the error's dynamics is governed by

$$\dot{\tilde{\mathbf{x}}} = (\mathbf{A}_a - \mathbf{L}\mathbf{C}_{\mathbf{y}a})\tilde{\mathbf{x}} + \mathbf{E}_a\mathbf{w} - \mathbf{L}\mathbf{v}\,. \qquad (5\text{-}23)$$

It turns out that the solution to the FARE is the error covariance, i.e., $\mathbf{S}_e(t) = E\left\{\tilde{\mathbf{x}}\tilde{\mathbf{x}}^T\right\}$. If the observer is asymptotically stable and $\mathbf{w}(t)$ and $\mathbf{v}(t)$ are stationary processes, the error $\tilde{\mathbf{x}}(t)$ will eventually reach a steady state in which it is also stationary with constant mean and covariance. The gain $\mathbf{L}$ will be chosen to minimize the steady state covariance $\mathbf{S}_e(t)$. Thus, the optimal gain $\mathbf{L}$ will be a constant matrix of observer gains (Stevens and Lewis, 2003).

Regarding the system's closed-loop stability properties, the conditions stated above also hold. It is stated as: if $(\mathbf{C}_{\mathbf{y}a}, \mathbf{A}_a)$ is observable and $(\mathbf{A}_a, \mathbf{E}_a\sqrt{\mathbf{C}_{\mathbf{z}}^T\mathbf{C}_{\mathbf{z}}})$ is reachable, the error system (5-23) using the gain $\mathbf{L}$ solved from FARE is asymptotically stable (Steven and Lewis, 2003). Generally $\mathbf{L}$ is selected such that poles of $(\mathbf{A}_a - \mathbf{L}\mathbf{C}_{\mathbf{y}a})$ are 2 to 6 times farther to the left than those of the matrix $(\mathbf{A} - \mathbf{B}\mathbf{K})$ so that the estimation error vanishes as quickly as desired.

Last, the force can be used as a measurement for the estimator, and in semiactive systems it is often necessary to do so. If the force is provided by active devices, then it is clear that $\mathbf{u} = \mathbf{f} = \mathbf{K}\hat{\mathbf{x}}$, where $\mathbf{f}$ is the actual force vector, and thus

$$\dot{\hat{\mathbf{x}}} = \mathbf{A}_a\hat{\mathbf{x}} + \mathbf{B}_a\mathbf{u} + \mathbf{L}(\mathbf{y} - \mathbf{C}_{\mathbf{y}a}\hat{\mathbf{x}} - \mathbf{D}_{\mathbf{y}a}\mathbf{K}\hat{\mathbf{x}}) = (\mathbf{A}_a - \mathbf{L}\mathbf{C}_{\mathbf{y}a} - (\mathbf{B}_a - \mathbf{L}\mathbf{D}_{\mathbf{y}a}))\hat{\mathbf{x}} + \mathbf{L}\mathbf{y}\,. \qquad (5\text{-}24)$$

However, for semiactive systems, the applied force $\mathbf{f}$ is not the commanded force $\mathbf{u}$, or the control action determined by the controller, i.e., $\mathbf{f} \neq \mathbf{Kx}$. Instead, the force $\mathbf{f}$ must be measured and fed into the controller resulting in the control action given by

$$\mathbf{u} = L^{-1}\left\{-\mathbf{K}L\left\{\begin{matrix}\mathbf{y}\\ \mathbf{f}_{meas}\end{matrix}\right\}\right\} \tag{5-25}$$

where $L\{.\}$ is the Laplace transform operator, and $\mathbf{f}_{meas}$ is the measured force. The estimator is now described by

$$\dot{\hat{\mathbf{x}}} = (\mathbf{A}_a - \mathbf{LC}_{\mathbf{y}a})\hat{\mathbf{x}} + \begin{bmatrix}\mathbf{L} & \mathbf{B}_a - \mathbf{LD}_{\mathbf{y}a}\end{bmatrix}\left\{\begin{matrix}\mathbf{y}\\ \mathbf{f}_{meas}\end{matrix}\right\}. \tag{5-26}$$

The controller is then designed for the combined filter / structure model, as shown in Figure 5-2.

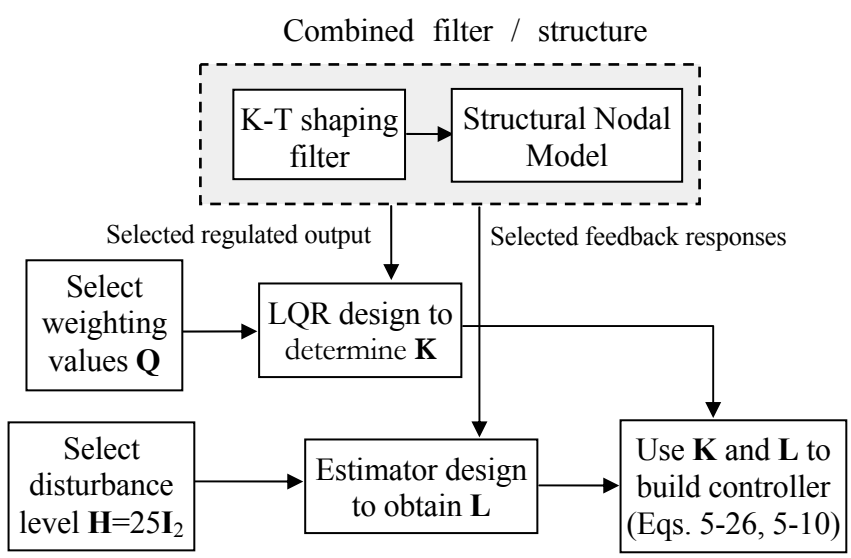

Figure 5-2 Flow Chart of the Nominal Controller Design Using the Nodal Approach

5.1.3 Selection of the Weighting Matrices

The discussion in section 5.1.2 shows that the observability of $(\mathbf{A}_a, \mathbf{E}_a\sqrt{\mathbf{C}_\mathbf{z}^T\mathbf{C}_\mathbf{z}})$ and controllability of $(\mathbf{C}_{\mathbf{y}a}, \mathbf{A}_a)$ are conditions to ensure the convergence of the closed-loop plant and the estimator, respectively. In this study, the feedback measurements selected corner accelerations and base drifts. For simplicity, the estimator model without noise is used for the study of weighting matrix selection. The matrix $\mathbf{C}_\mathbf{y}$ is

$$\mathbf{C}_\mathbf{y} = \begin{bmatrix} \begin{bmatrix} \mathbf{I}_{8\times 8} & \mathbf{0}_{8\times 46} \end{bmatrix} \\ [\mathbf{M}^{-1}\mathbf{K} \quad \mathbf{M}^{-1}\mathbf{C}]_{floors\,3\sim 8} \end{bmatrix}_{corners:2,4} . \tag{5-27}$$

The subscript is to remind that only the rows corresponding to corners 2 and 4 are to be used. The observability $(\mathbf{C}_\mathbf{y}, \mathbf{A})$ has been indirectly indicated in chapter 4, where all sensor location indices, and thus the associated Hankel singular values, are non-zero.

The goal of this section is to select the outputs $\mathbf{z}$, or the response gains $\mathbf{C}_\mathbf{z}$, on which weights should be placed. Responses to be weighted depend on the performance objectives. They should close all loops, and should result in larger control gains in the desired states or modes. The objective of the control of base isolated systems is to decrease the base drift while retaining the advantage of small inter-story drifts and accelerations. Table 5-1 gives six response combinations and the notations used for describing each case for testing the observability of $(\sqrt{\mathbf{C}_\mathbf{z}\mathbf{C}_\mathbf{z}^T}, \mathbf{A})$, or equivalently, the controllability of $(\mathbf{A}, \sqrt{\mathbf{C}_\mathbf{z}^T\mathbf{C}_\mathbf{z}})$, which is quantitatively measured by the grammians.

Table 5-1 Weighting Matrix Alternatives

1. All Accelerations (AA)	4. Base Drifts + Base Accelerations (BDBA)
2. Base Drifts + Inter-story drifts of the superstructure (AID)	5. Base Drifts + Accelerations of the base and top (8th)floor (BDBATA)
3. Base Drifts + All Accelerations (BDAA)	6. Base Drifts + Accelerations of the 5th and 8th floor (BD5ATA)

Figure 5-3 shows the observability grammian versus mode number for cases 1 and 2. It is clear that only the isolation modes (fundamental modes in each direction) are observable for the second case. That is, weightings placed on the base drifts and inter-story drifts would result in control gains near zero for the other higher modes. However, the first case, weighting all acceleration responses, has non-zero observability grammians in all modes, and the most observable modes are the isolation modes and the highest modes. The highest modes usually have small participation factors and thus contribute less to the responses. So although most modes have large observability grammians for the two cases, they are not a good choice to achieve the goal of controlling lower modes.

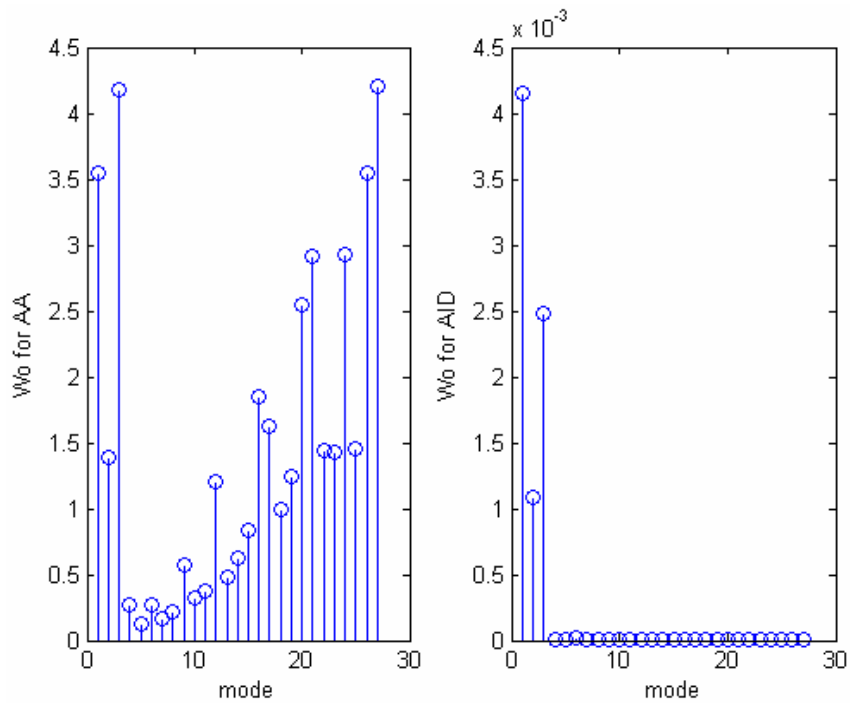

Figure 5-3 Weighting Observability Grammians for Cases AA and AID

The third case also includes the base drifts as weighted responses. The observability grammians for this case are shown in the left column of Figure 5-4. Notice that this modification does not change the observability significantly or the resulting control gains, from the first case. Thus it is important to carefully select the weighting used rather than simply weighting all responses. The fourth case weights only the base drifts and base

acceleration. The results (right column of Figure 5-4) show that most grammian values decrease, while the ratio of lower modes to isolation modes increases from 1/10 to 1/7. This choice is better if the control of the lower modes is the primary interest. Note that the absolute grammian values do not affect the control effort, because the control gains can be adjusted through the magnitude of the weighting value $\mathbf{Q}$.

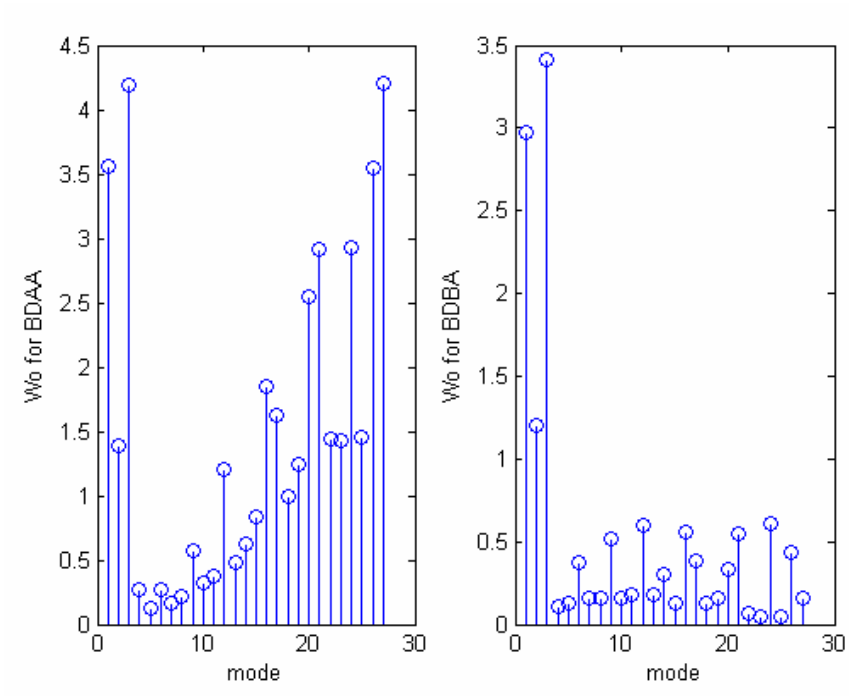

Figure 5-4 Weighting Observability Grammains for Cases BDAA and BDBA

Figure 5-5 provides two more cases, with the top floor accelerations and the fifth-floor accelerations added to the previous case. The results show that the ratio of the grammians of the flexible (structural) modes to those of the isolation modes increased to 1/5 when the top floor accelerations are added in case five (BDBATA). But the addition of weighting placed on the fifth-floor resulted in a decrease in this ratio (case six).

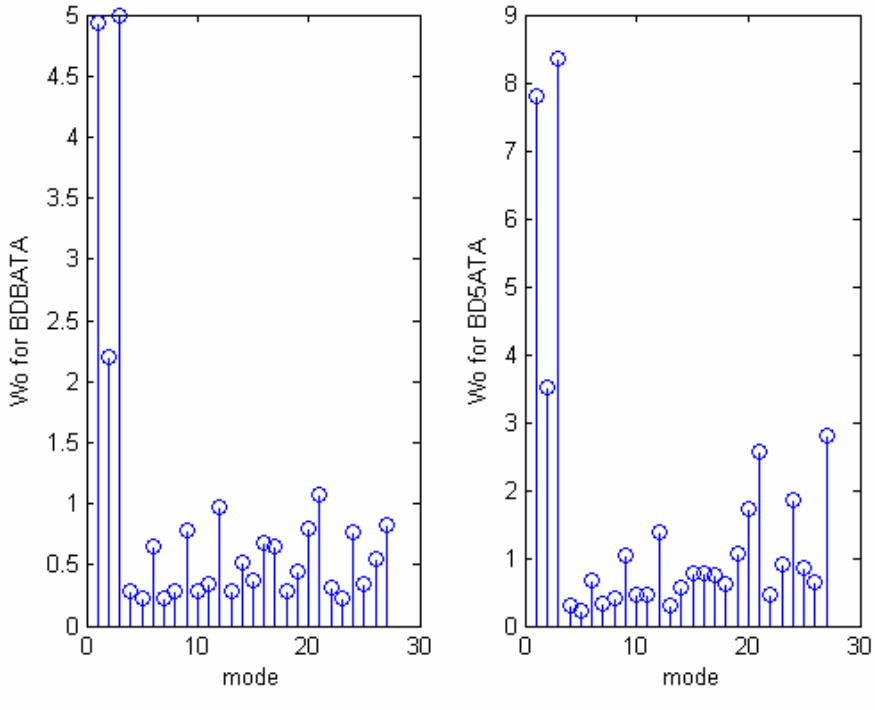

Figure 5-5 Weighting Observability Grammians for Cases BDBATA and BD5ATA

In summary, the fifth case of BDBATA is the most appropriate choice of weighting and will be used in the sequel.

5.2 Control of the Benchmark Building Subjected to Earthquakes

5.2.1 Modeling and Control of MR Dampers

MR dampers are semiactive control devices that use MR fluid to provide controllable force. MR fluids typically consist of micro-sized, magnetically polarizable particles dispersed in a carrier medium such as mineral or silicone oil. When a magnetic field is applied to the fluids, particle chains form, and the fluid becomes a semi-solid and exhibits viscoplastic behavior. The MR fluid can be readily controlled with a low voltage (i.e., 12~24 V), current-driven power supply outputting only 1~2 Amps. Transition to rheological equilibrium can be achieved in a few milliseconds, allowing construction of devices with high bandwidth. MR fluids have high strength, low power requirements, can

operate at temperatures from -40° to 150°C with only slight variations in the yield stress, and are insensitive to impurities commonly introduced during manufacturing. The future of MR devices for civil engineering applications appears to be quite bright (Dyke, 1996a).

A schematic of a type of MR damper is shown in Figure 5-6(a). The MR fluid valve is contained within the damper piston and consists of an annolar flow channel. The magnetic field is applied radially, perpendicular to the direction of fluid flow. The magnetic field varies with the current in the electromagnetic coil having a specified resistance. The current is proportional to a commanded DC input voltage. With the power supply, the damper can reach a maximum force determined by the design dimensions.

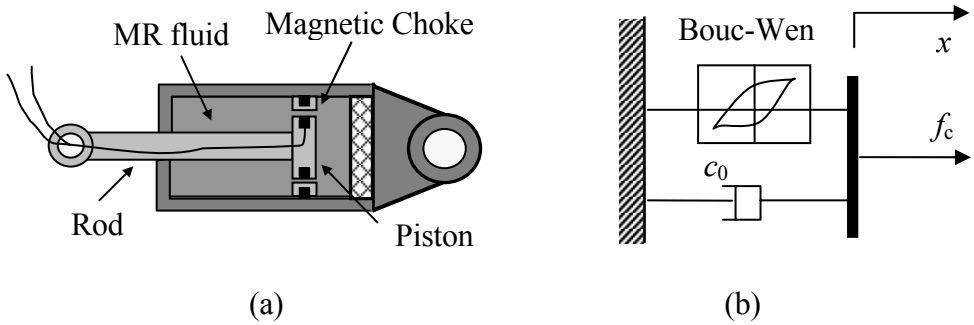

Figure 5-6 (a) Schematic of an MR Damper
(b) Bouc-Wen Model of the MR Damper (Spencer et al,1997)

To take full advantage of the unique features of the MR damper in control applications, a high fidelity model needs to be used to accurately reproduce the behavior of the MR damper. After reviewing several idealized mechanical models for controllable fluid dampers, Spencer et al (1997) proposed a new model that overcomes a number of the shortcomings of these models and can effectively portray the behavior of a typical MR damper. This phenomenological model is based on a Bouc-Wen hysteresis model, which is numerically tractable and is capable of exhibiting a wide variety of hysteretic behaviors. The schematic of this model is shown in Figure 5-6 (b).

The dashpot in series with the Bouc-Wen model is included to provide the roll-off observed in the force as the velocity approaches zero. Three parameters are assumed to

vary with the applied voltage. Additionally, a first order filter has been incorporated into the model to account for the dynamics involved in the MR fluid reaching rheological equilibrium. This simple model is shown to be able to accurately predict the response of the MR damper over a wide range of operating conditions (Spencer et al., 1997; Yi et al., 2001; Dyke et al., 1999). The equations governing the force *f* produced by this device model are

$$f = c_0\dot{x} + \alpha z \quad \text{and} \quad \dot{z} = -\gamma|\dot{x}|z|z^{n-1}| - \beta\dot{x}|z|^n + A\dot{x} \tag{5-28}$$

where x is the displacement accross the device, and z is an evolutionary variable that accounts for the history dependence of the response. By adjusting the parameters of the model γ, β, n, and A, one can control the linearity in the unloading and the smoothness of the transition from the pre-yield to post-yield region. The functional dependence of the device parameters on the command input u is modeled as

$$\alpha = \alpha_a + \alpha_b u \quad \text{and} \quad c_0 = c_{0a} + c_{0b}u \tag{5-29}$$

The first order filter that accounts for the dynamics involved in the MR fluid is given by

$$\dot{u} = -\eta(u - v) \tag{5-26}$$

where v is the command voltage applied to the control circuit and $1/\eta$ is the time constant of the filter.

The parameters of the MR damper used in this study are as follows: $\alpha_a = 1.0872e5$ N/cm, $\alpha_b = 4.9616e5$ N/cm, $c_{0a} = 4.40$ Nsec/(cm.V), $c_{0b} = 44.0$ N sec/(cm.V), $n = 1$, $A = 1.2$, $\gamma = 3$ cm^{-1}, $\beta = 3$ cm^{-1}, and $\eta = 50$ sec^{-1}. They were selected so that the device has a capacity of 1000 kN. These parameters are based on the identified model of a shear-mode prototype MR damper tested at Washington University (Yi et al.,

2001) and scaled up to have maximum capacity of 1000 kN with maximum command voltage $V_{\max} = 10$ V (Yoshida, 2003).

The response of the MR damper to a sinusoidal wave with amplitude of 20cm, frequency of 0.5 Hz is shown in Figure 5-7 for six constant voltage levels: 0V, 2V, 4V, 6V, 8V and 10V. The force levels increase with the command voltage levels. For the benchmark problem subjected to earthquakes, the MR dampers will experience displacements of 30cm to 50cm.

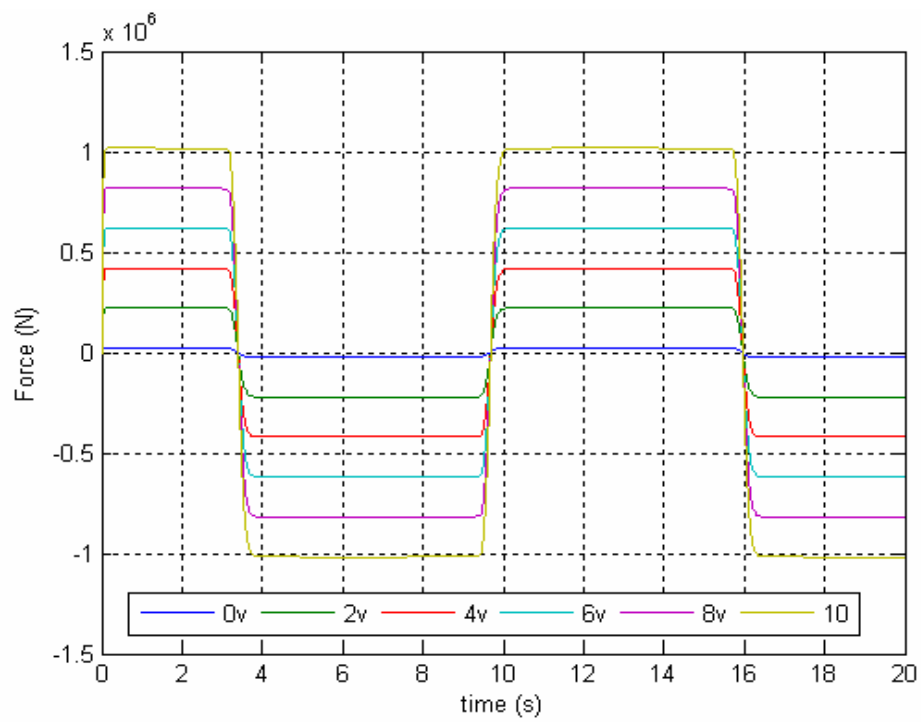

Figure 5-7 Force-Time Response of the MR Damper to 20sin(πt)

The force-displacement and force-velocity loops are shown in Figure 5-8 and Figure 5-9, respectively. Note that the force-displacement loops progress along a clockwise path with increasing time, whereas the force-velocity loops progress along a counter-clockwise path with increasing time, and the MR damper force is not zero when the voltage is zero. Also note that the model of the MR damper exhibits the dissipative characteristic of a viscous device.

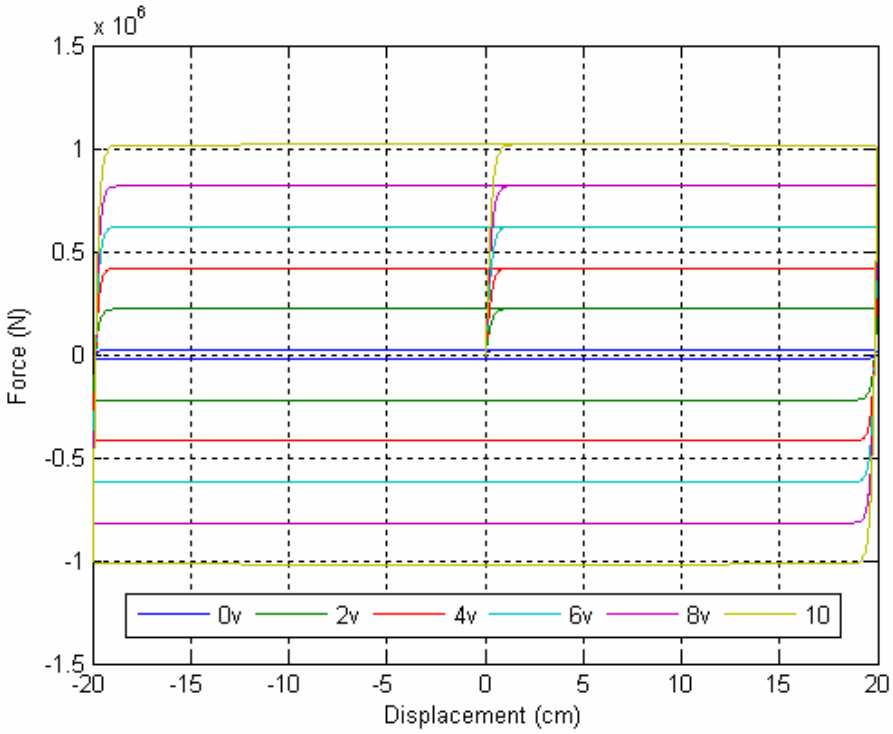

Figure 5-8 Force-Displacement Loop of the MR Damper to 20sin(πt)

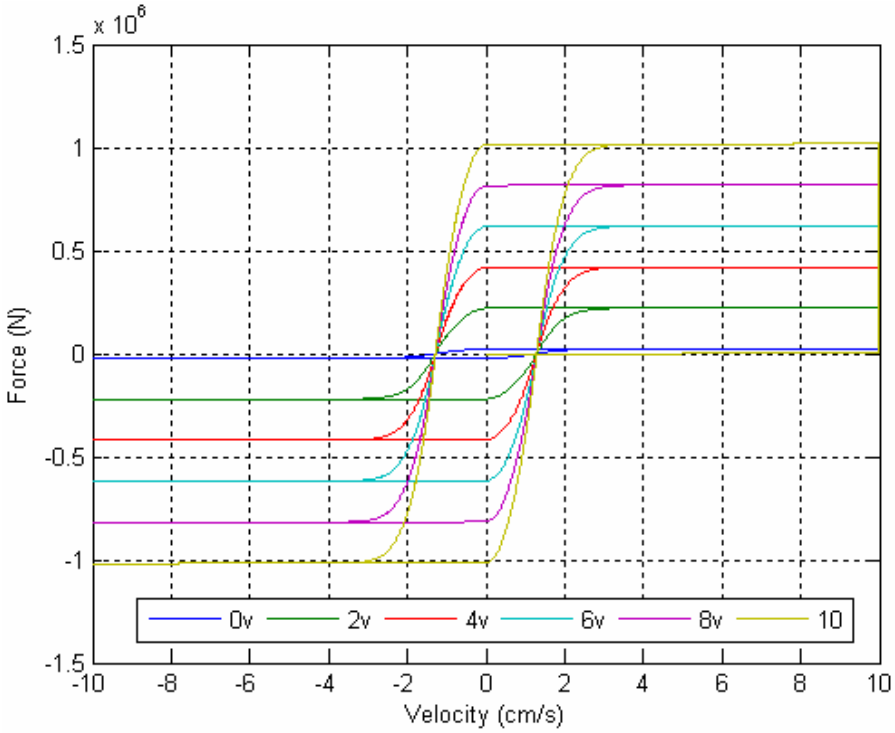

Figure 5-9 Force-Velocity Loop of the MR Damper to 20sin(πt)

Figure 5-9 also shows that the force-velocity relationship is not one-to-one but exhibits nonlinear behavior when the acceleration and velocity have opposite signs (or alternatively, when the velocity and displacement have the same sign). This behavior is crucial for control applications.

For employing this model in simulation, it is important to remember that semiactive devices are dissipative devices. Pure dissipative devices are capable of generating control force only in the second and fourth quadrants of the force-velocity plane. To enforce this physically-based behavior, a constraint is applied in the simulation as

$$f_i(t) = \begin{cases} u_i(t) & \dot{x}_i f_i(t) < 0 \\ 0 & otherwise \end{cases} \tag{5-30}$$

where u_i is the *i*th component of the desired force and $\dot{x}_i$ is the local velocity.

In this application, the measurements typically available for control force determination include the acceleration of selected points on the structure, the displacement of the MR damper, and the control force provided by the MR damper. The approach proposed here is to append a force feedback loop to induce the MR damper to produce a force $\mathbf{f}$ approximately equal to the desired (nominal) control force $\mathbf{u}$ (Dyke, 1996a). Thus a linear optimal controller is designed to calculate a vector of desired control forces based on the measured structural response $\mathbf{y}$ and the measured control force vector $\mathbf{f}_{meas}$. This approach has been shown in equation (5-25). The controller can be obtained from a variety of method. In this study, an LQG strategy is adopted.

Because of the nonlinear nature of the MR damper force and its dependence on the local response, it is not possible to directly command the *i*th MR damper to generate the specified force. The only way to control the force produced by the device is by adjusting the control voltage v_i. The $|f_i|$ increases when v_i increases.

Many approaches have been proposed to control semiactive devices. The clipped-optimal control algorithm based on acceleration feedback proposed by Dyke et al. (1996a, b,c) has found to be among the best performing of several nonlinear semiactive controllers for MR devices. The clipped-optimal algorithm selects the command signal as follows:

When the *i*th MR damper is providing the desired optimal force (i.e., $f_{meas} = u_i$), the voltage applied to the damper should remain at the present level. If the magnitude of the force produced by the damper is smaller than the magnitude of the desired optimal force, and the two forces have the same design, the voltage applied to the current driver is increased to the maximum level so as to increase the force produced by the damper to match the desired control force. Otherwise, the command voltage is set to zero. The algorithm for selecting the command signal for the *i*th MR damper is illustrated in Figure 5-10 and stated as

$$v_i = V_{\max} H(\{u_i - f_{meas}\} u_i) \tag{5-31}$$

where $V_{\max}$ is the maximum voltage to the current driver, $H(.)$ is the Heaviside step function, u_i is the desired force and f_{meas} is the measured force

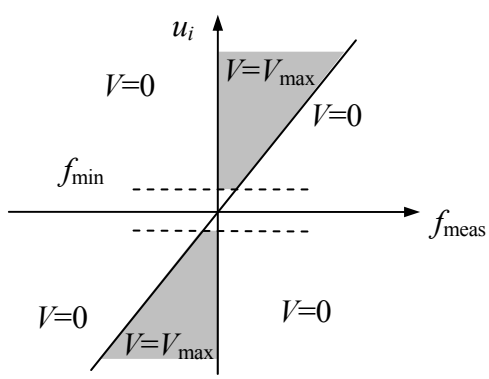

Figure 5-10 Graphical Representation for Selecting Command Signal (Dyke, 1996a)

With the clipped-optimal control algorithm for MR dampers, the simulink block diagram of this smart base isolation system is shown in Figure 5-11. The flow chart of the nominal controller design in the nodal coordinates was given in Figure 5-2. The flow chart of the nominal controller design in the modal coordinates will be given in chapter 6. The diagram also has a selection block for cases of passive-on (10 V to MR damper), passive-

off (0 V in MR damper), and semiactive. The passive (without MR damper) case will be controlled by the switch on/off block when it is on 0.

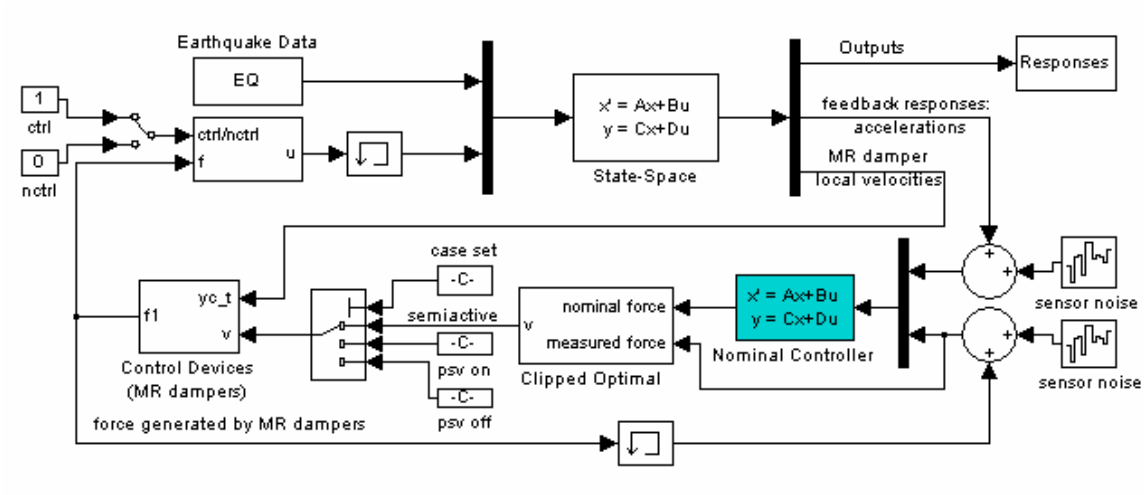

Figure 5-11 Simulink Block Diagram for Simulations

5.2.2 Weighting Determination

Engineering judgment plays an important role in modern LQ design for the selection of $\mathbf{Q}$ and $\mathbf{R}$. Once they are selected, the determination of the optimal feedback gain is a formal procedure relying on the solution of nonlinear coupled matrix equations. Because the ratio of the values in these two matrices are the critical parameters, it is assumed herein that $\mathbf{R} = \mathbf{I}_{20\times 20}$ without loss of generality, and $\mathbf{S}_{\ddot{x}_g\ddot{x}_g} = 25\mathbf{I}_2$ and $S_{v_i v_i} = \mathbf{I}_{ns\times 20}$ in solving the estimator gain.

In this study, the method to select $\mathbf{Q}$ used by Erkus and Johnson (2004) is adopted. Weightings are placed on displacements, velocities and accelerations at corner *j*, floor *i*. This choice is expressed as

$$\boldsymbol{\alpha}_i^j = \begin{bmatrix} (\alpha_{i,x}^j)^2 & 0 \\ 0 & (\alpha_{i,y}^j)^2 \end{bmatrix} \tag{5-32a}$$

$$\boldsymbol{\beta}_i^j = \begin{bmatrix} (\beta_{i,x}^j)^2 / \omega_x & 0 \\ 0 & (\beta_{i,y}^j)^2 / \omega_y \end{bmatrix} \tag{5-32b}$$

$$\boldsymbol{\gamma}_i^j = \begin{bmatrix} (\gamma_{i,x}^j / \omega_x)^2 & 0 \\ 0 & (\gamma_{i,y}^j / \omega_y)^2 \end{bmatrix} \tag{5-32c}$$

where $\boldsymbol{\alpha}$, $\boldsymbol{\beta}$, and $\boldsymbol{\gamma}$ represent the relative importance of displacements, velocities and accelerations, respectively. ω_x and ω_y are the frequencies of the dominant modes in the *x*- and *y*- directions, respectively. The frequencies are included in the weights to normalize the velocity and acceleration weights to be compatible with displacement weights in units and to have similar magnitudes. Here the mean of the first three frequencies (fundamental frequencies in *x*-, *y*- and *r*-directions) is used for both ω_x and ω_y; that is

$$\omega_x = \omega_y = \frac{\omega_{1,x} + \omega_{1,y} + \omega_{1,r}}{3} \tag{5-33}$$

In this study, all α, β and γ are set to unity. The weightings on drift, velocity, and acceleration are determined by scaling the values q_{drift}, q_{vel} and q_{accel}, respectively. An additional floor weighting of 100 is placed on the base displacements because these responses are the most important in our design goal.

The weighting matrix is composed of weights on displacements, velocities and accelerations of interest. It has been determined in section 5.2, i.e., corner base drifts, base accelerations, and top floor accelerations. The matrix is thus in the form

$$\mathbf{Q} = \begin{bmatrix} 100 \times q_{drift} \boldsymbol{\alpha}_b & \mathbf{0} & \mathbf{0} \\ \mathbf{0} & q_{accel} \boldsymbol{\gamma}_b & \mathbf{0} \\ \mathbf{0} & \mathbf{0} & q_{accel} \boldsymbol{\gamma}_8 \end{bmatrix} \tag{5-34}$$

where

$$\boldsymbol{\alpha}_b = \begin{bmatrix} \boldsymbol{\alpha}_b^1 & \cdots & 0 \\ \vdots & \ddots & \vdots \\ 0 & \cdots & \boldsymbol{\alpha}_b^4 \end{bmatrix}, \boldsymbol{\gamma}_b = \begin{bmatrix} \boldsymbol{\gamma}_b^1 & \cdots & 0 \\ \vdots & \ddots & \vdots \\ 0 & \cdots & \boldsymbol{\gamma}_b^4 \end{bmatrix}, \text{and } \boldsymbol{\gamma}_8 = \begin{bmatrix} \boldsymbol{\gamma}_8^1 & \cdots & 0 \\ \vdots & \ddots & \vdots \\ 0 & \cdots & \boldsymbol{\gamma}_8^4 \end{bmatrix}. \tag{5-35}$$

The responses at the four corners (marked in Figure 4-7) are used for weighting. $\boldsymbol{\alpha}_b^j$, $\boldsymbol{\gamma}_b^j$ and $\boldsymbol{\gamma}_8^j$ contain *x*- and *y*-components as shown in equation (5-30).

To determine the best weightings for structural response improvement, contour plots showing the ratio of improvement (maximum response of the semiactive system to the optimal passive system) at various q values (herein called q-Maps) for the Newhall earthquake are created. The highest frequency of the structure is 133Hz, so the integration step used for simulation is 0.0005 sec. The locations and numbers of MR dampers used are those determined in chapter 4, while sensors are the full set rather than the reduced set. Sensor noise is not considered in creating these q-maps.

The q-maps for the response reduction in the base drift and in the acceleration are shown in Figures 5-11 and 5-12, respectively. It is clear that for the semiactively controlled system, the accelerations increase and the base drifts decrease with larger values of q_{drift}. This behavior is the trade-off commonly observed in base-isolation systems. However, the responses do not change linearly with q_{accel}, so it is possible to find acceptable weighting values for both the base drifts and the accelerations.

Figure 5-12 shows that base drift can be reduced by up to 25% in the *x*-direction and up to 65% in the *y*-direction with $q_{drift} = 10^{6.5} \sim 10^{7.5}$. For these weighting values, accelerations are increased by 50% in the *x*-direction and 10% in the *y*-direction (Figure 5-13).

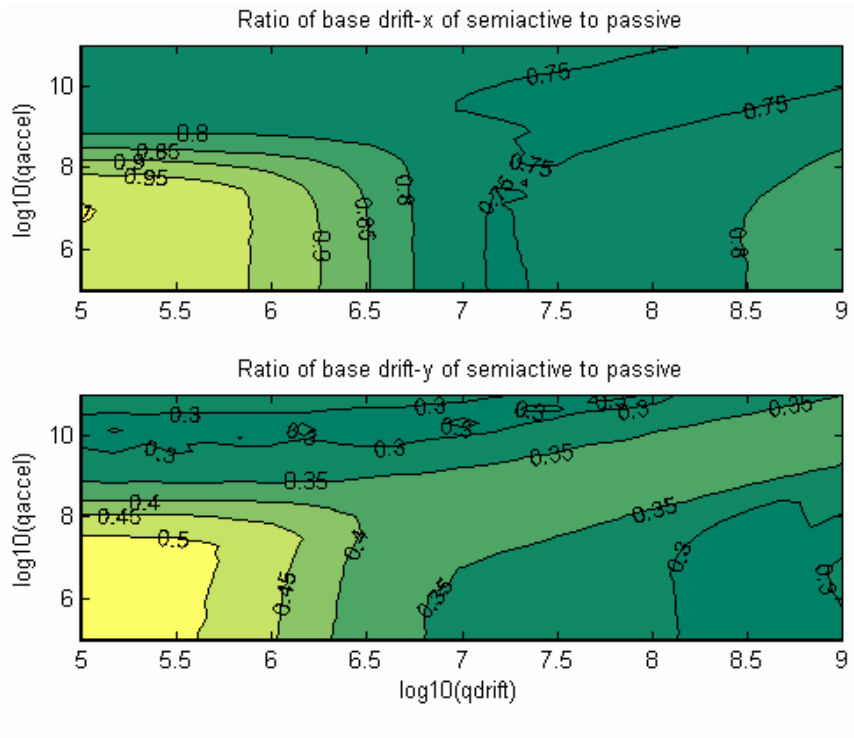

Figure 5-12 *q*-Maps of Base Drift Response

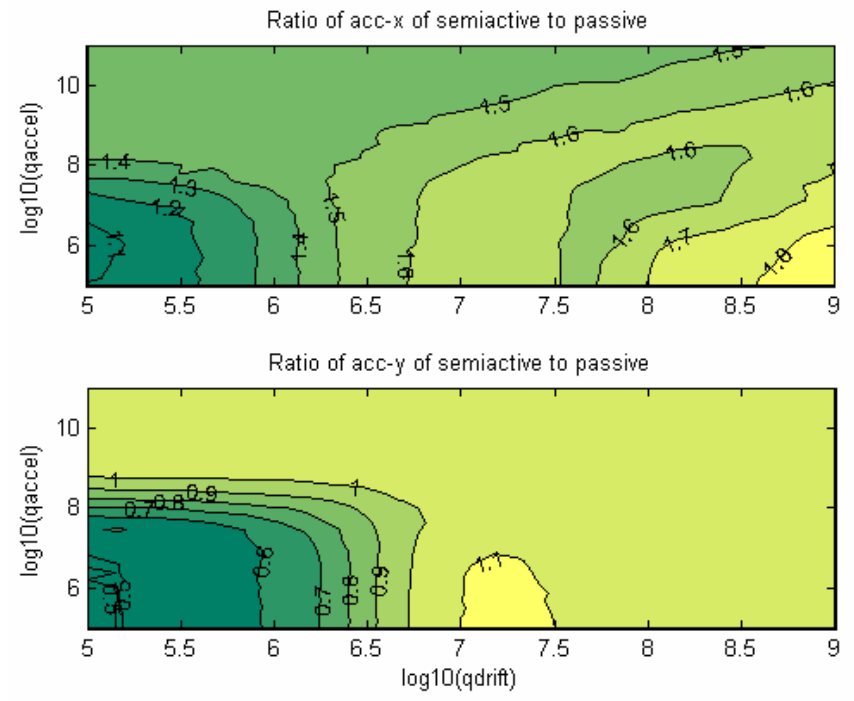

Figure 5-13 *q*-Maps of Acceleration Responses

The performance in the *y*-direction appears to be better because the responses are normalized by the larger of the two responses, which are those in the *x*-direction of the passive system. In subsequent earthquake simulations, $q_{drift} = 4.642 \times 10^6$ (with the factor 100 on base displacement, the actual $q_{drift} = 4.642 \times 10^8$) and $q_{acceleration} = 1.145 \times 10^9$ are used as the best weightings.

5.2.3 Earthquake Simulation Results

With the best set of weightings obtained through a thorough examination of the Newhall *q*-maps, the maximum responses subjected to all seven design earthquakes are computed. In addition to the responses of the semiactively controlled system, the performance of some other systems, passive (without MR damper), passive-on (10 V to MR damper), and passive-off (0 V in MR damper) systems are also computed for comparison. To be consistent with the *q*-maps, these simulations also use the full set of sensors without considering sensor noise. Results regarding the reduced-sensor and sensor noise will be shown in chapter 6. Figure 5-14 shows the maximum base drift, roof acceleration, and inter-story drift between the base and the 1st floor for the four cases (denoted by “semiactive”, “psv”, “psv on” and “psv off”, respectively, in the legend.) to the seven design earthquakes.

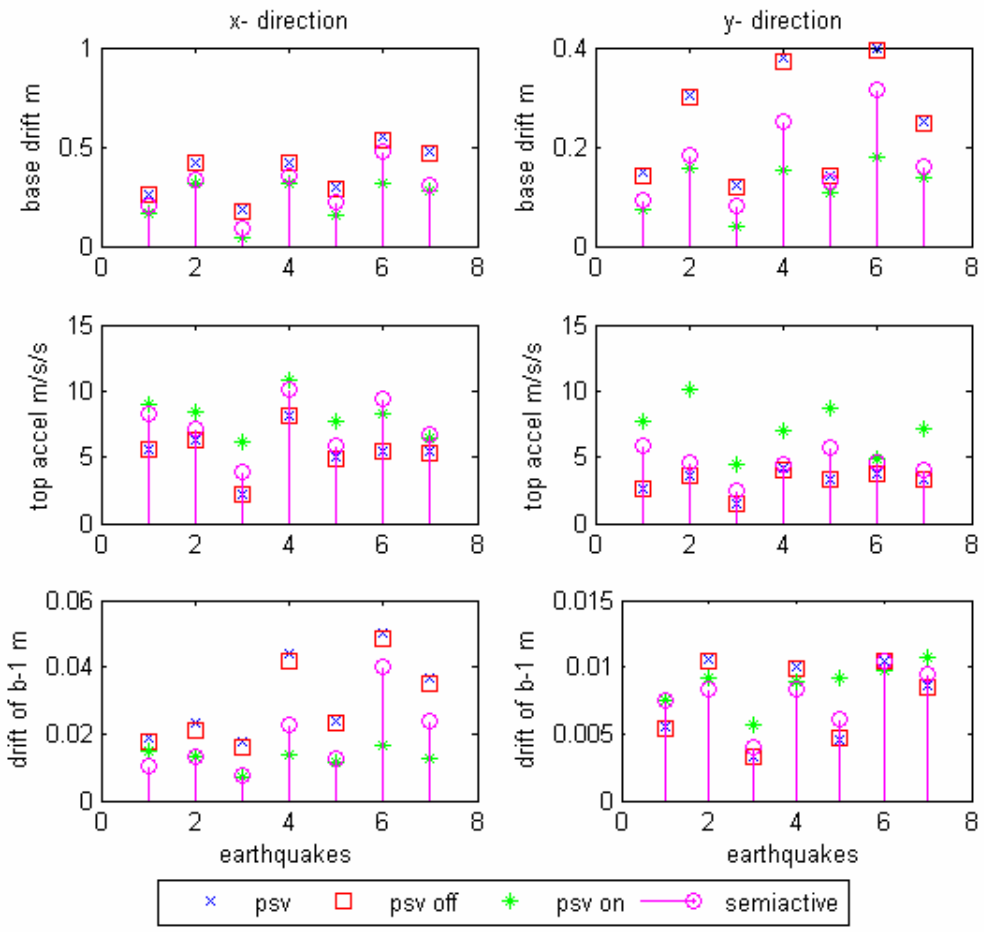

Figure 5-14 Maximum Responses to the Design Earthquakes (Nodal)

It is clear that the maximum responses of the ideal passive and MR-based passive-off systems are nearly equal. This result is because, with zero voltage, the damping force provided by MR damper is quite small. Passive-on is the most effective among the four strategies tested in limiting the base drift. However, it causes large accelerations and inter-story drifts in the superstructure. The semiactive system falls between the two cases. The base drift is limited to some extent at the cost of moderate acceleration and inter-story drift increases.

The performance of the passive-on and semiactive cases can also be compared using performance indices (Narasimhan, et al., 2004). Here six performance indices from Narasimhan et al. (2004) are compared (Table 5-2), and they correspond to the responses at the corners (unlike those defined in previous work). These numbers are also plotted in bar

graphs of Figure 5-15 and 5-16, where PI numbers 1, 2, 3 of the axis represent the performance indices 3, 4, 5, respectively, and 4, 5, 6 represent the performance indices 7, 11, and 8, respectively.

The values in Table 5-2 and the two figures demonstrate that both systems are able to decrease the base drift $(J_3 < 1, J_7 < 1)$ significantly for most of the earthquakes, especially in the case of the RMS responses. Though the semiactive system is not as good as the passive-on case at limiting the base drift, it is advantageous because it does not lead to the significantly larger story drifts and accelerations as the passive-on case. For the passive-on case, both peak and RMS accelerations for the earthquakes El Centro and Kobe are extremely large, while the semiactive case controls the accelerations within a range for all earthquakes, indicating the semiactively controlled system is particularly flexible in that it can adapt to various excitations and the designer has options regarding the design goals.

Table 5-2 Performance Indices

Earthquakes	Cases	Peak displ., drift, and accel.			RMS displ., drift, and accel.		
		J_3	J_4	J_5	J_7	J_{11}	J_8
Newhall	Passive-on	0.6416	1.2695	1.711	0.5147	0.8372	1.3951
	Semiactive	0.7660	1.2436	1.4942	0.6988	0.7644	1.1568
Sylmar	Passive-on	0.7380	1.1888	1.6139	0.5300	0.7655	1.1794
	Semiactive	0.7859	1.0669	1.1384	0.5904	0.6562	0.8829
El Centro	Passive-on	0.2468	0.9329	2.7857	0.3612	0.6900	2.8173
	Semiactive	0.5044	0.4962	1.7547	0.4783	0.3742	1.4551
Rinaldi	Passive-on	0.7360	0.7475	1.3323	0.3906	0.3707	1.3349
	Semiactive	0.8333	0.7498	1.2382	0.6503	0.4729	1.0482
Kobe	Passive-on	0.5333	0.9633	1.7454	0.4439	0.7523	1.8341
	Semiactive	0.7511	0.7478	1.2592	0.6380	0.5227	1.1794
Ji-ji	Passive-on	0.5725	0.5038	1.5323	0.4067	0.3647	0.9561
	Semiactive	0.8624	0.8001	1.7390	0.7597	0.6981	0.9967
Erzincan	Passive-on	0.5753	0.5058	1.3211	0.4786	0.4718	0.8771
	Semiactive	0.6457	0.6537	1.2372	0.6043	0.5172	0.8643

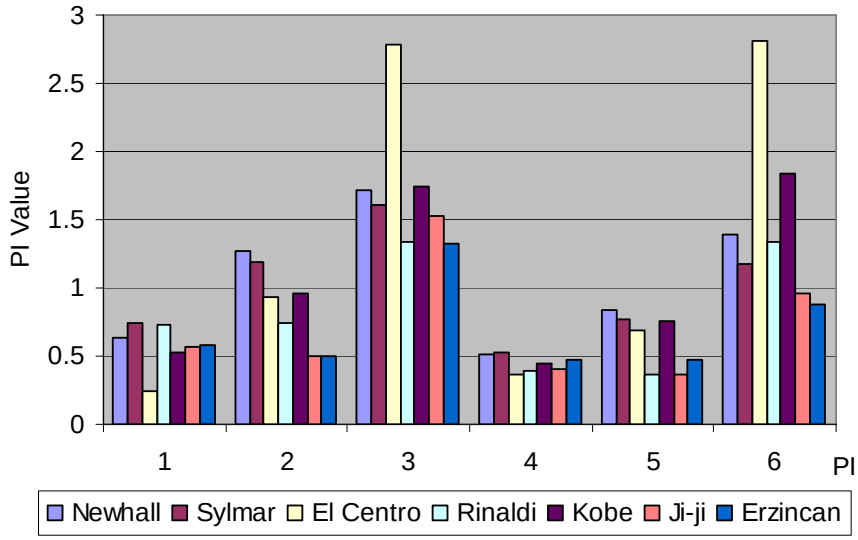

Figure 5-15 Performance Indices of the Passive-on System

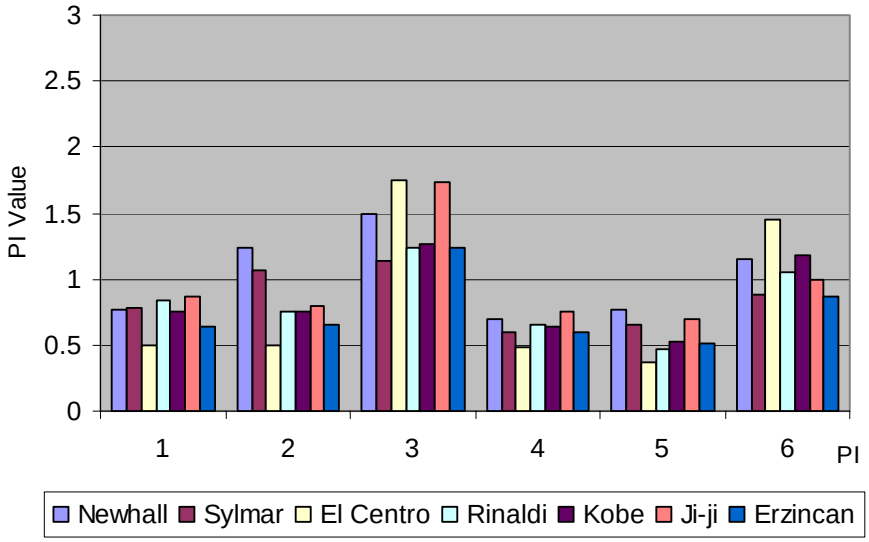

Figure 5-16 Performance Indices of the Semiactive System (Nodal)

Next, the responses to the Newhall earthquake are examined closely because *q*-maps were computed specifically for this earthquake. Figure 5-17 shows the base drift at corner 1 of the system to this earthquake. Though the semiactive case does not decrease the base drifts as much as the passive-on case, it has a similar decrease in the peak values than the passive and passive-off cases as the passive-on case.

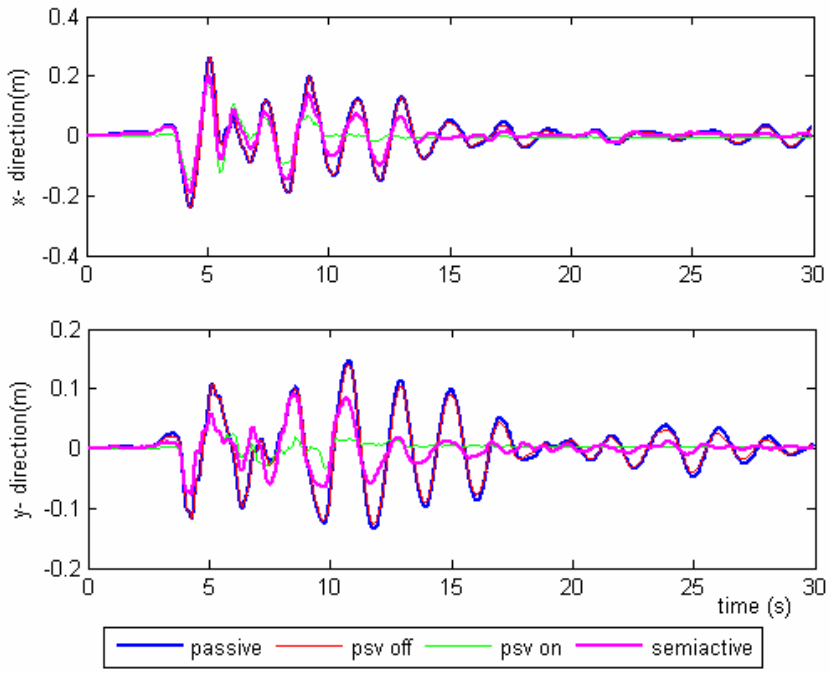

Figure 5-17 Base Drift Responses at Corner 1 to the Newhall Earthquake (Nodal)

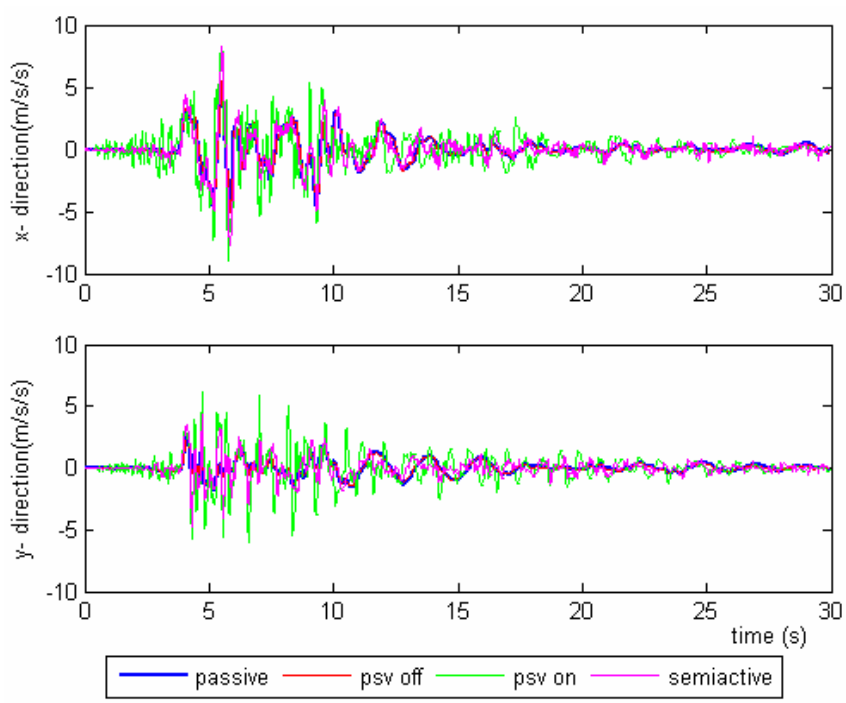

Figure 5-18 Acceleration Responses at Roof Corner 1 to the Newhall Earthquake (Nodal)

Figure 5-19 shows the top floor accelerations at corner 1 of the various systems for this earthquake. Note that the accelerations for the semiactive case are not as high as those of the passive-on case, although the peak values in *x*-direction are similar.

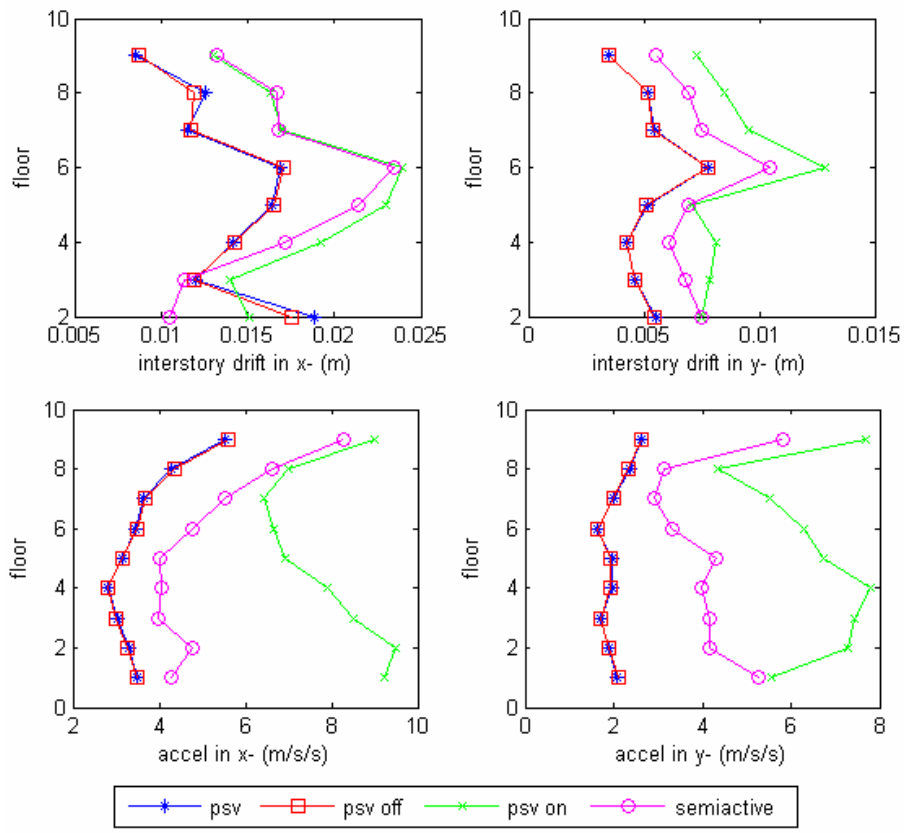

Figure 5-19 Response Profiles to the Newhall Earthquake (Nodal)

Figure 5-19 provides the peak response profiles for the Newhall earthquake. These plots show that maximum inter-story drift occurs at the 6th floor, while the maximum acceleration occurs at the roof. The semiactive system clearly performs better than the passive-on system in that it results in both lower accelerations and lower inter-story drifts.

The effective forces provided by MR dampers for the passive-on, passive-off and semiactive cases, and the effective bearing forces in the passive case are given in Figure 5-20. It shows that in the *x*- and *y*-directions, the effective control forces generated by the MR dampers do not exceed the maximum bearing forces used by the passive base isolation

system. This outcome satisfies the restrictions set forth in the benchmark problem. Also notice that the control forces in the passive-on case are greater than those in the semiactive case, and the forces with the MR-based passive-on controller do exceed the passive bearing forces in *r*-direction. This fact indicates that much less control effort (and smaller, less expensive devices) is needed for the semiactive strategy to achieve effective control performance than for the passive-on system.

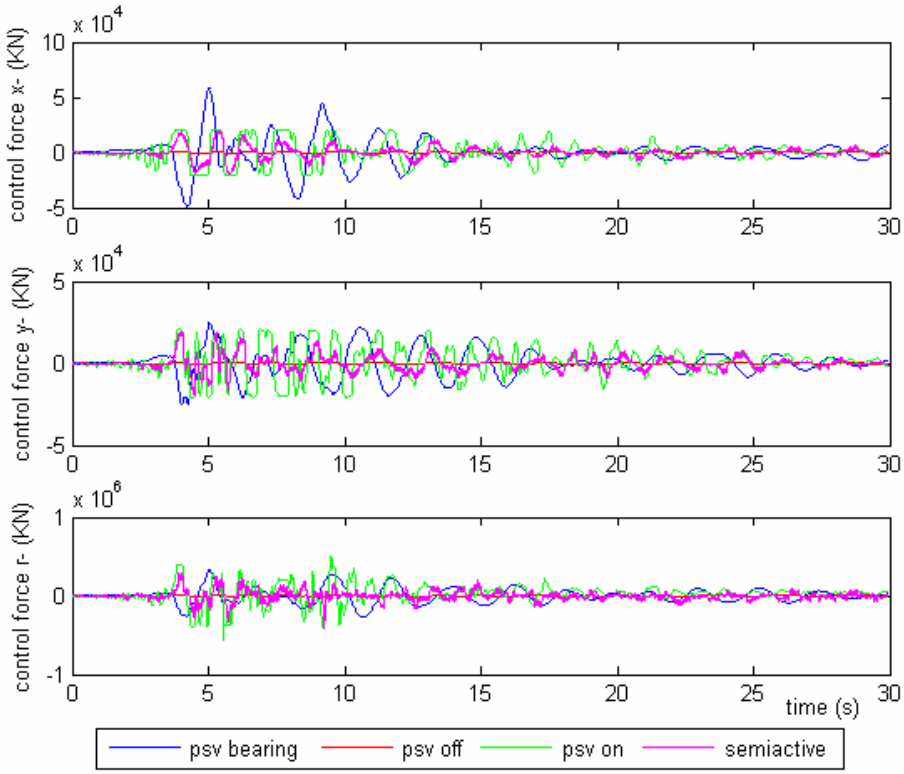

Figure 5-20 Effective Bearing Forces and Control Forces (Nodal)

As a final study, it is of interest to investigate how well the control forces generated by the MR dampers using the clipped-optimal strategy track the desired control forces computed from LQG algorithm. The forces shown in Figure 5-21 are the forces in one of the two MR dampers at bearing #3 in *x*- and *y*-directions, respectively. The ability of the MR damper to track the desired force generated by the nominal LQG controller are clearly seen here. The reason the peak force in the MR damper is lower is that the capacity of the MR dampers used in this study is 1000 kN (see chapter 3) and the desired force exceeds

this value. This outcome occurs often in the design of a semiactive controller and should not be considered a deficiency.

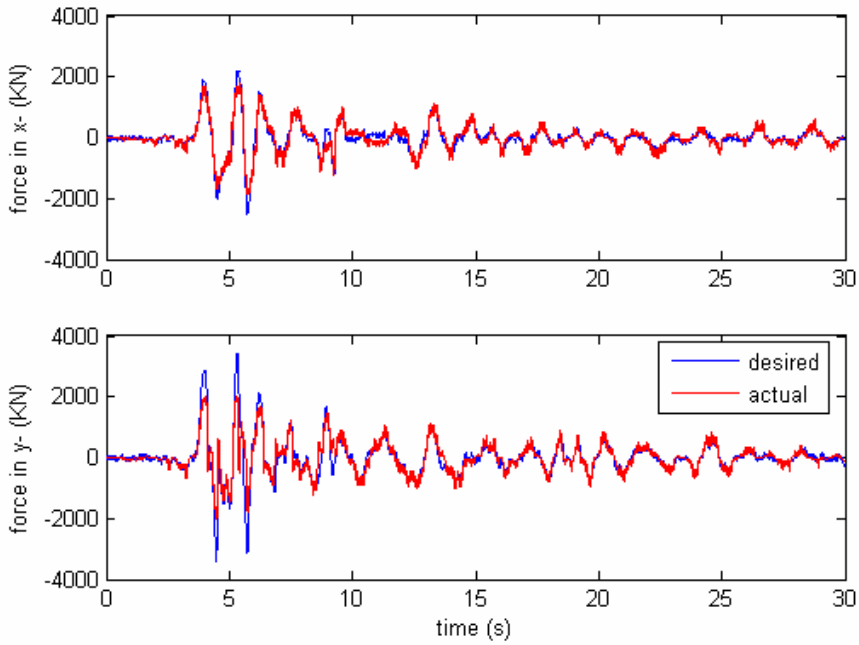

Figure 5-21 Desired and Actual Control Forces in MR Damper at Bearing 3 in the Newhall Earthquake (Nodal)

5.3 Pole Assignment and Order Reduction in Nodal Coordinates

With the weightings chosen, the controller gain matrix and estimator gain matrix have been determined, and thus the closed-loop poles of the plant $(\mathbf{A}-\mathbf{BK})$ and of the LQG compensator $(\mathbf{A}-\mathbf{LC}_y)$ are determined. It is of interest to examine how the control action changes the system configuration. Here the closed-loop poles are plotted together with the open-loop poles to gain some insight into the feedback control in the frequency domain.

Figure 5-22 shows that, with control, the first two modes in three directions (x, y, and r) are shifted to the left while other modes barely change. The two modes shifted roughly to the frequencies of the first two flexible modes, indicating that they are comparable to the frequencies of a traditional (fixed-base) building. However, the simulations shown above

demonstrated that the closed-loop system did not result in the large acceleration and drift levels typically present in fixed-based buildings. So the controlled structure has the ability to achieve better performance.

Also observed from Figure 5-22 is that these poles shift nearly horizontally and remain at approximately the same magnitude along the imaginary axes, indicating that the shifted poles have higher damping.

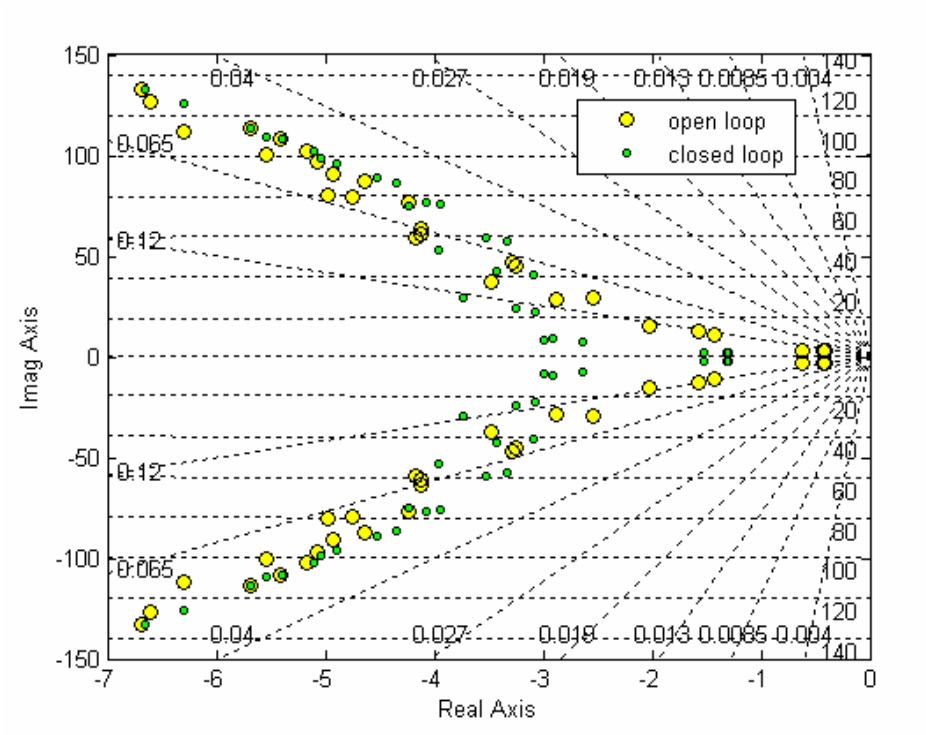

Figure 5-22 Poles of the Open-Loop and the Closed-Loop Plants (Nodal)

Figure 5-23 provides a plot of the compensator poles versus the open-loop plant poles. This plot shows that some poles shift far into the left-hand-plane with the selected weightings. Figure 5-24 is a zoom-in of Figure 5-23. Clearly, the poles corresponding to one isolation mode, and all the second and the third modes are shifted to the left, indicating that estimator errors of these modes decay quickly.

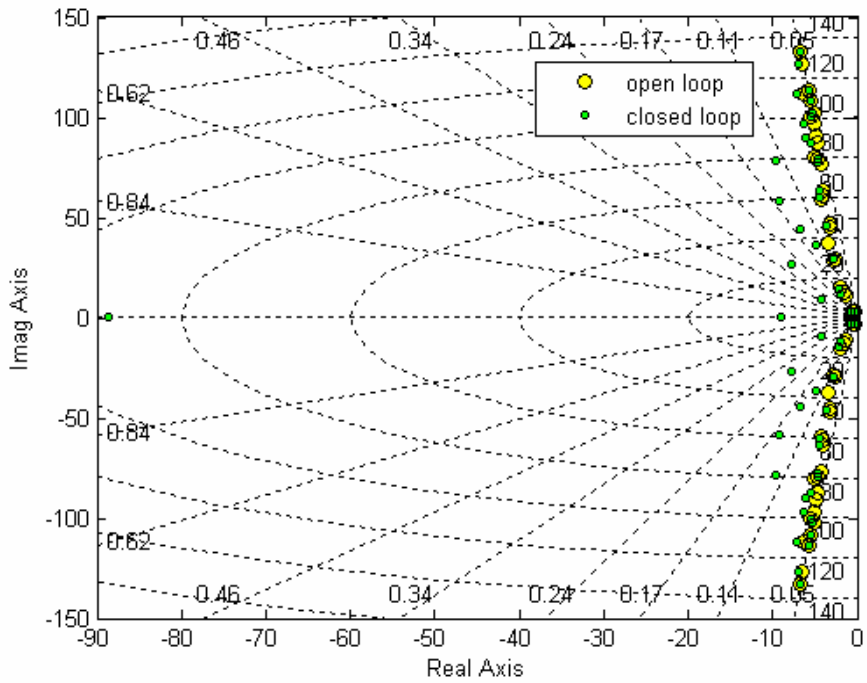

Figure 5-23 Poles of the Open-Loop Plant and the Closed-Loop Controller (Nodal)

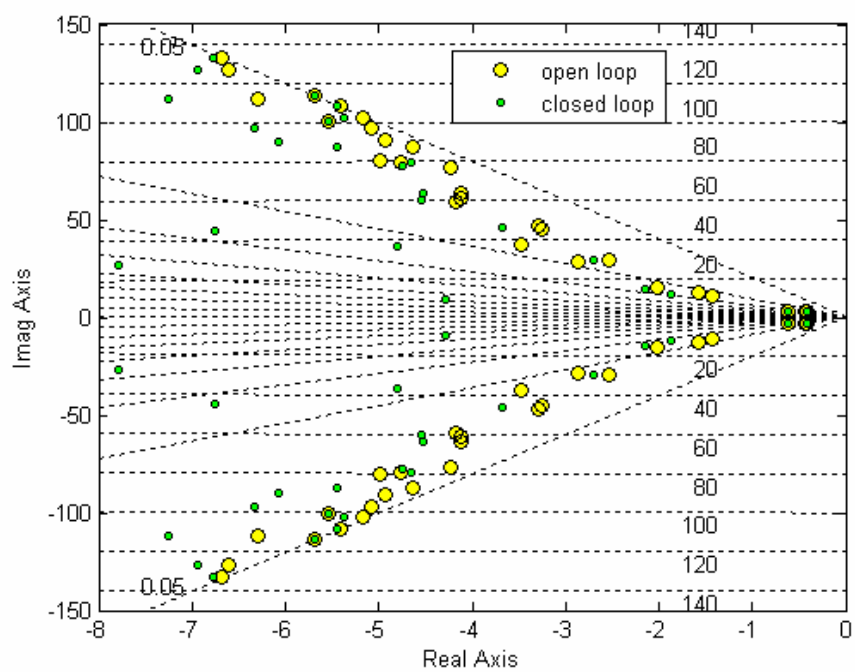

Figure 5-24 Zoom-In of the Poles of the Open-Loop Plant and the Closed-Loop Controller

5.4 Summary

Two issues for improving LQG design have been found to be very important: determination of the weightings and controller order. Weighting matrix selection is extensively studied in this chapter for a base isolated structural system by examining the observability of the selected responses so that all loops are closed and control gains are large in the desired modes. Optimal weighting values for the base isolated system examined herein are determined through trial simulations. The responses of the building to the design earthquakes with the selected weightings are presented.

However, using the trial-and-error method to determine the weightings fails to provide the insights into the effect of the control action on the structural dynamics and thus, prevents one from conducting more effective control and performance-oriented design. For example, the closed-loop pole locations are implicitly related to the weightings in the nodal approach. It is not clear how to choose $\mathbf{Q}$ and $\mathbf{R}$ to achieve larger gains for desired states or modes. It is similarly hard to determine the estimator gains such that the errors in the estimator states decay quickly while the dynamics do not override the control action. In nodal coordinates, it is also challenging to reduce the order of the controller, because the insignificant states or modes are not explicitly shown in the weightings. However, in modal coordinates, the answers to the above questions are explicit and straightforward, which will be discussed and studied in the next chapter.

Chapter 6

LQG Control and Order Reduction Using the Modal Approach

Constraints on the controller order are frequently employed in classical controller design. For example, proportional control constrains the controller to have an order of zero, and a lead compensator constrains the order to be one (Burl, 1999). State-space control strategies tend to yield controllers of excessively high order. The basic order of an LQ methodology generates controllers with an order equal to the plant order. Frequency-shaped loop transfer recovery, integral control, and other modifications of the controller's frequency domain characteristics increase the controller order. High order controllers not only increase the hardware quantity and complexity, which translates directly to increased cost, but also increase software complexity, which increases coding and debugging time. High order controllers typically contain faster poles and thus require faster sampling rates, which may increase the cost of A/D and D/A conversion. For digital control, high order controllers increase the computational burden and therefore the speed of the required processor. For these reasons, it is desirable to reduce the order of the controllers whenever possible (Burl, 1999).

Controller order can be reduced in three ways: (1) generate a reduced order approximation of the plant before designing the controller; (2) constrain the order of the controller during the design; (3) generate an approximate reduced order controller after the controller design. For MIMO systems combined with modern control technique like LQG, order reduction is usually performed after the full order controller design. A variety of techniques exist for controller order reduction. In this study, a technique referred to as LQG-balancing is adopted, for it assumes that the system to be balanced is closed with a standard LQG feedback loop. Studies have shown that the LQG approach is the most natural way to balance closed-loop systems (Jonckheer and Silverman, 1983). An approximate LQG-balanced method that simplifies the procedure will also be introduced

and evaluated in this chapter. The approximate procedures only apply to the modal coordinate system.

6.1 LQG Balancing and Order Reduction

6.1.1 LQG Control in Modal Coordinates

For an LQG strategy in a modal coordinate system, consider a simple case of $\mathbf{D_z} = \mathbf{0}$, $\mathbf{R} = \mathbf{I}$, $\mathrm{E}\{\mathbf{v}\mathbf{v}^T\} = \mathbf{P} = \mathbf{I}$. There is no loss of generality with these assumptions because they can be compensated by adjusting $\mathbf{Q}$ and $\mathbf{H}$. The CARE and FARE of the system represented by equations (5-7) and (5-21) then reduce to

$$\mathbf{0} = \mathbf{S}_c\mathbf{A} + \mathbf{A}^T\mathbf{S}_c - \mathbf{S}_c\mathbf{B}\mathbf{B}^T\mathbf{S}_c + \widetilde{\mathbf{Q}} \tag{6-1}$$

$$\mathbf{0} = \mathbf{S}_e\mathbf{A}_a + \mathbf{A}_a^T\mathbf{S}_e - \mathbf{S}_e\mathbf{C}_{\mathbf{y}a}^T\mathbf{C}_{\mathbf{y}a}\mathbf{S}_e + \underset{\sim}{\mathbf{H}} \tag{6-2}$$

where

$$\widetilde{\mathbf{Q}} = \mathbf{C}_{\mathbf{z}}^T\mathbf{Q}\mathbf{C}_{\mathbf{z}}, \quad \underset{\sim}{\mathbf{H}} = \mathbf{E}_a\mathbf{H}\mathbf{E}_a^T, \quad \mathrm{E}\{\mathbf{w}\mathbf{w}^T\} = \mathbf{H}\delta(\tau) \tag{6-3}$$

and the control gain and the estimator gain are given by

$$\mathbf{K} = \mathbf{B}^T\mathbf{S}_c, \quad \mathbf{L} = \mathbf{S}_e\mathbf{C}_{\mathbf{y}a}^T. \tag{6-4}$$

Weightings can be placed directly on the responses of particular modes with the modal approach, so the model does not require a shaping filter in the controller design, i.e., $\mathbf{A}_a = \mathbf{A}$, $\mathbf{C}_{\mathbf{y}a} = \mathbf{C}_{\mathbf{y}}$, and $\mathbf{E}_a = \mathbf{E}$.

The control design process usually begins with the required closed-loop system performance, such as the tracking error, or the pole locations. Thus, one must determine appropriate weights to meet the performance requirement. Generally, weighting selection is

a trial and error process and is dependent on experience. For example, using the nodal approach in chapter 5, weights are determined through q-maps by numerical simulation. However, with the modal approach, weightings can be placed directly on modes of interest. Moreover, an analytical solution can be obtained for low-authority LQG controllers.

A low-authority controller only moderately modifies the system properties. For a structure with LQG control, the controller is of low-authority if the plant closed-loop matrix and the estimator closed-loop matrix in (6-5a) can be approximately replaced by (6-5b)

$$\mathbf{A}_{pcl} = \mathbf{A} - \mathbf{B}\mathbf{B}^T\mathbf{S}_c\,,\ \mathbf{A}_{ecl} = \mathbf{A} - \mathbf{S}_e\mathbf{C}^T\mathbf{C} \tag{6-5a}$$

$$\mathbf{A}_{pcl} \cong eig(\mathbf{A} - diag(\mathbf{B}\mathbf{B}^T)\mathbf{S}_c)\,,\ \mathbf{A}_{ecl} \cong eig(\mathbf{A} - \mathbf{S}_e diag(\mathbf{C}^T\mathbf{C}))\,. \tag{6-5b}$$

In other words, for a low-authority controller, $\mathbf{B}\mathbf{B}^T$ and $\mathbf{C}^T\mathbf{C}$ can be replaced with their diagonal terms (Gawronski, 1998).

Low-authority LQG controllers in modal representations produce diagonally dominant solutions of CARE and FARE equations, and weights are explicitly implied in pole shifts. These results are summarized in properties 6, 7 and 8 provided below.

Consider the diagonal weight matrices $\widetilde{\mathbf{Q}}$ and $\underset{\sim}{\mathbf{H}}$, i.e., $\widetilde{\mathbf{Q}} = diag(q_i\mathbf{I}_2)$ and $\underset{\sim}{\mathbf{H}} = diag(h_i\mathbf{I}_2)$. The solutions to the Ricatti equations (6-1) and (6-2) can be obtained from properties 6 and 7, respectively.

6. There exist $q_i \le q_{o,i}$, where $q_{o,i} > 0$, $i = 1,\cdots,n$, such that $\mathbf{S}_c \cong diag(s_{c,i}\mathbf{I}_2)$ is the solution of (6-1), where

$$s_{c,i} = \frac{\beta_{c,i} - 1}{2w_{c,i}} = \frac{\beta_{c,i} - 1}{2\gamma_i^2}, \quad \beta_{c,i}^2 = \frac{1 + 2q_i\gamma_i^2}{\zeta_i\omega_i} \tag{6-6}$$

7. There exist $h_i \le h_{o,i}$, where $h_{o,i} > 0$, $i = 1, \cdots, n$, such that $\mathbf{S}_e \cong diag(s_{e,i}\mathbf{I}_2)$ is the solution of (6-2), where

$$s_{e,i} \cong \frac{\beta_{e,i} - 1}{2w_{o,i}} = \frac{\beta_{e,i} - 1}{2\gamma_i^2}, \quad \beta_{e,i}^2 = \frac{1 + 2h_i\gamma_i^2}{\zeta_i \omega_i}. \tag{6-7}$$

Here, γ_i is the ith Hankel singular value, $w_{o,i}$ and $w_{o,i}$ are the ith controllability and observability grammians, respectively, ξ_i the ith modal damping ratio, and ω_i the ith circular frequency.

Figure 6-1 shows the change in β_c with the weight q or Hankel singular value square from equation (6-6). Similar results can be obtained for β_e based on the weight h.

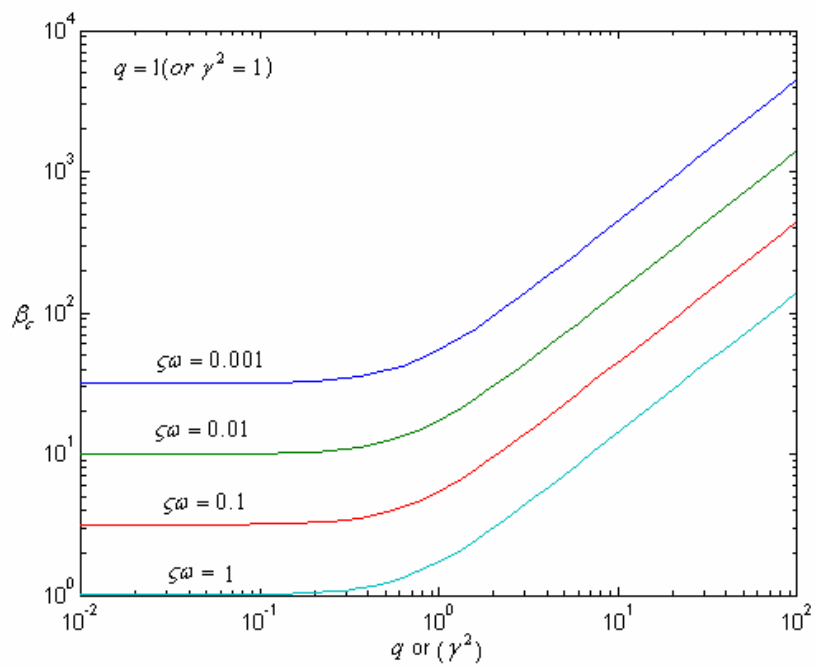

Figure 6-1 Coefficient β_c vs. Weight q or Hankel Singular Value γ^2

Also, the approximate diagonal CARE and FARE solutions allow one to determine the relationship between the weights and root loci. Let weighting matrices be

$$\widetilde{\mathbf{Q}} = (0,0,\ldots,q_i\mathbf{I}_2,\cdots,0,0), \text{ and } \underset{\sim}{\mathbf{H}} = (0,0,\ldots,h_i\mathbf{I}_2,\cdots,0,0). \tag{6-8}$$

Then property 8 (the LQG root-locus) holds (Gawronski, 1994, 1998).

8. For the weights (6-8) and $q_i \le q_{o,i}$, $h_i \le h_{o,i}$, the pair of closed-loop poles $(\mathrm{Re}(\lambda_{cc,i}) \pm j\,\mathrm{Im}(\lambda_{cc,i}))$ (controller) and $(\mathrm{Re}(\lambda_{ec,i}) \pm j\,\mathrm{Im}(\lambda_{ec,i}))$ (estimator) related to the pair of open-loop poles $(\mathrm{Re}(\lambda_{co,i}) \pm j\,\mathrm{Im}(\lambda_{co,i}))$ (controller) and $(\mathrm{Re}(\lambda_{eo,i}) \pm j\,\mathrm{Im}(\lambda_{eo,i}))$ (estimator) by

$$\mathrm{Re}(\lambda_{cc,i}) \pm j\,\mathrm{Im}(\lambda_{cc,i}) \cong \beta_{c,i}\,\mathrm{Re}(\lambda_{co,i}) \pm j\,\mathrm{Im}(\lambda_{co,i}) \tag{6-9a}$$

$$\mathrm{Re}(\lambda_{ec,i}) \pm j\,\mathrm{Im}(\lambda_{ec,i}) \cong \beta_{e,i}\,\mathrm{Re}(\lambda_{eo,i}) \pm j\,\mathrm{Im}(\lambda_{eo,i}) \tag{6-9b}$$

where $q_{o,i}$ and $h_{o,i}$ are limiting values for damping authority. They are the weights at which the *i*th resonant peak of the plant transfer function flattens (Gawronski, 1994,1998).

Property 8 implies that the *i*th pair of closed-loop poles shifts the *i*th pair of open-loop poles by factors of $\beta_{c,i}$ and $\beta_{e,i}$ on the real axis for the controller and estimator, respectively (Gawronski, 1994, 1998). The imaginary parts $\mathrm{Im}(\lambda_{co,i}) = \omega_{d,i}$, and other pairs of poles, remain unchanged.

Proofs regarding the low-authority property, the approximate CARE and FARE solutions, and the root-loci to weight relationships are given in Gawronski (1994, 1998) and are summarized in Appendix B.

An investigation of the root locus characteristic results in additional insights. Note that the real part of the poles is $\mathrm{Re}(\lambda_{co,i}) = \zeta_i\omega_i$, and the resonant peak is $\alpha_{o,i} = \kappa/2\zeta_i\omega_i$, where κ is a constant. One obtains

$$\beta_{c,i} = \zeta_{c,i}/\zeta_i = \alpha_{o,i}/\alpha_{c,i}. \tag{6-10}$$

$\beta_{c,i}$ is thus a ratio of the closed-loop to the open- loop damping ratio, and the open-loop to the closed-loop resonant peak. Therefore, to suppress the resonant peak by $\beta_{c,i}$ times, the required weighting is (from property 6)

$$q_i \cong \frac{(\beta_{c,i}-1)^2 \zeta_i \omega_i}{2\gamma_i^2}. \tag{6-11}$$

$\beta_{c,i}$ can also be interpreted as a ratio of the open-loop to closed-loop Hankel singular value, or as a ratio of the variances of the open-loop $\sigma_{o,i}^2$ and the closed-loop $\sigma_{c,i}^2$ states excited by the white noise input (Gawronski, 1998) as

$$\beta_{c,i} \cong \frac{\gamma_{o,i}^2}{\gamma_{c,i}^2} = \frac{Var_{o,i}^2}{Var_{c,i}^2}. \tag{6-12}$$

This interpretation can be obtained using modal coordinate properties and Lyaponov equations.

These formulas and related insights provide a direct approach to the design of the controller. Note that, although the controller and estimator gain matrices might not be completely accurate with the assumptions of $\mathbf{D_z} = \mathbf{0}$ and $\mathbf{E}_y = \mathbf{0}$, they do not pose a problem for assigning pole location because, as property 8 illustrated, the desired solutions of $(\mathbf{S}_c, \mathbf{S}_e)$, and thus the desired gains, can be found by adjusting weightings. So these assumptions do not result in a loss of generality.

6.1.2 LQG-Balanced and Approximately LQG-Balanced Controllers

The LQG methodology generates controllers with an order equal to the plant order. The state-space model of the base isolated benchmark structure has an order of 54. It is desirable that the controller have a lower order. However, reducing the controller order based on Moore balanced realization (chapter 2) uses the assumption that the plant and the

controller are operating separately as open loops. One still has to be cautious about the feedback properties of the loop made up with the full system and a compensator based upon the reduced model.

In this study, a new balancing and reduction approach, the LQG-balancing technique, is adopted. It was initiated by Jonckheer and Silverman (1983) and extended by Opdenacker and Jonckheer (1985), which considered the plant, from the beginning, within the LQG loop. Jonckheer and Silverman (1983) found that the eigenvalues of the solutions to the two algebraic Riccati equations (CARE and FARE) are similarity invariants, and there exists a state-space representation in which $\mathbf{S}_c$ and $\mathbf{S}_e$ are equal and diagonal. An LQG-balanced system is thus defined in the sense that the solutions to CARE and FARE are equal and diagonal, that is

$$\mathbf{S}_c = \mathbf{S}_e = \boldsymbol{M}_{lqg} = diag(\mu_1, \mu_2, \cdots, \mu_N),\ \mu_1 \geq \mu_2 \geq \cdots \geq \mu_N \tag{6-13}$$

where $\Sigma_{lqg} = diag(\mu_i)$, and μ_i, $(i = 1, \cdots, N)$ are LQG characteristic (or singular) values. The characteristic values are used to measure how important each state of the plant is in the closed loop. It makes it possible to construct a reduction index for the LQG compensator that remains approximately the same as the full order version.

Let $\mathbf{T}_{lqg}$ be the transformation matrix of the LQG-balanced state such that $\mathbf{x} = \mathbf{T}_{lqg}\overline{\mathbf{x}}$. The transformation matrix $\mathbf{T}_{lqg}$ is computed by decomposing $\mathbf{S}_c$ and $\mathbf{S}_e$, forming the matrix $\mathbf{F}$, and then performing singular value decomposition to $\mathbf{F}$, as

$$\mathbf{S}_c = \mathbf{P}_c^T \mathbf{P}_c,\ \mathbf{S}_e = \mathbf{P}_e^T \mathbf{P}_e \tag{6-14}$$

$$\mathbf{F} = \mathbf{P}_c \mathbf{P}_e \tag{6-15}$$

$$\mathbf{F} = \mathbf{V}\boldsymbol{M}_{lqg}\mathbf{U}^T \tag{6-16}$$

where the singular values are the LQG characteristic values. $\mathbf{T}_{lqg}$ is obtained using

$$\mathbf{T}_{lqg} = \mathbf{P}_e \mathbf{U} \boldsymbol{M}_{lqg}^{-1/2} \quad \text{or} \quad \mathbf{T}_{lqg} = \mathbf{P}_c^{-1} \mathbf{V} \boldsymbol{M}_{lqg}^{-1/2} . \tag{6-17}$$

The solutions of CARE and FARE, and the weighting matrices in the new coordinate system, are (Jonckheer and Silverman, 1983)

$$\overline{\mathbf{S}}_c = \mathbf{T}_{lqg}^T \mathbf{S}_c \mathbf{T}_{lqg} , \ \overline{\mathbf{S}}_e = \mathbf{T}_{lqg}^{-1} \mathbf{S}_e \mathbf{T}_{lqg} \tag{6-18}$$

$$\overline{\mathbf{Q}}_c = \mathbf{T}_{lqg}^T \widetilde{\mathbf{Q}} \mathbf{T}_{lqg} , \ \overline{\mathbf{Q}}_e = \mathbf{T}_{lqg}^{-1} \underset{\sim}{\mathbf{H}} \mathbf{T}_{lqg} . \tag{6-19}$$

The most striking result Opdenacker and Jonckheer (1985) obtained for the LQG balancing method is that, in a system without energy dissipation, the LQG-balanced coordinates coincide with the modal coordinates and that the characteristic values of the balancing all equal one. A characteristic value not equal to one is a clear indication of the existence of dissipation in the system. Other types of balancing, or related techniques, do not have this property. Thus, LQG-balancing is a procedure that accounts for the physical characteristics of the problem throughout.

The results for low-authority controllers lead to approximate, but greatly simplified procedures of LQG balancing in modal coordinates. The system is approximately LQG-balanced in the sense that $\mathbf{S}_c \cong \mathbf{S}_e \cong \boldsymbol{M}_{lqg}$, i.e., their diagonal terms satisfy $s_{c,i} + \varepsilon_{c,i} = \mu_i$, $s_{e,i} + \varepsilon_{e,i} = \mu_i$ with $\varepsilon_{c,i} / s_{c,i} << 1$ and $\varepsilon_{e,i} / s_{e,i} << 1$. Gawronski (1994) derived approximate, closed-form balanced-LQG-controller gains from Riccati equations in modal coordinates, stated in property 9.

9. For the diagonally dominant solutions of CARE and FARE for a Moore-balanced modal model, i.e., $\mathbf{S}_c \cong diag(s_{c,i}\mathbf{I}_2)$ and $\mathbf{S}_e \cong diag(s_{e,i}\mathbf{I}_2)$, an approximate balanced-LQG solution is obtained. It is diagonally dominant, i.e.,

$$\boldsymbol{M}_{lqg} \cong diag(\mu_i \mathbf{I}_2) \ \text{and} \ \ \mu_i = \sqrt{s_{c,i} s_{e,i}} \tag{6-20}$$

where $\mathbf{T}_{lqg}$ is the transformation matrix from the balanced modal representation $(\mathbf{A}_{mb}, \mathbf{B}_{mb}, \mathbf{C}_{mb}, \mathbf{D}_{mb})$ to the LQG-balanced representation $(\mathbf{A}_{lqg}, \mathbf{B}_{lqg}, \mathbf{C}_{lqg}, \mathbf{D}_{lqg})$. It is diagonally dominant as well,

$$\mathbf{T}_{lqg} \cong diag(T_{lqg,1}\mathbf{I}_2, T_{lqg,2}\mathbf{I}_2, \cdots, T_{lqg,n}\mathbf{I}_2), \quad T_{lqg,i} = (\frac{s_{e,i}}{s_{c,i}})^{1/4} \tag{6-21}$$

and $(\mathbf{A}_{lqg}, \mathbf{B}_{lqg}, \mathbf{C}_{lqg}, \mathbf{D}_{lqg})$ is approximately obtained by

$$(\mathbf{A}_{lqg}, \mathbf{B}_{lqg}, \mathbf{C}_{lqg}, \mathbf{D}_{lqg}) \cong (\mathbf{A}_{mb}, \mathbf{T}_{lqg}^{-1}\mathbf{B}_{mb}, \mathbf{C}_{mb}\mathbf{T}_{lqg}, \mathbf{D}_{mb}). \tag{6-22}$$

$\mathbf{T}_{lqg}$ is obtained either from the singular value decomposition (SVD) method or the approximate method; the control gain and the estimator gain based on the LQG-balanced model are given by

$$\overline{\mathbf{K}} = \mathbf{B}_{lqg}^T \overline{\mathbf{S}}_c, \quad \overline{\mathbf{L}} = \overline{\mathbf{S}}_e \mathbf{C}_{\mathbf{y},lqg}^T. \tag{6-23}$$

The LQG-balanced controller for the semiactive system is then

$$\dot{\hat{\overline{\mathbf{x}}}} = (\mathbf{A}_{lqg} - \overline{\mathbf{L}}\mathbf{C}_{\mathbf{y},lqg})\hat{\overline{\mathbf{x}}} + \begin{bmatrix} \overline{\mathbf{L}} & \mathbf{B}_{lqg} - \overline{\mathbf{L}}\mathbf{D}_{\mathbf{y},lqg} \end{bmatrix} \begin{Bmatrix} \mathbf{y} \\ \mathbf{f}_{meas} \end{Bmatrix} \tag{6-24a}$$

$$\mathbf{f} = \overline{\mathbf{K}}\hat{\overline{\mathbf{x}}} \tag{6-24b}$$

These results provide a means for controller order reduction.

6.1.3 Reduction Index and Reduction Strategy

A balanced model was introduced above for model reduction. However, determining the order and the retained states that best reproduce the complete system needs a measure

of importance, i.e., a reduction index. Generally, system norms are used as reduction indices (Burl, 1999). However, system norms, including Hankel norms, reflect only the system controllability and observability properties of the open-loop systems. For closed-loop, Jonckheer and Silverman (1983) used the LQG characteristic values as the reduction indices to measure the importance of the compensator performance. This study uses an order-reduction index that was introduced by Gawronski (1994, 1998). This order-reduction index accounts for both the system controllability and observability properties of the open-loop system and the compensator performance. It is the product of Hankel singular value and the LQG characteristic value; that is,

$$\sigma_i = \gamma_i^2 \mu_i . \tag{6-25}$$

From equations (6-6), (6-7) and (6-20), one obtains

$$\sigma_i = \frac{\sqrt{(\beta_{c,i} - 1)(\beta_{e,i} - 1)}}{2} . \tag{6-26}$$

Equation (6-26) reflects the degree of damping of motion, which depends on the pole mobility to the left-hand side of the complex plane (Gawronski, 1994, 1998). If a pair of poles is easily moved (i. e., a small weight is required), the corresponding states are easy to control and estimate; otherwise, if poles hardly move even for large weights, the states are difficult to control and estimate. If the *i*th controller pole is stationary, then $\beta_{c,i} = 1$; if the *i*th estimator pole is stationary, then $\beta_{e,i} = 1$. For both cases, $\sigma_i = 0$. For shifted controller poles and estimator poles, $\beta_{c,i} > 1$, $\beta_{e,i} > 1$ and thus $\sigma_i > 0$. In addition, from equations (6-12) and (6-26), one obtains

$$\sigma_i \cong \frac{\gamma_{o,i}^2 - \gamma_{c,i}^2}{2\gamma_{c,i}^2} \cong \frac{Var_{o,i}^2 - Var_{c,i}^2}{2Var_{c,i}^2} . \tag{6-27}$$

That is, the reduction index is proportional to the relative change of the responses of the open- and closed-loop systems due to white noise. So σ_i is a proper indicator of the importance of states and thus can serve as the reduction index.

A matrix of the reduction indices matrix is formed by the product of the Hankel singular matrix and LQG characteristic value matrix

$$\mathbf{\Sigma} = \mathbf{\Gamma}_h^{\,2} \boldsymbol{M}_{lqg} \,. \tag{6-28}$$

The large entries of $\mathbf{\Sigma}$ are to be retained and the small entries are be truncated. Arranging the σ_i's in descending order, and denoting retained entries with a subscript *r*, truncated with a subscript *t*, modal coordinate with a subscript *m*, the reduction matrix becomes

$$\mathbf{\Sigma} = diag(\mathbf{\Sigma}_r, \mathbf{\Sigma}_t) \,. \tag{6-29}$$

To truncate the insignificant states or modes, the estimator model is partitioned as

$$\begin{Bmatrix} \dot{\hat{\bar{\mathbf{x}}}}_r \\ \dot{\hat{\bar{\mathbf{x}}}}_t \end{Bmatrix} = \begin{bmatrix} \mathbf{A}_{lqr,r} - \overline{\mathbf{L}}_r \mathbf{C}_{\mathbf{y},lqr,r} & \mathbf{0} \\ \mathbf{0} & \mathbf{A}_{lqr,t} - \overline{\mathbf{L}}_t \mathbf{C}_{\mathbf{y},lqr,t} \end{bmatrix} \begin{Bmatrix} \hat{\bar{\mathbf{x}}}_r \\ \hat{\bar{\mathbf{x}}}_t \end{Bmatrix} + \begin{bmatrix} \overline{\mathbf{L}}_r & \mathbf{B}_{lqr,r} - \overline{\mathbf{L}}_r \mathbf{D}_{\mathbf{y},lqr,r} \\ \overline{\mathbf{L}}_t & \mathbf{B}_{lqr,t} - \overline{\mathbf{L}}_t \mathbf{D}_{\mathbf{y},lqr,t} \end{bmatrix} \begin{Bmatrix} \mathbf{y} \\ \mathbf{f}_{meas} \end{Bmatrix} \tag{6-30}$$

where $(\mathbf{A}_{lqg}, \mathbf{B}_{lqg}, \mathbf{C}_{lqg}, \mathbf{D}_{lqg})$ is the LQG-balanced model, the transformation matrix of which is obtained either from accurate singular value decomposition (equation (6-21)) or approximation (equation (6-19)). Note that the states should be arranged with the same sorting order as the reduction index matrix $\mathbf{\Sigma}$ is arranged.

The reduced estimator is

$$\dot{\hat{\bar{\mathbf{x}}}}_r = (\mathbf{A}_{lqr,r} - \overline{\mathbf{L}}_r \mathbf{C}_{\mathbf{y},lqr,r}) \hat{\bar{\mathbf{x}}}_r + (\overline{\mathbf{L}}_r \quad \overline{\mathbf{B}}_r - \overline{\mathbf{L}}_r \mathbf{D}_{\mathbf{y},lqr,r}) \begin{Bmatrix} \mathbf{y} \\ \mathbf{f}_{meas} \end{Bmatrix} . \tag{6-31}$$

The output of the controller is the control force. The full order control force is $\overline{\mathbf{K}}\hat{\overline{\mathbf{x}}}$. Partitioning $\overline{\mathbf{K}}$ as $\left[\overline{\mathbf{K}}_r \quad \overline{\mathbf{K}}_t\right]$, the order-reduced control force is

$$\mathbf{f} = \mathbf{K}_r \hat{\mathbf{x}}_r . \tag{6-32}$$

6.1.4 Spillover in Modal Control

The modal approach requires one to decouple the system equations into sets of two equations, each dealing with a single modal coordinate. However, as shown in equations (6-9a, b), the effect of the action of the control system is similar to that of high damping, and it is possible that some modes can even become over-damped. The small damping assumption does not hold any more. Some modes may be coupled again with the addition of the control system, and the coupling can be very strong (much stronger than if they were coupled with non-proportional damping). As a result, energy might be inadvertently pumped into one of the uncontrolled modes. This phenomenon has been called “spillover” (Genta, 1999). Spillover can cause the system to behave differently than predicted, and in some cases can even results in instabilities.

However, when the full-order model of the system is used for control law design, the LQR control law using full-state feedback, and the LQG control law using a Kalman filter, guarantee closed-loop stability. Moreover, the focus of this study is on semiactive systems using MR dampers as control devices instead of an active system using actuators. The device itself is inherently passive and cannot generate instabilities in the controlled system. Therefore, it is only necessary to refine the control strategy that works efficiently within this bound for vibration mitigation as well as spillover suppression.

A key to achieving this objective is the understanding that most of the structural vibration energy is typically contained in the lowest modes of vibration, especially for base isolation systems. Because we are dealing with linear systems, energy is not able to transfer to the higher modes for base isolation systems and thus spillover is avoided. Note that there are some design constraints for the benchmark problem, one of which is the limitation on the number and capacity of the control devices. This restriction is included to define an

upper bound of the control force, thus ensuring that the system still acts as a base isolation system even when the control force is introduced.

Further spillover mitigation for modal LQG control in this study is through closed-loop pole placement. Through the use of larger β_c values in the lower modes and smaller β_c values in the higher modes, the closed-loop poles can be placed at the desired locations so that only lower modes are coupled (through the presence of the controller) while higher modes are not effected. This outcome will be shown in the figures of the closed-loop poles of the plant in the section 6.2. In addition, the control devices are placed only at locations with higher placement indices (stronger controllability) at lower modes. This approach also helps to avoid the potential of spillover.

6.2 Application to the Benchmark Building

6.2.1 LQG-Balanced Controller for the Benchmark Building

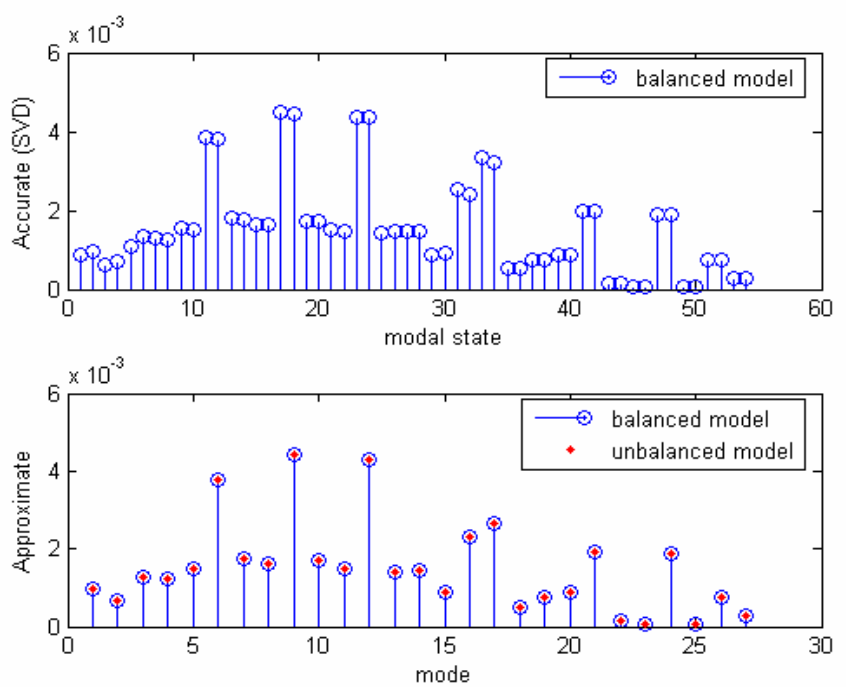

Figure 6-2 Hankel Singular Values from SVD of Balanced Nodal Model and from Approximation of Balanced and Unbalanced Modal Model

Before designing the LQG-balanced controller, Hankel singular values that represent the open-loop controllability and observability are computed and are shown in Figure 6-2.

The upper figure shows the accurate values obtained from Moore-balanced modal model using the singular value decomposition method. The lower figure shows the comparisons of the unbalanced and Moore-balanced modal model using the approximate closed-form equations. The results agree very well, which confirms the fact that Hankel singular values are invariant under linear transformation, and the approximate method is sufficient for Hankel singular value computation.

The first step in the LQG compensator design is to determine the closed-loop pole locations. As is shown in the approximate LQG-balancing algorithm, the closed-loop pole locations are determined by the solutions of the Ricatti equations, which are consequently determined by the weightings, and thus by β_c and β_e. In this study, the design procedures for the reduced-order LQG controller start from the trial values of β_c and β_e. A block diagram is shown in Figure 6-3.

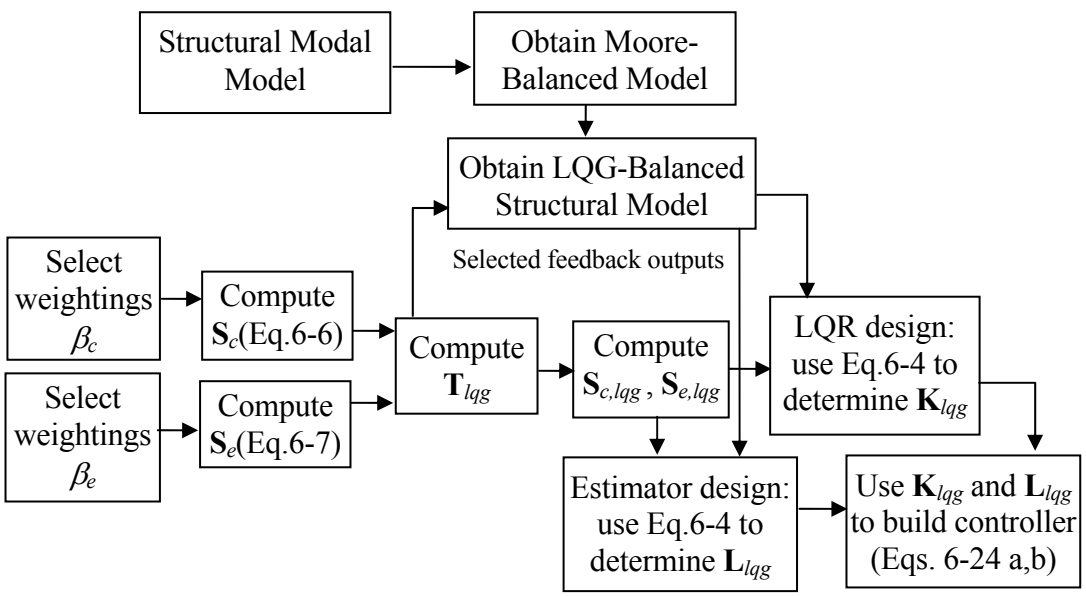

Figure 6-3 Flow Chart of the Nominal Controller Design Using the Modal Approach

The procedure is described as follows:

- Balance the form 2 modal state-space representation of the plant using equations (2-55) and (2-56).
- Place the closed-loop poles of the plant and the estimator at desired positions. This is done by assuming β_c and β_e values are known. Determine the weighting matrices $\tilde{\mathbf{Q}}$ and $\underset{\sim}{\mathbf{H}}$, solve $\mathbf{S}_c$ and $\mathbf{S}_e$ (equations (6-6) and (6-7)) and then $\mathbf{K}$ and $\mathbf{L}$ (equations (6-4)). Adjust β_c and β_e values so that the two equations of (6-5a) have the desired eigenvalues.
- Use either the singular value decomposition algorithm (equation (6-17)) or the approximation algorithm (equation (6-21)) to obtain the LQG-balanced transformation matrix $\mathbf{T}_{lqg}$. The LQG-balanced representation $(\mathbf{A}_{lqg}, \mathbf{B}_{lqg}, \mathbf{C}_{lqg}, \mathbf{D}_{lqg})$ and the LQG characteristic values $\boldsymbol{M}_{lqg}$ are then easily obtained using equations (6-16) or (6-20).
- Compute the reduction indices using equation (6-25) or (6-26), form the reduction index matrix and decide which modes are to be retained.
- Based on the LQG-balanced representation, construct the full-order LQG-balanced controller (equation 6-24). Now that the retained modes have been identified, the reduced-order controller is then obtained (equations (6-30) and (6-31)).
- Apply the full-order and reduced-order controller to the plant. Examine the performance of the reduced-order LQG controller. If the desired performance is not achieved, repeat the procedure by testing other β_c and β_e values.

Because the goal of controlling base isolation systems is to decrease the response of the fundamental modes while maintaining low responses for the higher modes, $\beta_{c,i}$ values for the first six modes (first two modes in *x*-, *y*- and *r*-directions, respectively) are chosen as 4.8, 14.6, 3.1, 1.4, 1.4, 1.02, while $\beta_{c,i}$ values for other modes are 1.1. The corresponding weightings on modes, q_i, are then obtained, the first six of which are: 5314.9, 4627.1, 4267.8, 1012.6, 691.97, 748.8, respectively. Others are between 200 and 500, much smaller than the first three. Similarly, $\beta_{e,i}$ values for the first three modes are chosen as 5.2, 4.8,

and 3.0, while the others are 2. Such selection is to ensure that the estimator poles stay at least two times farther into the left hand plane than the plant poles. h_i values are obtained from equation (6-7), the first three of which are: 6103.6, 4616.3, 7272.3.

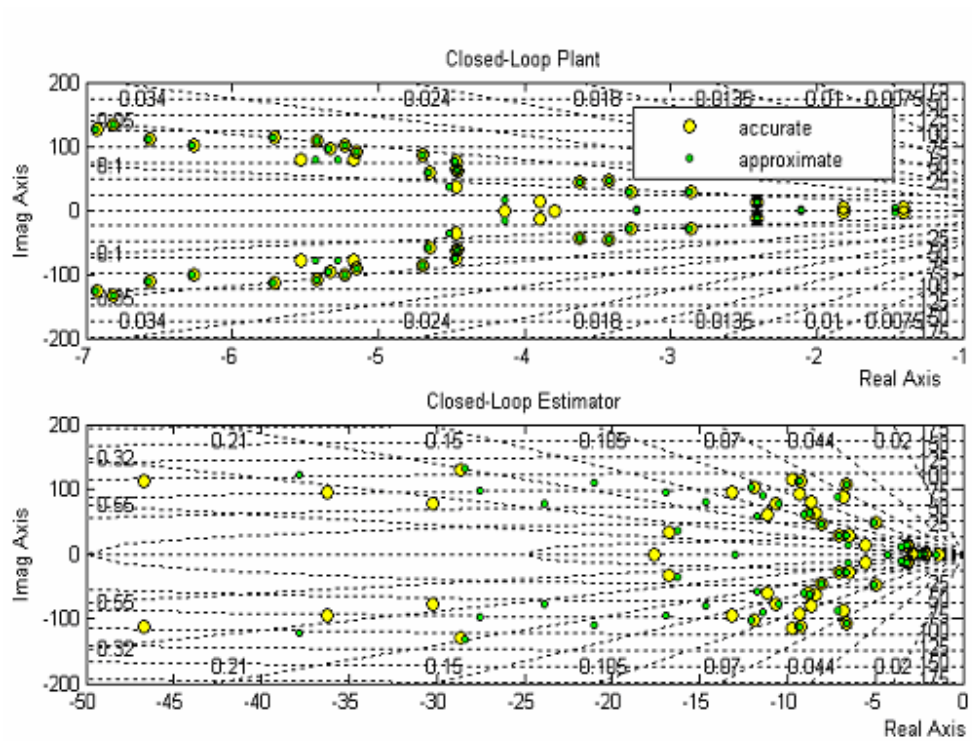

Figure 6-4 Test of Low-Authority Property

Figure 6-4 shows the closed-loop poles in expressions (6-5a) and (6-5b), to see if $\mathbf{BB}^T$ and $\mathbf{C}^T\mathbf{C}$ can be replaced by their diagonal terms, that is, if the controller is of low-authority for the selected weightings. It is demonstrated that all closed-loop plant poles nearly coincide except for a few lower modes. This outcome is because the lower modes are highly damped and highly weighted. As the estimator poles are purposely placed farther into the left hand plane, the β_e values are large, and thus the estimation of the closed-loop poles using the diagonal terms of $\mathbf{C}^T\mathbf{C}$ deviates from the accurate poles. Figure 6-3 also shows that using $\beta_e = 2$ for the last several high modes is too large for low-authority properties. However, these modes of the estimator will be truncated in the controller order reduction as shown later because they have small order reduction indices. The frequencies of the sensor noise are not this high (>100 Hz), so truncating these modes would not affect

the estimator's noise rejection ability. So simulations below would still use the low-authority approximation of the LQG-balanced controller for the above selected β_e's.

It is of interest to examine how the LQG-balanced controller with the selected weightings changes the structural properties. Thus, the open-loop poles of the plant and the LQG-balanced closed-loop poles for the two algorithms are shown in Figure 6-5. Computations have confirmed that $\mathbf{S}_c \cong \mathbf{S}_e \cong \boldsymbol{M}_{lqg}$ using the approximate method. The plot demonstrates that the approximate LQG-balancing algorithm using the low-authority property agrees well with the accurate LQG-balancing using complicated singular value decomposition methods. Also, it shows that the feedback only changes the lower modes as desired. The three pairs of poles move to the left, comparable to the fundamental flexible modes. So the closed-loop system behaves like a fixed-base system without base isolation for the passive-on case. However, MR dampers in the semiactive case do not provide the maximum force all the time as in the passive-on case, so the semiactively controlled system would still behave like an isolation system with feedback.

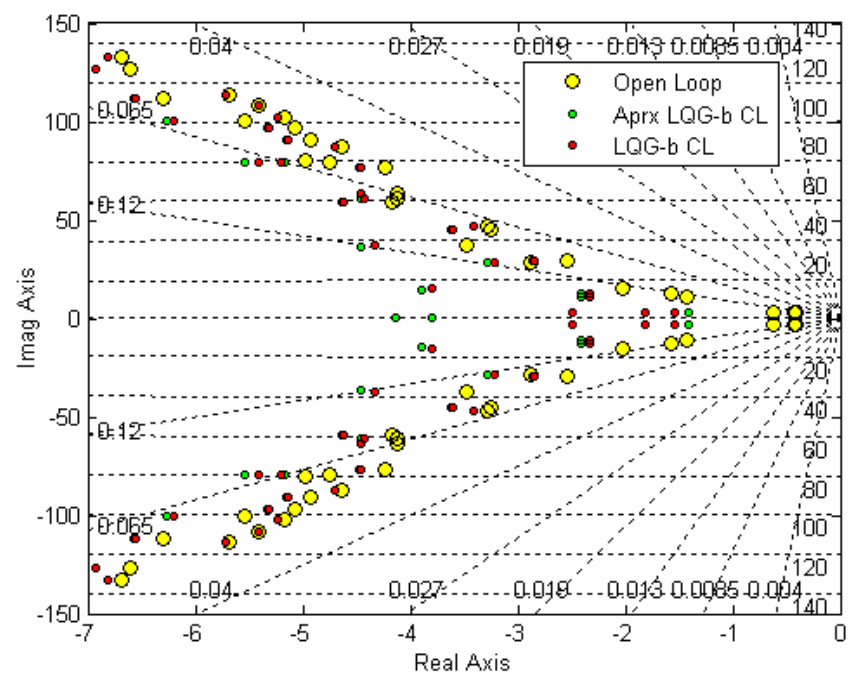

Figure 6-5 Poles of the Open-Loop and the Closed-Loop Plants (Modal, 1)

Figure 6-6 shows the close-loop estimator poles using the two LQG-balancing algorithms versus the open-loop plant poles. With the selected weights, all the poles move about twice as far to the left as those of the plant. The poles from the two LQG-balancing methods do not coincide for some modes, so the β_e values are a little large for these modes. However, larger β_e values are necessary for sensor noise rejection, which will be discussed later.

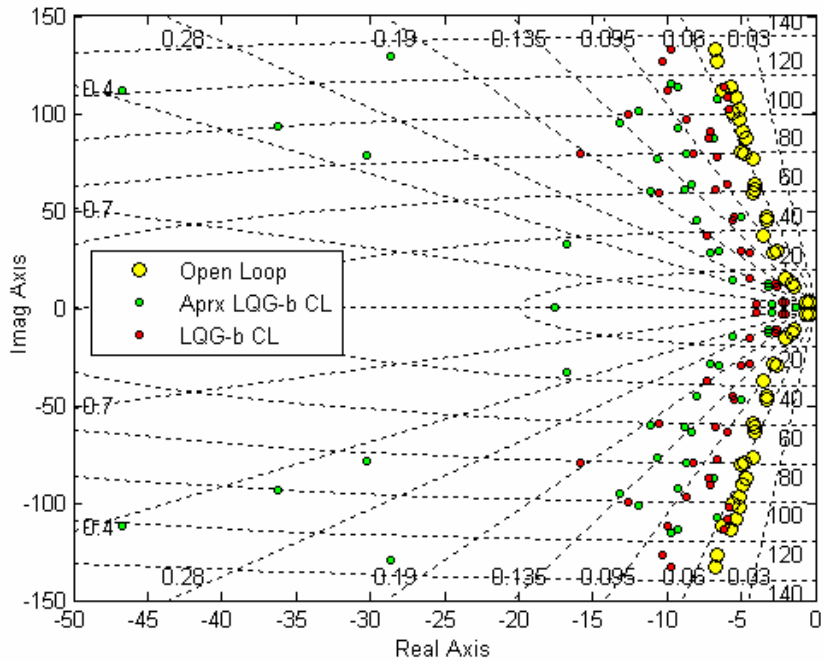

Figure 6-6 Poles of the Open-Loop Plant and the Closed-Loop Controller (Modal, 1)

It is desirable to see the frequency responses of the LQG-balanced control system. However, for MIMO systems, it is neither informative nor necessary to compute every transfer function. The frequency-dependent singular values of the transfer function matrix provide sufficient information regarding the maximum and minimum margins of the frequency response. The singular values are an extension of the Bode magnitude response for MIMO systems.

Figure 6-7 shows the MIMO Bode magnitudes of base drifts at corner 1 to the control devices (MR dampers) of the open- and closed-loop systems without disturbances applied.

It shows that for the weightings chosen above, the controlled (closed-loop) system has lower peak frequency response in the fundamental modes (-81.4 dB) than the uncontrolled (open-loop) system (-91.2), and the first peak of the closed-loop system moves slightly to the left (2.77 rad/s to 1.13 rad/s), indicating the control force makes the system a little more rigid. However, from the third peak, the maximum frequency response margin of the controlled system is higher than the uncontrolled value, though weightings are also put on these modes. It also shows the difference between the LQG-balancing and Moore balancing (balancing such that controllability grammians and observability grammians are equal) is not significant for this base isolation system.

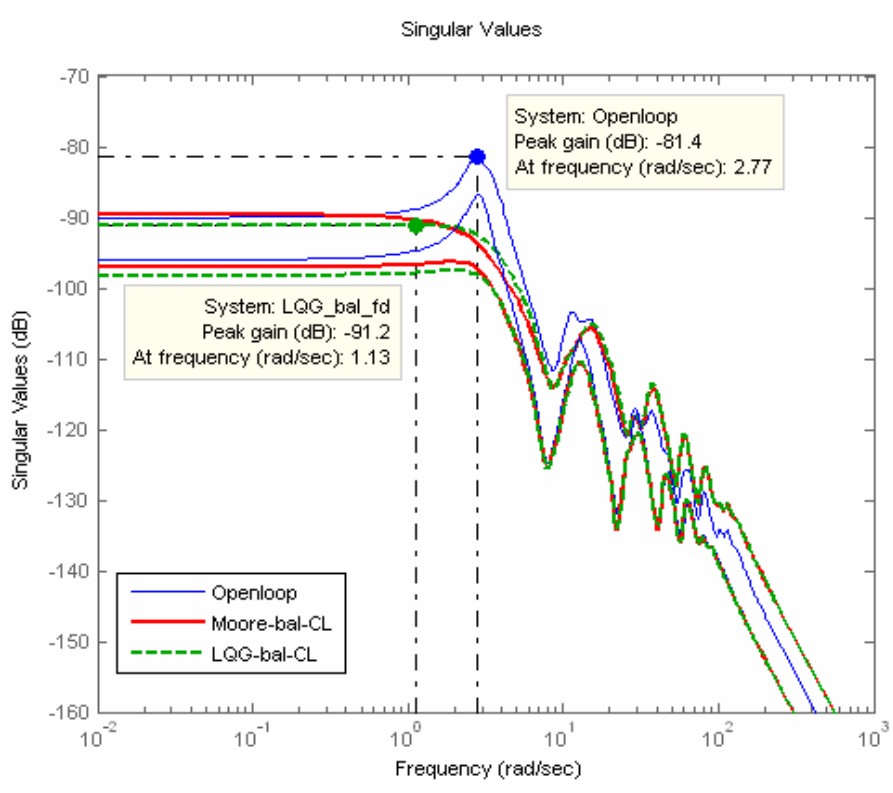

Figure 6-7 MIMO Bode Magnitude Plots of Base Drifts to MR Damper at Bearing 3 of the Open- and Closed-Loop Systems (Modal, 1)

Figure 6-8 shows the MIMO Bode magnitudes of the top floor accelerations at corner 1 to control devices (MR dampers) of the open- and closed-loop system without disturbances. Similar results are obtained for the acceleration frequency responses.

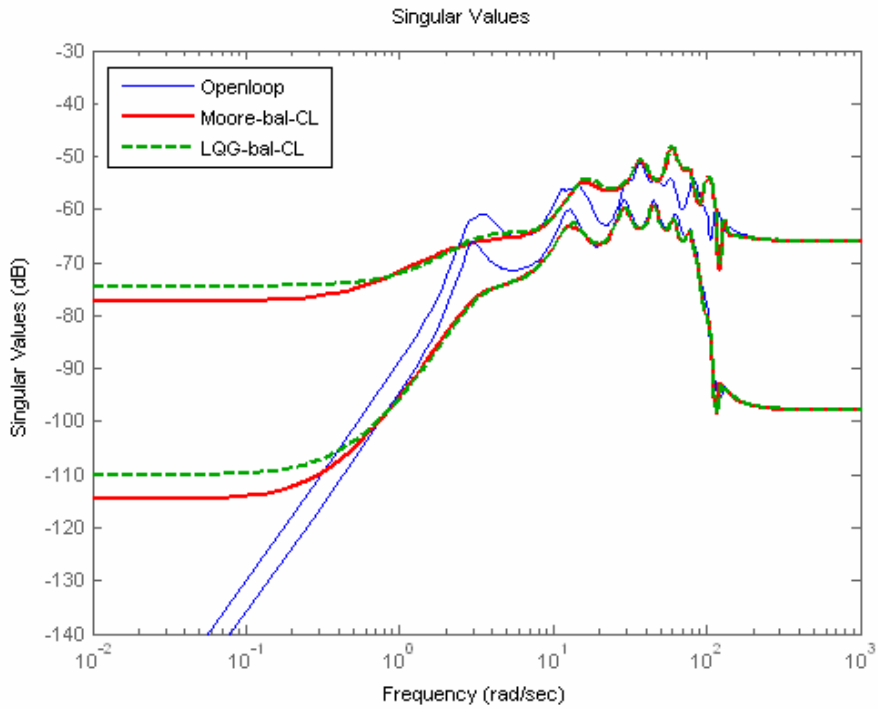

Figure 6-8 MIMO Bode Magnitude Plots of Roof Corner Accelerations to MR Damper at Bearing 3 of the Open- and Closed-Loop Systems (Modal, 1)

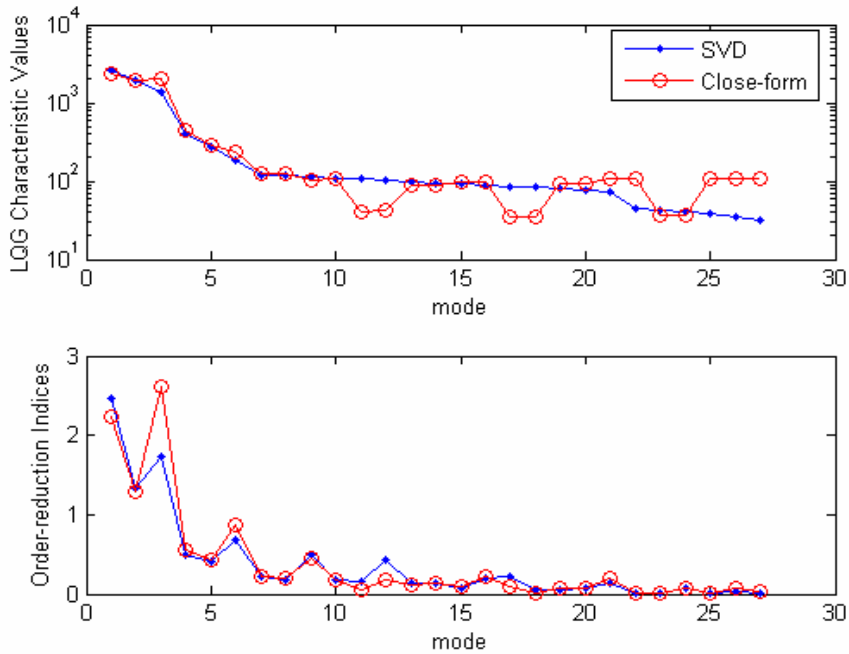

Figure 6-9 LQG Characteristic Values and Order Reduction Indices (Modal, 1)

Figures 6-7 and 6-8 show that the LQG-balanced controller is able to decrease the fundamental modes without sacrificing the higher modes for the undisturbed system. The order of this controller is then reduced to improve the design. Figure 6-9 shows the LQG characteristic values and controller order reduction index. As shown in Figure 6-9, both the LQG characteristic values and the order-reduction indices are large for the isolation modes. The order-reduction indices show that retaining first twelve modes seem to be good sufficient to capture the main features of the full-order controller.

6.2.2 Earthquake Simulations

In this section, the performance of the benchmark building with the designed controller is to be examined for earthquake excitations. Sensor noises are simulated by adding band-limited white noises with an RMS magnitude of 3% of the RMS responses at the corresponding locations in the passive case to each of the measurements.

The response profiles of the system with base-drift and all corner acceleration feedback and full order balanced-LQG controller subjected to the Newhall earthquake are shown in Figure 6-10. This plot shows that the semiactively controlled system only allows minor increases in inter-story drifts and accelerations over the passive system in the upper floors, and significantly decreases all responses as compared with the passive-on system. These results are better than the previous results using the nodal approach (Figure 5-16). This fact shows that the selected weightings for the modal approach are effective.

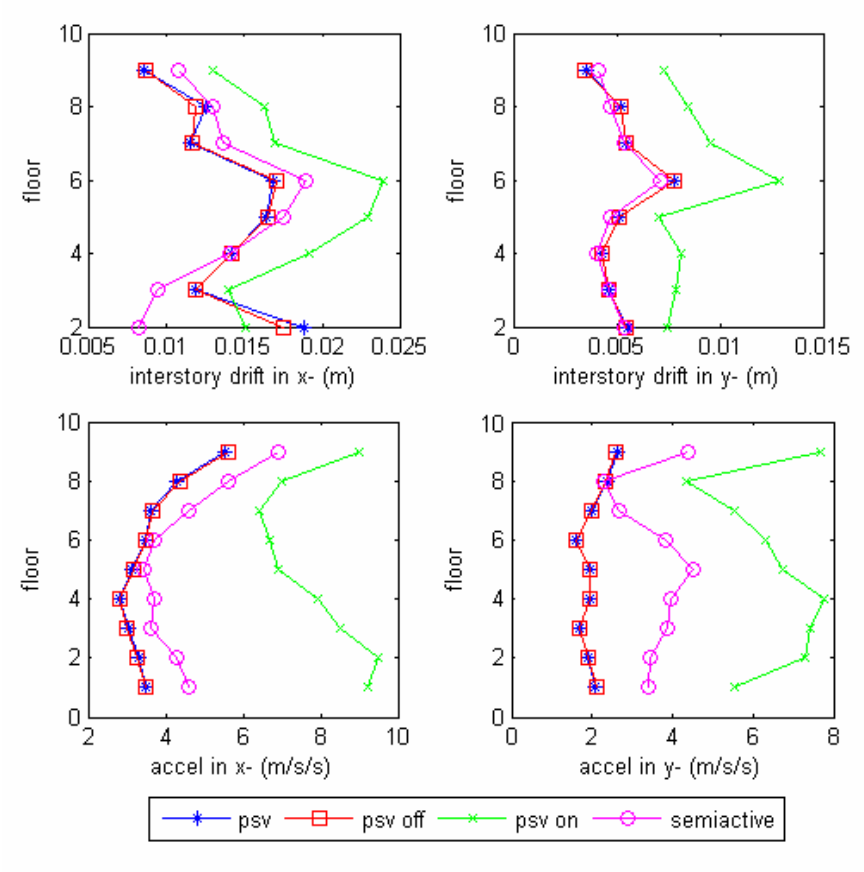

Figure 6-10 Response Profiles with Full-Sensor, Full-Order Controller to the Newhall Earthquake (Modal, 1)

Figure 6-11 shows the response profiles with the set of reduced sensors determined in Chapter 4. Compared with Figure 6-10, it is clear that reduced set of sensors is able to capture the response. The responses of the two systems are very close indicating that the reduced set of accelerometers is sufficient. This set of sensors is adopted in all subsequent studies.

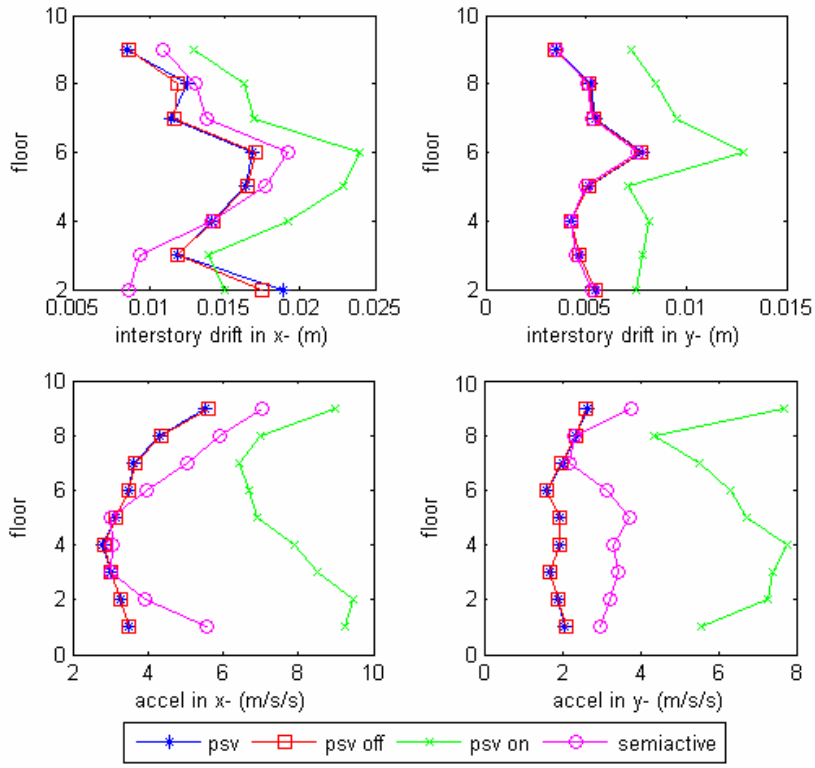

Figure 6-11 Response Profiles with Reduced-Sensor, Full-Order Controller to the Newhall Earthquake (Modal, 1)

Figure 6-12 shows the response profiles with reduced sensors and the reduced-order controller with only 12 modes retained. Compared with Figure 6-10 and 6-11, it can be seen that reduced-order control results in an error in the story drift between floor 1 and the base. Further study shows that the reduced-order controller with 18 modes retained results in nearly the same performance as the full-order controller.

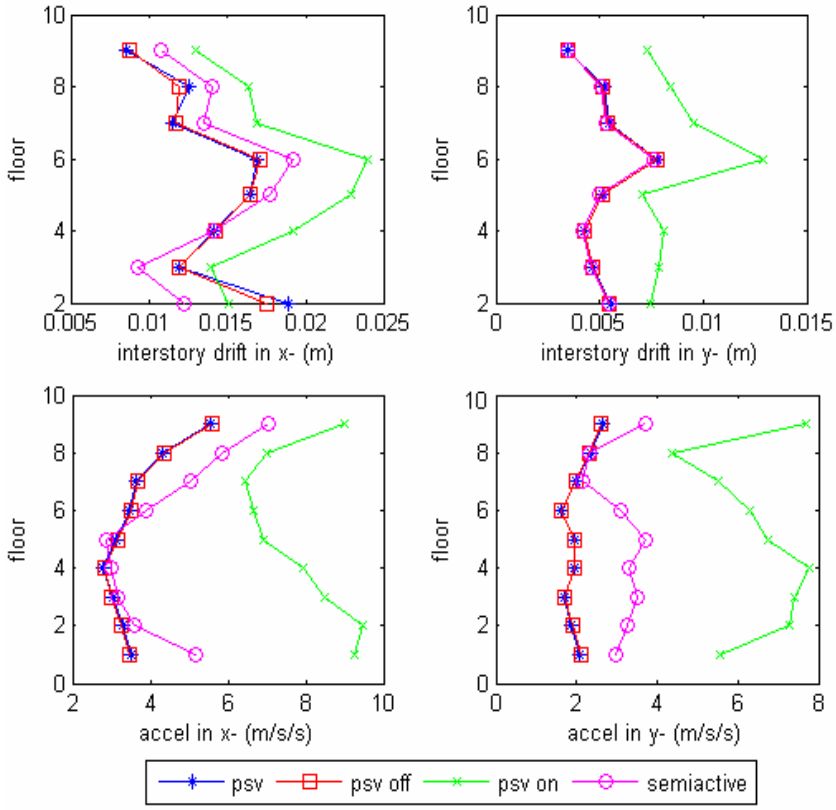

Figure 6-12 Response Profiles with Reduced-Sensor, 12-Mode Controller to the Newhall Earthquake (Modal, 1)

The responses using these weightings, the reduced set of sensors and the reduced-order controller were computed. The time histories of the base displacement at bearing 3 are shown in Figure 6-13. This plot shows that the peak base drifts are smaller than those in nodal approach (Figure 5-9). The acceleration response at the same location as that in chapter 5 (Figure 5-18) is shown in Figure 6-14. The semiactive system results in smaller accelerations than the passive-on case although the base drifts are decreased at the same time. Again, this result is better than those using the nodal approach.

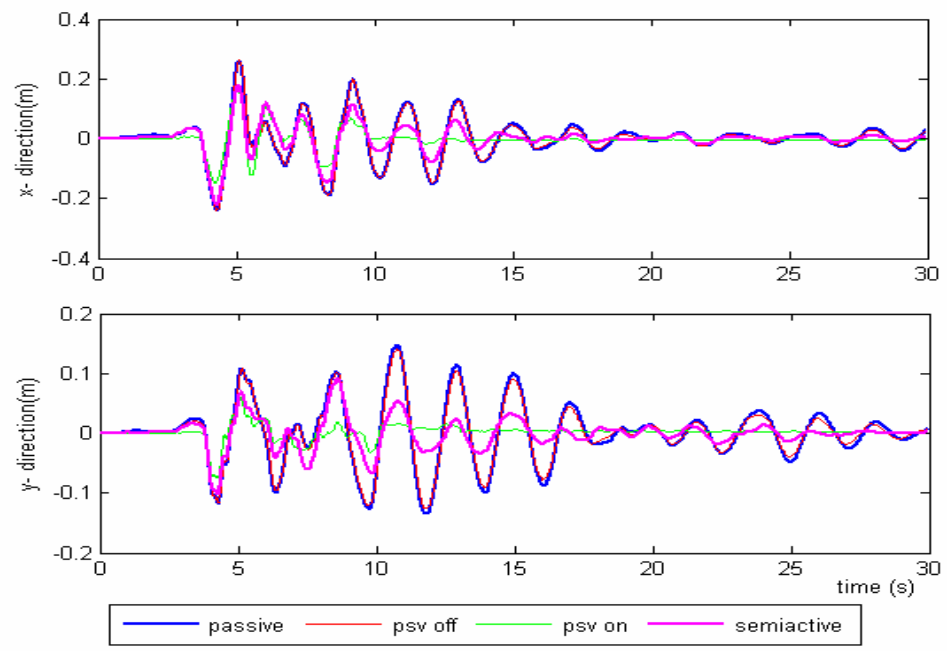

Figure 6-13 Base Drift Responses at Corner 1 to the Newhall Earthquake (Modal, 1)

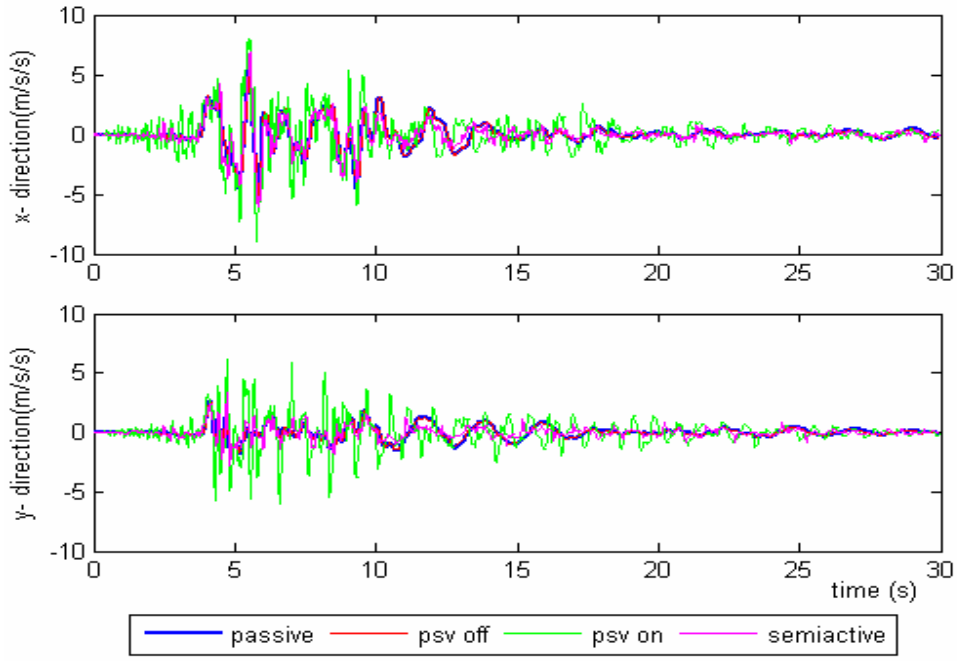

Figure 6-14 Acceleration Responses at Roof Corner 1 to the Newhall Earthquake (Modal, 1)

The forces generated by MR dampers using this approach (Figure 6-15) indicate that the modal approach uses less control force in achieving much better performance than the nodal approach (Figure 5-20).

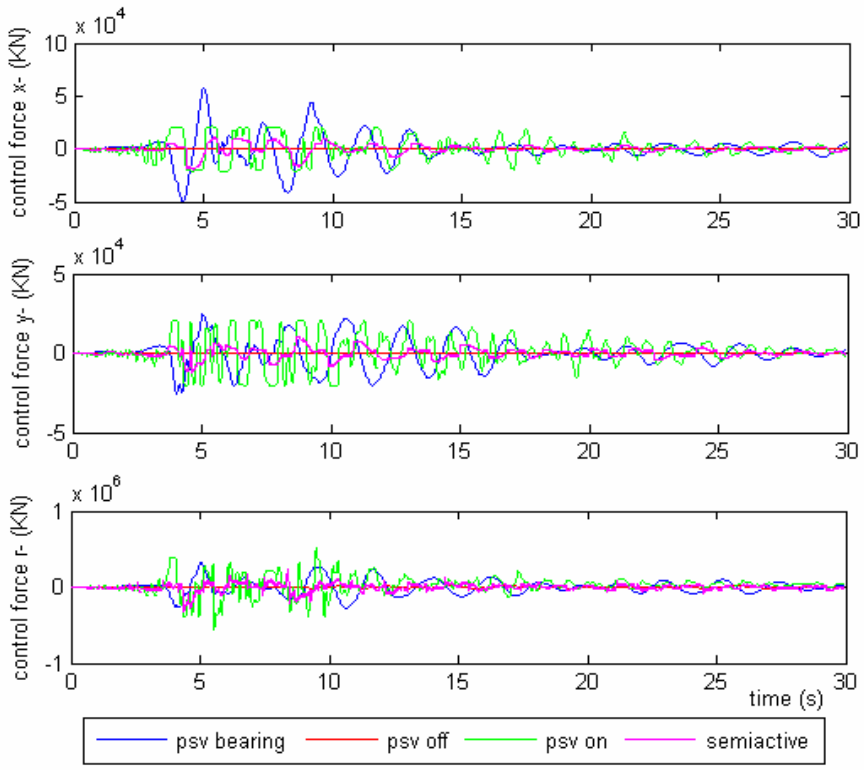

Figure 6-15 Effective Bearing Forces and Control Forces (Modal, 1)

The maximum responses using these weightings for all seven design earthquakes are shown in Figure 6-16 (compared to Figure 5-8). Clearly, the semiactive system has smaller responses in inter-story drifts and accelerations, for all earthquakes than the passive-on system, and even the base drifts in the *y*-direction.

The performance indices 3, 4, 5, 7, 11, 8 of the semiactive system for the seven earthquakes are compared in a bar graph (Figure 6-17). Comparing these results with those in Figure 5-16, it is clear that nearly all of the performance indices for all earthquakes are better than those corresponding to the nodal approach. Peak and RMS base drifts, inter-story drifts and accelerations are all smaller. The modal approach turns out to be very effective, simple and straightforward.

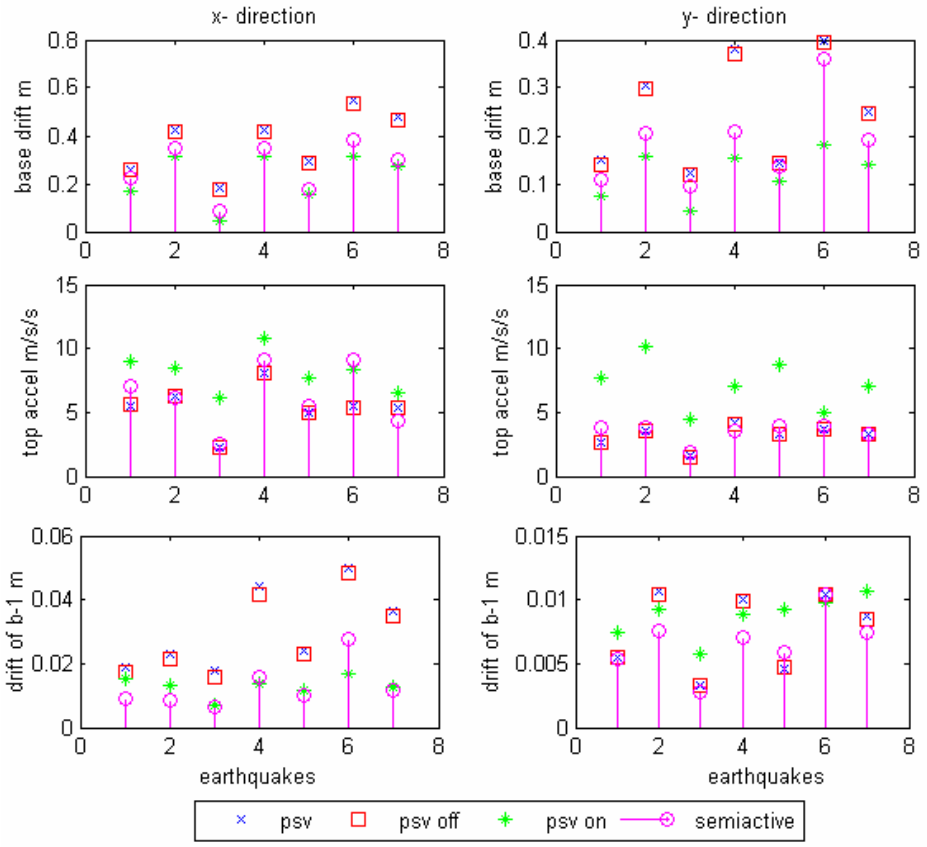

Figure 6-16 Max Responses to the Design Earthquakes (Modal, 1)

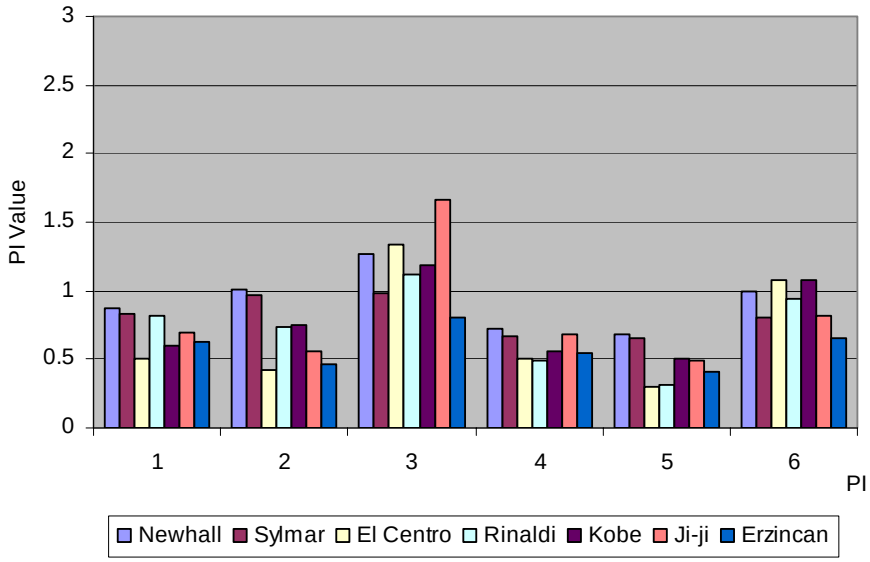

Figure 6-17 Performance Indices of the Semiactive System (Modal, 1)

6.2.3 Control Performances for Different Weightings

When selecting pole locations, it is useful to keep in mind that the control effort required is generally related to how far the open-loop poles are moved by feedback. Furthermore, when a zero is near a pole, the system may be nearly uncontrollable and moving such poles requires large control gains and thus large control effort. Therefore, a pole-placement philosophy that aims to modify only the undesirable aspects of the open-loop response and avoid either large increases in bandwidth or efforts to move poles that are near zeros will typically allow smaller gains and thus smaller control devices than a philosophy that arbitrarily picks all the poles without regard to the original open-loop pole and zero locations (Steven and Lewis, 2003).

In comparison with the selection of controller poles, estimator pole selection requires us to consider a different perspective. As in the controller, there is a feedback term in the estimator that grows in magnitude as the requested speed of its response increases. However, this feedback is in the form of an electronic signal or a digital word in a computer, so its growth causes no special difficulty (in theory). In the controller, increasing the speed of the response requires an increase in device size, weight and cost. The important consequence of increasing the speed of response of an estimator is that the bandwidth of the estimator becomes higher, thus causing more sensor noise to pass through to the control device. Thus, as with controller design, the best estimator design is a balance between good transient responses and low-enough bandwidth that sensor noise does not significantly impair actuator activity (Franklin et al., 2002).

As a rule of thumb, the estimator poles can be chosen to be faster than the controller poles by a factor between 2 and 6. This ensures a faster decay of the estimator errors compared with the desired dynamics, thus causing the controller poles to dominate the total response. If the estimator poles are slower than the controller poles, we would expect the system response to disturbances to be dominated by the dynamic characteristics of the estimator rather than by those selected by the control law.

For the measurement with sensor noise $\mathbf{v}$, the estimator equation is

$$\dot{\hat{\mathbf{x}}} = \mathbf{A}\hat{\mathbf{x}} + \mathbf{B}\mathbf{u} + \mathbf{E}\mathbf{w} + \mathbf{L}(\mathbf{y} - \mathbf{C}_y\hat{\mathbf{x}} - \mathbf{D}_y\mathbf{u} - \mathbf{v}) . \tag{6-33}$$

The associated estimator error is

$$\dot{\tilde{\mathbf{x}}} = (\mathbf{A} - \mathbf{L}\mathbf{C}_y)\tilde{\mathbf{x}} + \mathbf{E}\mathbf{w} - \mathbf{L}\mathbf{v}\,. \tag{6-34}$$

Here the sensor noise is multiplied by $\mathbf{L}$. If $\mathbf{L}$ is very small, then the effect of sensor noise is removed but the estimator's dynamic response will be slow, so the error will not reject the effects of $\mathbf{w}$ very well. On the other hand, if $\mathbf{L}$ is large, then the estimator's dynamic response will be fast, but the sensor noise, multiplied by $\mathbf{L}$, results in large errors. Also, different weighting selection usually results in different control force.

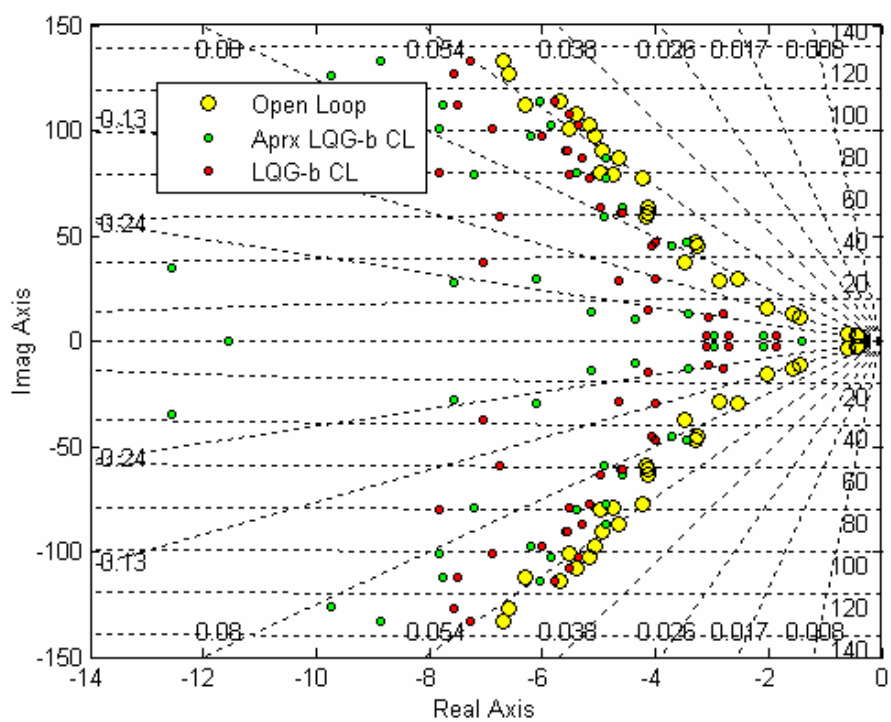

Figure 6-18 Poles of the Open-Loop Plant and the Closed-Loop Controller (Modal, 2)

In this section, examples are given to show how the weightings change the pole locations. First, a comparison is made between the two cases of β_e values with the β_c values unchanged. Larger β_e values in low modes and smaller in higher modes are chosen for the second case. The first nine β_e's are: 7.0, 4.5, 2.5, 2.5, 2.2, 1.8, 2.1, 1.9, 1.7. The

resulting estimator poles are shown in Figure 6-18. This controller is expected to be truncated into a lower order, possibly 9 or 12. The controller order indices are shown in Figure 6-19.

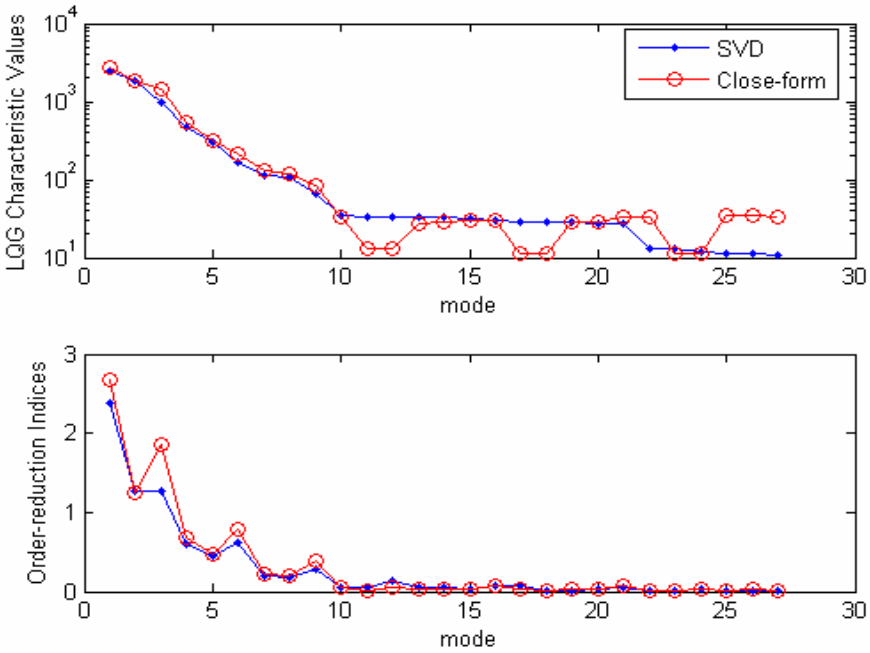

Figure 6-19 LQG Characteristic Values and Order Reduction Indices (Modal, 2)

Figure 6-20 shows the step response of the closed-loop system and of the controller. It shows that the controller needs a longer time to settle, which indicates that the controller may not be very good for error and noise rejection. Further simulation shows that this controller is nearly as good at improving the performance as the controller discussed in the last section. The effective MR damper forces at the center of the base mass are given in Figure 6-21. It shows that this set of weightings results in smaller MR damper forces in the *y*-direction than the previous controller.

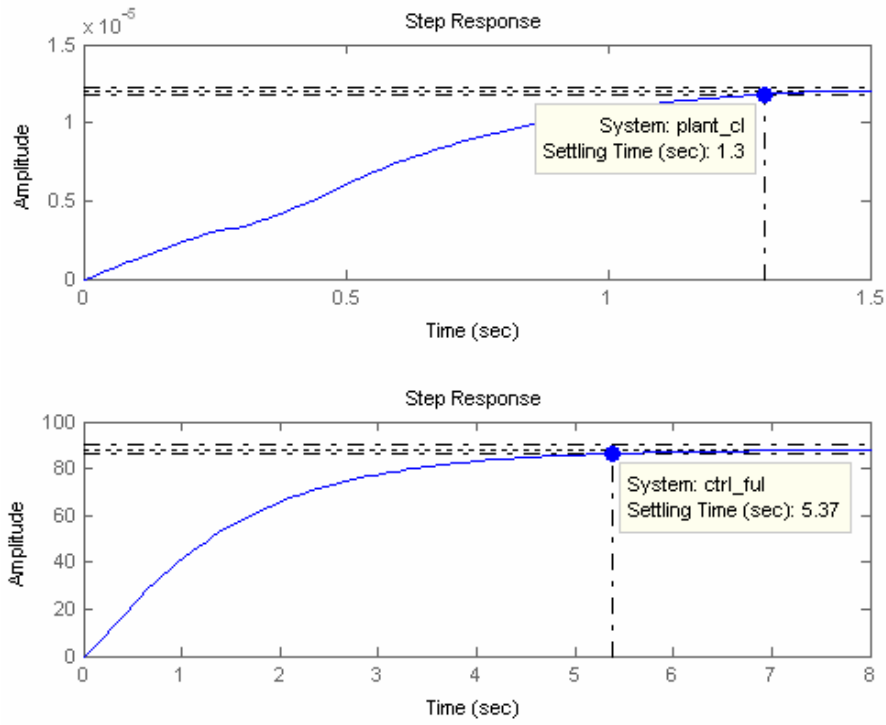

Figure 6-20 Step Responses of the Closed-Loop Plant and the Full-Order LQG Controller (Modal, 2)

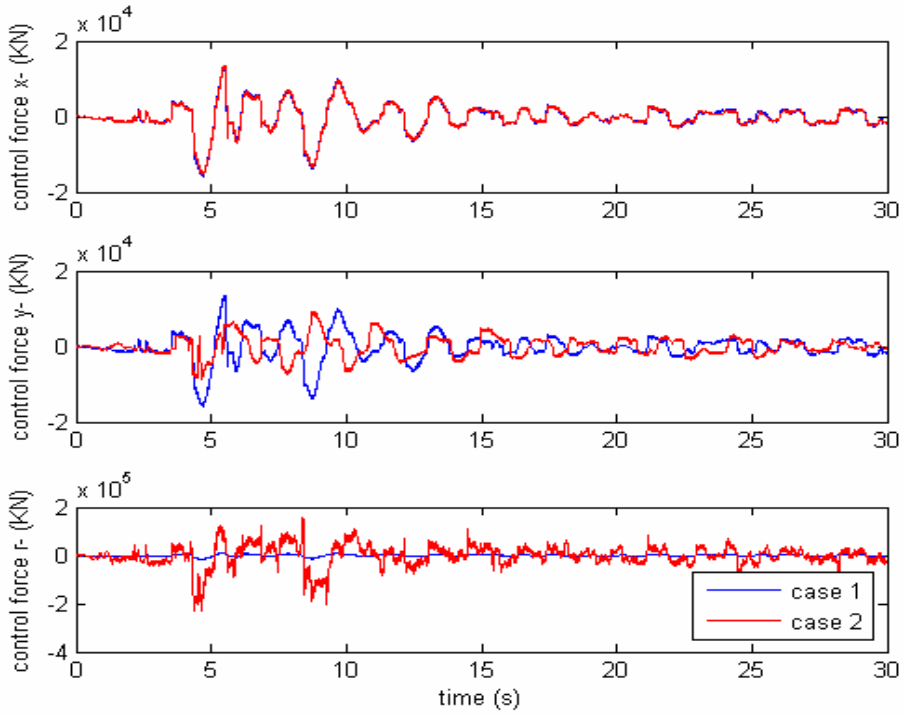

Figure 6-21 Effective Bearing Forces and Control Forces (Modal, 2)

Next, a comparison is made between different β_c values for the second case of β_e. The second set of β_c are smaller. They are 4.0, 3.5, 2.0, 2.0, 1.5, 1.2 for the first six modes, and 1.05 for all other modes. The open-loop and closed-loop poles of the plant are shown in Figure 6-22. It shows that smaller weightings do not push the closed-loop poles to the left as far as the larger weightings do.

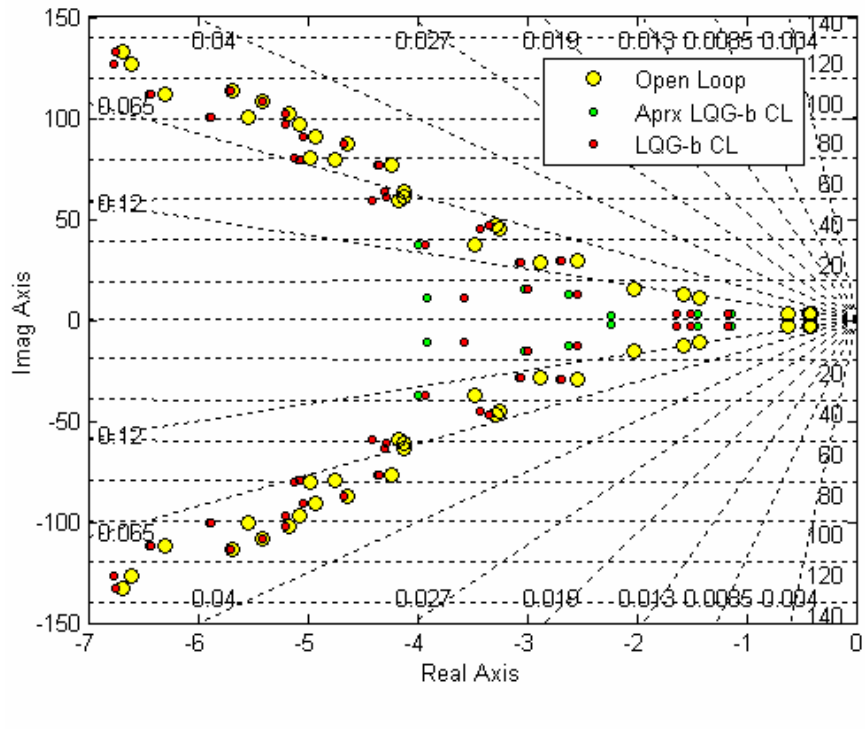

Figure 6-22 Poles of the Open-Loop and the Closed-Loop Plants (Modal, 2)

The MIMO Bode magnitudes of the system with smaller weightings confirmed that the fundamental modes decreased less (-89.3) than the system with larger weightings (-91.2), and frequencies shifted less (1.96 Hz vs. 1.13 Hz), as is shown in Figure 6-23.

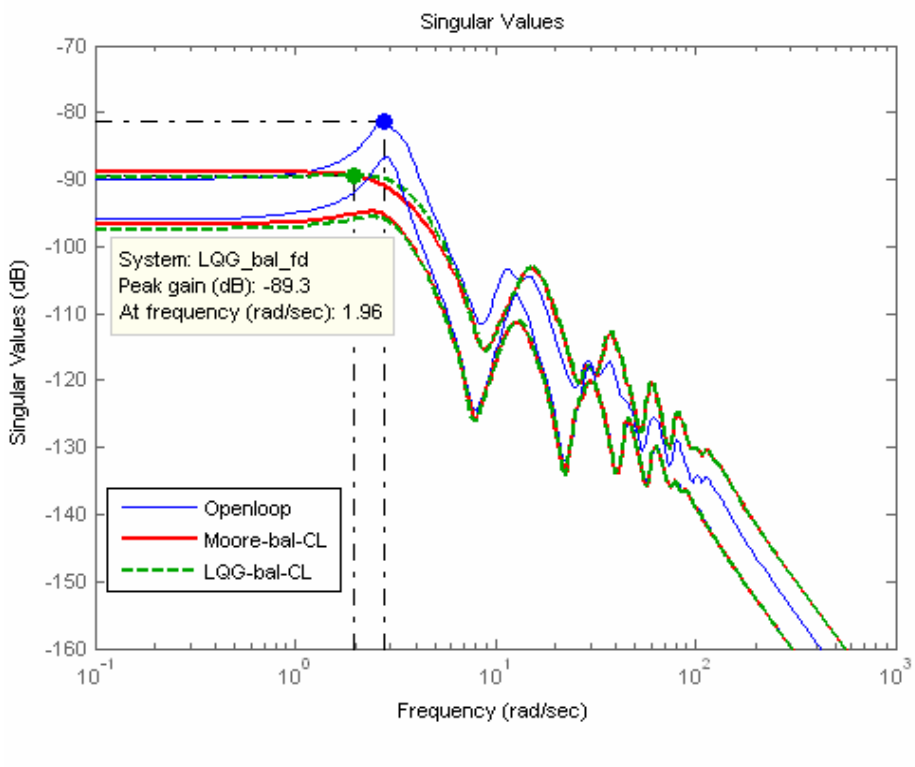

Figure 6-23 MIMO Bode Magnitude Plots of Base Drifts to MR Damper at Bearing 3 of the Open- and Closed-Loop Systems (Modal, 2)

Simulations with the Newhall earthquake for this set of weightings yield the same conclusions. From figure 6-24, it is obvious that the maximum base displacement is much larger than that in Figure 6-11. In Figure 6-25, the base drifts are larger than those in Figure 6-13. So, if the weightings are too small, neither the acceleration nor the base displacement can be controlled very effectively. However, the relative positions of the plant and controller poles are better assigned according to the rule of thumb, because the controller decays faster (Figure 6-26) than in the first case (Figure 6-19).

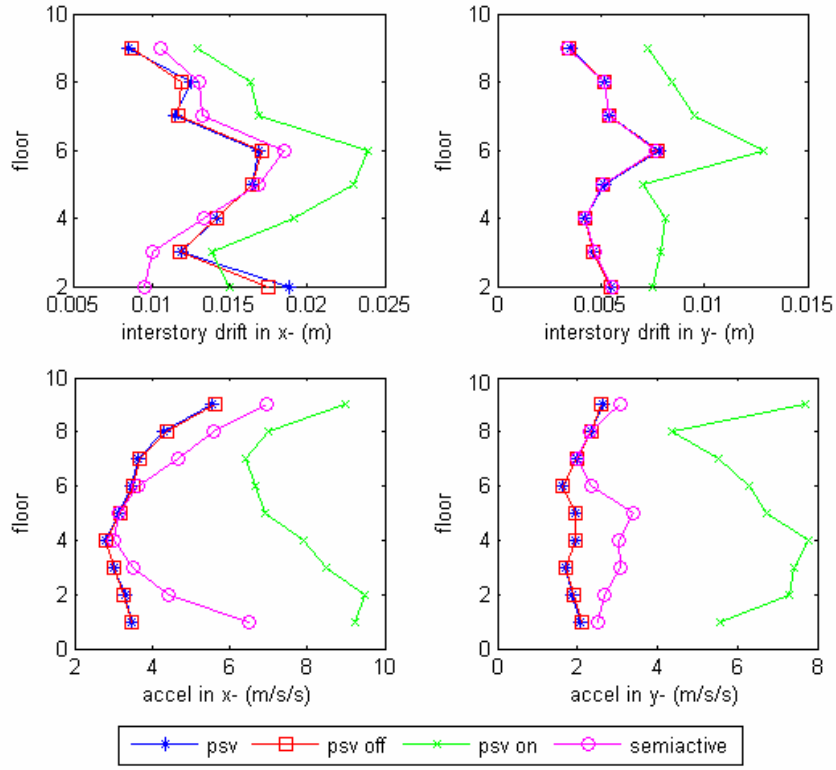

Figure 6-24 Response Profiles with Reduced-Sensor, 18-Mode Controller to the Newhall Earthquake (Modal, 2)

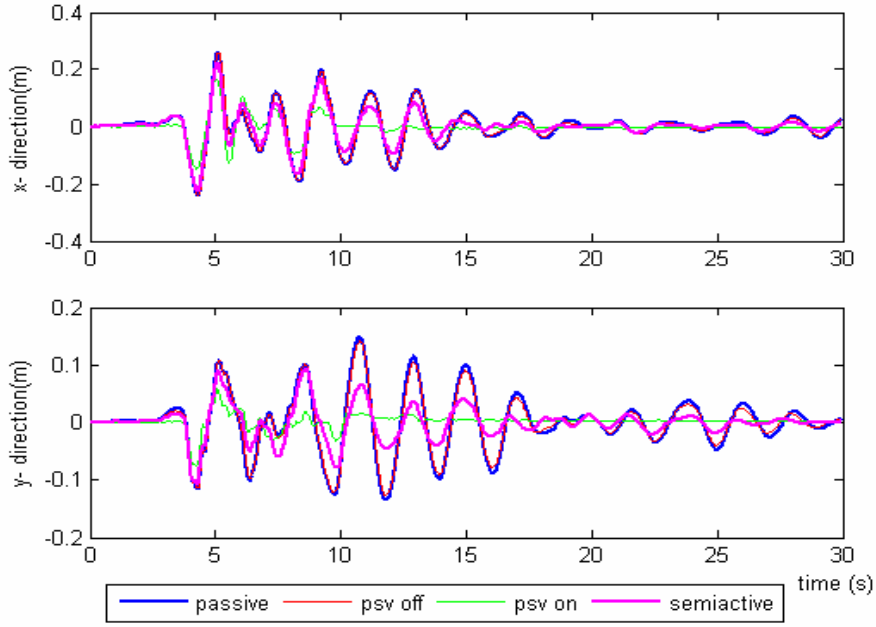

Figure 6-25 Base Drift Responses at Corner 1 to the Newhall Earthquake (Modal, 2)

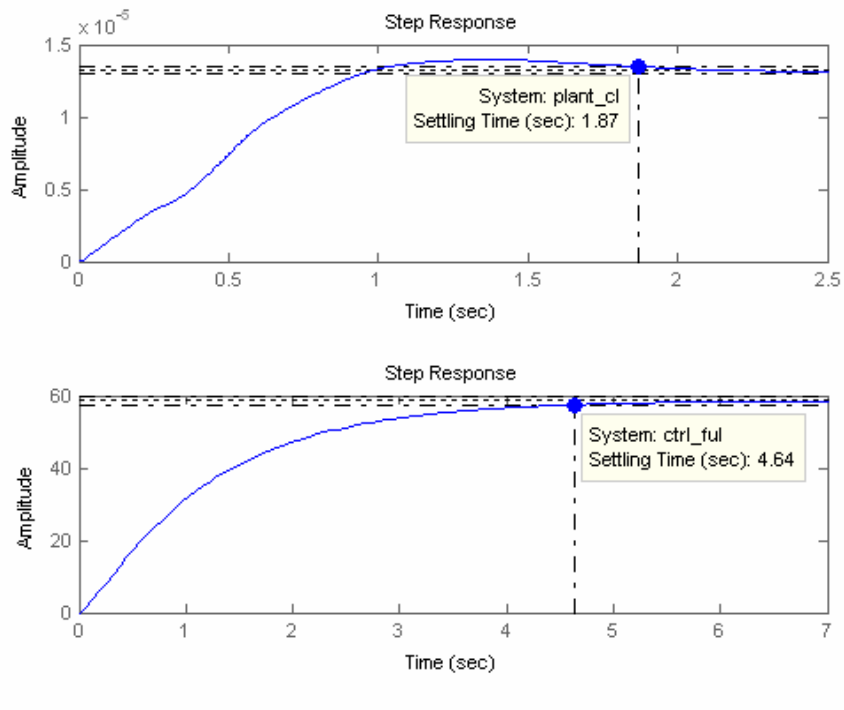

Figure 6-26 Step Response of the Closed-Loop Plant and the Full-Order LQG Controller (Modal, 2)

From the above analysis, it is clear that the weightings on the responses govern the system responses. The weightings of the controller determine whether the estimator gain $\mathbf{L}$ is optimal or not but have less effect on the system responses. Also, the control performance might be improved if the MR damper used is specifically designed for this building.

The modal design procedures demonstrate that the LQG-balanced controller does ensure the desired closed-loop properties, and the pole locations can be easily assigned by adjusting the β_c and β_e values which relate to weightings through closed-form expressions. Thus, unlike the trial and error weighting selection in the nodal approach, the weighting selection using the modal approach is quite straightforward, simple, and has an explicit physical interpretation.

6.3 Sources of Error

The errors considered in this chapter are mainly modeling errors. There are basically three sources: (1) Transformation from the nodal model to the modal model. For the 3D irregular structure, the equations of motion cannot be fully decoupled with modal decomposition. When they are written into decoupled modal equations, some non-proportional damping and stiffness are eliminated, which results in errors; (2) Approximate solutions to the Riccati equations using the modal approach. Even for the structure that can be fully decoupled, the closed-form expressions are approximated by disposing of many insignificant off-diagonal terms. The balance-LQG controller applies to more assumptions such as low-authority controller, low damping ratios, and so on. The isolation-modes to be eliminated in base isolation systems are highly damped. This fact can be seen in the optimal passive design part. These modes have damping ratios of 15% or so. (3) The **D** matrix cannot be reflected in the controllability and observability analysis and, for simplicity, this matrix is often ignored in the control design procedure.

6.4 Summary

This chapter introduced a controller order reduction technique that takes into account both open-loop and closed-loop effects for computing a LQG-balanced representation. A convenient closed-form approximation using the modal approach was also introduced and applied to the base isolated benchmark building. Pole-location assignment with weighting selection was examined and the earthquake simulation results were compared for different cases of weightings, reduced-order controllers and sensors. The results in this chapter demonstrate that the modal approach is straightforward, efficient and physically explicit.

Chapter 7

Conclusions and Recommendations

The purpose of this study was to develop an approach for the design of a seismic control system that is based on physical understanding of the system and thus is particularly suitable to the design of a smart base isolation system. The effectiveness of the proposed control strategies have been demonstrated and evaluated through application to the benchmark smart base isolation problem. An approach for optimal placement of control devices and sensors was also considered, and was demonstrated within the context of this benchmark problem. Evaluation of the designed controllers has been performed using a set of earthquakes defined within the smart benchmark problem. MR dampers are the semiactive devices selected for use throughout this dissertation because of their promise for civil engineering applications.

Using well established controllability and observability properties (they have often been overlooked in civil engineering applications), the distribution of control devices and the number and locations of the sensors are determined by the proposed placement indices. These devices indicate the importance of each potential control device location and of each sensor (accelerometer) location for each mode. Locations that have low placement indices for selected modes are rejected. Due to the complexity of this problem, a correlation index has also been proposed to reject highly correlated locations that would be redundant. The seismic performance of the structure with the selected MR damper and sensor locations demonstrates the efficacy of this placement algorithm.

LQG is a modern optimal control technique that provides the designer with great flexibility to perform trade-offs among various objectives. It has been successfully applied in many civil engineering studies. However, from a civil engineering implementation point of view, this approach may not be obvious to the designer. The control gains require the selection of weighting values that require the designer to have considerable experience with the system. However, in the modal coordinate system, such experience is not as critical as

the modal characteristics of the system are physically based and clear to the design engineer. Thus, the modal approach not only results in many approximate closed-form relationships between weightings and closed-loop pole locations, but also provides explicit physical interpretations, and thus helps the designer to facilitate the design.

This study first considered a nodal coordinate system for the design of controllers. In the traditional nodal coordinate system, the weighting matrix in the LQG controller was determined based on the controllability / observability concepts considering the closed-loop stability requirements and the loop closure. The best weighting matrix was selected from several options because it was more effective in suppressing the desired modes with less control effort. Earthquake simulations showed that the nodal approach was effective in limiting the base drifts without sacrificing the low inter-story drifts and accelerations typical for base isolation systems. However, the nodal approach could not provide an understanding of the relationship between the weightings and the control objectives for assigning the closed-loop pole locations. Finding the optimal weighting values required a trial and error approach.

Due to the challenges in applying physical knowledge of the system in the nodal approach, the modal approach was considered for the base isolation system. Using the modal approach, the closed-loop poles could be placed at desired locations by adjusting the weightings on individual modes. Thus the responses of the specified mode can be suppressed. In addition, this study adopted a new balanced model, the LQG-balanced model, for controller order reduction. This balanced model can be conveniently obtained using approximate closed-loop formulas and this balancing technique accounts for feedback effects. Combining the LQG characteristic values with Hankel singular values, the order reduction indices thus take into account both the open-loop and the closed-loop effects. Earthquake simulations confirmed the effectiveness of the order-reduction technique. Responses of the base isolated building subjected to earthquakes using the modal approach displaced more base drift reduction combined with lower inter-story drift and acceleration responses, all while using less control force than in the nodal approach.

In all, the proposed approach integrating knowledge of the modal characteristics of the system with optimal placement techniques and LQG control in the modal coordinate

system was found to be very effective in improving the seismic performance of base isolation systems.

Some recommendations for futures studies related to this work are:

- Due to the limitations set forth in the base isolation benchmark problem statement constraints, control devices can only be installed at the base level in this study. This constraint rule is necessary for the benchmark problem participants to compare their control strategies, but can not make full use of control strategies and the control devices, and thus the achievable performance of the building is only partially realized within this study. To achieve better performance, future researchers are recommended to test the control strategies for general locations of control devices.
- This benchmark building model is three dimensional, modeled with two translational and one rotational degree of freedom at each floor. However, this study did not focus specifically on torsional behavior, but controlled translations and rotations simultaneously. Future researchers could further investigate the potential for controlling the torsional behaviors.
- The benchmark building is a tool to demonstrate the techniques developed and synthesized in this research. Future researchers should apply these techniques to even more complex structural models. For example, these techniques should be eventually applied to structures with nonlinear behaviors to evaluate their performance. The base isolation benchmark problem also allows for the use of nonlinear bearings.
- Experiments are a necessary step in the validation of control strategies. It is recommended that some experiments be conducted to verify the performance of the proposed strategies. Further comparisons to other control methods should also be performed.
- MR damper studies so far have been limited to consideration of the versatile and controllable damping properties of these devices. However, MR dampers can serve as a tunable interaction element between a primary system and a secondary subsystem to control the energy flow between the two systems for the protection of the primary system. Research of the active interaction algorithm has been successfully conducted

using a friction device as the interactive element (Hayen and Iwan, 1994; Iwan and Wang, L.-J., 1998; Zhang and Iwan, 2002a, b, c).

Appendix A

Structural Parameters of the Benchmark Building

Coordinates of 92 the bearings (unit: m)

(The origin of the coordinate system is the center of the mass of the base)

1	1.82 , -47.79 ;	***24***	32.83 , -11.16 ;	***47***	1.82 , -24.05 ;	***70***	-17.25 , -4.63 ;
2	-7.32 , -47.79 ;	***25***	25.97 , -11.16 ;	***48***	1.82 , -31.88 ;	***71***	-17.25 , 3.23 ;
3	-17.25 , -47.79 ;	***26***	18.17 , -11.16 ;	***49***	1.82 , -39.75 ;	***72***	-17.25 , 11.06 ;
4	-17.25 , -39.93 ;	***27***	12.53 , -16.18 ;	***50***	10.21 , 23.04 ;	***73***	-17.25 , 18.93 ;
5	-17.25 , -31.88 ;	***28***	12.53 , -24.05 ;	***51***	10.21 , 15.21 ;	***74***	-17.25 , 26.76 ;
6	-17.25 , -24.05 ;	***29***	12.53 , -31.88 ;	***52***	10.21 , 7.35 ;	***75***	-12.28 , 30.69 ;
7	-17.25 , -16.18 ;	***30***	12.53 , -39.75 ;	***53***	10.21 , -0.49 ;	***76***	-2.41 , 30.69 ;
8	-17.25 , -8.35 ;	***31***	12.53 , -47.79 ;	***54***	18.17 , 23.04 ;	***77***	6.00 , 30.69 ;
9	-17.25 , -0.49 ;	***32***	-7.32 , 23.04 ;	***55***	18.17 , 15.21 ;	***78***	14.17 , 30.69 ;
10	-17.25 , 7.35 ;	***33***	-7.32 , 15.21 ;	***56***	18.17 , 7.35 ;	***79***	22.07 , 30.69 ;
11	-17.25 , 15.00 ;	***34***	-7.32 , 7.35 ;	***57***	18.17 , -0.49 ;	***80***	29.41 , 30.69 ;
12	-17.25 , 22.83 ;	***35***	-7.32 , -0.49 ;	***58***	25.97 , 23.04 ;	***81***	32.83 , 26.88 ;
13	-17.25 , 30.69 ;	***36***	-7.32 , -8.35 ;	***59***	25.97 , 15.21 ;	***82***	32.83 , 19.11 ;
14	-7.32 , 30.69 ;	***37***	-7.32 , -16.18 ;	***60***	25.97 , 7.35 ;	***83***	32.83 , 11.28 ;
15	1.82 , 30.69 ;	***38***	-7.32 , -24.05 ;	***61***	25.97 , -0.49 ;	***84***	32.83 , 3.41 ;
16	10.21 , 30.69 ;	***39***	-7.32 , -31.88 ;	***62***	-12.28 , -47.79 ;	***85***	32.83 , -5.82 ;
17	18.17 , 30.69 ;	***40***	-7.32 , -39.75 ;	***63***	-2.80 , -47.79 ;	***86***	29.35 , -11.16 ;
18	25.97 , 30.69 ;	***41***	1.82 , 23.04 ;	***64***	7.10 , -47.79 ;	***87***	22.07 , -11.16 ;
19	32.83 , 30.69 ;	***42***	1.82 , 15.21 ;	***65***	-17.25 , -43.86 ;	***88***	12.53 , -11.16 ;
20	32.83 , 23.04 ;	***43***	1.82 , 7.35 ;	***66***	-17.25 , -36.03 ;	***89***	12.53 , -20.12 ;
21	32.83 , 15.21 ;	***44***	1.82 , -0.50 ;	***67***	-17.25 , -28.16 ;	***90***	12.53 , -27.95 ;
22	32.83 , 7.35 ;	***45***	1.82 , -8.35 ;	***68***	-17.25 , -20.33 ;	***91***	12.53 , -35.81 ;
23	32.83 , -0.49 ;	***46***	1.82 , -16.18 ;	***69***	-17.25 , -12.47 ;	***92***	12.53 , -43.65;

Coordinates of the corners:

Floors 1 to 6

1 -17.25, 30.69
2 -17.25, -47.79;
3 12.53, -47.79;
4 32.83, 30.69;

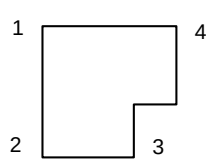

Floors 7 to 8

1 -17.25, 30.69;
2 -17.25, -47.79
3 12.53, -47.79;
4 12.53, 30.69

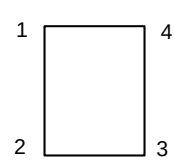

Masses of the base in the *x*-, *y*-, *r*- directions (units: x- y-: kN-sec^2/m, r-: kN-sec^2-m)

mb_x = 3565.73; mb_y = mb_x; mb_r = 2706868;

Masses and moments of inertia of the superstructure in the *x*-, *y*-, *r*-directions:

floor	*x*	*y*	*r*
1	2051,	2051,	1560994;
2	2051,	2051,	1560994;
3	2051,	2051,	1560994;
4	2051,	2051,	1560994;
5	2051,	2051,	1560994;
6	2057,	2057,	1560994;
7	2247,	2247,	1705017;
8	2580,	2580,	1957503;

Offsets of the center of the mass of the floors with respect to the base (unit: m):

0,	0
-0.3500,	-1.4200
-0.3200,	-5.8000
0.1100,	-7.2000
0.1600,	-9.2000
0.1600,	-9.2000
0.1600,	-9.2000
0.1600,	-9.2000

Eigenvectors of the fixed-base superstructure (24×24): first 12 columns.

-0.012202	0.000184	0.000114	0.000365	0.009757	-0.002245	0.000492	-0.00893	0.002504	-5.74E-05	-0.006898	0.003499
-0.000198	-0.012259	-0.000485	0.010182	-0.000321	0.000221	0.009585	0.000507	0.000118	-0.007028	9.34E-05	-0.000272
1.73E-05	-2.54E-05	0.000453	9.28E-06	-5.86E-05	-0.000361	-8.9E-06	9.45E-05	0.000325	7.44E-06	7.94E-05	0.000226
-0.011049	0.000156	0.00018	0.000182	0.005184	-0.001264	2.49E-05	-0.0011	0.000262	5.07E-05	0.002892	-0.002455
-0.00019	-0.011139	-0.000526	0.005478	-0.000162	0.000279	0.000252	-1.99E-06	-0.000139	0.003526	-2.68E-05	0.000223
1.59E-05	-1.9E-05	0.000402	1.25E-06	-2.53E-05	-0.00018	-7.17E-06	8.22E-06	5.95E-06	-1.7E-07	-3.53E-05	-0.00012
-0.009695	0.000134	0.000366	-2.74E-05	-0.000209	-0.000022	-0.000405	0.006784	-0.002009	7.97E-05	0.008707	-0.004302
-0.000159	-0.009675	-0.000504	-0.000269	5.3E-07	0.000131	-0.008583	-0.00049	-0.000214	0.00877	-0.000113	0.000233
9.22E-06	-1.73E-05	0.000352	-6.62E-06	1.58E-05	3.61E-05	1.25E-06	-7.83E-05	-0.000294	-8.07E-06	-0.000103	-0.000291
-0.008202	0.000115	0.000432	-0.000216	-0.00522	0.001237	-0.00053	0.009749	-0.003009	-4.71E-05	0.004008	0.000351
-0.000135	-0.007998	-0.000458	-0.005663	0.000152	-1.37E-05	-0.010729	-0.000563	8.25E-05	0.002104	-7.93E-05	-0.000245
6.74E-06	-1.54E-05	0.000285	-9.69E-06	4.96E-05	0.000225	8.3E-06	-0.000104	-0.000359	-8.83E-06	-4.35E-05	-6.97E-05
-0.006099	9.95E-05	0.000188	-0.000342	-0.00978	0.001738	-0.000183	0.004686	-0.001343	-0.000155	-0.009102	0.00496
-8.44E-05	-0.005651	-0.000438	-0.010319	0.000286	-0.000224	-0.002784	-0.000122	0.000454	-0.011125	9.95E-05	-0.000198
-1.06E-06	-8.76E-06	0.000199	-1.55E-05	6.93E-05	0.000378	9.81E-06	-3.34E-05	-7.48E-05	1.8E-07	0.000113	0.000384
-0.00408	7.28E-05	0.000331	-0.000389	-0.011066	0.00141	0.00032	-0.004768	0.001636	-2.26E-05	-0.008133	-0.000332
-5.05E-05	-0.004186	-0.000283	-0.010525	0.000293	-0.000545	0.005171	0.000262	7.95E-05	-0.00649	7.24E-05	0.00017
-8.04E-06	-7.46E-06	0.000137	-1.5E-05	7.51E-05	0.000385	7.42E-06	4.28E-05	0.000228	6.5E-06	9.4E-05	0.000207
-0.002251	4.74E-05	0.000128	-0.00029	-0.008805	0.000941	0.000584	-0.010694	0.001808	0.00013	0.006101	-0.000579
-2.8E-05	-0.002768	-0.000213	-0.008456	0.000238	-0.000523	0.009677	0.000507	-0.000271	0.006098	-3.65E-05	0.000105
-1.02E-05	-1.94E-06	7.73E-05	-8.86E-06	3.35E-05	0.000287	2.12E-06	8.64E-05	0.000369	9.28E-06	-9.66E-05	-0.000269
-0.00087	2.73E-05	0.000119	-0.000153	-0.004212	0.000556	0.000385	-0.007299	0.001657	0.000136	0.009157	-0.002121
-2.11E-05	-0.001328	-0.000115	-0.004624	0.000139	-0.000344	0.007559	0.000439	-0.00016	0.01052	-0.000137	-0.000313
-7.71E-06	-1E-07	3.21E-05	-2.23E-06	9.28E-06	0.000141	1.33E-06	4.41E-05	0.000242	8.23E-06	-8.45E-05	-0.000319

Eigenvectors of the fixed-base superstructure (24×24): last 12 columns.

0.000543	-0.005638	-0.000165	0.005144	0.004363	-0.001019	0.000262	0.000434	-0.001274	0.004171	0.000368	-0.00093019;
0.00715	0.000525	-0.005023	-0.000248	0.00013	3.95E-05	-0.002965	0.003551	0.000278	-0.000264	5.51E-05	-0.00019508;
-6.88E-06	8.7E-05	8.26E-06	-0.000105	0.000155	0.000171	2.39E-05	1.56E-05	-0.000172	-0.000033	7.7E-05	-0.00013789;
-0.000615	0.006347	0.000289	-0.008505	-0.007353	0.002934	-0.000418	-0.001004	0.002414	-0.011693	-0.001257	0.00263041;
-0.009135	-0.00069	0.0091	0.000458	-0.000337	-0.000185	0.007644	-0.010017	-0.000696	0.000723	-0.000253	0.00055375;
8.29E-06	-9.23E-05	-1.03E-05	0.000145	-0.000189	-0.000242	-3.62E-05	-1.61E-05	0.000316	9.48E-05	-0.000198	0.00039482;
-0.000543	0.00597	-1.81E-05	-0.001254	-9.15E-05	-0.002617	-7.45E-05	0.000758	-0.000111	0.014118	0.000972	-0.00321618;
-0.005763	-0.000447	-0.000458	6.03E-05	0.000142	-6.58E-05	-0.007276	0.012645	0.001222	-0.000889	0.000215	-0.00076490;
6.59E-06	-0.000102	-1.03E-06	7.04E-05	-0.000165	-8.79E-05	1.61E-06	-3.32E-05	-2.69E-05	-0.000119	0.000171	-0.00048109;
0.000524	-0.005878	-0.000292	0.009465	0.006923	-0.001401	0.000528	-9.41E-05	-0.002403	-0.009571	8.79E-05	0.00231962;
0.009985	0.000726	-0.008964	-0.000465	0.000155	0.000212	0.001687	-0.009587	-0.001308	0.000637	-3.55E-05	0.00058690;
-1.02E-05	6.68E-05	1.49E-05	-0.000146	0.000214	0.000257	2.51E-05	6.81E-05	-0.0003	8.47E-05	-1.83E-05	0.00034387;
0.00063	-0.007654	0.000295	-0.006241	-0.006577	0.007132	-0.000572	-0.00019	0.002358	0.004184	-0.001759	-0.00127519;
0.004121	0.000345	0.010343	0.000323	-0.000316	-4.48E-05	0.006388	0.007026	0.001493	-0.000381	-0.000255	-0.00038160;
-5.7E-07	0.000127	-9.4E-06	-1.71E-05	0.000182	-2.55E-05	-1.64E-05	-6.08E-05	0.000385	-3.46E-05	-0.000208	-0.00019856;
-0.000758	0.009587	-5.12E-05	-0.0025	0.00507	-0.010421	0.000474	0.000131	-0.000767	-0.001725	0.003828	0.00122197;
-0.008946	-0.000629	-0.002355	-8.79E-06	0.000699	1.16E-05	-0.012476	-0.006601	-0.00154	0.000316	0.000399	0.00030596;
1.58E-05	-6.2E-05	1.65E-06	7.7E-05	-0.000334	-0.000145	-4.5E-07	2.61E-05	-0.000171	1.87E-05	0.000407	0.00015387;
-0.000135	0.003418	-0.000228	0.009701	-0.004981	0.007939	-0.000332	5.41E-05	-0.001084	0.000671	-0.003146	-0.00077024;
-0.003665	-0.000368	-0.009085	-0.000203	-0.000759	4.25E-05	0.0109	0.004213	0.000954	-0.000167	-0.000308	-0.00012790;
-9.5E-06	-4.04E-05	-1.08E-06	-3.58E-05	4.33E-06	-6.78E-05	-3.9E-07	2.39E-05	-0.000238	-1.51E-05	-0.000442	-0.00010451;
0.000618	-0.010579	0.000262	-0.00891	0.003813	-0.00396	0.00018	-7.59E-05	0.000972	-0.000216	0.001083	0.00022340;
0.009281	0.000716	0.008813	0.000157	0.00047	-8.36E-06	-0.005337	-0.001728	-0.000335	5.45E-05	8.05E-05	0.00004858;
-1.58E-05	1.59E-06	-7.79E-06	3.45E-05	0.000207	0.000284	1.53E-06	-3.47E-05	0.000334	1.53E-05	0.000282	0.00005275;

Eigenvalues of the superstructure:

49.62	65.66	91.05	496.42	557.82	860.45	1674.41	1793.83
2858.65	3292.8	3511.06	5583.47	5743.95	5958.46	7453.32	7928.58
9248.47	9702.5	10431.08	11673.94	12011.94	12912.83	15828.77	17720.57

Appendix B

Properties of Modal Low-Authority LQG Controllers

The relationship between $\mathbf{A}_m$, $\mathbf{B}_m$ and $\mathbf{C}_m$ for the low-authority LQG controller is discussed here.

Let $\|\mathbf{S}_c\|_2 \le s_0$ and $\|\mathbf{S}_e\|_2 \le s_0$. For a controllable and observable flexible system, there exists $s_0 > 0$ such that the controller is of low-authority. Furthermore, if $\mathbf{A}_m$ is in the modal form 2, the following approximations hold

$$\mathbf{B}_m\mathbf{B}_m^T \cong -\mathbf{W}_c(\mathbf{A}_m + \mathbf{A}_m^T) = diag(w_{c,1}\alpha_1, w_{c,1}\alpha_1, w_{c,2}\alpha_2, w_{c,2}\alpha_2, \cdots, w_{c,n}\alpha_n, w_{c,n}\alpha_n) \quad \text{(B-1)}$$

$$\mathbf{C}_m^T\mathbf{C}_m \cong -\mathbf{W}_o(\mathbf{A}_m + \mathbf{A}_m^T) = diag(w_{o,1}\alpha_1, w_{o,1}\alpha_1, w_{o,2}\alpha_2, w_{o,2}\alpha_2, \cdots, w_{o,n}\alpha_n, w_{o,n}\alpha_n) \quad \text{(B-2)}$$

or, for the *i*th block,

$$\mathbf{B}_{m,i}\mathbf{B}_{m,i}^T \cong -w_{c,i}(\mathbf{A}_{m,i} + \mathbf{A}_{m,i}^T) = w_{c,i}\alpha_i\mathbf{I}_2 \quad \text{(B-3)}$$

$$\mathbf{C}_{m,i}^T\mathbf{C}_{m,i} \cong -w_{o,i}(\mathbf{A}_{m,i} + \mathbf{A}_{m,i}^T) = w_{o,i}\alpha_i\mathbf{I}_2 \quad \text{(B-4)}$$

where $\alpha_i = 2\varsigma_i\omega_i$, $\mathbf{B}_{m,i}$ is the *i*th two-row block, and $\mathbf{C}_{m,i}$ is the *i*th two-column block.

Proof: Note that for the positive semi-definite matrix $\mathbf{B}_m\mathbf{B}_m^T$, one obtains that $(b_{m,i}b_{m,j}^T)^2 \le (b_{m,i}b_{m,i}^T)(b_{m,j}b_{m,j}^T)$, i.e., the off-diagonal terms do not exceed the geometric mean value of the corresponding diagonal terms. Therefore, if $\mathbf{A}_m$ is in modal form 2, for small $\mathbf{S}_c$ such that $\|\mathbf{S}_c\|_2 \le s_0$, the off-diagonal terms of $\mathbf{B}_m\mathbf{B}_m^T$ do not influence the eigenvalues of $\mathbf{A}_{pcl}$, i.e., $\mathbf{A}_{pcl} = \mathbf{A}_m - \mathbf{B}_m\mathbf{B}_m^T\mathbf{S}_c$ (this is one of the equations (6-5) in modal

cordinates). Similar applies to the eigenvalues of $\mathbf{A}_{ecl} = \mathbf{A}_m - \mathbf{S}_e \mathbf{C}_m^T \mathbf{C}_m$. From Lyapunov equations (2-30), one obtains the above relationships.

Substituting $\mathbf{B}_{m,i}\mathbf{B}_{m,i}^T \cong -w_{c,i}(\mathbf{A}_{m,i} + \mathbf{A}_{m,i}^T) = w_{c,i}\alpha_i \mathbf{I}_2$ into the Lyapunov equations, one obtains

$$s_{c,i}(\mathbf{A}_{m,i} + \mathbf{A}_{m,i}^T) - s_{c,i}^2 \mathbf{B}_{m,i}\mathbf{B}_{m,i}^T \cong 0 \tag{B-5}$$

and thus

$$s_{c,i}^2 + \frac{s_{c,i}}{w_{c,i}} - \frac{q_i}{2\varsigma_i \omega_i w_{c,i}} \cong 0 . \tag{B-6}$$

Therefore, $s_{c,i} = \dfrac{\beta_{c,i} - 1}{2w_{c,i}} = \dfrac{\beta_{c,i} - 1}{2\gamma_i^2}$, where $\beta_{c,i}^2 = \dfrac{1 + 2q_i\gamma_i^2}{\zeta_i \omega_i}$. This is equation (6-6) used for the property 6 stated in chapter 6. Property 7 in chapter 6 can be obtained similarly.

LQG Root-Locus shown as property 8 in chapter 6 is proven as follows:
For the weighting $\widetilde{\mathbf{Q}} = diag(0,0,\cdots,q_i\mathbf{I}_2,\cdots,0,0)$, where q_i is small, the closed-loop matrix $\mathbf{A}_{pcl}$ is diagonally dominant, i.e.,

$$\mathbf{A}_{pcl} \cong diag(\mathbf{A}_{pcl,i}) \text{, where } i = 1,\cdots,n \text{, and } \mathbf{A}_{pcl,i} = \mathbf{A}_{m,i} - \mathbf{B}_{m,i}\mathbf{B}_{m,i}^T s_{c,i} . \tag{B-7}$$

Introducing (B-3) yields $\mathbf{A}_{pcl,i} \cong \mathbf{A}_{m,i} - 2\gamma_i s_{c,i}(\mathbf{A}_{m,i} + \mathbf{A}_{m,i}^T)$. Then introducing $\mathbf{A}_{m,i}$ in form 2 (2-26b) into (B-7) yields

$$\mathbf{A}_{pcl,i} \cong \begin{bmatrix} -\beta_{c,i}\varsigma_i\omega_i & -\omega_i \\ \omega_i & -\beta_{c,i}\varsigma_i\omega_i \end{bmatrix} \text{, with } \beta_{c,i}^2 = \frac{1 + 2q_i\gamma_i^2}{\zeta_i\omega_i} . \tag{B-8}$$

References

Abdullah, M. M. (1999). "Optimal Placement of DVFC Controllers On Buildings Subjected To Earthquake Loading", *Earthquake Engineering and Structural Dynamics*, **28**(2): 127-141.

Abdullah, M. M., Richardson, A. and Hanif, J. (2001). "Placement of Sensors/Actuators On Civil Structures Using Genetic Algorithms", *Earthquake Engineering and Structural Dynamics*, **30**(8): 1167-1184.

Ahmadi H., Fuller K. Fischinger M. and Isakovic T. (2005). "A Smart Elastomeric Isolator", *9th World Seminar on Seismic Isolation, Energy Dissipation and Active Vibration Control of Structures*, Kobe, Japan, June 13-16.

Agrawal, A.K., Yang, J.N. and He, W.L. (2003). "Performance Evaluation of Some Semiactive Control Systems for a Benchmark Cable-stayed Bridge", *Journal of Structural Engineering*, **129**(7):884-894.

Balas, M. (1978). "Modal Control of Certain Flexible Dynamic Systems", *Journal on Control and Optimization*, **16**(3):450-462.

Barbat, A. H., Rodellar J., Ryan, E. P. and Molinares, N. (1995). "Active Control of Nonlinear Base Isolated Buildings", *Journal of Engineering Mechanics*, **121**(6): 676-684.

Barnett S., (1975), *Introduction to Mathematical Control Theory*, Oxford University Press, Ely House, London.

Bhatia, K. M. (2001). "Spillover Reduction for Magnetorheological Damping Systems in Structural Control", *MSCE thesis*, Purdue University, West Lafayette, Indiana, USA.

Boyd S. P., and Barratt, C. H. (1991), *Linear Control Design*, Prentice Hall, Englewood Cliffs, NJ.

Burl, J. B. (1999). *Linear Optimal Control, H_2 and H_∞ Method*, Addison Wesley Longman, Inc.

Chang, C.C. and Roschke, P. N. (1999). "Neural Network Modeling of a Magnetorheological Damper", *Journal of Intelligent Material Systems and Structures*, **9**(9), September.

Chen, C.Q. and Chen, G. (2004a). "Shake Table Tests of A Quarter-Scale Three-Storey Building Model With Piezoelectric Friction Dampers", *Journal of Structural Control and Health Monitoring*, **11**: 239-257.

Chen, G. and Chen, C.Q. (2004b). "Semi-Active Control of the 20-Story Benchmark Building with Piezoelectric Friction Dampers", *Journal of Engineering Mechanics*, ASCE, **130**(4): 393-400.

Cho, S.-W., Kim, B.-W., Jung, H.-J., and Lee, I.-W. (2005). "Implementation of Modal Control for Seismically Excited Structures Using Magnetorheological Dampers", *Journal of Engineering Mechanics*, **131**(2): 177-184.

Choi, J. W., Park, U. S., and Lee, S. B. (2000). "Measures of modal controllability and observability in balanced coordinates for optimal placement of sensors and actuators: a flexible structure application", *Proceedings of SPIE, Smart Structures and Materials 2000: Mathematics and Control in Smart Structures*, **3984**: 425-436.

Chopra, A.K. (1995). *Dynamics of Structures: Theory and Applications to Earthquake Engineering,* Prentice Hall, Inc., A Simpson & Schuster Company, Upper Saddle River, NJ.

D'Azzo J. J, and Houpis C. H. (1988), *Linear Control System Analysis & Design*, McGraw-Hill, Inc.

Dullerud, G. E., Paganini F. (2000). A Course in Robust Control Theory: A Convex Approach, Springer-Verlag New York, Inc.

Dyke, S. J., (1996a), "Acceleration Feedback Control Strategies for Active and Semiactive Control Systems: Modeling, Algorithm Development, and Experimental Verification", *PhD Thesis*. University of Notre Dame.

Dyke, S. J., Spencer Jr., B. F., Sain, M. K. and Carlson, J. D. (1996b). "Seismic Response Reduction Using Magnetorheological Dampers", *Proceedings of the IFAC World Congress*, San Francisco, CA, June 30-July 5.

Dyke, S. J. Spencer, Jr., B. F., Sain, M. K. and Carlson, J. D. (1996c). "Modeling and Control of Magnetorheological Dampers for Seismic Response Reduction", *Smart Materials and Structure*s, **5**: 565-575.

Dyke, S. J., Spencer, Jr., B. F., Quast, P., Kaspari, Jr., D. C., and Sain, M. K. (1996d). "Implementation of an AMD Using Acceleration Feedback Control," *Microcomputers in Civil Engineering: Special Issue on Active and Hybrid Structural Control*, **11**: 305–323.

Dyke, S. J., Spencer, Jr., B. F., Quast, P., Sain, M. K., Kaspari, Jr., D. C. and Soong, T. T. (1996e). "Acceleration Feedback Control of MDOF Structures" *Journal of Engineering Mechanics*, ASCE, **122**(9): 907–918.

Dyke, S. J., Spencer Jr., B. F., Sain, M. K. and Carlson, J. D. (1997). "An Experimental Study of MR Dampers for Seismic Protection", *Smart Materials and Structures: Special Issue on Large Civil Structures*.

Dyke, S. J. (1999). "Application of Magnetorheological Dampers to Seimically Excited Structures", *Proceedings of the International Modal Analysis Conference*, Kissimmee, FL, February 8-11.

Dyke, S. J., Wang, Y., Taylor, E. (2005) "Seismic Response Modification Using Innovative Damping Devices", *Proceedings of the 3rd Columbian Conference on Steel Structures*, October 12-13, Tokyo, Japan.

Erkus, B. and Johnson, E. A. (2004). "Smart Base Isolated Benchmark Building Part III: A Sample Controller for Bilinear Isolation", *Journal of Structural Control and Health Monitoring*, Pub. Online, DOI: 10.1002/stc.101.

Franklin, G. F., Powell, J. D., and Emami-Naeini, A. (2002). *Feedback Control of Dynamic Systems*, Prentice-Hall, Inc., Upper Saddle River, New Jersey.

Fortuna, L., Muscato, G. and Nunnari, G. (1993a). "Parameterization of Discrete-Time Models in Open-Loop Balanced Form", *Proceedings of the 32nd IEEE Conference on Decision and Control*, San Antonio, U.S.A.

Fortuna L., G. Muscato and Nunnari, G. (1993b). "Closed-Loop Balanced Realizations of L.T.I. Discrete-Time Systems", *Journal of the Franklin Institute*, **330**(4): 695-705.

Fujita, T., Feng, Q., Takenaka, E., and Suizu, H. (1988). "Active Isolation of Sensitive Equipment for Weak Earthquakes", *Proceedings of the 9th World Conference of Earthquake Engineering*, Tokyo and Kyoto, Japan VIII, 459-464.

Furuta, K., Sano, A., and Atherton, D . (1988). *State Variable Method in Automatic Control*, Wiley, Chichester.

Gahinet, P. and Apkarian, P. (1994). "A Linear Matrix Inequality Approach to H_∞ Control", *International Journal of Robust and Nonlinear Control*, **4**:421-448.

Gawronski, W. K. (1994). "A Balanced LQG Compensator for Flexible Structures", *Automatica*, **30**(10), 1555-1564.

Gawronski, W. K. (1998). *Dynamics and Control of Structures: A Modal Approach*, Springer-Verlag New York, Inc.

Genta, G. (1999). *Vibration of Structures and Machines: Practical Aspects*, Springer-Verlag New York, Inc.

Geromel, J. C., 1989, "Convex Analysis and Global Optimization of Joint Actuator Location and Control Problems", *IEEE Tranactions On Automatic Control*, **34**(7), 711-720.

Gordaninejad F., Wang X., Hitchcock G., Bangrakulur K., Fuchs A., Elkins J., Evrensel C., Ruan S., Siino M., and Kerns M. (2004a). "A New Modular Magneto-Rheological Fluid

Valve For Large-Scale Seismic Applications", *Proceedings of the Fourth International Workshop on Structural Control*, *Ed. A. Smith and R. Betti*, New York, New York: 140-145.

Gordaninejad F., Wang X., Hitchcock G., Bangrakulur K., Fuchs A., Elkins J., Evrensel C., Ruan S., Siino M., Zemanek T., and Kerns M. (2004b). "A New Modular Seismic Magneto-Rheological Fluid Damper", *Proceedings of the Third International Conference on Earthquake Engineering*, Nanjing, China: 717-727.

Hamdan, A. M. A., and Nayfeh, A. H. (1989) "Measures of Modal Controllability and Observability for First- and Second- Order Linear Systems", *Journal of Guidance, Control, and Dynamics*, **12**(3), 421-428.

Hayen, J. C., and Iwan, W. D. (1994). "Response Control of Structural Systems Using Active Interface Damping", *Proceedings of 1st World Conference on Structural Control*, **1**: WA2-23-WA2-33.

He, W. L., Agrawal A. K. and Yang J. N. (2003). "A Novel Semiactive Friction Controller for Linear Structures against Earthquakes", *Journal of Structural Engineering*, **129**(7): 941-950.

He, W. L. and Agrawal, A. K. (2005), "Passive and Hybrid Control Systems for Seismic Protection of a Benchmark Cable-Stayed Bridge", *Accepted for publication in Journal of Structural Control and Health Monitoring*, 2005.

Inaudi, J. A., and Kelly, J. M. (1990). "Active isolation", *Proceedings of U. S. National. Workshop on Structural Control Research*, Los Angeles, CA, 125-130.

Inaudi, J. A., and Kelly, J. M. (1992). "Optimum Damping in Base Isolated Structures", *Proceedings of the 10th World Conference in Earthquake Engineering*, Madrid, Spain, July 1992.

Inaudi, J. A., and Kelly, J. M., (1993a). "Hybrid Isolation Systems for Equipment Protection", *Earthquake Engineering and Structural Dynamics*, **22**: 297-313.

Inaudi, J. A., and Kelly, J. M. (1993b). "Optimum Damping in Linear Isolation Systems", *Earthquake Engineering and Structural Dynamics*, **22**: 583-596.

Iwan, W. D. and Wang, L.-J. (1998). "A comparison of Control Algorithms for Active Interaction Control of Civil Structures", *Proceedings of the 2nd World Conference on Structural Control*, **2**:1559-1566.

Iwasaki, T. and Skelton, R. E. (1995). "All Controllers for the General H_∞ Control Problem", *automatica*, **30**(8):1307-1317.

Jansen, L. and Dyke, S. J. (1999). "Investigation of Nonlinear Control Strategies for the Implementation of Multiple Magnetorheological Dampers", *Proceedings of the 1999 ASCE Engineering Mechanics Conference*, Baltimore, Maryland, June 16.

Jansen, L. M. and Dyke, S. J. (2000). "Semiactive Control Strategies for the MR Damper: A Comparative Study", *Journal of Engineering Mechanics*, **126**(8): 795-803.

Jonckheer, E. A., and Silverman, L. M. (1983), "A New Set of Invariants for Linear Systems – Application to Reduced Order Compensator Design", *IEEE Transactions on Automatic Control*, **28**(1), 953-964.

Johnson, E. A., and Erkus, B. (2002a). "Structural Control with Dissipative Damping Devices", *Proceedings of the American Control Conference*, New York, 2463-2468.

Johnson, E. A., and Erkus, B. (2002b). "Structural Vibration Mitigation Using Dissipative Smart Damping Devices", *CD-ROM Proceedings of the 15th ASCE Engineering Mechanics Conference*, Anchorage, Alaska, June 2-5.

Johnson, E. A., and Erkus, B. (2004). "Dissipativity and Performance Analysis of Semiactive Systems with Smart Dampers via LMI Synthesis", *submitted to the Journal of Structural Control and Health Monitoring*.

Kelly, J. M., Leitmann, G., and Soldatos, A. (1987). "Robust Control of Base-Isolated Structures Under Earthquake Excitation", *Journal of Optimization Theory Application*, **53**: 159-180.

Kelly, J. M. and Tsai, H. -C. (1985). "Seismic Response of Light Equipment in Base-Isolated Structures", *Earthquake Engineering and Structural Dynamics*, **13**: 711-732.

Ko, J. M., Zheng, G., Chen, Z. Q. and Ni, Y. Q. (2002). "Field Vibration Tests of Bridge Stay Cables Incorporated with Magneto-Rheological (MR) Dampers". *Smart Structures and Materials 2002: Smart Systems for Bridges, Structures, and Highways* [C], Liu, S.-C. and Pines ,D. J. (eds.), 2002, SPIE, **4696**: 30-40.

Kobori, T., Koshika, N., Yamada, N. and Ikeda, Y. (1991). "Seimic Response Controlled Structure with Active Mass Driver System, Part I: Design", *Earthquake Engineering and Structural Dynamics*, **20**:133-139.

Kwakernaak, H. and Silvan, R. (1972). *Linear Optimal Control Systems*, Wiley-Interscience, New York.

Liu, Y., Gordaninejad, F., Evrensel, C. A., and Hitchcock, G. (2001). "An Experimental Study on Fuzzy Logic Vibration Control of a Bridge Using Fail-Safe Magneto-Rheological Fluid Dampers", *Smart Systems and Materials - Smart Systems for Bridges, Structures, and Highways*, Newport Beach, USA, 281-288.

Longman, R. W., Siilin, S. W., Li, T., and Sevaston, G., 1982, "The Fundamental Structure of the Degree of Observability", *AIAA/AAS paper 82-1434*, San Diego.

Lu, L.Y. (2001). "Seismic Test of Modal Control with Direct Output Feedback for Building Structures", *Structural Engineering and Mechanics*, **12**(6): 633-656.

Lu, L. Y. and Chung, L. L. (2001). "Modal Control of Seismic Structures Using Augmented State Matrix", *Earthquake Engineering and Structural Dynamics*, **30**: 237-256.

Maciejowski, J. M.(1989). *Multivariable Feedback Design*, Addison-Wesley, Wokingham.

Makris, N., (1997), "Rigidity-Plasticity-Viscosity: Can Electrorheological Damper Protect Base-Isolated Structures from Near-Source Ground Motions?" *Earthquake Engineering and Structural Dynamics*, **26**(5): 571-591.

Manolis, G., Juhn, G., Constantinou M. And Reinhorn, A. (1990). "Secondary Systems in Base-Isolated Structures: Experimental Investigation, Stochastic Response and Stochastic Sensitivity", *Technical Report NCEER-90-0013*, State University of New York at Buffalo, July, 1990.

Matlab version 7.0, The Mathworks inc., 2005.

Mei, G., and Kareem, A. and Kantor, J. C. (2001). "Real-Time Model Predictive Control of structures under earthquakes", *Earthquake Engineering and Structural Dynamics*, **30**: 995-1019.

Mei, G., Kareem, A. and Kantor, J. C. (2002). "Model Predictive Control of Structures Under Earthquakes Using Acceleration Feedback", *Journal of Engineering Mechanics*, ASCE, **128**(50): 574-586.

Meirovitch, L., and Stemple, T. J. (1997). "Nonlinear Control of Structures in Earthquakes", *Journal of Engineering Mechanics*, **123**(10): 1090-1095.

McClamroch, N.H. and Gavin, H. P. (1995). "Closed Loop Structural Control Using Electrorheological Dampers", *Proceeding of the American Control Conference*, Seattle, Washington, 4173–77.

Midorikawa, M., Otani, S., Wada, A., Kitagawa, Y. and Fujita, T. (2004). "Research Project on Smart Structural Systems – Part of the U.S. / Japan Joint Research Program", Proceedings of the US-Korea Joint Seminar/Workshop on Smart Structures Technologies, Seoul, Korea, September 2-4, 2004.

Moore, B. C., 1981, "Principle Component Analysis in Linear Systems: Controllability, Observability, and Model Reduction", *IEEE Transactions on Automatic Control*, **26**(1), 17-32.

Naeim, F., and Kelly, J. M. (1999). "Design of Seismic Isolated Structures: from Theory to Practice", Wiley, Chichester, England.

Nagarajaiah, S. and Nadathur, V. (2005). "Semiactive Control of Wind Excited Building with Variable Stiffness TMD Using Short Time Fourier Transformation", *Journal of Engineering Structures*, **27**: 431-441.

Narasimhan S., Nagarajaiah S., Gavin H. P., and Johnson E.A. (2002). "Benchmark Problem for Control of Base Isolated Buildings", *Proceedings of the 3rd World Conference on Structural Control*, Como, Italy. CDROM

Narasimhan S., Nagarajaiah S., Johnson E.A., and Gavin H. P. (2004). "Smart Base Isolated Benchmark Building, part I: Problem Definition", Proceedings of the 4th *International Workshop on Structural Control and Health Monitoring*, Columbia University, June 10-11, 2004. CDROM.

Nagarajaiah S. and Narasimhan S. (2005). "Smart Base Isolated Benchmark Building Part II: Sample Controllers for Linear and Friction Isolation", *Journal of Structural Control and Health Monitoring*, Pub. Online, DOI: 10.1002/stc.100.

Nagarajaiah S. and. Mate, D. (1998). "Semiactive Control of Continuously Variable Stiffness System", *Proceedings of the 2nd World Conference of Structural Control*, 1: 397-405.

Nagarajaiah S., Reinhorn A. M, and. Constantinou, M. C. (1991). "3D-BASIS: Nonlinear Dynamic Analysis of Three Dimensional Base Isolated Structures: Part II", *Technical Report NCEER-91-0005*, National Control for Earthquake Engineering, Res., 1991b; State University of New York, Buffalo.

Nagarajaiah, S., and Xiaohong, S. (2000). "Response of Base-Isolated USC Hospital Building in Northridge Earthquake", *Journal of Structural Engineering*, **126**(10), 1177-1186.

Ni, Y. Q, Chen, Y., Ko, J. M, Cao, D. Q. (2002a). "Neuro-control of Cable Vibration Using Semi-active Magnetorheological Dampers", *Engineering Structures*, **24**: 295-307.

Ni, Y. Q., Chen, Y., Ko, J. M. and Zheng, G. (2002b). "Optimal Voltage/Current Input to ER/MR Dampers for Multi-Switch Control of Stay Cable Vibration", *Proceedings of the 3rd International Conference on Structural Control*, Como, Italy, 2002.

Nunnari G, Fortuna L., and Muscato G. (1994) "LQG-Controller Reduction: A Structured Perturbation Approach Based on Closed Loop Balanced Realizations", *Proceedings of the 1994 IFAC Symposium on Robust Control Design*, Rio de Janeiro, Brazil, Sep. 1994.

Ohtori, Y., Christenson, R. E., Spencer Jr., B. F., and Dyke, S. J. (2004). "Benchmark Control Problems for Seismically Excited Nonlinear Buildings", *Journal of Engineering Mechanics*, ASCE, **130**(4): 366-385.

Oliveira, M. C. and Geromel, J. C. (2000) "Linear Output Feedback Controller Design with Joint Selection of Sensors and Actuators", *IEEE Transactions on Automatic Control*, **45**(12): 2412-2419.

Opdenacker, P. H. and Johckheer, E. A. (1985). "LQG Balancing and Reduced LQG Compensation of Symmetric Passive Systems", *International Journal of Control*, **41**(1): 73-109.

Park, K. S. Jung, H. J., Spencer Jr., B. F. and Lee, I. W. (2003). "Hybrid Control Systems for Seismic Protection of a Phase II Benchmark Cable-Stayed Bridge", *Journal of Structural Control*, **10**: 231-247.

Panossian, H., Gawronski, W. and Ossman, J. (1998) "Balanced Shaker and Sensor Placement for Modal Testing of Large Flexible Structures", IMAC-XVI, Santa Barbara, CA.

Reigles, D. G. and Symans, M. D. (2005a). "Supervisory Fuzzy Control of Base-Isolated Benchmark Building utilizing Neuro-Fuzzy Model of Controllable Fluid Viscous Damper", *Special Issue of the Journal of Structural Control and Health Monitoring on Structural Control Benchmark Problem: Smart Base-Isolated Building*, *Subjected to Near Fault Earthquakes*.

Reigles, D. G. and Symans, M. D. (2005b). "Systematic Performance Evaluation of Smart Seismic Isolation Systems", *Proceedings of Seventeenth Conference on Analysis and Computation held in Conjunction with ASCE Structures Congress 2005*, ASCE, New York, NY, April, 2005, *in press*.

Ribakov, Y. and Gluck, J. (2002). "Selective Controlled Base Isolation System with Magnetorheological Dampers", Earthquake Engineering and Structural Dynamics, **31**:1301-1324.

Richardson, A. and Abdullah, M. M. (2003). "Vibration control of multiple structures: theory and application." *Doctoral Thesis*, Florida A & M.

Ramallo, J. C., Johnson, A. M., and Spencer Jr., B. F. (2002). ""Smart" Base Isolation Systems", *Journal of Engineering Mechanics*, **128**(10): 1088-1099.

Sahasrabudehe, S. S. and Nagarajaiah, S. (2005). "Semiactive Control of Sliding Isolated Bridges Using MR Dampers: An Experimental and Numerical Study", *Earthquake Engineering and Structural Dynamics*, **34**:965-983.

Scruggs, J. T. and Iwan, W. D. (2004). "Dissipative Capabilities of Regenerative Force Actuators", *International Symposium on Network and Center-Based Research for Smart Structures Technologies and Earthquake Engineering*, Osaka, 115-120.

Scruggs, J. T. and Iwan, W. D. (2005). "Structural Control Using Regenerative Force Actuation Networks", *Journal of Structural Control and Health Monitoring*, 12: 25-45.

Scruggs, J. T., Taflanidis, A. A., and Beck, J. L. (2005). "Reliability-Based Control Optimization for Active Base Isolation Systems", *Journal of Structural Control and Health Monitoring*, *in press*.

Silva, S. and Lopes Jr., V. (2002). "Técnicas de Controle Ótimo para Supressão de Vibração Utilizando Sensores e Atuadores Piezelétricos", *II Congresso Nacional de Engenharia Mecânica* - CONEM 2002, João Pessoa-PB.

Silva, S. and Lopes Jr., V. (2004) "Robust Control to Parametric Uncertainties in Smart Structures Using Linear Matrix Inequalities", *Journal of the Brazil Society of Mechanical Science & Engineering*, vol. XXVI (4), 2004, 430-437.

Skinner, R. I., Robinson, W. H., McVerry G. H. (1993). An Introduction to Seismic Isolation, Willey, Chichester, England.

Soong, T. T, and Grigorio, M. (1996). Random Vibration of Mechanical and Structural Systems, Prentice Hall.

Spencer Jr., B. F., Dyke, S. J., Sain, M. K. and Carlson, J. D. (1997). "Phenomenological Model for Magnetorheological Dampers", *Journal of Engineering Mechanics*, 123(3): 230-238.

Spencer Jr., B. F., Dyke, S. J., and Deoskar, H. S. (1998a). "Benchmark Problems in Structural Control: Part I – Active Mass Driver System", *Earthquake Engineering and Structural Dynamics*, 27(11): 1127-1139.

Spencer Jr., B. F., Dyke, S. J., and Deoskar, S. S. (1998b). "Benchmark Problems in Structural Control: Part II – Active Tendon System", *Earthquake Engineering and Structural Dynamics*, 27(11): 1141-1147.

Spencer Jr., B. F. and Yang, G. (2004). "Recent Developments in Structural Control Research in the U.S.", *Proceedings of the 4th International Workshop on Structural Control*, Columbia University, New York, NY USA.

Stevens, B. L., and Lewis, F. L., (2003), "Aircraft Simulation and Control", 2nd version, S John Wiley & Sons, INC, Hoboken, New Jersey.

Symans, M. D. and Reigles, D. G. (2004). "Supervisory Fuzzy Logic Control of Smart Seismic Isolation Systems", *Proceedings of 2004 ASCE Structural Congress*, ASCE, Nashville, TN, May.

Talbot, M. E. and Shinozuka, M. (1990). "Active Isolation for System Protection of Operating Rooms", *Technical Report NCEER-90-0010*, Natural Center of Earthquake Engineering, Buffalo, New York.

Tan, P., and Agrawal, A. K. (2005a). "A Nonlinear Benchmark Model of Highway Bridge Crossing for Structural Response Control, Part II: Sample Active and Semi-Active Controller Design". *to be published in Journal of Structural Control and Health Monitoring*.

Tan, P. and Agrawal, A. K. (2005b). "A Nonlinear Benchmark Model of Highway Bridge Crossing for Structural Response Control, Part II: Sample Active and Semiactive Controller Design", *to be published in Journal of Structural Control and Health Monitoring*.

Tan P., Dyke, S.J., Richardson, A., and Abdullah, M. (2005c). "Integrated Device Placement and Control Design in Civil Structures Using Genetic Algorithms", *Journal of Structural Engineering*, ASCE, **131**(10): 1489-1496.

Tsai, H. C. and Kelly, J. M. (1989). "Seismic Response of the Superstructure and Attached Equipment in a Base-Isolated Building", *Earthquake Engineering and Structural Dynamics*, **18**: 551-564.

Walsh, K. K. and Abdullah, M. M. (2005). "Semi-active Control of Civil Structures Using Variable Amplification", *Journal of Structural Engineering*, *in review*.

Wang, X. Gordaninejad, F., Bangrakulur, K. K., Hitchcock, G., Fuchs, F., Elkins, J., Evrensel, C., Ruan, S., Siino, M., and Kerns, M. (2004). "A New Modular Magneto-Rheological Fluid Valve for Large-Scale Seismic Applications, Damping and Isolation", *Proceedings of SPIE Conference on Smart Materials and Structures*, *Ed. Kon-Well Wang*, 5386: 226-237.

Wen, Y. K. (1976). "Method of Random Vibration of Hysteretic Systems", *Journal of Engineering Mechanics Division*, ASCE, **102**(2): 249-263.

Watanabe, T. and Stoorvogel, A. A. (2002). "Plant Zero Structure and Further Order Reduction of a Singular H_∞ Controller", *International Journal of Robust and Nonlinear Control*, **12** (2): 591-619.

Wereley, N. M., Kamath, G. M. and Madhavan, V. (1999). "Hysteresis Modeling Of Semiactive Magnetorheological Helicopter Dampers", *Journal of Intelligent Material systems and Structures*, **10**(8): 624-633.

Whalen, T. M., Bhatia, K. M., and Archer, G. C. (2002). "Semi-Active Vibration Control for the 3rd Generation Benchmark Problem Including Spillover Suppression", *The 15th ASCE Mechanics Conference*, June 2-5th, 2002, Columbia University, New York, NY.

Wilson, C. M. D. and Abdullah, M. (2005a). "Fuzzy Control of Magnetorheological Dampers in Civil Structures", *6th European Conference on Structural Dynamics (EURODYN)*, September 4-7th, Paris, France, 2005.

Wilson, C. M. D. and Abdullah, M. (2005b). "Structural Vibration Reduction Using Fuzzy Control of Magnetorheological Dampers", *ASCE Structures Congress*, April 20-24th, New York, 2005.

Xia, X., Liu, L. and Dyke, S. J. (2005). "Semiactive Control for Seismic Protection of a Railway Bridge with Tall Piers", *to be submitted to the 4th World Conference on Structural Control and Monitoring*, July 11-13, San Diego, CA, 2006

Xu, Z. D., Shen, Y. P. and Guo, Y. Q. (2003). "Semi-active Control of Structures Incorporated with Magnetorheological Dampers Using Neural Networks", *Smart Material and Structures*, **12**(2): 80-87.

Yalla, S.K. and Kareem, A. (2000). "Optimum Absorber Parameters for Tuned Liquid Column Dampers", *Journal of Structural Engineering*, ASCE, **126**(8): 906-915.

Yalla, S.K. and Kareem, A. (2003). "Semi-Active Tuned Liquid Column Dampers: An Experimental Study", *Journal of Structural Engineering*, ASCE, **129**(7): 960-971.

Yang, J. N. (1982). "Control of Tall Buildings under Earthquake Excitations", Journal of Engineering Division, **108**(5): 833-849.

Yang, J. N., Lin, S. Kim, J. H. and Agrawal, A. K. (2002). "Optimal Design of Passive Energy Dissipation Systems Based on H-Infinity and H2 Performance", *Journal of Earthquake Engineering and Structural Dynamics*, **31**(4): 921-936.

Yang, J. N., Lin, S. and Jabbari, F. (2004a). "Linear Multi-objective Control Strategies for Wind-Excited Buildings", *Journal of Engineering Mechanics*, ASCE. **130**(4):471-477.

Yang, J. N., Agrawal, A. K., Samali, B. and Wu, J. C. (2004b). "A Benchmark Problem for Response Control of Wind-Excited Tall Buildings", *Journal of Engineering Mechanics*, ASCE, **130**(4): 437-446.

Yang, G. (2001). "Large-Scale Magnetorheological Fluid Damper for Vibration Mitigation: Modeling, Testing and Control", *Ph.D dissertation*, Department of Civil Engineering and Geological Sciences, University of Notre Dame, Notre Dame, Indiana.

Yang, G., Spencer Jr., B. F., Carlson, J. D. and Sain, M. K. (2002a). "Large-Scale MR Fluid Dampers: Modeling and Dynamic Performance Considerations", *Engineering Structures*, **24**: 309–323.

Yang, G., Spencer Jr., B.F., Carlson, J. D. and Sain, M. K. (2002b). "Large-Scale MR Fluid Dampers: Modeling and Dynamic Performance Considerations", *Chinese Journal Earthquake Engineering and Engineering Vibration*, **21**(4): 8–23. (translated into Chinese).

Yi, F., Dyke, S. J., Frech, S. and Carlson, J. D. (1998). "Investigation of Magnetorheological Dampers for Earthquake Hazard Mitigation", *Proceedings of the 2nd World Conference on Structural Control*, Kyoto, JAPAN, June 29 - July 2.

Yi, F., Dyke, S. J., Caicedo, J. M., and Carlson, J. D. (2001). "Experimental Verification of Multi-Input Seismic Control Strategies for Smart Dampers", *Journal of Engineering Mechanics*, ASCE, **127**(11): 1152-1164.

Yoshida O. (2003). "Torsionally Coupled Response Control of Earthquake Excited Asymmetric Buildings: Development and Application of Effective Control Systems Using Smart Dampers", *Doctoral Dissertation*, Washington University in St. Louis.

Yoshida, O., Dyke, S.J., Giacosa, L.M., and Truman, K.Z. (2003). "Experimental Verification of Torsional Response Control of Asymmetric Buildings Using MR Dampers", *Earthquake Engineering and Structural Dynamics*, **32**(13): 2085-2105.

Yoshida O., and Dyke, S.J. (2005). "Response Control of Full Scale Irregular Buildings Using MR Dampers", *Journal of Structural Engineering*, ASCE, *in press*.

Zhang, Y., and Iwan, W. D. (2002a). "Active Interaction Control of Civil Structures, Part 1: SDOF Systems", *Earthquake Engineering and Structural Dynamics*, **31**(1): 161-178.

Zhang, Y., and Iwan, W. D. (2002b). "Active Interaction Control of Civil Structures, Part 2: MDOF Systems", *Earthquake Engineering and Structural Dynamics*, **31**(1): 179-194.

Zhang, Y., and Iwan, W. D. (2002c). "Protecting Base-Isolated Structures from Near-Field Ground Motion by Tuned Interaction Damper", *Journal of Engineering Mechanics*, **128**(3): 287-295.

Zhang, J. and Roschke P. N. (1998). "Neural Network Simulation of Magnetorheological Damper Behavior", *Proceedings of the International Conference on Vibration Engineering '98*, Dalian, China, August 6-9.

Zhang, Y., and Zhu, S. (2005). "A Superelastic Shape Memory Alloy Wire Damper with Tunable Hysteretic Behaviors", *submitted to the Journal of Structural Engineering*, ASCE.

Vita

Yumei Wang

Place of Birth Heilongjiang, P. R. China

Degrees
B.ENG., Tongji University, Shanghai, China, July, 1991
M.ENG., Tongji University, Shanghai, China, July, 1999
M.S., University of Illinois at Urbana-Champaign, May, 2003
D.Sc., Washington University in St. Louis, May, 2006

Publications

Wang, Y., and Dyke, S. J., (2006), "Smart System Design for a 3D Base Isolated Building", to be submitted to *Journal of Structural Control and Health Monitoring*.

Wang, Y., and Dyke, S. J., (2006), "Modal-Based Smart System Design for Seismic Response Control", to be submitted to *Earthquake Engineering and Structural Dynamics*.

Wang, Y., McFarland, D. M., Vakakis A. F., and Bergman, L.A, (2005), "Seismic Base Isolation by Nonlinear Mode Localization", *Archive of Applied Mechanics (Ingenieur Archiv)*, **74**(5-6): 387-414.

Wong, Kevin K. F. and Wang, Y., (2001), "Probabilistic Structural Damage Assessment and Control Based on Energy Approach", *The Structural Design of Tall Buildings*, **10**(12): 283-308.

Wong, Kevin K. F. and Wang, Y., (2001), "Energy-based Damage Assessment on Structures during Earthquakes", *The Structural Design of Tall Buildings*, **10**(6): 135-154.

Wang, Y. and Luo, Q., (2000), "Study on Ideological Weakness of Earthquake Resistant Code Based on Damages to Masonry Buildings", *Journal of Seismological Research (in Chinese)*, **23**(3): 361-367.

Wang, Y., Dyke, S. J. (2005), "A Comparative Study of the Base Isolation Benchmark Problem Using H_2/LQG Algorithm and MR Dampers", *the 17th Analysis & Computation Specialty Conference*, May 18-21, 2006, St. Louis, MO, USA.

Wang, Y., McFarland, D. M., Vakakis A. F., and Bergman, L. A., (2002), "Efficacy of a Nonlinear Base Isolation System Subjected to Near-field Earthquake Motions", *Proceedings of International Conference on Advances and New Challenges in Earthquake Engineering Research*, August 15-17, 2002, Harbin, China.

May 2006